CLINICAL AND MOLECULAR INVESTIGATION OF RARE CONGENITAL DEFECTS OF THE PALATE

RIMANTE SESELGYTE

A thesis submitted for the degree of

Doctor of Philosophy to University College London

August 2019

DECLARATION

I, Rimante Seselgyte, confirm that the work presented in this thesis is my own. Where information has been derived from other sources, I confirm that this has been indicated in the thesis.

Signed……..

ABSTRACT

Cleft palate (CP) affects around 1/1500 live births and, along with cleft lip, is one of the most common forms of birth defect.

The studies presented here focus on unusual defects of the palate, especially to understand better the rarely reported but surprisingly common condition called submucous cleft palate (SMCP). The frequency and consequences of SMCP from a surgical perspective were first investigated based on the caseload of the North Thames Cleft Service at Great Ormond Street Hospital and St Andrew's Centre, Broomfield Hospital, Mid Essex Hospitals Trust. It was previously reported that up to 80% of individuals with unrepaired SMCP experience speech difficulties as a consequence of velopharyngeal insufficiency (VPI). Attempted repair of the palatal defect can sometimes give poor results, so controversies still exist about the correct choice of surgical technique to use. Over 23 years, 222 patients at The North Thames Cleft Service underwent operations to manage SMCP. Nearly half of them (42.8%) were diagnosed with 22q11.2 deletion syndrome (22q11.2 DS). The first operation was palate repair, with an exception of one case, followed by a second surgical intervention required in approximately half of the patients. A third procedure to manage VPI was carried out in 6% of patients.

To better understand the histological anatomy of the palatal muscles in cleft patients, biopsies were taken from levator veli palatini (LVP) and/or palatopharyngeus (PP) muscles during surgical correction of CP. Muscles were compared from patients with SMCP to those with overt CP and also to controls. The controls consisted of descending PP muscle fibres from healthy children who underwent a tonsillectomy operation for obstructive sleep apnoea or recurrent chronic tonsillitis. Fifty-seven biopsy samples were available from children between 10 months to 9 years of age. Individual biopsy samples were also available from patients with achondroplasia, Apert, Cornelia de Lange and Kabuki syndromes. The study showed a prevalence of fast fibres in both muscles in all CP types. However, in both SMCP LVP and SMCP 22q11.2 DS LVP, this trend was reversed in favour of slow fibres. Single cases with syndromes did not reveal any obvious differences compared to more common cleft types.

Mutations in *TBX22* are a frequent genetic cause of cleft palate and SMCP. The functional role of the encoded TBX22 transcription factor was investigated in a mouse model with SMCP. Cell lineage-specific fluorescence activated cell sorting of a conditional allele of *Tbx22,* was used to look at the RNA-Seq transcriptome in developing palatal shelves, with a view to identify downstream target genes. Eleven up regulated genes reached statistical significance after multiple testing correction in cranial mesoderm (CM) derived cells when comparing $Tbx22^{null/Y}$ and WT samples (*Cspg4, Foxp2, Reln, Bmpr1b, Adgrb3, Sox6, Zim1, Scarna13, Fat1, Notch3, Peg3*). Eleven genes were down regulated in the same comparison (*Nr2f2, Lars2, Ahr, Aplnr, Emcn, Npnt, Apln, Ccr2, Tll1, Snord34, Snord99*). Comparing $Tbx22^{null/Y}$ and WT in cranial neural crest (CNC) derived cells, only *Cxcl14* was up regulated, while *Tbx22* was down regulated. Osteoclast differentiation, calcium signalling, focal adhesion, Wnt signalling and cell adhesion molecule pathways were the most enriched pathways in functional annotation of significantly differentially expressed genes analysis.

Finally, a family with an unusual velopharyngeal anatomy was investigated in order to determine the likely genetic cause. This involved the implementation of genetic technologies in an autosomal dominant multigeneration Egyptian family with 8 affected individuals who presented with absent uvula, short posterior border of the soft palate and abnormal pillars of the fauces. Using a combination of cytogenetic, linkage analysis and exome sequencing, followed by more detailed segregation and functional analysis, a dominantly acting missense mutation in the activation domain of *FOXF2* was revealed. This variant was found to co-segregate with a copy number variant of unknown significance that could not at this stage be causally distinguished from the point mutation.

IMPACT STATEMENT

Orofacial clefts are among the most common birth defects worldwide, affecting 1 in 700 births. Facial clefts, including cleft lip and/or cleft palate, have a very serious impact on the quality of life, requiring repeated surgical interventions in childhood and specialist medical attention throughout life. Recent research has emphasized the importance for a better understanding of cleft pathogenesis and genetic background using a combination of epidemiology, genome-wide association studies, linkage analysis, candidate gene sequencing and the study of animal models. Despite intensive research worldwide, much of the genetic basis of cleft lip and palate still remains unknown. It is an important goal to develop these research methods with a view to the gradual transition and application in the everyday clinical cleft patient management.

The main focus of this work was the study of rare forms of cleft palate (CP), a group of congenital abnormalities that present a significant challenge since treatment outcomes are on the whole less successful. In this PhD, extensive palate muscle histology was analysed in patients with submucous cleft palate for the first time. The findings add to our understanding why surgical cleft repair is not always successful and provides evidence which can assist surgeons to manage expectations of patients and their families. At the same time, these results can form the basis of a larger prospective study into palatal muscle repair.

A second aim was to examine the molecular basis of *Tbx22* loss in a mouse model of CP. Mutations in *TBX22* cause X-linked CP, which ranks as one of the most common genetic causes of CP in humans. Experiments were performed to identify consequential gene expression disbalances that occur in embryonic mouse palatal shelves, when the TBX22 transcription factor is silenced. This work has revealed several likely downstream target genes and highlighted biochemical pathways that are likely to be required for normal palatogenesis. This is of interest to a large international group of orofacial biologists and provides an important platform for future studies.

Finally, a family with an unusual, and possibly unique, inherited palate phenotype, characterised by an absent uvula, short posterior border of the soft palate and

abnormal pillars of the fauces was studied in order to identify the molecular cause. Using a combination of technologies including cytogenetic analysis, linkage, exome sequencing and cell-based functional studies identified *FOXF2* as playing an important role in palatal, oropharyngeal and uvula development. Recent publication of this work benefits the broad society of researchers and clinicians, particularly raising awareness of this rare condition. The family has been fully informed for the benefit of future genetic counselling, especially since our findings also have implications for preventable late-onset glaucoma.

The work in this PhD was funded by 'CLEFT-bridging the gap', which included a generous donation by the Childwick Trust and the results will be reported to the charity. Dissemination of the PhD project's results via the Charity's events, publications and website, helps to raise awareness about the importance of cleft lip and palate research.

Much of the research reported in this thesis has been presented at national or international conferences. The genetic study of absent uvula and hypernasality has been published as a peer review article (Seselgyte et al., 2019), with a follow up clinical report currently under revision prior to final acceptance (The Cleft Palate-Craniofacial Journal). Other manuscripts are currently being prepared for publication.

ACKNOWLEDGEMENTS

My recent years have been a profound journey accompanied by outstanding support that I am very grateful for. Without my supervisors and mentors Prof Philip Stanier, Dr Erwin Pauws and Mr Brian Sommerlad this work would have never reached the daylight. My PhD was funded by 'CLEFT - bridging the gap', and I highly appreciate everyone who has been involved in fund raising.

Huge thanks to Prof Gudrun Moore for constant inspiration throughout my PhD. Our conversations enlightened me well beyond the research.

Dale Bryant, Emma Peskett, Miho Ishida, Charalambos Demetriou, Melissa Riachi and Nita Solanky patiently shared their expertise in research and along with others, were my best friends when support, understanding and encouragement were needed.

I am grateful to my mentors and colleagues at Great Ormond Street Hospital Ms Lesley Cochrane, Mr Norman Hay, Mr Loshan Kangesu, Mr Paul Morris, Ms Marie Pinkstone, Dr Debbie Sell, Mr Marc Swan and Mr Guy Thorburn. Also, very sincere thanks to the Clinical Nurse Specialists Julie, Helen, Clair and all others who were not only wonderful to work with but also are 'GOSH family'.

I would like to express appreciation to my mentors Prof Samir Mardini, Mr Nho Tran and Prof Uldis Bite from the Mayo Clinic, Minnesota and also Prof Philip Kuo-Ting Chen, Prof Yu-Ray Chen and Mr Zung-Chung Chen from the Chang Gung Memorial Hospital, Taiwan for shaping my professional path and future research aspirations.

Big thanks to Prof Tomas Poškus, Mr Renaldas Vaičiūnas and Prof Alina Pūrienė, my Lithuanian colleagues who led me at the beginning of my career.

Finally I can't thank enough to my family: my mother, my sister and my niece. They were always standing by my side, behind the scene with love, care and support in all my endeavours.

Apart of all those that I have mentioned above, there were many more who offered their hands and hearts to allow this work to be completed and thank you very much for this.

TO MY MOTHER AND SISTER.

LIST OF CONTENTS

LIST OF FIGURES

LIST OF TABLES

ABBREVIATIONS

Abbreviation	Long form
22q11.2 DS	22q11.2 deletion syndrome
AP	Anteroposterior
Av exp	Average expression; average normalised read count
bp	Base pairs
CAMs	Cell adhesion molecules
cDNA	Complementary DNA
CL	Cleft lip
CLP	Cleft lip and palate
CL/P	Cleft of the lip and/or the palate
CM	Cranial mesoderm
CN	Cranial nerve
CNC	Cranial neural crest
CNV	Copy number variant
COX	Cytochrome oxidase
CP	Cleft palate
CPX	X-linked cleft palate
CS	Carnegie stage

Abbreviation	Long form
DAVID	Database for annotation, visualization and integrated discovery
dsDNA	Double-stranded DNA
ECM	Extracellular matrix
EMSA	Electrophoretic mobility shift assay
EMT	Epithelial to mesenchymal transformation
EtOH	Ethanol
ExAC	The Exome Aggregation Consortium
FACS	Fluorescence activated cell sorting
FC	Fold change
FDR	False discovery rate
FSC	Forward scatter
GO	Gene ontology
GOSH	Great Ormond Street Hospital
GFP	Green fluorescent protein
GSEA	Gene set enrichment analysis
GWAS	Genome-wide association studies
HA	Hyaluronic acid
HCl	Hydrogen chloride

Abbreviation	Long form
HDBR	Human Developmental Biology Resource
H&E	Haematoxylin and eosin
HLH	Helix-loop-helix
ICP	Isolated cleft palate
iDC	Immature dendritic cells
IVVP	Intravelar veloplasty
KCl	Potassium chloride
KOH	Potassium hydroxide
LAR	Leukocyte antigen related
LMS	Lateral meningocele syndrome
LOD	Logarithm of the odds
LVP	Levator veli palatini
MDT	Multidisciplinary team
MEE	Medial edge epithelium
MEHT	Mid Essex Hospitals Trust
MES	Midline epithelial seam
$MgCl_2$	Magnesium chloride
MRFs	Myogenic regulatory factors

Abbreviation	Long form
MRI	Magnetic resonance imaging
MSCs	Muscle stem cells
MyHC	Myosin heavy chain isoform
NaAc	Sodium acetate
NADH-TR	Nicotinamide adenine dinucleotide-tetrazolium reductase
NC	Neural crest
NCBI	National Centre for Biotechnology Information
NS	Non-syndromic
OSMCP	Occult submucous cleft palate
PBS	Phosphate-buffered saline
PCA	Principal component analysis
PCP	Planar cell polarity
PCR	Polymerase chain reaction
pcw	Post conception week
PFA	Paraformaldehyde solution
PMT	Photomultiplier tubes
PP	Palatopharyngeus muscle
R26	*Rosa26*

Abbreviation	**Long form**
RA	Retinoic acid
RIN	RNA integrity number
rRNA	Ribosomal RNA
ROI	Region of interest
RS	Robin sequence
RT-PCR	Reverse transcription PCR
RTqPCR	Real-time quantitative PCR
SMCP	Submucous cleft palate
SNP	Single-nucleotide polymorphism
SNV	Single nucleotide variant
SSC	Side scatter
ssDNA	Single-stranded DNA
StSC	Standard sodium citrate
SDH	Succinate dehydrogenase
TAD	Topologically associated domain
TVP	Tensor veli palatini
UCLP	Unilateral cleft lip and palate
UMI	Unique molecular identifier

Abbreviation	Long form
VF	Velopharyngeal function
VPD	Velopharyngeal dysfunction
VPI	Velopharyngeal insufficiency
VWS	Van der Woude syndrome
WES	Whole exome sequencing
WGS	Whole genome sequencing
WT	Wildtype
w/v	Weight by volume
x g	Relative centrifugal force
YFP	Yellow fluorescent protein
µg	Microgram
µL	Microliter
µm	Micrometer
µM	Micromolar mass

Chapter I: Introduction

I. 1. Introduction

Orofacial clefts may affect the lip (CL), the palate (CP) or both lip and palate (CLP). Collectively they are referred to as clefts of the lip and/or palate (CL/P) which as a group rank amongst the most frequent birth defects seen in humans, occurring in around 1/700 births worldwide (Mossey et al., 2009), Figure I. 1. The prevalence of CL and CLP varies according to geographic origin, racial and ethnic grouping, as well as socioeconomic status and environmental exposure. The highest prevalence rates are reported in Asian and Amerindian populations being 1 in 500, intermediate rates are observed in European derived populations at 1 in 1000 and African populations have the lowest prevalence rates at about 1 in 2500. The prevalence of CP is more stable worldwide, occurring at around 1/1500 births. There is a 2 to 1 male to female ratio for clefts involving the lip and a 1 to 2 male to female ratio for clefts of the palate only (Dixon et al., 2011, Younkin et al., 2014).

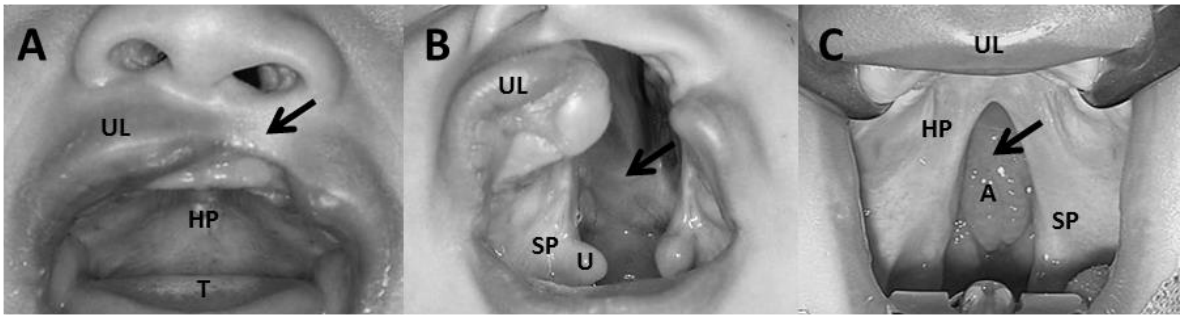

Figure I. 1. Cleft lip and/or palate (CL/P) phenotypes.
A) Left cleft lip (CL); **B)** left cleft lip and palate (CLP); **C)** cleft palate (CP). **UL** - upper lip; **HP** - hard palate; **SP** - soft palate; **U** - uvula; **A** - adenoid tissue; **T** – tongue. Arrows indicate cleft.

Historically, in 1825 Roux described a case of a girl whose speech was nasal and unintelligible. She had a cleft of the posterior portion of the soft palate, a notch in the posterior border of hard palate which was palpable under an intact mucosa. Roux described an operation to repair this soft palate cleft, calling it ‘staphylorraphy’ and was the first to draw attention to submucous cleft palate (SMCP) (Roux, 1825). Roux actually performed his first staphylorraphy in 1819,

which was three years after von Graefe's introduced his comprehensive surgical method for closing clefts in the velum in 1816 (Rogers, 1967). The triad of SMCP was later described by Calnan in 1954 (bony notch, soft palate translucency and bifid uvula) and the term occult submucous cleft palate (OSMCP) was first used in 1975 when Kaplan recognized that muscle malposition can occur in the absence of the triad of overt signs (Kaplan, 1975). Kaplan also believed that isolated cleft of secondary palate, SMCP and OSMCP are variations of the same embryological disorder and that there is, in fact, a continuous spectrum of severity of muscle malformation and actual clefting. However, CP associated with craniosynostosis (Apert syndrome), branchial arch syndromes (Treacher-Collins), mandibular micrognatia (Robin sequence (RS)) and CLP were all considered as embryologically distinct conditions (Burdi and Faist, 1967). There has also been a proposed scoring system, which takes into account individual components of the triad of SMCP. This provides a total score reflecting the spectrum of deformity, although preoperative speech parameters do not correlate with SMCP severity (Sommerlad et al., 2004). However, SMCP and OSMCP terms are more commonly used in clinical practice to represent two extremities rather than describe the complexity of the velum pathology (Rourke et al., 2017).

Orofacial clefts exhibit a wide phenotypic spectrum which may include complete or incomplete bilateral or unilateral CL, with or without CP, as well as isolated cleft secondary palate. Isolated palate defects are considered aetiologically distinct from CL due to the different timing of various fusion events during development and the contribution of different cell lineages to the relevant tissues (Stanier and Moore, 2004, Harville et al., 2005, Mossey et al., 2009). Defects of the secondary palate range from complete overt cleft of the hard and soft palate, to cleft of the soft palate only.

The spectrum of abnormality as well as the functional impact differs between a classical CP and OSMCP (Sommerlad et al., 2004). The consequences of SMCP can be very mild, remaining undiagnosed (Meskin et al., 1964) or identified incidentally, e.g. when the patient requires adenoidectomy. In more severe cases, similar problems to an overt cleft are experienced (Swanson et al., 2017). These can include significant difficulties with feeding including nasal regurgitation,

conductive hearing loss due to otitis media and poor speech (de Blacam et al., 2018). Speech may be characterized by hypernasality with audible nasal emission and the cleft characteristics of passive and nonoral articulation errors (Sell et al., 1999), all of which significantly compromise intelligibility. This is due to the SMCP resulting in significant effects on the anatomy of the velopharynx. The velopharyngeal mechanism is usually described as a muscular valve that extends from the posterior surface of the hard palate to the posterior pharynx and includes the soft palate and lateral and posterior pharyngeal walls. When functioning correctly, the velopharyngeal mechanism is able to achieve a tight seal between the velum and pharyngeal walls, which separates the oral and nasal cavities during speech and swallowing (Perry, 2011, Mardini et al., 2016). Failure of the velopharyngeal sphincter to close appropriately may either be due to an anatomical or a physiological deficit depending on the severity of the palate defect, and may lead to velopharyngeal insufficiency (VPI).

I. 2. Embryology, cleft lip and cleft palate development

The human face is formed by the union, growth and differentiation of five embryonic prominences or processes (Merritt, 2005). The forehead, supraorbital ridges, nose, philtrum and primary palate are derived from the frontonasal process. The zygomatic arches, lateral upper lip, secondary palate are derived from both the left and right maxillary processes, while the lower lip and lower jaw are derived from the left and right mandibular processes. The maxillary and mandibular processes themselves originate from the paired first pharyngeal arches. The pharyngeal arches consist of a core of mesenchymal tissue, which is both cranial mesoderm (CM) and cranial neural crest (CNC) and is lined on the inside by endoderm and covered by ectoderm, the origin of epithelium. The skeletal elements of these developing structures, together with the connective tissues and tendons, originate from the CNC cells, while the associated muscles derive mainly from the CM cells (Grenier et al., 2009).

By the end of the fourth week the nasal placodes invaginate creating the primitive nostrils. During the 6th and 7th weeks, maxillary prominences derived from the first

pharyngeal arches grow medially and will eventually form the upper lip. The lateral nasal prominences form the alar structures of the nose. Failure of fusion of the medial nasal process and maxillary prominence result in CL (Figure I. 2).

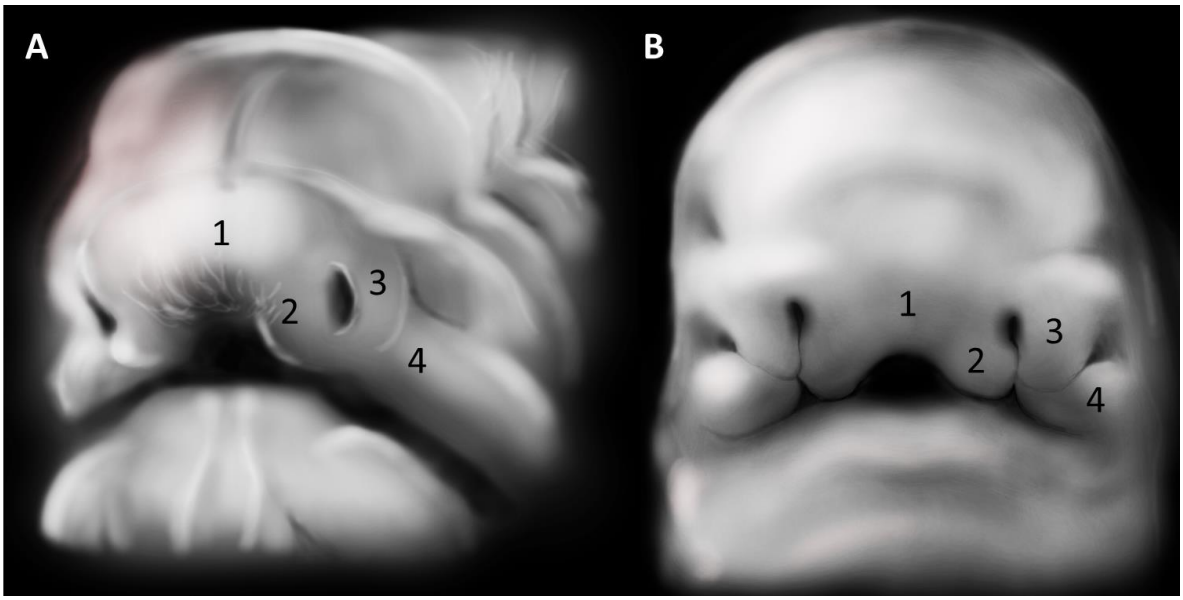

Figure I. 2. Graphical illustration of the human embryonic face.
A) 6th gestation week; **B)** 7th gestation week. **1** - Frontonasal prominence; **2** - medial nasal process; **3** - lateral nasal process; **4** - maxillary process. Adapted from Sulik K. K. and Bream P. R., Jr. *Embryo images: Normal and abnormal mammalian development,* https://syllabus.med.unc.edu/courseware/embryo_images.

The area of the palate posterior to the incisive foramen is called the secondary palate. It forms through the fusion of two paired outgrowths of the maxillary prominences called palatal shelves. These structures appear during the 6th week of development as vertical projections on either side of the tongue. These processes assume a horizontal orientation and fuse during the 7th week, closing the secondary palate. The soft palate is formed by merging of the growth centres in the caudal end of the palatal shelves. Failure of fusion of the palatal shelves results in CP. An example of human embryo palatal shelf fusion is presented in Figure I. 3. The fetal face is formed completely by 9 to 10 weeks gestation (Canick, 1954).

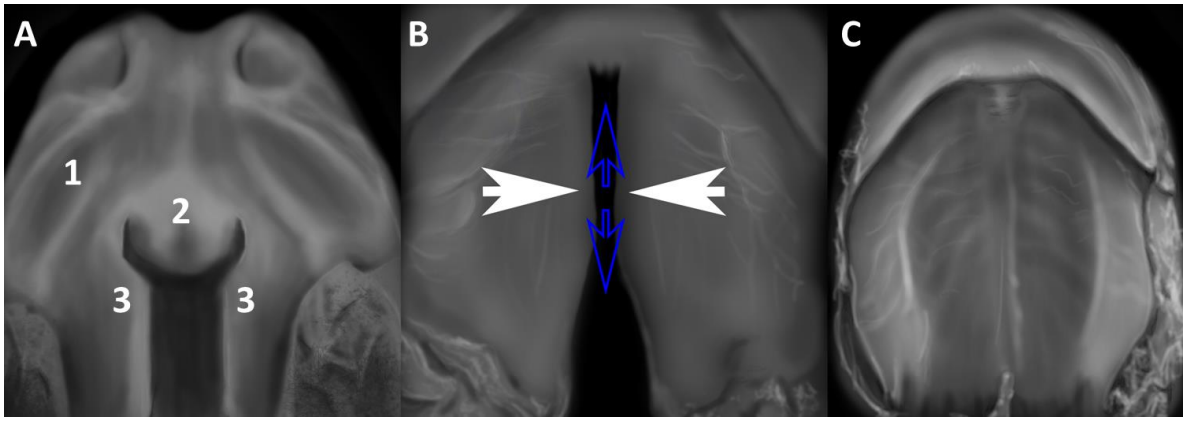

Figure I. 3. Graphical illustration of human embryonic palate.

A) Transverse view of the head at 7th gestation week, showing the maxilla and palatal shelves. **1** - Upper lip; **2** - primary palate; **3** - vertical palatal shelves. **B)** At 9th gestation week, the palatal shelves have elevated to the horizontal position. The white arrows indicate the location of initial contact and fusion; blue arrows the direction of further fusion. **C)** At 10th gestation week, the palatal shelves have completed fusion. Adapted from Sulik K. K. and Bream P. R., Jr. *Embryo images: Normal and abnormal mammalian development,* https://syllabus.med.unc.edu/courseware/embryo_images.

I. 3. The developmental biology underlying craniofacial development and palatogenesis

One of the most important cell types in understanding normal and abnormal craniofacial morphogenesis is the CNC cell. These cells arise from the final stages of the formation of the embryonic neural tube (Bronner and Simoes-Costa, 2016, Birgbauer et al., 1995). Neural crest specificity is the result of an inductive action by non-neural ectoderm adjacent to the developing neural tube. Wnt signalling appears to be essential for this process (Garcia-Castro et al., 2002). This affects the lateral cells of the neural plate as it transforms from a plate of ectoderm into the definitive neural tube. Cells of the induced neural crest separate from the embryonic epithelial layer and subsequently migrate as mesenchymal cells away from the base site (Keynes and Cook, 1995). CNC cells have the capacity to differentiate into a wide variety of anatomical structures throughout the body (Thesleff et al., 1996), including connective, skeletal, dentin, and muscle tissues of the face. CNC cells follow specific migratory pathways into specific regions of the

embryonic head, unlike trunk neural crest cells, which show diffuse migratory pathways (Minoux and Rijli, 2010). These neural crest cells essentially arise from eight segmented regions on either side of the hindbrain (rhombencephalon) called rhombomeres (R1-R8) and subsequently migrate into specific pharyngeal arches (Carstens, 2002) . Crest cells from R1 and R2 migrate into the first pharyngeal arch and play important roles in the formation of Meckel's cartilage and the malleus and incus ear ossicles.

As CM and CNC cells populate the first pharyngeal arch, there are several categories of transcription, growth factors and signalling pathways that play essential roles in completion of normal craniofacial morphogenesis and palatogenesis. This includes an early role in patterning of the pharyngeal arches by Homeobox (HOX) genes which establish CNC identity. Interestingly, the first arch is derived from *HOX* gene negative cells (Couly et al., 1996). CNC-derived mesenchyme cells stream into and proliferate within this structure and are influenced by a series of *Dlx* genes that show nested expression patterns as the lower and upper jaws differentiate (Cobourne and Sharpe, 2003, Depew et al., 2005).

Palatogenesis primarily involves the upper jaw and can be considered as developing as bilateral extensions (palatal shelves) of the maxillary processes, which contact each other and fuse to form the secondary palate. Fusion of these palatal shelves has been linked to a variety of growth factors (e.g. Tgfβ superfamily) and protein activities (Darling et al., 2003, Kaartinen et al., 1997). This has a number of roles, not least eliciting changes to cell proliferation as well as synthesis and remodelling of the extra cellular matrix (D'Angelo et al., 1994, Brown et al., 2002). Bone morphogenetic proteins (BMPs) are members of the Tgfβ superfamily and have been implicated in various aspects of palatogenesis. These include CNC migration, maxillary and nasal process fusion, epithelial-mesenchymal interactions for bone and cartilage formation and tooth development (Greene and Pisano, 2011).

Sonic hedgehog (SHH) is an important ligand effecting Hedgehog signalling and is critical for craniofacial morphogenesis. Shh is expressed in the palate epithelium

yet effectively activates *Bmp2*, *Bmp4*, and *Fgf10* expression in the palatal mesenchyme (Lan and Jiang, 2009). In this reciprocal signalling cycle, activation of FGF signals back to the epithelium to regulate epithelial expression of *Shh* (Rice et al., 2004, Welsh et al., 2007). This plays an important role in differentiation of the medial edge epithelium (MEE).

Complete or partial failures in MEE regulation along the palatal shelves can lead to various forms of palatal clefts. The future midpalatine suture marks the line of fusion between shelves. Fusion also occurs between the shelves and the inferior edge of nasal septum, except in the posterior region where the soft palate and uvula remain free. After the secondary palatal shelves fuse, the mesenchymal cells differentiate into osteogenic cells which form the skeletal elements of the premaxillary, maxillary and palatine parts of the palate.

Formation of the soft palate and uvula takes a different path to that of the regions of the secondary palate which gives rise to the hard palate (Burdi, 1968). The soft palate and uvula develop from two separate tissue bulks located at the most posterior parts of the secondary palatine shelves. Unlike the fusion along the length of the palatal shelves, soft palate primordia are brought together by a selective proliferation of mesenchymal cells located between the two primordia. As a consequence of proliferation and merging, the valley between the two distal shelf primordia disappears, and the contour smooths to form soft palate and uvula (Burdi, 2006).

I. 4. Signalling mechanisms that are known to regulate palatogenesis

Mammalian palatogenesis is a tightly regulated process where protrusions from the medial nasal and maxillary prominences eventually form the embryonic primary and secondary palate. The primary palate contains the philtrum and the upper incisor region of the upper jaw, anterior to the incisive foramen. The secondary palate consists of the rest of the hard and soft palate (Bush and Jiang, 2012). These palatal regions differentiate and fuse, dividing the nasal and oral cavities. The posterior palate creates a complex functional muscular structure, essential for

swallowing, hearing, breathing and speech. Research over many years has found a large number of genes that are required for normal palate development. Recent studies have focused on understanding the role of multiple signalling pathways, most notably those of Shh, Bmp, Fgf, Tgfβ and Wnt signalling (Li et al., 2019a). These have extensive interactions occurring between numerous growth factors and transcription factors that combine together in the regulation of palatal shelf growth, elevation and fusion.

Palatogenesis is initially characterised by the appearance of two rudimentary palatal shelf outgrowths that emanate from the maxillary prominences at E11.0. These continue to extend in a downward direction on each side of the tongue up to E14.0. The growth of the palatal shelves is controlled by epithelial-mesenchymal interactions. Defects in palatal shelf growth are the most common causes of cleft palate in transgenic animal models with well documented examples such as *Fgf10*, *Fgfr2b* (Rice et al., 2004), *Lhx8* (Zhao et al., 1999), *Msx1* (Satokata and Maas, 1994), *Pdgfc* (Ding et al., 2004), *Sim2* (Shamblott et al., 2002) and *Tgfβr2* (Ito et al., 2003) mutant mice. Key components of the signalling network driving palatal shelf growth are Shh, Fgf10 and Bmp. Shh protein expressed throughout the early oral epithelium, is an early signal that initiates palatal shelf growth, although the mechanism instigating the Shh switch is not completely understood (Rice et al., 2006). Both mesenchymal Fgf10 and Bmp4 have been shown to induce the expression of Shh in the palatal oral epithelium where it signals back to the palatal mesenchyme to control the expression of its own receptor *Ptc1* and another growth factor *Bmp2* (Lan and Jiang, 2009). Exogenous application of Shh induces a mitogenic response in palatal explant cultures (Zhang et al., 2002, Rice et al., 2004) and is mediated partly by the *Ccnd1* and *Ccnd2* (Lan and Jiang, 2009). The expression of *Ccnd1* and *Ccnd2* is reduced in the palatal mesenchyme of embryos with mesenchyme specific inactivation of *Smo.* It is suggested that the transcription factors *Foxf1a*, *Foxf2* and *Osr2* genes might be downstream effectors of *Shh* signalling as their expression is also reduced in the palatal mesenchyme (Lan and Jiang, 2009). It has been shown that *Smo* function is not required in the epithelium for palatal shelf growth, although disruption of *Smo* in the palatal mesenchyme affects palatal epithelial cell proliferation (Rice et al., 2004). This indicates that Shh

signalling is necessary to activate a mesenchymal signal that regulates palatal epithelial cell proliferation (Lan and Jiang, 2009).

The interaction between Shh and Bmp signalling pathways is also notable, where loss of *Smo* in palatal mesenchyme leads to *Bmp4* upregulation and *Bmp2* downregulation (Lan and Jiang, 2009). Effect on Bmp2 was confirmed in studies using palatal explant cultures showing that exogenous Shh resulted in induced *Bmp2* expression while exogenous Bmp2 regulated cell proliferation in the palate mesenchyme (Zhang et al., 2002). In the maxillary mesenchyme and the oral epithelium, complete Bmp4 inactivation resulted in early embryonic death, while partial ablation of *Bmp4* function causes a CL with no secondary palate defect (Liu et al., 2005). Bmo antagonist Noggin overexpressed in the palatal mesenchyme caused retarded palatal growth and CP in mice (Xiong et al., 2009). Bmp signalling during palatogenesis occurs through its receptor Bmpr1a. Disruption of *Bmpr1a* in the maxillary mesenchyme and the oral epithelium result in CLP (Liu et al., 2005). Inactivation in the epithelium alone does not cause any palate phenotype, indicating that *Bmpr1a* acts through the palatal mesenchyme (Andl et al., 2004). Interestingly, disruption of *Bmpr1a* in the neural crest has a more explicit effect on the anterior region of palatal shelves (Li et al., 2011) resulting in severe craniofacial anomalies including a hypoplastic mandible and maxilla. Palate defects are shown to be either primary or secondary related to altered maxillary prominences. The specific disruption of *Bmpr1a* function within the palate mesenchyme using the *Osr2-IresCre*; *Bmpr1a*$^{f/f}$ mice resulted in a cleft palate with reduced cell proliferation in the anterior palatal mesenchyme (Baek et al., 2011). *Shh* was down regulated in both the primary palate and anterior secondary palate together with significantly reduced cell proliferation in the developing primary palate suggesting that interaction between Bmp and Shh signalling are required to regulate primary and secondary palate growth (Baek et al., 2011). There is also evidence that loss of Noggin function results in CP due to aberrant apoptosis in the palatal epithelium and reduced cell proliferation of the anterior palatal mesenchyme (He et al., 2010b). This finding also confirms the requirement of Bmp signalling regulation in palate development.

Fgf10 is another crucial mesenchymal signal that is required for palatal shelf growth. Mutant homozygous mice null for either *Fgf10* or *Fgfr2b* present with impaired palatal shelf growth causing CP (Rice et al., 2004). *Fgf10* mRNA expression is predominantly in mesenchyme, while *Fgfr2b* mRNA is detected in the overlying epithelium. Deletion of *Fgfr2b* in mouse epithelial tissue results in a CP indicating its functional importance in the epithelium (Hosokawa et al., 2009). Cell proliferation in epithelial and mesenchymal tissue are reduced in the absence of either *Fgf10* or *Fgfr2b. Shh* expression was found to be down regulated in the epithelium of *Fgf10*$^{-/-}$ and *Fgfr2b*$^{-/-}$ embryos, implying that the decreased palatal mesenchymal cell proliferation observed in these mutants might be due to the reduced epithelial *Shh* expression (Rice et al., 2004). Embryos lacking mesenchymal *Smo* also showed a reduction of *Fgf10* expression in the palatal mesenchyme. This suggested that Shh and Fgf10 function in a positive feedback loop that drives the palatal shelf growth (Lan and Jiang, 2009).

It is thought that Fgf10 is required for maintenance of *Shh* expression in the palatal epithelium (Rice et al., 2004) while Fgf7, a related FGF family member inhibits *Shh* expression in palatal epithelium (Han et al., 2009). *Fgf7* expression is regulated by Dlx5 in the medial side of the palatal mesenchyme and restricts Shh expression to the lateral palatal epithelium during palatal shelf outgrowth (Han et al., 2009). It is important to mention that recent genetic and explant culture studies revealed a novel Shh-Foxf-Fgf18-Shh molecular circuit critical for palatal shelf outgrowth (Xu et al., 2016). *Foxf2*$^{-/-}$ mouse embryos develop CP caused by impairment in growth together with ectopic activation of *Fgf18* expression in specific subdomains of the palatal mesenchyme and loss of *Shh* expression in corresponding domains of palatal epithelium (Xu et al., 2016). Mouse embryos with CNC specific inactivation of *Foxf1* and *Foxf2* demonstrate only rudimentary palatal outgrowths accompanied by ectopic *Fgf18* expression in palatal mesenchyme (Xu et al., 2016). Palatal shelf culture assays show that exogenous Fgf18 protein inhibits *Shh* expression in the palatal epithelium. These studies suggest that Shh signalling coordinates several pathways involving FGF ligands and multiple transcription factors in the regulation of palatal shelf growth.

Osr2 is an intrinsic regulator of palatal mesenchymal cell proliferation and depends on the Pax9 transcription factor (Lan et al., 2004, Zhou et al., 2013). Osr2 and Pax9 both play important roles in a gene regulatory network involving Shh and Fgf10. This is evidenced by the reduced expression in the developing palatal mesenchyme of *Fgf10* in *Osr2*$^{-/-}$ and *Pax9*$^{-/-}$ embryos along with a CP (Zhou et al., 2013, Lan et al., 2004). Failure of palatal shelf elevation and reduction in expression of both *Osr2* and *Pax9* in *Ldb1*$^{-/-}$ embryos (a cofactor for LIM domain containing transcription factors), suggest that molecular control of palatal shelf growth is closely linked to the regulation of palatal shelf elevation (Almaidhan et al., 2014).

Another category of molecules that play important roles in the regulation of palatal shelf growth are extracellular matrix (ECM) proteins. Examples of this are the defects in early growth, elevation and approximation of the palatal shelves leading to a CP caused by simultaneous disruption of the two members of the ADAMTS family metalloproteases genes encoding Adamts9 and Adamts20 (Enomoto et al., 2010). These enzymes bind to the cell surface where they are actively involved in pericellular ECM proteolysis. A major substrate for these proteases is a proteoglycan called versican which has space-filling properties. In *Adamts9*$^{+/-}$; *Adamts20*$^{bt/bt}$ complex mutants, breakdown of versican is reduced. Simultaneous disruption of versican and Adamts20 function results in reduced palatal cell proliferation (Enomoto et al., 2010). Meanwhile, in *Foxf2*$^{-/-}$ mutant mice (Nik et al., 2016) it was noted that failure of palatal shelf elevation was accompanied by significantly reduced expression of several ECM components such as tenascin-C and fibronectin as well as reduced expression of an ECM receptor integrin-β1.

Morphological and molecular diversity along the anteroposterior (AP) axis in the developing palatal shelves is a characteristic feature and several molecular pathways have been described that operate specifically in the anterior and posterior parts, respectively. For example, Meox2 and Tbx22 are transcription factors crucial to the development of the posterior palate (Li and Ding, 2007, Pauws et al., 2009a), while Msx1 and Shox2 are more limited to anterior palatal mesenchyme, where each plays an important role in anterior palatal mesenchyme proliferation (Zhang et al., 2002, Yu et al., 2005). *Meox2*$^{-/-}$ embryos exhibit a post

fusion split of the posterior palate even after successful fusion and removal of the midline epithelial seam (MES), suggesting that the Meox2 transcription factor is required for the maintenance of palatal integrity (Jin and Ding, 2006b). Meanwhile, *Tbx22*, which is expressed from E12.5 to E14.5, plays a more significant role post fusion, where it regulates palatal bone formation at the soft palate and mid palate boundary. *Tbx22*$^{-/-}$ mice develop a SMCP (Pauws et al., 2009). Msx1 is required for maintenance of *Shh* expression in the anterior palatal epithelium through a role in maintaining *Bmp4* expression in the anterior palatal mesenchyme (Zhang et al., 2002). *Shox2* has a limited expression domain restricted to the anterior part of the developing palatal shelves and results in a highly unusual cleft affecting only the anterior palate in null mice (Yu et al., 2005).

A recent study showed that Wnt signalling in developing palatal mesenchyme, detected by using the *BATGAL* transgenic reporter, is restricted to the most anterior region and dependent on Gpr177-mediated Wnt secretion by the neural crest derived mesenchyme (Liu et al., 2015). Wnt5a is expressed in the anterior palatal mesenchyme and together with its receptor Ror2, regulates anterior directed palatal mesenchyme migration and palatal shelf elongation (He et al., 2008). Interesting to note that *Wnt5a*$^{-/-}$ and *Ror2*$^{-/-}$ mice fail in palatal shelf elevation (He et al., 2008) while Ror2 forms co-receptor complexes with Fzd2 which binds to Wnt ligands while activating pathways involved in palatal shelf elevation (Yu et al., 2010). A transposable element derived enhancer has been shown to confer Msx1 mediated activation of *Wnt5a* expression in the anterior palatal mesenchyme (Nishihara et al., 2016). Neural crest specific inactivation of *Ldb1*, causes ectopic expression of *Wnt5a* in the posterior palatal mesenchyme (Almaidhan et al., 2014). This suggests that LIM domain containing transcription factors are important for palatal shelf growth and AP patterning. Cesario et al. (2015) showed that Lhx6 and Lhx8 function partly redundantly to regulate maxillary arch and palatal mesenchyme proliferation through repression of expression of the cell cycle inhibitor gene *Cdkn1c* and of several FOX family transcription factor genes including *Foxc1*, *Foxd1*, *Foxd2*, *Foxp1*, and *Foxp2*. Given the recent discovery of the Shh-Foxf-Fgf18-Shh molecular circuit in early palate development (Xu et al.,

2016), it remains to be determined whether Lhx6/8 also modulates the Shh and FGF signalling network during palatal shelf growth.

Around E14.0 the palatal shelves begin to elevate to the horizontal position above the tongue. The anterior region flips first, followed by the posterior region (Ferguson, 1988). The elevation of the palatal shelves often occurs asynchronously, with one palatal shelf elevating before the other (Walker and Fraser, 1956). Shelf elevation is a rapid process and understanding the exact molecular mechanisms have remained a significant challenge, not least defining the physical forces driving this rapid change in position and shape. Although many different mutant mouse models show defects in shelf elevation, Gritli-Linde, 2007 discuss that there little significant advance in the understanding of the mechanism of shelf elevation. Our current understanding still largely histomorphological (Walker and Fraser, 1956, Coleman, 1965) and from *in vitro* studies (Ferguson, 1978) conducted more than four decades ago. In 1940 Lazzaro described rapid rotation of the shelves and growth based regression of the distal portion of the shelves and outgrowth in the horizontal direction to explain palatal shelf elevation process (Lazzaro, 1940). Coleman, 1965 proposed that the mechanism of palatal shelf elevation is heterogeneous along the AP axis and anterior part of the palatal shelves elevate by a swinging 'flip-up' process, while the posterior and middle parts of the palatal shelves reorient through an 'flow' remodelling mechanism (Coleman, 1965). Walker and Fraser, 1956 described the process of palatal shelf elevation as too quick to be explained by growth changes and proposed instead that the palatal shelves remodel themselves by a bulging of the medial wall and regression of the distal end (Walker and Fraser, 1956).

Meanwhile *in vivo* observation of defective palatogenesis indicates that elevation is impaired either by intrinsic or extrinsic factors such as tongue obstruction or inappropriate fusion with oral epithelium. There are several hypotheses to explain palatal shelf elevation. It has been proposed that an intrinsic elevating force is regulated by extrinsic factors that are associated with development of other orofacial structures. Theories include the involvement of accumulation of ECM prior to and during shelf elevation (Larsson, 1960). Another prevalent hypothesis is that the extracellular hydrophilic glycosaminoglycan hyaluronic acid (HA), accumulates

in specific regions of the palatal shelf mesenchyme through its capacity to bind a large amount of water, generating osmotic pressure to drive medial directed remodelling movement (Brinkley and Morris-Wiman, 1984, Ferguson, 1988). Direct detection of HA using biotin labelled HA binding peptides has confirmed differential distribution of HA in the developing palatal shelf mesenchyme (Lan et al., 2016). Embryos that are deficient in the Golgi-associated protein Golgb1 fail in palatal shelf elevation together with a significant reduction in accumulation of HA in palatal mesenchyme (Lan et al., 2016). However, none of the hypothesis are completely proven (Brinkley and Bookstein, 1986, Ferguson, 1988). It has also been suggested that alignment of type I collagen and mesenchymal cells occurs within the palatal shelf facilitate elevation (Greene and Pratt, 1976, Brinkley and Morris-Wiman, 1984). Another hypothesis has suggested that palatal rugae serve as structural supports that stiffen the palatal shelves or provide the force that drives shelf elevation (Brinkley, 1980, Luke, 1984). However, this was disproved in studies when canonical Wnt signalling was ablated in the palatal epithelium causing a complete loss of rugae formation with no disruption to outgrowth or elevation of the palatal shelves (He et al., 2011). It has been also showed that F-actin stress fibres align with nuclear orientation of palatal mesenchyme cells between the distal tip and the newly forming medial wall protrusion in the middle and posterior regions of the elevating shelf (Chiquet et al., 2016). This finding allows a hypothesis that palatal shelf reorientation in the middle and posterior regions is driven by actin-based cell contraction where palatal shelf stiffness and differences in ECM structure contribute to reshaping of tissue.

A useful model to investigate the palatal shelf elevation process is the *Zfhx1a* (*Zeb1*) mutant mouse strain which has a delayed palatal shelf elevation (Jin et al., 2010). In homozygous mutant embryos palatal shelf elevation is delayed by 24-48 hours, but they do not exhibit apparent deficits in palatal cell proliferation or patterning (Jin et al., 2008). At E14.5, *Zfhx1a*$^{-/-}$palatal shelves remain vertical and express markers of the MEE along the medial side of the palatal epithelium while littermates exhibit complete shelves elevation at this stage. This result support the hypothesis of Walker and Fraser, 1956, that remodelling and horizontal outgrowth from the medial wall of the vertical palatal shelves give rise to the elevated palatal

shelves (Walker and Fraser, 1956). It also indicates that the MEE of post elevation palatal shelves corresponds to the medial rather than the distal region of the pre elevation palatal epithelium. Yu and Ornitz, 2011 presented a histomorphological study which refined timing for palatal shelf remodelling along the AP axis with overall support for the findings of Walker and Fraser, 1956 (Yu and Ornitz, 2011). They reported horizontal outgrowth from the medial wall of the vertically oriented palatal shelves which starts from the mid-posterior region. Palatal shelf reorientation then occurs in a dynamic and regionalized manner (Yu and Ornitz, 2011). In contrast, Walker and Fraser, 1956 described palatal shelf reorientation as wave-like from posterior to anterior (Walker and Fraser, 1956). In *Osr2*$^{-/-}$ homozygous embryos, apart from defects in growth, they also fail at palatal shelf elevation (Lan et al., 2004). It is possible that the reduced medial palatal mesenchyme proliferation affect the horizontal outgrowth or contractile force in the medial area disturbing normal palatal shelf elevation (Chiquet et al., 2016). Specifically, comparison of gene expression patterns in the middle and posterior regions of the palatal shelves before and after elevation suggests that the entire lingual part of the vertical shelves moves close to the midline, while the mesenchyme at the distal tip of the vertical shelves ends up ventrolaterally (Chiquet et al., 2016, Jin et al., 2010). A more sophisticated study by Brock et al. (2016) investigated nucleus-golgi orientation in serial sections of palatal shelves at growth and elevation stages. They demonstrated that mesenchyme cells in the anterior region actively switch direction by about 90° and in the posterior palatal shelf switch their direction by almost 180°. (Brock et al., 2016)

It has been suggested that the Wnt-mediated planar cell polarity (PCP) pathway might play an important role in organising palatal cell orientation and migration (Yu et al., 2010, Yang et al., 2014). The most direct evidence comes from mice deficient in the Wnt-Frizzled receptors Fz1 and Fz2, which resulted in disrupted palatal shelf elevation (Yu et al., 2010). Half of *Fz2*$^{-/-}$ mice and all of *Fz1*$^{-/-}$; *Fz2*$^{-/-}$ mutants develop CP giving high importance to these receptors in palate development. Similarly, mice deficient in *Prickle1*, another PCP component also fail to elevate their palatal shelves (Yang et al., 2014). PCP signalling is mediated by GTPases Rac1, RhoA, and Cdc42 (Sedgwick and D'Souza-Schorey, 2016).

Interestingly, Rac1 protein levels were found to be differentially regulated in palatal mesenchyme just prior to palatal shelf elevation while overexpression of Rac1 in embryonic maxillary explant cultures disrupted palatal shelf elevation (Tang et al., 2015). These studies therefore implicate a potentially critical role for the Wnt/PCP pathway in orienting and directing palatal mesenchyme during palatal shelf elevation.

A putative role for another potentially Wnt-related pathway was identified by conditional disruption of *Gsk3β* in the palatal epithelium. This resulted in a failure of palatal shelf elevation together with defects in epithelial cell proliferation and increased epithelial cell death (He et al., 2010a). Targeted disruption of *Gsk3β* induced CP could be rescued by chemically dependent re-expression of *Gsk3β* between E13.5 and E15.0 (Liu et al., 2007). *Gsk3β* which mediates degradation of β-catenin also plays roles in other signal transduction pathways. In this case, loss of *Gsk3β* did not affect Wnt/β-catenin reporter activity and the epithelial-specific ablation of β-catenin do not result in faulty palatal shelf elevation, strongly suggesting that regulation of palatal shelf elevation mediated by Gsk3β was potentially via a different pathway (He et al., 2011, He et al., 2010a).

A targeted point mutation in *Fgfr2* (*Fgfr2*$^{C342Y/C342Y}$) resulted in CP through delayed elevation and increased mesenchyme proliferation in the lateral half of the palatal shelf (Snyder-Warwick et al., 2010). These embryos also showed reduced glycosaminoglycan accumulation, suggesting a correlation between palatal shelf elevation and glycosaminoglycan levels. It is interesting to note, that the mediolateral cell proliferation was disturbed in the same way as is observed in *Osr2*$^{-/-}$ embryos. This indicates that the regulation of cell proliferation along the mediolateral axis is linked to processes involved in palatal shelf elevation. There is also evidence that disruption of *Spry2* (a negative regulator of the ERK/MAPK signal transduction pathway) results in failure of palatal shelf elevation, as well as in an increased cell proliferation rate in the anterior palatal shelves. The ERK/MAPK signal transduction pathway is commonly utilized downstream of Fgf receptor signalling, and would be expected to be hyperactivated in *Fgfr2*$^{C342Y/C342Y}$ mutant palates. More recently, it was shown that overexpression of Fgfr2 in a conditional overexpression model (*R26R*$^{Fgfr2c;Bact}$) similarly resulted in CP at a high

penetrance although the expected craniosynostosis was not present (Lee et al., 2018). ERK/MAPK signalling was upregulated in both *Fgfr2*$^{C342Y/C342Y}$ and *R26R*$^{Fgfr2c;Bact}$ mice, together with earlier data, implicating this pathway as playing an important role in palatal shelf elevation although not crucial for suture morphogenesis (Matsumura et al., 2011, Lee et al., 2018).

Disturbed palatal shelf elevation and subsequently CP is also known on occasion to be a secondary effect to other deficiencies within the craniofacial complex. An example of this is when CP occurs as a secondary consequence of what is described as RS in humans. RS describes micrognathia and glossoptosis which in turn result in a physical obstruction to palatal shelf elevation (Robin, 1994). CP as a secondary effect of mandibular or tongue developmental abnormalities has been reported in several mutant mouse strains, for example, the physical obstruction by the tongue as a consequence of mandibular defects in *Csp1*, *Prdm16*^{Gt683Lex} mouse (Bjork et al., 2010); mandibular hypoplasia leading to a small oral cavity preventing proper movements of tongue and palatal shelves in *Wnt1Cre*; *Alk2*$^{flox/flox}$ mouse (Dudas et al., 2007); failure of palatal elevation due to physical obstruction by the tongue in *Snai1*$^{-/-}$; *Snai2*$^{-/-}$ (Murray et al., 2007); and defective attachment of the hyoglossus muscle to the hyoid bone and consequently an inability to depress the lateral edges of the tongue in *Hoxa2*$^{-/-}$ mouse (Gendron-Maguire et al., 1993).

The palatal shelves continue to grow horizontally towards each other following elevation, until eventually the MEE cells contact and fuse between E14.5 and E15.0. Fusion then occurs toward both anterior and posterior directions starting from the point of first contact between the 3rd and the 4th rugae (Biddle, 1980, Sakamoto et al., 1989). At this stage the crucial aspect is the programmed regulation of MEE differentiation which occurs independently of palatal shelf contact (Jin et al., 2008). CP can be caused by inappropriate MEE differentiation or adhesion, both in time and space. Disruption of the Notch ligand Jag2 in *Jag2*$^{DSL/\Delta DSL}$ mice result in aberrant adhesion of the palatal shelves to the tongue, leading to CP (Jiang et al., 1998). The periderm cells are flat epithelial surface cells that regulate fusion competence (Fitchett and Hay, 1989). Direct genetic ablation of periderm cells cause aberrant oral epithelial adhesions suggesting that the periderm acts as a non-stick barrier to prevent pathological epithelial adhesion

(Richardson et al., 2014). The periderm cells are maintained by Jag2 which is expressed throughout the oral epithelium (Casey et al., 2006). Less severe palatal shelf-tongue fusion also occurs in *Fgf10*$^{-/-}$ embryos which have reduced *Jag2* expression in palatal epithelium (Alappat et al., 2005). This suggests that Fgf10 signalling acts upstream of Jag2-Notch signalling in order to regulate palatal epithelial differentiation.

Another gene important in the role of the periderm is Irf6, which regulates its differentiation in collaboration with Jag2. Compound *Irf6*$^{R84C/+}$; *Jag2*$^{\Delta DSL/+}$ mice presented with palatal shelf-tongue fusion defects as well as other oral adhesions leading to CP, similar to what was observed in mice that are homozygous for either individual allele (Richardson et al., 2009). Irf6 does not directly regulate *Jag2* expression as the expression of each gene is unaffected in the reciprocal individual mutant. Also R84C point mutation mice embryos (Ingraham et al., 2006) developed undifferentiated epidermis hyperproliferation with inappropriate oral adhesions and CP (Richardson et al., 2006). *Irf6* expression was reduced in the palatal epithelium of *p63*$^{-/-}$ embryos (Thomason et al., 2010). The p63 protein binds to an enhancer upstream of the *Irf6* gene and can activate luciferase reporter expression driven by the *Irf6* enhancer. This indicates that *Irf6* is likely to be a direct target of p63 (Thomason et al., 2010). A CP and a thin, undifferentiated epidermis were also observed in mice deficient for *p63* (Mills et al., 1999, Yang et al., 1999). Compound *p63*$^{+/-}$; *Irf6*$^{R84C/+}$ mice had CP due to failed palatal shelf fusion which was associated with inappropriate maintenance of periderm cells. p63 positively regulates *Jag2* and *Fgfr2* expression in other cell types (Sasaki et al., 2002, Candi et al., 2007). These studies have revealed a genetic network involving p63, Irf6, Fgf10-Fgfr2b and Jag2-Notch signalling in the control of palatal epithelial differentiation.

After the periderm differentiation is complete, MES must then be removed to achieve mesenchymal continuity in the palate. Although lots of studies have attempted to clarify the cell biological mechanisms involved, some aspects of this complex process remain unclear (Gritli-Linde, 2007). There are three theories proposed: apoptosis or non-apoptotic removal mechanisms of MES; epithelial to

mesenchymal transformation (EMT) and migration of the MEE cells along the midline to the nasal and oral epithelia.

To trace the fate of MES cells *in vivo*, epithelially-restricted Cre expressing transgenic lines are coupled with the R26R reporter line (Vaziri Sani et al., 2005). When either *ShhGFPCre* or *K14-Cre* mice are crossed to R26R reporter mice, *lacZ* expression is activated within the epithelium. The subsequent examination of β-galactosidase staining during and following MES elimination allowed the fate of MEE cells to be followed to see whether they contributed to the mesenchyme if they were subject to EMT. Under this experimental design *lacZ* expressing mesenchymal cells were not detected (Vaziri Sani et al., 2005) suggesting that EMT is not a major contributor to the regression of the MES. This finding was independently confirmed by utilizing *K14-Cre; R26R* lineage tracing (Xu et al., 2006). Here a contradiction was noticed where some mesenchymal β-galactosidase activity was present during and immediately after regression of the MES in *K14-Cre; R26R* embryos. The discrepancy might be explained by differences in Cre expression levels and patterns in the palatal epithelium in the different *K14-Cre* transgenic mouse lines used (Jin and Ding, 2006a).

To determine MES cells migration, palatal shelves derived from WT embryos were recombined in culture with palatal shelves expressing *lacZ* in all cells (Jin and Ding, 2006a). *LacZ* expressing epithelial cells migrated onto the WT palatal shelves suggesting that MES migration occurs during palatal fusion stage.

Several studies indicate that MES cells are TUNEL and activated Caspase-3 (apoptotic marker) positive during palatal shelf fusion showing the importance of apoptosis during MES dissolution (Cecconi et al., 1998, Martinez-Alvarez et al., 2004, Cuervo and Covarrubias, 2004, Vaziri Sani et al., 2005). *Apaf1* is a gene that encodes a crucial component of Caspase-3 mediated apoptosis and can be used as another method to investigate MES cell dissolution through a genetic approach. *Apaf1*$^{-/-}$ embryos have normal palate fusion and MES disintegration (Jin and Ding, 2006a). This result contrasts with the earlier one, showing that palatal shelves made contact but failed to fuse in *Apaf1*$^{-/-}$ embryos (Cecconi et al., 1998).

It has also been proposed that MES dissolution differs along the AP axis (Charoenchaikorn et al., 2009). MES cells at the midline of the fusing secondary palatal shelves are positive for TUNEL staining while only a few are detected between the fusing primary and secondary palate. In unpaired palatal shelf culture used to monitor MES cell behaviour in the opposite shelf, one palatal shelf is removed before midline contact. Here, the MEE disappeared without contact or adhesion from the middle and posterior regions of the palatal shelf although not from the region anterior to the second ruga (Charoenchaikorn et al., 2009). These contradictory studies still require further experimentation, especially to understand the mechanism for fusion of the anterior secondary and between the primary and secondary palate.

Tgfβ signalling is well known as an important pathway required for palatal shelves fusion (Iwata et al., 2014). Embryos lacking *Tgfβ3* develop a complete CP even though the palatal shelves make appropriate contact in the midline (Proetzel et al., 1995, Kaartinen et al., 1995). *Tgfb3*$^{-/-}$ palatal shelves in culture fail to eliminate MES suggesting that *Tgfb3* is significant in MES abolition (Kaartinen et al., 1995). *Tgfb1* expression is lower compared to *Tgfb3*, but both are expressed in the MEE prior to palatal shelf elevation, and their expression is maintained in the MES during palatal fusion (Yang and Kaartinen, 2007). *Tgfb1* and *Tgfb3* have partially overlapping functions. A knock-in of the *Tgfb1* cDNA into the *Tgfb3* locus partially rescues palate fusion in the *Tgfb3*$^{-/-}$ mice (Yang and Kaartinen, 2007). Epithelial ablation of Tgfβ receptors *Tgfbr1* or *Tgfbr2* led to CP phenotypes. Adhesion of palatal shelves was observed initially but the MES failed to dissolve, causing the palatal shelves to fall apart (Dudas et al., 2006, Xu et al., 2006). In these studies reduction in apoptosis throughout MES was observed confirming that Tgfβ3 signalling regulates programmed cell death in the palatal epithelium (Xu et al., 2006, Dudas et al., 2006).

Tgfβ1 and Tgfβ3 are expressed in the MEE and Tgfβ2 is expressed in the mesenchyme beneath the MEE (Fitzpatrick et al., 1990, Pelton et al., 1990). The Tgfβ signalling pathway is initiated by heterotetramerization of type I receptor and type II receptor dimers. Activated type I receptors phosphorylate Smad2, which

then cooperates with Smad4 to regulate transcription. MES degeneration fails in palatal explant cultures with knockdown of Smad2 function. It has also been shown that conditional inactivation of Smad4 in oral epithelium results in much milder phenotypes than those seen with the corresponding receptor mutants, *Bmpr1a* and *Tgfbr2*. The transgenic overexpression of Smad2 in the palatal epithelium partially rescues palate fusion in *Tgfb3*$^{-/-}$ mice (Shiomi et al., 2006, Cui et al., 2005). Disrupting Smad4 in epithelium of *K14-Cre; Smad4*$^{f/f}$ mice do not cause CP, suggesting that Smad signalling is not the only pathway responsible for MES degeneration (Shiomi et al., 2006, Xu et al., 2008). Tgfβ signalling also activates other intracellular signal transduction pathways, including p38 MAPK (Mapk14) which is elevated in the epithelium of fusing palatal shelves (Xu et al., 2008). Treating *K14-Cre; Smad4*$^{f/f}$ palatal shelves in culture with an inhibitor of p38 MAPK, blocks Tgfβ-dependent expression of the *Cdkn1a* gene in the MES. *Cdkn1a* expression is known to correlate with reduced apoptosis and failed MES degeneration (Xu et al., 2008). The p38 MAPK is activated by TGFβ and can function as a complementary effector to mediate Smad4 independent TGFβ signalling during palate development (Xu et al., 2008).

β-catenin has been reported as a regulator of MES disappearance through *Tgfb3* expression in the MEE. Epithelial disruption of *Ctnnb1* results in loss of *Tgfb3* expression in the MEE. A CP occurred potentially due to reduced apoptotic MES cells impacting upon shelf fusion (He et al., 2011). However, β-catenin functions in the Wnt signalling pathway or as a component of adherent junctions, as previously described (He et al., 2011).

Transcription factors of the Snail family have also been shown to regulate palate fusion. *Snai1*$^{+/-}$; *Snai2*$^{+/-}$ compound mutants develop CP due to palatal shelves failed fusion associated with a reduction in MES apoptosis (Murray et al., 2007). It is thought that these transcription factors regulate palatal fusion downstream or in parallel to the Tgfβ3 pathway, although *Tgfβ3* expression is not itself affected in these mutants.

In summary, a great deal of progress has been made in understanding the role of the many growth factors, transcription factors and associated signalling pathways

in palatogenesis. This spans the initial appearance of rudimentary palatal shelves, their growth, elevation and fusion, with cell proliferation and patency of the MEE being critical events. The analysis of mutant mouse embryos and associated technologies has provided important tools to interrogate the underlying events. There is still more work required to better connect the basic mechanisms and molecular events that occur during normal palate development. This will help in revealing the complex aetiology of CP.

I. 5. Genetics of clefting

Although more than 300 malformation syndromes which can include orofacial clefts have been described, non-syndromic (NS) forms account for about 70% cases of all CL/P and about 50% of cases with CP only (Leslie and Marazita, 2013, Seto-Salvia and Stanier, 2014). Research suggests multiple layers of heterogeneity underlie the aetiology for NS clefts. It is thought that both genes and environmental factors interacting with one another or acting independently are likely to be responsible (Stanier and Moore, 2004). As a consequence of the complex genetic and environmental contributions, modest recurrence rates, along with orofacial clefts arising early in embryological development, it has proven difficult to identify specific causal factors. Nevertheless, using a combination of epidemiology, careful phenotyping, genome-wide association studies (GWAS) and analysing animal models, several distinct risk factors have been confirmed for NS CL/P (Dixon et al., 2011). These include a variety of signalling molecules which play important roles in facial epithelial differentiation and palate shelves remodelling during development such as ECM, MEE molecules, growth and transcription factors (Shh, Bmp, Fgf, Tgfα, Dlx, Hox, Gli) and members of the Tgfβ superfamily (Nakajima et al., 2018).

The study of syndromic clefts has been a rich source of identifying genes involved in lip and palate development, including NS CL/P (Stanier and Moore, 2004). These include identification of the *TBX22* gene, a member of the T-box containing transcription factor family, in X-linked CP and ankyloglossia (CPX; OMIM 303400) (Braybrook et al., 2001). T-box genes are known to play important role in early

development (Stanier and Moore, 2004) and, in addition to *TBX22*, several other T-box genes have been implicated in human syndromes that occasionally involve CLP (e.g. *TBX1, TBX3, TBX5* and *TBX10* (Naiche et al., 2005)). Meanwhile, Van der Woude syndrome (VWS; OMIM 119300) is one of the best-known models for NS CL/P, and is most commonly caused by mutations in *IRF6* (Khandelwal et al., 2016). VWS patients can have CL or CP, but are characterized by the presence of lower lip pits as an additional feature. Other well known syndromes are caused by mutation in *TP63*, which is responsible for autosomal dominant ectrodactyly, ectodermal dysplasia and CL/P (EEC; OMIM 604292) (Celli et al., 1999), while *MSX1* mutations are found in patients with clefting and hypodontia (OMIM 106600) (Van den Boogaard et al., 2000, Mitsui et al., 2016). A variety of other genes causing syndromic CL/P are reviewed by Seto-Salvia and Stanier (2014), Leslie and Marazita (2013), Table I. 1. Clear cut causal mutations are more rarely found in patients with NS CL/P but large scale GWAS have implicated a number of potentially important loci, Table I. 2, (Ludwig et al., 2012, Younkin et al., 2014, Leslie et al., 2016, Mangold et al., 2016), which include 8q24 and *IRF6*. The increasing use of whole exome sequencing (WES) in multiplex families has also expanded the identification of genes with a role in NS CL/P: *VAX1, MSX1*, *FOXE1*, *MYH9*, *FGFR2, ARHGAP29* and others (Li et al., 2017b, Liang et al., 2016, Leslie et al., 2017, Wang et al., 2018, Jin et al., 2018, Paul et al., 2017). A second gene for VWS has been described, where mutations in *GRHL3* were found in *IRF6* mutation negative patients (Peyrard-Janvid et al., 2014). Interestingly, further studies utilizing a combination of GWAS, WES and Sanger sequencing identified further mutations, including a common variant predisposing to clefts (Ludwig et al., 2012, Leslie et al., 2016). These studies concluded that mutations in *GRHL3* are more likely to cause CP than CL and are more likely to be found in patients without lip pits. This provides an interesting example of cross-over between syndromic and NS clefting.

Table I. 1. Selected CL/P syndromes with an identified genetic cause.

Syndrome	Cleft type	Gene	Other anomalies	Reference
Ankyloblepharon-Ectodermal Defects-Clefting (AEC) syndrome, Ectrodactyly, ectodermal dysplasia, and cleft lip/palate syndrome 3 (EEC3)	CL/P	*TP63*	AEC: Skin erosions; changes in skin colour; brittle, sparse, or missing hair; misshapen or absent fingernails and toenails; malformed or missing teeth. EEC3: Split-hand/foot malformation; ectodermal dysplasia	(Rinne et al., 2007, Maas et al., 1996, Celli et al., 1999)
Apert	CP	*FGFR2*	Craniosynostosis; syndactyly; hypertelorism	(Riley et al., 2007)
Bamforth-Lazarus	CP	*FOXE1*	Thyroid dysgenesis (in most cases athyreosis); spiky hair; +/- choanal atresia; bifid epiglottis.	(Baris et al., 2006)
Bartsocas-Papas	CL/P	*RIPK4*	Neonatal or intrauterine death in most cases; severe popliteal webbing; oligosyndactyly; genital abnormalities; typical face with craniofacial anomalies.	(Kalay et al., 2012, Mitchell et al., 2012)
Branchio-oculo-facial	CL/P	*TFAP2A*	Skin abnormalities on the neck; deformities of the ears and eyes; slow growth; mental retardation; premature greying of hair.	(Milunsky et al., 2008)
Robin sequence with or without campomelic dysplasia	CP	*SOX9*	RS: micrognathia; glossoptosis. CD: short legs; dislocated hips; underdeveloped shoulder blades; 11 pairs of ribs; bone abnormalities in the neck; clubfeet.	(Benko et al., 2009, Foster et al., 1994)
CHARGE	CP	*CHD7*	Coloboma; choanal atresia; brain and spinal cord problems; malformed ears (hearing loss); short stature.	(Stromland et al., 2005)
CLP ectodermal dysplasia 1 (CLPED1)	CL/P	*PVRL1*	Abnormal nails; abnormal or missing teeth; decreased skin pigmentation); low nasal bridge; thin, sparse hair; learning disabilities.	(Suzuki et al., 2000)

Table I. 1. (continued).

Cornelia de Lange	CP	*NIPBL*	Slow growth before and after birth leading to short stature; intellectual disability; abnormalities of bones in the arms, hands, and fingers; distinctive facial features.	(Krantz et al., 2004, Tonkin et al., 2004)
Crouzon	CP	*FGFR2*	Craniosynostosis; wide set, bulging eyes; vision problems; strabismus.	(Riley et al., 2007)
22q11.2DS, s. DiGeorge	CP	*TBX1*	Developmental and learning delay; hearing and vision problems; short stature; frequent infections; bone, spine, muscle problems; unusual facial features, including an underdeveloped chin, low-set ears, and wide set eyes.	(Yagi et al., 2003)
Ectrodactyly-ectodermal dysplasia-clefting	CL/P	*TP63*	Abnormalities of structures derived from the embryonic ectoderm and affects epidermis, mammary, pituitary and sweat glands, enamel, nail, lens and ears.	(Rinne et al., 2007)
Familial gastric cancer and CLP	CL/P	*CDH1*	High risk for diffuse gastric and lobular breast cancer.	(Frebourg et al., 2006)
Gorlin	CL/P	*PTCH1*	Pits in the skin of the palms of the hands and soles of the feet; macrocephaly with a prominent forehead; skeletal abnormalities involving the spine, ribs, skull.	(Ming et al., 2002)
Culler-Jones	CL/P	*GLI2*	Pituitary anomalies resulting in hypopituitarism; polydactyly; unusual facial features.	(Roessler et al., 2003)
Holoprosencephaly	CL/P	*SHH, SIX3, TGIF*	Failure of prosencephalon (the forebrain of the embryo) to develop into two hemispheres.	(Orioli et al., 2002, Wallis et al., 1999, Gripp et al., 2000)

Table I. 1. (continued).

***SATB2*-associated syndrome; Pierre Robin sequence with or without ankyloglossia; Intellectual disability**	CP	*SATB2*	Mild to severe intellectual disability; developmental delay.	(Rainger et al., 2014, Leoyklang et al., 2007)
Kabuki	CL/P	*MLL2, KDM6A*	Distinctive facial appearance, which includes long palpebral fissures; everted lower eyelids; prominent eyelashes; arched eyebrows; a broad nose with a flattened or depressed tip; large, misshaped ears.	(Ng et al., 2010a, Lederer et al., 2012)
Kallmann	CL/P	*FGFR1*	Delayed or absent puberty; an impaired sense of smell.	(Dode et al., 2003, Bick et al., 1992)
Lethal and Escobar multiple pterygium	CP	*CHRNG*	Short stature; spine defects; joint contractures; webbing of the neck, armpit, elbow, knee, between the legs, fingers and toes.	(Morgan et al., 2006)
Loeys-Dietz	CP	*TGFBR1, TGFBR2*	Hypertelorism; instability or malformation of the spine in the neck.	(Loeys et al., 2005)
Miller	CP	*DHODH*	Underdeveloped cheekbones; micrognathia; small, protruding ears; drooping of the lower eyelids.	(Ng et al., 2010b)
Oculofaciocardiodental	CP	*BCOR*	Abnormally small deep set eyes; cataracts; long narrow face; a broad nasal tip that is divided by a cleft; heart defects; teeth with very large roots.	(Ng et al., 2004)
Opitz G/BBB	CL/P	*MID1*	Midline defects including hypertelorism; hypospadias, laryngotracheal clefts; imperforate anus.	(Quaderi et al., 1997)
Oro-facial-digital	CL/P	*GLI3*	Problems with development of the oral cavity; facial features; digits.	(Johnston et al., 2010)

Table I. 1. (continued).

Oro-facial-digital type 1	CL/P	*OFD1*	Affected development of the oral cavity (the mouth and teeth); facial features; fingers and toes; polycystic kidney disease.	(Ferrante et al., 2001)
Otopalatodigital types 1 and 2	CP	*FLNA*	Generalized skeletal dysplasia; mild mental retardation; hearing loss; typical facial anomalies.	(Hidalgo-Bravo et al., 2005)
Popliteal pterygium; Van der Woude	CL/P	*IRF6*	PP: lip pits; skin and genital anomalies. VW: lip pits.	(Kondo et al., 2002)
Saethre-Chotzen	CP	*TWIST1*	Craniofacial and limb anomalies.	(Howard et al., 1997)
Stickler type 1	CP	*COL2A1*	Distinctive facial features; eye abnormalities; hearing loss; joint problems. Myopia; retinal detachment.	(Bonaventure et al., 1992, Zlotogora et al., 1992)
Stickler type 2	CP	*COL11A1, COL11A2*	Distinctive facial features; eye abnormalities; hearing loss; joint problems. Myopia; retinal detachment	(Zlotogora et al., 1992, Annunen et al., 1999)
Tetra-amelia with CLP	CL/P	*WNT3*	Complete absence of all four limbs and other anomalies.	(Niemann et al., 2004)
Tooth agenesis with or without cleft, Witkop syndrome	CL/P	*MSX1*	WS: Nail dysplasia and several congenitally missing teeth.	(Van den Boogaard et al., 2000, Jezewski et al., 2003, Jumlongras et al., 2001)
Treacher Collins	CP	*TCOF1*	Craniofacial development disorder; conductive hearing loss.	(Dixon, 1996)
X-linked cleft palate and ankyloglossia	CP	*TBX22*	Ankyloglossia; problems with feeding; speech; hearing; dentition; psychological development.	(Braybrook et al., 2001)
Siderius X-linked mental retardation	CL/P	*PHF8*	Mental retardation.	(Laumonnier et al., 2005)

Table I. 2. Selected non-syndromic CL and CLP loci implicated by GWAS.

Locus	Gene	Population	Reference
1p22.1	*ABCA4*	European and Asian	(Beaty et al., 2010)
1p22.1-p21.3	*ARHGAP29*	European and Asian	(Beaty et al., 2010, Ludwig et al., 2012)
1p36.13	*PAX7*	European and Asian	(Ludwig et al., 2012)
1q32.3-q41	*IRF6*	Norway, Denmark, EUROCRA, Philippines	(Rahimov et al., 2008)
2p21	*THADA*	European and Asian	(Ludwig et al., 2012)
3p11.1	*EPHA3*	Chinese	(Pan et al., 2013)
8q21.3	*DCAF4L2*	European and Asian	(Ludwig et al., 2012)
8q24	*MYC*	European	(Birnbaum et al., 2009, Grant et al., 2009)
9q22.2	*GADD45G*	European and Asian	(Beaty et al., 2013)
9q22.33	*FOXE1*	European and Asian	(Beaty et al., 2013)
10q25	*VAX1*	European	(Mangold et al., 2010)
13q31.1	*SPRY2*	European and Asian	(Beaty et al., 2013)
15q22.2	*TMP1*	European and Asian	(Beaty et al., 2013)
17p13.1	*NTN1*	European and Asian	(Ludwig et al., 2012)
17q22	*NOG*	European	(Mangold et al., 2010)
17q25.3	*RBFOX3*	European and Asian	(Beaty et al., 2013)
20q12	*MAFB*	European and Asian	(Beaty et al., 2010)

Despite intensive research worldwide, much of the genetic basis of NS CL/P remains unknown. Further research carried out on large families, especially with rare forms of clefts or rare cleft syndromes, may assist in the difficult process of identify novel genes and pathways required for normal palatogenesis.

I. 6. Cleft palate classification

At a basic level, orofacial clefts fundamentally include three anatomical defects: CL, CLP and CP (Sandy, 2019), Figure I. 1. Although there is some overlap through embryological development and similarities in epidemiological evidence, there are distinct differences in their aetiology and pathogenesis. Most of our understanding of the embryonic processes required for lip and palate development has come from the study of animal models. Primarily this has used either chick or mouse models. It is interesting to note though that the chick has a natural CP (Lőw et al., 2016), and although many mouse mutants have a CP, they more rarely have a CL (Juriloff and Harris, 2008). This differs to most human genetic studies which tend to focus on defects of the lip, since this is more commonly affected than the palate.

In contrast this thesis deals predominantly with CP and with a special interest in rare forms. Orofacial clefts, including CP also differ in severity and clinical presentation (Sommerlad et al., 2004). Palate pathology can be considered as a spectrum of complete CP to more minor anatomical variations such as bifid or absent uvula. The range of severity seen in the palate phenotype can make classification difficult and is illustrated by the scheme used by the North Thames Cleft Team (Figure I. 4). There has always been a great need to create a universal, but simple and practical classification system. The evolution of ideas for suitable schemes has been described by Davis and Ritchie (1922), Brophy (1923), Veau (1931), Fogh-Andersen (1943), Kernahan and Stark (1958), Harkins et al. (1962), Broadbent et al. (1968), Spina (1973), and others (Allori et al., 2015).

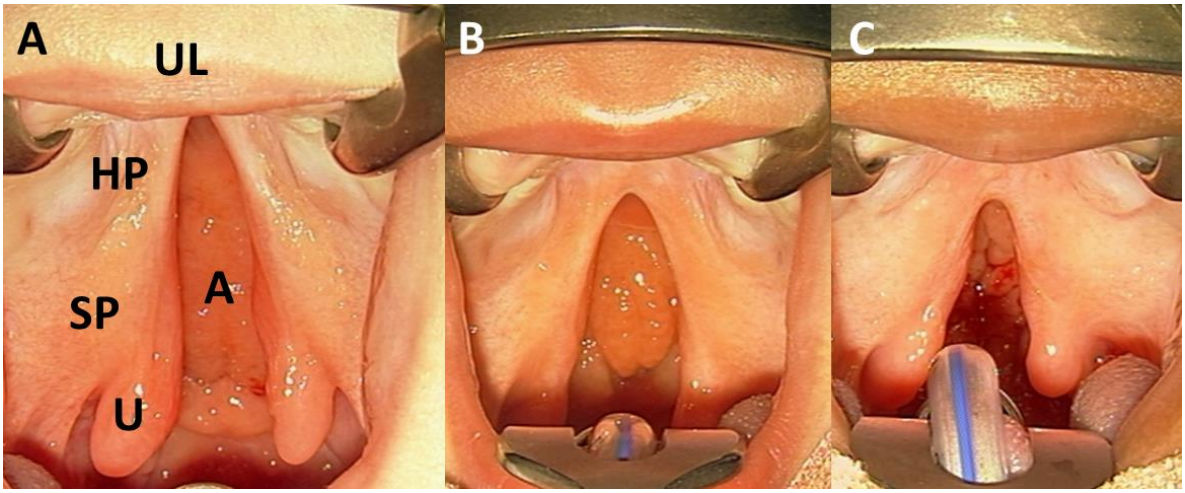

Figure I. 4. Cleft palate classification, currently used by the North Thames Cleft Team at Great Ormond Street Hospital and St Andrew's Centre.

In this scheme, the hard and soft palate are divided into 3 parts each and the cleft is then graded depending on the severity or involvement of one or both palate regions. **A)** A complete cleft of the hard and soft palate**:** 3/3 HP 3/3 SP; **B)** partial cleft of the hard palate and complete cleft of the soft palate: 1/3 HP 3/3 SP; **C)** Soft palate cleft only: 0/3 HP 3/3 SP. **UL** - upper lip; **HP** - hard palate; **SP** - soft palate; **U** - uvula; **A** - adenoid tissue.

I. 7. Surgical palate repair

The first surgical repair of CP was performed by the French dentist Le Monnier in 1764, who used three stages. The process involved approximation of the cleft edges with sutures, followed by cauterizing and then realigning the edges (Tempest, 1981). Since then the surgical management of CP became more complex and an elaborate art. There are a variety of techniques used worldwide that have been developed and used mainly because of surgeon preference (Sadove et al., 2004). The challenge of modern palatoplasty is not only to effectively close the cleft but must also achieve an optimal speech outcome, without compromising maxillofacial growth (Leow and Lo, 2008).

One of the most accepted and widely applied techniques for CP repair in the UK and internationally was originally described by Mr Brian Sommerlad (Sommerlad, 2006, Andrades et al., 2008, Doucet et al., 2013, Luyten et al., 2013) and uses the operating microscope with radical muscle retropositioning. The technique involves

mobilization of mucoperiosteal flaps of the hard palate. Then, using an operating microscope, dissection of the soft palate muscles from their abnormal anterior insertions so that they can be realigned transversely at the posterior limit of the soft palate. Special attention is required for dissection and mobilization of the levator veli palatini (LVP) muscle. The nasal mucosa is closed before the muscle dissection. Finally, the oral layer is closed, making relaxing incisions laterally where necessary.

Leonard T. Furlow Jr. introduced the double opposing Z-palatoplasty in 1978 and most of his work was published in 1986 (Furlow, 1986). The technique involves dissection of two mirror image Z-plasty flaps, with one on the oral side and one on the nasal side, with their central limbs along the cleft. The anteriorly based flap of each Z-plasty is mucosal and the posteriorly based flap is myomucosal (involving LVP muscle). Transpositioning of Z-plasty flaps rotate the levator sling across the cleft. The arch of vault of the hard palate allows the CP closure without releasing incisions. Furlow Z-palatoplasty is not considered anatomical and does not address the uvula muscle structure, but nevertheless, overall reported speech and growth results are comparable with other widely used techniques (Mardini et al., 2016).

Possibly one of the oldest surgical techniques that was adopted in clinical practice for quite long time is the von Langenbeck palatoplasty. It was originally introduced in 1859. This technique closes an incomplete cleft of the hard and soft palate without lengthening the palate by medially mobilizing bipedicled mucoperiosteal flaps (Strong and Buckmiller, 2001). A modification of the von Langenbeck technique, which is designed to increase the palatal length, is called Veau-Wardill-Kilner or V-Y pushback palatoplasty. The flap design is similar to the von Langenbeck palatoplasty with V to Y incision and closure on the hard palate. This approach requires extensive dissection (Leow and Lo, 2008) and appears to impair maxillary growth.

Although the majority of techniques described can still be recommended for use in routine cleft patient management, other controversies exist, particularly regarding the optimal timing of surgery, and the specific technique in relation to speech outcome and maxillofacial growth. Early postoperative surgical complications may

involve bleeding, wound dehiscence/healing problems and airway obstruction, while late postoperative complications can be palatal fistula and obstructive sleep apnoea (Perkins et al., 2005). Even more challenges arise when dealing with rare forms of clefts. SMCP and OSMCP occur in 0.02% to 0.08% of children and diagnosis is often delayed until VPI becomes apparent (Sullivan et al., 2011, Kaplan, 1975). Up to 80% of individuals with unrepaired SMCP experience speech difficulties secondary to VPI (Boyce et al., 2018). Attempted repair of the associated palatal defects has often given poor results and controversies still exist regarding the best choice for the management of these patients (Park et al., 2000). An example of SMCP repair with radical muscle retropositioning technique is presented in Figure I. 5. Proper comparison between studies are limited due to the use of different operative techniques, procedure timing, diverse patient populations with varying physiologic and anatomic profiles, along with inconsistent and subjective outcome measures. Further research is therefore required regarding best practice when aiming to modify or correct specific features of clefts as well as for the development and testing of novel therapies to improve cleft patient management while reducing complication risks (Crockett and Goudy, 2014).

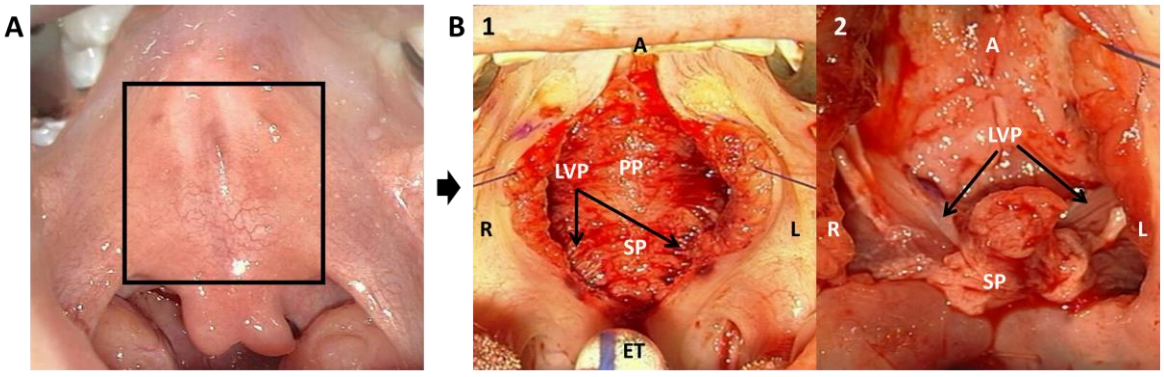

Figure I. 5. Submucous cleft palate repair.

A) The representation of area in picture B. **B)** Intraoperative view of SMCP repair. **1.** LVP exposure under mucosa, **2.** LVP retropositioning. **A** – Anterior; **R** – right; **L** – left; **SP** – soft palate; **LVP** – levator veli palatini; **PP** - palatopharyngeus; **ET** – endotracheal tube.

I. 8. Multidisciplinary team approach in cleft patient management

In 1998 the Clinical Standards Advisory Group (Sandy et al., 1998) reported that outcomes for children born with a CLP in the United Kingdom would be improved if care was provided by a multidisciplinary team (MDT). Within the MDT, coordinated care can be provided from a wide range of clinical and nonclinical professionals including ear, nose and throat, plastic, maxillofacial surgeons, orthodontists, paediatric, restorative dentists, audiologists, cleft nurse specialists, clinical geneticists, paediatricians, speech and language therapists, clinical psychologists, dieticians, medical photographers and other support staff (Sandy et al., 2001, Chuo et al., 2008, Scott et al., 2015).

CL/P has a very serious impact on quality of life, often requiring repeated surgical intervention at intervals throughout childhood until late teens. Frequently dental and orthodontic treatment, speech therapy and help for hearing may be required as well as psychological support and genetic counselling (Stanier and Moore, 2004). Furthermore, over the long-term, it has been reported that individuals born with clefts may face an increased risk of mental health problems, cancer and overall mortality, along with lifestyle effects including alteration to their child bearing patterns (Dixon et al., 2011).

I. 9. Aims

I. Investigation of SMCP soft palate muscle integrity:

- To identify the surgical management pathway in patients with SMCP, operated on at the North Thames Cleft Service at Great Ormond Street Hospital (GOSH) and St Andrew's Centre, Broomfield Hospital, Mid Essex Hospitals Trust (MEHT), over a 23 year period.
- To investigate the histological structure of the palatopharyngeus (PP) and LVP muscles in patients with SMCP and isolated cleft palate (ICP) in comparison to UCLP and controls at the time of surgery.

II. To investigate the transcriptional role of TBX22 in mouse palate development:

- The primary defect in *Tbx22* null mice is SMCP therefore it was intended to perform RNA-Seq to compare flow sorted palatal shelf tissue specific cells between wildtype (WT) and *Tbx22*$^{null/Y}$ in order to identifying potential downstream transcriptional targets in both CM and CNC derived tissue that underlie SMCP development.

III. To investigate the genetic cause of absent uvula and hypernasality in an Egyptian family:

- To describe the clinical presentation, surgical management and outcome in a patient presenting with a rare palate phenotype causing velopharyngeal dysfunction (VPD).
- Pursue gene discovery in a large multiplex family with an unusual autosomal dominant hypernasality and absent uvula phenotype.
  - To perform cytogenetic analysis, single-nucleotide polymorphism (SNP) genotyping, linkage analysis and WES to identify the likely candidate gene and causal variant.
  - Screen a cohort of patients with palate defects (NS CP and SMCP) to determine the frequency of mutations in the best candidate gene *FOXF2*,

to both review the phenotypic spectrum and to determine if SMCP was a plausible alternative phenotype for similar mutations.

- Perform functional analysis of the likely causal variants in FOXF2.
- Confirm appropriate developmental expression analysis in human embryos for *FOXF2*.

Chapter II: Materials and methods

II. 1. Collection of palate muscle biopsies

Both cleft patients and patients undergoing a tonsillectomy operation were recruited to the study with approval of the National Research Ethics Service (NRES Committee East of England - Cambridge South) REC reference 11/EE/0032. The cleft patient samples were collected during their palate repair, while the control group samples were collected during their tonsillectomy operation, all under general anaesthesia. Indication for tonsillectomy was either obstructive sleep apnoea or recurrent chronic tonsillitis. Otherwise these children were considered healthy. In the control group PP muscle descending fibres were sampled since only these (but not LVP) were exposed during the tonsillectomy operation. The PP sample from this site was considered to be a reasonable proxy for comparison to the PP muscle in the palate. Biopsy sites are indicated in Figure II. 1. Each of the collected muscle biopsies were transported to the Histopathology Department, GOSH, where they were snap frozen, sectioned and stained by Histopathology Department staff under the supervision of Prof Thomas Jacques. Slides were then returned to perform digital scanning and analysis.

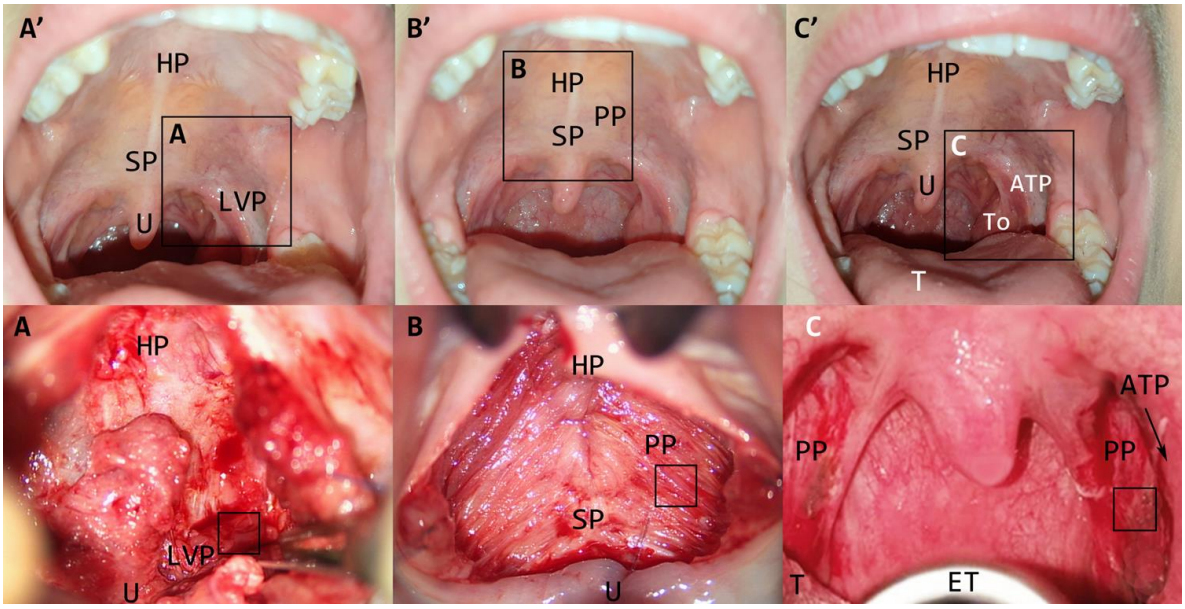

Figure II. 1. Sites for muscle biopsy.

A', B', C' - The normal anatomy of the palate is represented in pictures A, B and C. During a CP operation, the site of **A)** the LVP (left side) biopsy and **B)** the PP (left side) biopsy is indicated. **C)** During a tonsillectomy operation, the site of the PP muscle biopsy (left side) is indicated. **HP** - hard palate; **SP** - soft palate; **U** - uvula; **T** - tongue; **ET** - endotracheal tube; **ATP** - anterior tonsillar pillar; **LVP** - levator veli palatini; **PP** - palatopharyngeus; □ - biopsy site.

II. 2. Histological analysis of human palate muscle biopsies

Muscle biopsies were snap frozen, wrapped in foil within 1 hour by immersing in a bath of hexane cooled by an acetone/cardice mixture, air dried and stored at -80°C. At a later date, muscle biopsies were mounted at the optimal cutting temperature compound, orientated such that sections were taken transversely through the muscle fibres. Sections were cut at 10 µm with a cryostat at -25°C. The following histological and immunohistochemical staining techniques were applied to consecutive sections of each biopsy. An initial haematoxylin and eosin (H&E) stain was performed on all biopsies to confirm transverse sectioning. Each stain was then performed according to standard protocols for: Gomori trichrome; picrosirius; Oil Red O; cytochrome oxidase (COX); nicotinamide adenine dinucleotide-tetrazolium reductase (NADH-TR); succinate dehydrogenase (SDH); fast, slow, developmental and fetal myosins.

II. 3. Haematoxylin and eosin stain

Haematoxylin is a natural compound extracted from a species of tree found in the West Indies and Mexico. The active staining component of the haematoxylin stain is haematein, which is achieved from oxidized extracted compound. Aluminium salts are used as a mordant in haematoxylin staining and makes the nuclear components of cells a dark blue colour. Eosin stains cytoplasmic organelles varying shades of pink and therefore is often used in combination with haematoxylin (Figure II. 2). The combination of the two stains provides a broad range of morphological information about the muscle section (Wang et al., 2017).

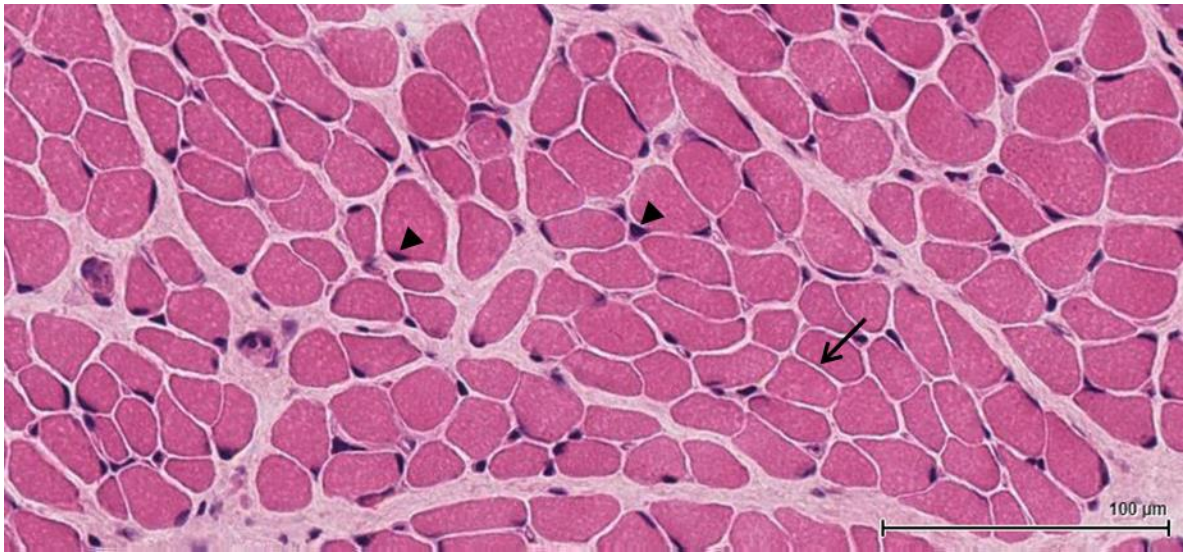

Figure II. 2. Normal palatopharyngeus muscle stained with haematoxylin and eosin. H&E is useful to examine the overall architecture of the muscle fibres. In this example, there is little variation in size and shapes of fibres. The sarcolemma nuclei (dark blue) are situated peripherally (arrow heads). The fibres in a fascicle fit closely together with no intervening fibrous connective tissue (arrow).

II. 4. Special stains

II. 4. 1. Gomori trichrome stain

Gomori trichrome staining is named after George Gömöri, a Hungarian-American physician who became famous as a histochemist and developed the method in 1950. Gomori trichrome stain allows visualization of the mitochondrial activity and collection by the red staining (ragged red fibres) of tubular aggregates, nemaline rods, reducing bodies, cytoplasmic bodies, membranous whorls or rimmed vacuoles. Muscle fibres stain a greenish-blue colour and the collagen is a lighter but clearly distinguishable blue-green colour (Figure II. 3).

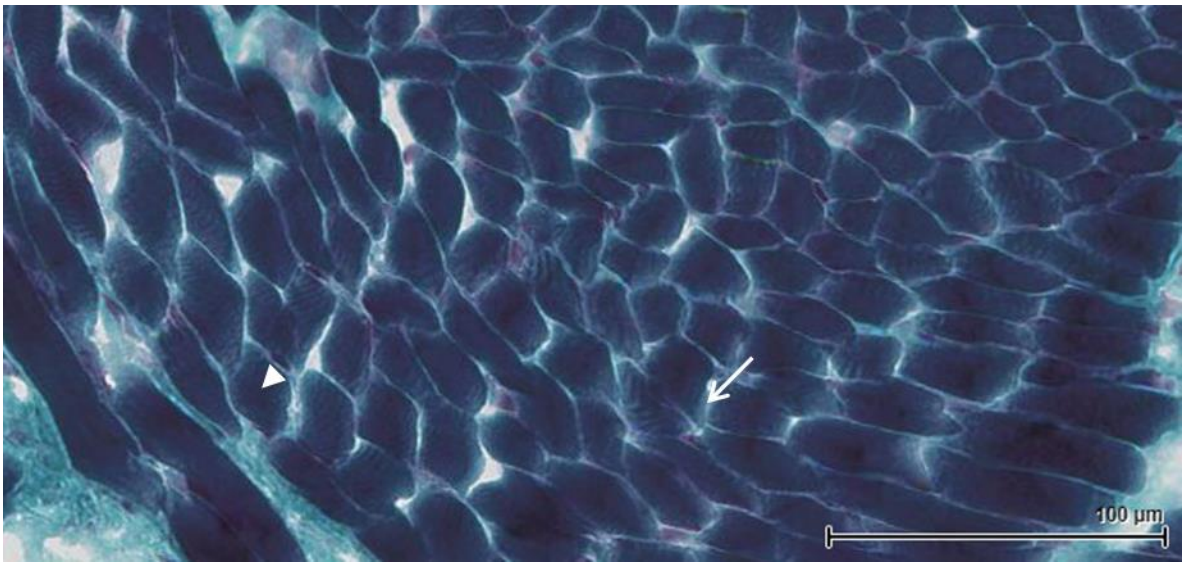

Figure II. 3. Normal palatopharyngeus muscle stained with Gomori trichrome.
This stain is used to demonstrate cytoarchitectural disturbances with an increase in the intermyofibrillar constituents, which are stained purplish-red (such as mitochondria or inclusions such as nemaline rods). This biopsy shows no nemaline rod accumulation with any substantial change in the cytoarchitecture of the fibres. Muscle fibres stain a greenish-blue colour (arrow head) and the collagen is a lighter but clearly distinguishable blue-green colour (arrow).

II. 4. 2. Picrosirius stain

Picrosirius (Figure II. 4) reveals connective tissue staining collagen bright red in contrast to the yellow - green of the fibres (Lattouf et al., 2014).

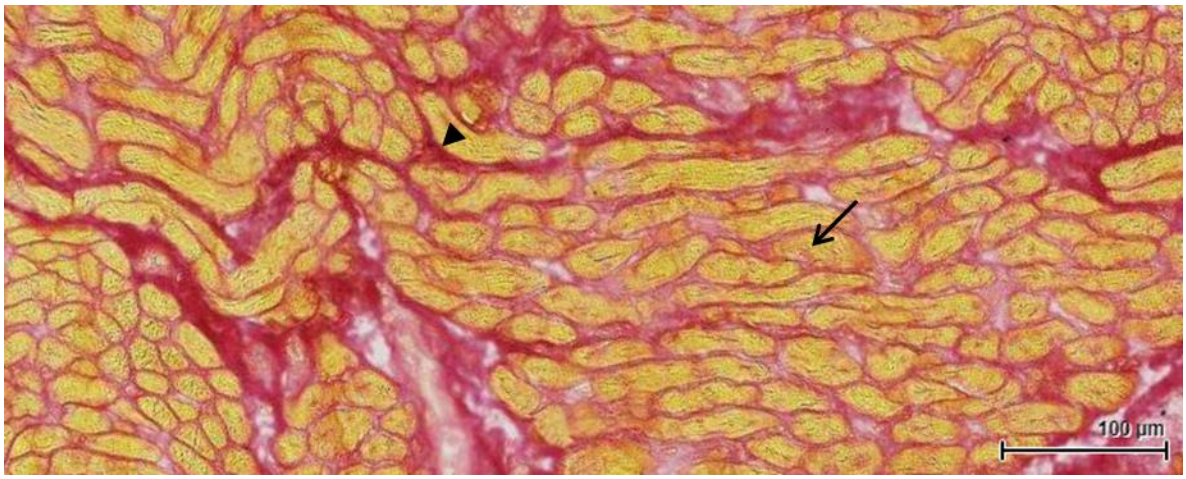

Figure II. 4. Normal palatopharyngeus muscle stained with picrosirius.
This stain highlights connective tissue, staining collagen bright red (arrow head) and the muscle fibres yellow (arrow).

The connective tissue was quantified using Image J software (http://imagej.nih.gov/ij/index.html). To designate the total region of interest (ROI) the drawing tool was used. Within the ROI the connective tissue was selected using the colour threshold tool. The settings were adjusted to select red as the ROI for analysis. The data was exported to the ROI manager and the area of connective tissue (i.e. red hue) was measured. To normalize the data the area of connective tissue was divided by the total ROI. Statistical test one-way ANOVA was applied to calculate statistical significance and graphs generated in GraphPad PRISM (Version 6.01). Multiple comparisons were carried out using the Tukey multiple comparisons method (McHugh, 2011).

II. 4. 3. Oil Red O stain

Staining with the Oil Red O technique (Figure II. 5) demonstrates neutral lipids which in normal muscle take the form of small droplets with a distribution similar to that of mitochondria. The concentration and size of the droplets varies with the fibre type.

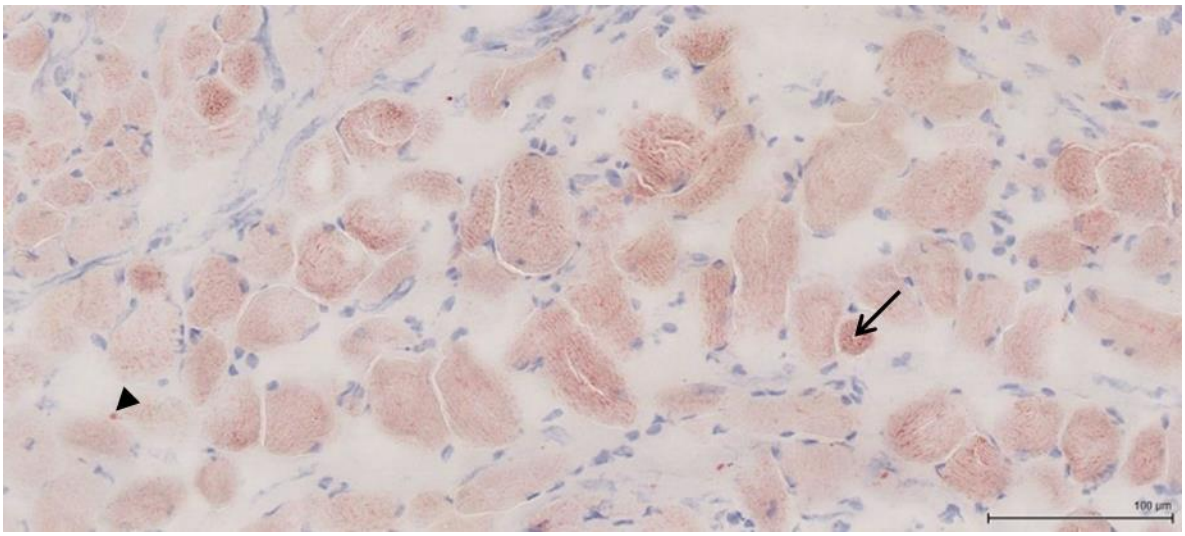

Figure II. 5. Normal palatopharyngeus muscle stained for neutral lipid with Oil Red O.

Lipid droplets are stained red (arrow head). Only faint red dots are visible in slow twitch type fibres (arrow).

To evaluate muscle infiltration with fat, a scale based on 4 grades (Figure II. 6) was used. These were: none - no fat staining was noted; detectable - low amount of fat observed; apparent - obvious fat deposit in muscle tissue; significant - muscle infiltration with fat.

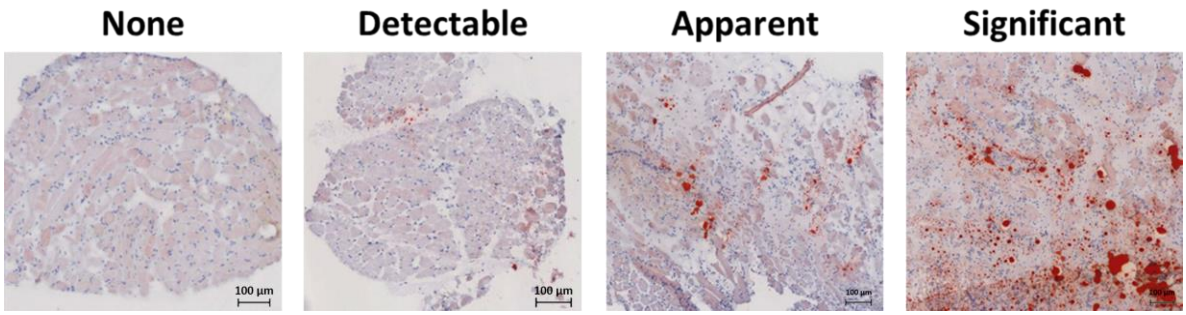

Figure II. 6. Grading system for fat evaluation in muscle tissue.

Four levels of fat infiltration were distinguished in biopsies. Red staining indicates accumulated lipid droplets.

II. 5. Histochemical reactions

II. 5. 1. Nicotinamide adenine dinucleotide-tetrazolium reductase stain

The NADH-TR reaction is based on the ability of the mitochondrial enzyme NADH - dehydrogenase to transfer electrons to the colourless, soluble tetrazolium salt and convert it into an insoluble formazan compound. This highlights the intermyofibrillary matrix - the space between the myofibrils, Figure II. 7.

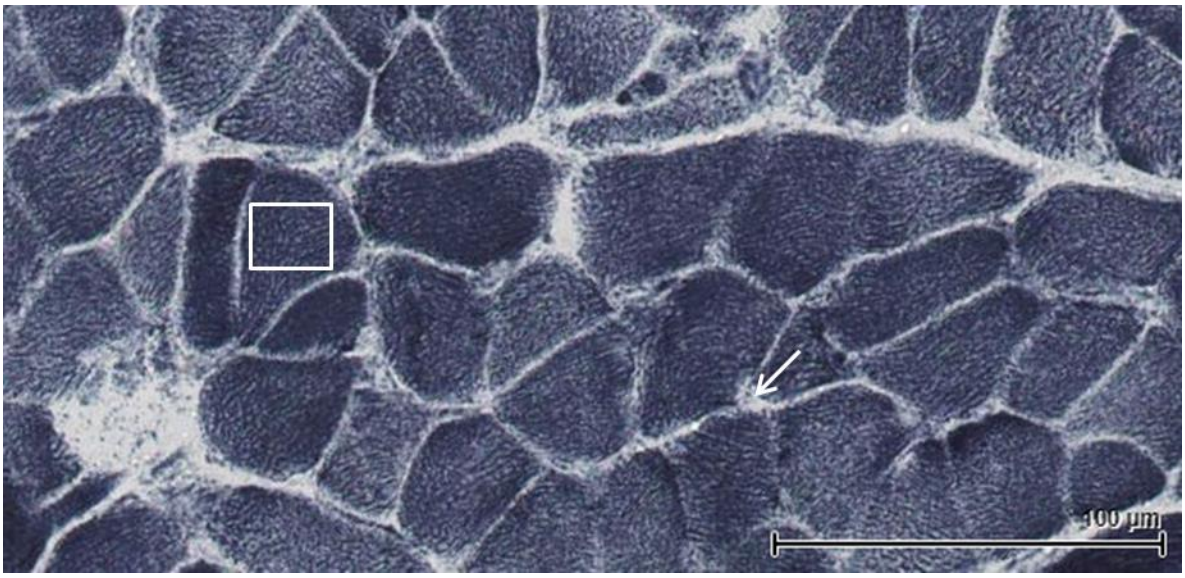

Figure II. 7. Normal palatopharyngeus muscle stained with NADH-TR.
This stain distinguishes cell organelles (□), particularly mitochondria and displays the orderly cytoarchitecture with intermyofibrillary matrix - the space between the myofibrils (arrow).

II. 5. 2. Succinate dehydrogenase stain

SDH is a mitochondrial enzyme catalysing the conversion of succinate to fumarate in the citric acid cycle. By providing an excess of sodium succinate, the cytochrome oxidase (COX) system reduces a tetrazolium salt into the insoluble deep blue or purple formazan compound. This reaction provides a specific stain for mitochondria. Since the gene for SDH is encoded in the nucleus and not in the mitochondrial genome, it is not affected by deletions on the latter and is considered among the best screening reactions for mitochondria (Figure II. 8).

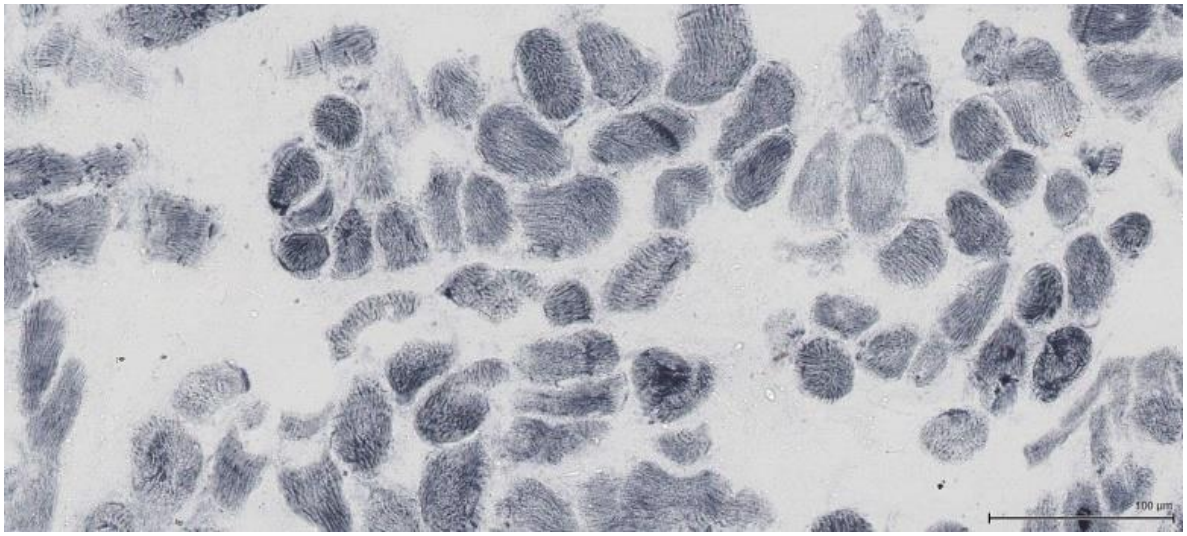

Figure II. 8. Normal palatopharyngeus muscle stained with SDH.
The SDH stain distinguishes cell organelles, particularly mitochondria and displays the orderly cytoarchitecture.

II. 5. 3. Cytochrome oxidase stain

COX is another mitochondrial enzyme often used in conjunction with SDH stain. Since the COX gene is located in the mitochondrial genome, it can be subject to mitochondrial genome alterations. In mitochondrial cytopathies, the COX stain helps in a differential diagnosis (Figure II. 9).

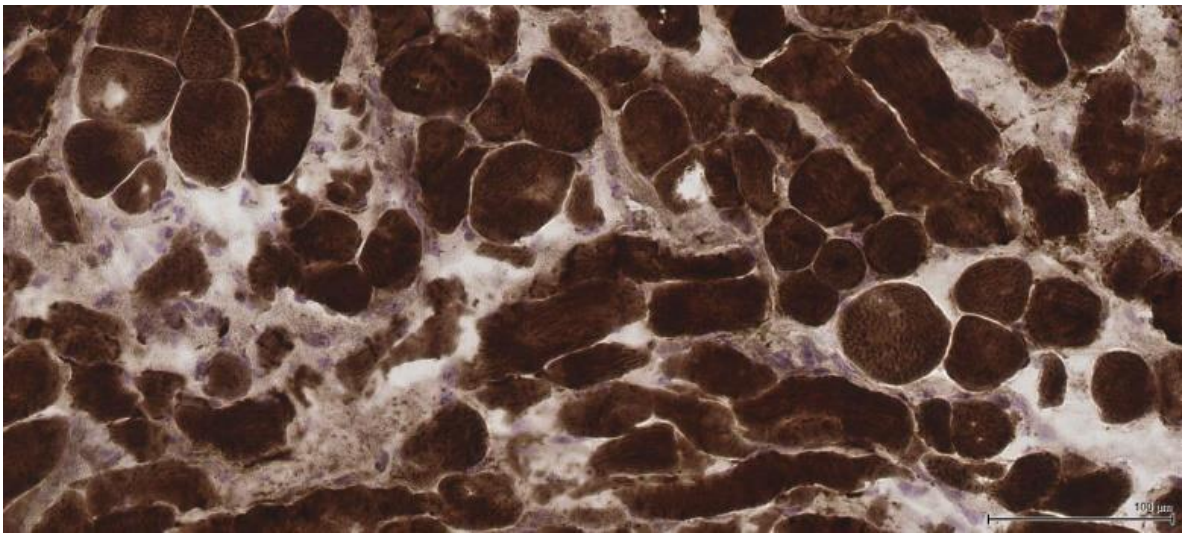

Figure II. 9. Normal palatopharyngeus muscle stained with COX.
This biopsy shows the level of cytochrome oxidase activity in muscle fibres.

II. 6. Immunohistochemistry

II. 6. 1. Fast, slow, neonatal and developmental myosin

Immunohistochemistry is used to visualize and localize specific protein components of a tissue. The principle of the technique is based on the specific affinity of an antibody for its corresponding protein or protein fragment (antigen). Allied techniques are the labelling of glycoproteins with lectins, the labelling of receptors with a ligand and labelling of nucleic acids by *in situ* hybridization. Similar methods of detection and amplification have been developed for all these techniques but their diagnostic role is less than that of immunohistochemistry (Vogel and Zamecnik, 2005, Duraiyan et al., 2012). To identify slow and fast

muscle fibres Mouse Monoclonal Antibodies Myosin Heavy Chain (slow [NCL-MHCs] and fast [NCL-MHCf]) were used.

In the neonate, an additional fibre type can be identified. In reality these are immature fibres that will go on to mature during the first year of life. Very few are found in normal adult muscle. Both neonatal and developmental myosin isoforms are transiently expressed during embryonic and fetal development and usually disappear shortly after birth, at which point adult fast and slow myosins become prevalent (Figure II. 10). However, developmental myosins can persist throughout adult ages in specialized muscles, such as the extraocular and jaw closing muscles, and in the intrafusal fibres of the muscle spindles. These myosins can also be re-expressed during muscle regeneration and can be a useful marker of regenerating fibres in the pathologic skeletal muscle (Schiaffino et al., 2015). To identify neonatal and developmental muscle fibres Mouse Monoclonal Antibodies Myosin Heavy Chain (neonatal [NCL-MHCn] and developmental [NCL-MHCd]) were used.

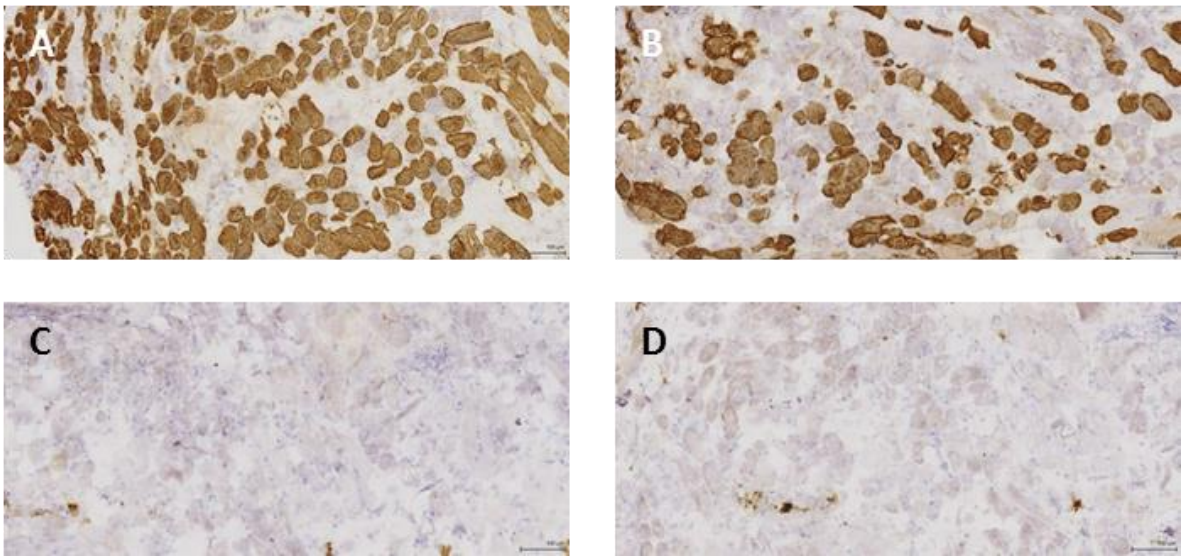

Figure II. 10. Normal palatopharyngeus muscle stained for myosin.
Different pH conditions is used to visualize and localize different types of myosin fibre (brown stain). **A)**, **B)** Samples of PP muscle from an ICP patient at age 9 months; **A)** fast myosin; **B)** slow myosin. **C)**, **D)** Samples of PP muscle from a SMCP patient at age 3 years (note the lack of muscle fibres in this patient); **C)** neonatal myosin; **D)** developmental myosin.

For fast and slow fibres analysis, either the area of the best quality stain or the whole sample was marked using Image J software (http://imagej.nih.gov/ij/index.html). The ROI was designated using the drawing tool to select the area containing the fibres based on the myosin signal. Within the ROI the number of fibres was then counted using the multipoint tool and exported to the ROI manager. The fibre's density per 10,000 μm^2 was compared between cleft and muscle types. One-way ANOVA was applied to calculate statistical significance and graphs were generated in GraphPad PRISM (Version 6.01). Multiple comparisons were carried out using the Tukey multiple comparisons method (McHugh, 2011).

II. 6. Polymerase chain reaction

Polymerase chain reaction (PCR) is a primer mediated enzymatic amplification of cloned or genomic DNA sequences (Kolmodin and Birch, 2002). To design locus specific primers, genomic sequences for respective genes were obtained from their National Centre for Biotechnology Information (NCBI) reference sequence (https://www.ncbi.nlm.nih.gov/gene). Primer3 (version 4.1.0) software (http://primer3.ut.ee/) was used to choose optimal primer sequences, which were also screened for the presence of SNPs using SNPcheck3 (https://genetools.org/SNPCheck/snpcheck.htm). The chosen primers were 18-24 base pairs (the recommended size for binding specificity) and were obtained from Sigma-Aldrich in a lyophilized state (Table II. 1). An initial dilution was made using the required amount of DEPC-treated water in order make a stock solution with a final concentration of 1 µg. A working solution was then prepared by mixing 10 µL of stock solution with 190 µL of DEPC-treated water to give a final concentration of 50 ng. Both stock and working solutions were stored at -20°C. Primers were first tested with a control DNA sample and if necessary optimized using a temperature gradient (up to 62°C) (Dieffenbach et al., 1993). After primers were successfully optimized, they were used to amplify DNA using BIOTAQ^{TM} DNA polymerase (Bioline, #21040) and 1 µL of the sample DNA (Table II. 2).

Table II. 1. Primers used for gene amplification and sequencing.

Genotyping	Primer sequence 5' to 3'	t (°C)	PCR	Product size (bp)	Notes
PLB1	F: tgggcttctcagtttgacca R: ctgtctctggccaagtgaga	60	Standard	354	for DNA
FOXF2 **Exon 1**	F: agccccagaggagctgag R: gcctgcaggaactggtagat	58	HotStar	569	for DNA
	F: aagccgccctactcgtacat R: ctggccatgtaggtggaac	58	Standard	563	for DNA
	F: gcggcctcgacatgat R: gccctcagacctcctagctt	58	HotStar	555	for DNA
FOXF2 **Exon 2**	F: gggctttctctaccagctgt R: tgtgacttgaatccgtccca	60	Standard	386	for DNA
SNX10	F: gtccagactcctaacccctg R: aacctcctcaagcaacccat	60	Standard	318	for DNA
PLIN2	F: ccctcctgtccaacatccaa R: gcactagtgataggggcagg	60	Standard	316	for DNA
IGDCC3	F: ggagattgaggtggagtccc R: agccgatgatctccttggtg	60	Standard	341	for DNA
THSD4	F: gcaggagttaaagccacagc R: aacttagtcaccacccctgc	60	Standard	334	for DNA
SEMA7A	F: tggtcttctgaaccctctgg R: agacgtggtcctctgtgctt	60	Standard	347	for DNA
SCAPER	F: cggaaagatgctgaaggatgg R: tttcggcaagaggatggtca	60	Standard	212	for DNA
SH2D7	F: caggcaggtctgttctggat R: ccttttcaagccctccctat	60	Standard	351	for DNA
IL16	F: aaccattgattcccggggta R: tgctggtctatggtaaatgctg	60	Standard	336	for DNA

Table II. 2. Standard Bioline PCR reaction mix.

Reagent	Volume (µL) per reaction
NH_4 reaction buffer (10x)	2.5
$MgCl_2$ (50 mM)	1
dNTPs (10 mM)	0.5
Forward primer (50 ng/µL)	1
Reverse primer (50 ng/µL)	1
Taq DNA polymerase	0.25
Betaine (5 M)	5
DEPC-treated water	12.75
DNA (50-100 ng)	1

PCR reactions were carried out in a Veriti® 96-well Thermal Cycler (Applied Biosystems) using a heated lid, which was set at 100°C in order to prevent evaporation. A standard PCR cycle consisted of an initial denaturation at 94°C for 5 min and 35-40 cycles of: denaturation at 94°C for 30 sec, annealing at 58-62°C for 30 sec and extension at 72°C for 30 sec and a final extension at 72°C for 2 min. PCR products (5 µL of each) were analysed by electrophoresis (see below II. 8. Agarose gel electrophoresis) to confirm product size and quality.

II. 7. HotStar polymerase chain reaction

Occasionally, it was necessary to change to a different Taq polymerase when encountering regions that were difficult to amplify. HotStar Taq is a higher fidelity enzyme and uses a modified protocol, involving heating at 96°C for a longer period to ensure complete denaturation of the dsDNA. In addition, the protocol contains Q-solution that enables more efficient amplification of difficult templates including templates that have a high degree of secondary structure or are GC rich (Table II. 3).

Table II. 3. A standard HotStar PCR reaction mix.

Reagent	Volume (µL) per reaction
10x PCR buffer	2
dNTPs (10 mM)	0.5
Forward primer (50 ng/µL)	1
Reverse primer (50 ng/µL)	1
HotStar Taq DNA polymerase	0.5
Q-solution (5 M)	6
DEPC-treated water	8
DNA (50-100 ng)	1

II. 8. Agarose gel electrophoresis

Agarose gel electrophoresis was used to visualise the size and integrity of PCR products. It involved the separation of DNA fragments depending on their molecular weight/size. Negatively charged DNA molecules move towards the positively charged anode in an electric field. Gels were made using 1 g UltraPureTM agarose powder mixed with 100 mL of TAE (Tris base, acetic acid and EDTA) buffer (1% agarose gel). The solution was microwaved until the agarose powder had completely dissolved and 1.5 µL of ethidium bromide (10 mg/mL) was added to the solution once it had cooled down. The solution was then poured into a gel tray with a comb to form the wells and left to solidify. Then 5 µL of commercially available blue/orange loading dye (Promega, #G1881) was mixed with 15 µL of PCR product and loaded on the gel adding 5 µL of 100 bp DNA ladder (Promega, #G2101) in an adjacent well as a size marker. The gel tank was run at 100 V for 30 min, before visualizing the ethidium-stained DNA in a Genosmart UV machine.

II. 9. Real-time quantitative polymerase chain reaction assays

Real-time quantitative PCR (RTqPCR) is a technique that allows an amplified PCR product to be detected and quantified in 'real time'.

II. 9. 1. Power SYBR Green assay

Power SYBR Green (ThermoFisher, #4368577) binds to dsDNA but not to ssDNA. This binding causes bright fluorescence. Increased DNA synthesis binds more dye and results in increased levels of fluorescence (Ma H, 2006). Fluorescence is continuously measured by a sensitive detector in each well of the plate, which enables the quantity of a PCR product to be measured at any time during amplification.

Relative quantification e.g. of a cDNA to measure gene expression levels, allows relative target quantity comparisons between the samples, with expression of each sample normalised to an endogenous control gene. In this study we used *ACTB* expression as an RTqPCR endogenous control. The 'comparative Ct method' was used in this study, which relies on the assumption that the amplification of the target and endogenous control genes are equally efficient. The RTqPCR reactions were run in triplicate with the gene of interest and housekeeping gene on the same 96-well plate (microAmp Fast Optical 96-well reaction plates). Each reaction contained 10 µL of template and 15 µL of SYBR Green master mix (Table II. 4). Primers used for quantitative analysis are shown in Table II. 5. All primer sets were free of primer-dimer products.

Table II. 4. Standard SYBR Green reaction mix.

Reagent	Volume (µl) per reaction
***Power* SYBR® Green PCR master mix**	12.5
Forward primer (50 ng/µL)	1
Reverse primer (50 ng/µL)	1
DEPC-treated water	0.5

Table II. 5. Primers designed for Power SYBR Green assay.

Gene	Primer sequence 5' to 3'	t (°C)	Product size (bp)	Accession number	Notes
SHOX2	F: gcttctccgttacccctttg R: ccgagtccaagatgcgatag	60	90	NM_006884	for cDNA
FOXF2	F: cccgttaccagcatcactct R: gctagctgagggatggaaag	60	92	NM_001452	for cDNA
FGF18	F: tacacgacggtgaccaagag R: ttctgggagtgtgagtgtgg	60	107	NM_003862	for cDNA
TBX22	F: atacctgcccaatgtcaacc R: tcaggagccggtaaaacaag	60	90	NM_001109878	for cDNA

The plate was sealed with optical adhesive covers (ThermoFisher, #4311971) and spun briefly to remove air bubbles, then placed in the StepOne Plus™ RTqPCR Systems to be analysed. The amplification reaction was programmed for an initial incubation at 50°C for 2 min, polymerase activation at 95°C for 10 min, and 40 cycles of denaturation at 95°C for 15 sec, and annealing and extension step at 60°C for 1 min. Each RTqPCR reaction was subjected to melt curve analysis in order to confirm the fidelity of the target sequence amplification.

II. 9. 2. TaqMan® gene expression assay

RTqPCR assay was carried out to detect gene expression using TaqMan® gene expression master mix (ThermoFisher, #4444556). Each reaction contained 10 µL of TaqMan® gene expression master mix, 4 µL of complementary DNA (cDNA) sample, 1 µL of TaqMan® assay (ThermoFisher, Mm00467433_m1, Mouse *Tbx22*, #4331182) and 5 µL of water (Table II. 6). Each reaction was run in triplicate and a cDNA template negative control reaction was set up for each assay used. TaqMan® assay were run on a program for 2 min at 50°C which was followed by 10 min at 95°C before 40 cycles of 15 sec at 95°C and 1 min at 60°C. The program was carried out using C100™ Thermal Cycler and CFX96™ Real-Time System (BIO-RAD). In this study, *Sdha* expression was used as a TaqMan® RTqPCR endogenous control.

Table II. 6. TaqMan® PCR reaction mix.

PCR reaction mix component	Single reaction (µL)
20x TaqMan® gene expression assay	1.0
2x TaqMan® gene expression master mix	10.0
cDNA template	4.0
RNase-free water	5.0

II. 9. 3. Gene expression analysis

After amplification, quantitative expression levels were obtained using the StepOne software (version 2.1). This determines the cycle number at which the fluorescence crosses an arbitrary line, the threshold. The crossing point gives the C_T value (cycle threshold). The increment of fluorescent signal at each cycle point is measured as ΔRn, which is calculated as: ΔRn (cycle) = Rn (cycle) - Rn (baseline), where normalised reporter (Rn) is the fluorescence of the reporter dye divided by that of passive reference which produces a consistent fluorescent signal.

The threshold is set automatically and is usually high enough to distinguish amplification rather than noise. In the logarithmic view, the threshold is on the linear part of the reaction. In the regular view, the threshold will be close to the bottom of the curve. The difference in the C_T values (ΔC_T) is calculated as the control C_T value subtracted from the target C_T value.

ΔC_T = average target C_T (gene of interest) - average control C_T (endogenous gene)

Although the C_T value for each sample triplicate should be the same, pipetting errors can contribute to variation. Therefore, C_T values that were not within one cycle of the other two repeats were excluded from the analysis. The relative quantity of the target gene was calculated using the formula $2^{\wedge -\Delta Ct}$.

II. 10. Mouse tissue DNA extraction and genotyping

A small piece of mouse tissue (usually an ear clipping from an adult or limb from an E13.5-E17.5 embryo) was first air dried. Then 45 µL of proteinase K lysate buffer and 5 µL proteinase K (10 mg/mL) were added to it in a PCR tube. This was placed in a thermal cycler (DNA Engine Dyad Peltier Thermal Cycler, Bio-Rad) at 37°C for 1 hour 40 min. To precipitate the DNA, 50 µL isopropanol was added and mixed, followed by centrifugation (Sigma® 1-14 centrifuge) at 15700 x g for 10 min. The supernatant was discarded and the pellet was washed in 70% ethanol (EtOH). This was again centrifuged at 15700 x g for 10 min and the supernatant was discarded. The DNA was then allowed to dry and the pellet suspended in 20 µL of DEPC-treated water. Primer sequences designed for mice genotyping is presented in Table II. 7.

Table II. 7. Primers designed for mice genotyping.

Genotyping	Primer sequence 5' to 3'	t (°C)	Product size (bp)	Notes
WT	F: cagcttccaaaacagtggag R: catgtgtgtaccatcagtcc	60	190	for cDNA
Tbx22^{flox}	F: cagcttccaaaacagtggag R: catgtgtgtaccatcagtcc	60	230	for cDNA
Tbx22^{null}	F: cagcttccaaaacagtggag R: gattgggaagactttagcagg	60	N/A	for cDNA
YFP	F: tgaaccgcatcgagctgaaggg R: tccagcaggaccatgtgatcgc	58	320	for cDNA
Cre	F: accctgatcctggcaatttcggc R:gatgcaacgagtgatgatgaggttcg	60	600	for cDNA
Sex **F:** single band **M:** two bands	F: tgaagcttttggctttgag R: ccgctgccaaattctttgg	58	209 209 & 216	for cDNA

II. 11. Alcian blue and alizarin red skeletal staining

E17.5 embryo heads after the removal of the skin were fixed and dehydrated in 75% EtOH overnight. This was followed by incubation overnight in 0.01% alcian blue staining solution (20% acetic acid, 80% EtOH, 0.01% alcian blue). The stained specimens were washed in 75% EtOH for 24 hours. The soft tissue was then treated by alkaline hydrolysis and glycerol clearing. The specimens were immersed in 1% potassium hydroxide (KOH) and kept for 3 hours at room temperature on the shaker. When the heads started to become clear, 0.01% alizarin red was added and kept overnight at room temperature. A further 1% KOH wash was performed overnight at room temperature. The embryo heads were then transferred into 20% glycerol 1% KOH solution and incubated overnight. Specimens were stored and photographed in 80% glycerol (Nagy et al., 2009).

II. 12. Methods to dissociate palate shelf tissue into cells

To identify the best method to dissociate cells from the dissected palatal shelf tissues, 4 different methods were tested for optimization. The cell dissociation was induced either with trypsin (ThermoFisher, #25200056), accutase (Sigma-Aldrich, #A6964), dispase/collagenase/$CaCl_2$ solution (Table II. 8) or affected by mechanical dissociation. The dispase/collagenase/$CaCl_2$ solution was chosen as the optimal method and subsequently used for cell preparation prior to flow sorting (IV. 3. 3. Optimization of palate shelf tissue dissociation into single cells for flow sorting).

Table II. 8. Dispase/collagenase/$CaCl_2$ solution.

Reagent	Details	Concentration
Collagenase D	Roche, #11088858001	1.5 U/mL
Dispase II	Specialty Media, #2643607	2.4 U/mL
$CaCl_2$	Sigma-Aldrich, #10043-52-4	2.5 mM

II. 13. Palate shelf dissection and cells preparation for flow sorting

Timed pregnant female mice (E13.5) were killed by CO_2 asphyxiation and cervical dislocation. For each female, the uterus containing the embryos was removed and placed in cold PBS on ice. Palatal shelves were dissected in Knockout DMEM (Figure II. 11) and a limb from each embryo was taken for genotyping. Samples were carefully numbered and labelled. The tissues were collected into Eppendorf tubes containing fluorescence activated cell sorting (FACS) medium (Table II. 9). The samples were pelleted by centrifugation followed by FACS medium aspiration. 150 µL of dispase/collagenase/$CaCl_2$ solution was added to each sample and then incubated at 37ºC for 7 min. This was followed by adding 500 µL of FACS medium and pipetting up and down to dissociate the tissue into a single cell suspension. The cell suspension was then moved to a 15 mL Falcon tube and centrifuged at 76 x g at room temperature for 5 min (Eppendorf Centrifuge 5810R). The

supernatant was aspirated and the cells washed again with FACS medium to remove residual enzyme. The suspension was centrifuged again followed by aspiration of the medium. The pellets were resuspended in 1 mL FACS medium and passed through a 100 µm filter, then repeated using a 40 µm filter (Scientific Laboratory Supplies, #352360 and #352340) and collected into a 50 mL Falcon tube. The suspension was centrifuged at 76 x g for 5 min. The pellet was resuspended in 200 µL of FACS medium and transferred to an Eppendorf tube. Flow sorted cells collection tubes were prepared by adding 100 µL of PBS into fresh Eppendorf tubes. After flow sorting, the cells were then pelleted at 200 x g for 5 min and frozen, first placing them on dry ice and subsequently transferring them to a -80ºC freezer.

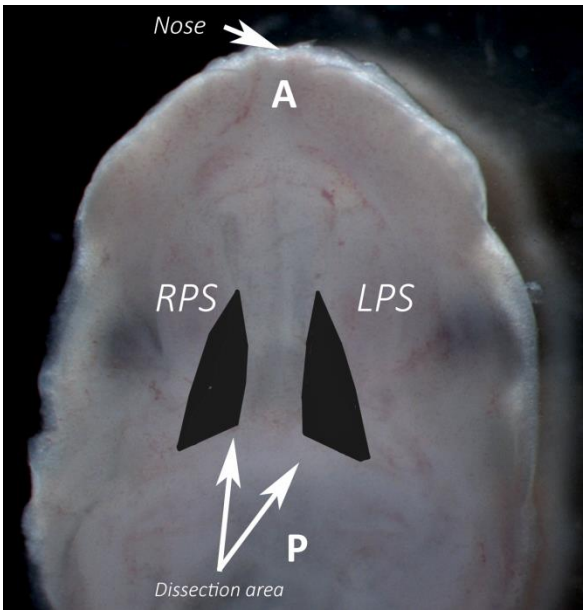

Figure II. 11. Dissection of palate shelves for FACS.

Ventral view of the maxilla, palatal shelves and palate of E13.5 mouse embryo. Arrows indicate the regions of dissection. **A** - anterior; **P** - posterior; **RPS** - right palatal shelf; **LPS** - left palatal shelf.

Table II. 9. The medium used for flow sorting.

The medium
Knockout DMEM (Life Technologies, #A12861-01 CTSTM KnockOutTM DMEM 500 mL)
10% KSR (Life Technologies, #10828010 KnockOutTM Serum Replacement 100 mL)
1X N2 supplement (Life Technologies, #A13707-01 CTSTM (Cell Therapy Systems) N-2 Supplement 5 mL)
2% cell culture grade albumin (Life Technologies, #15260-037 Bovine Albumine Fraction V (7.5% solution) 100 mL)
Penicillin 25 U/mL and streptomycin 25 µg/mL (Life Technologies, #15070-063 Penicillin-Streptomycin (5.000 U/mL))

II. 14. Flow cytometry

Flow cytometry or FACS is used to identify, analyse, and/or sort different populations of cells (Shapiro, 2018). It is based on the principles of light scattering caused by particles crossing a beam of light. This causes excitation and fluorescence emission of fluorochromes that may be attached to either specific molecules or expressed by a particular cell type. A population of single cells can be analysed by suspending them in a medium and injecting them into a stable stream that forces the cells to travel one by one through the flow cytometer. To analyse each cell, one or more beam of laser light can be used. The information about the cell's properties is provided by scattered light and fluorescence emission. The flow cytometer can analyse cells at up to 100,000 events per second and is capable of detecting low signals, count cells and simultaneously analyse several different physical and chemical properties with high sensitivity and in a very short period of time (Ormerod, 1994).

Forward scatter (FSC) is a parameter which is obtained when light detector converts a confocal lens focused laser beam into an electrical signal that

subsequently becomes digitilised (Radbruch, 1992). The FSC signal gives information about the size and shape of the cell. The side scatter (SSC) signal is gathered by a side confocal lens and detected by a sensor reading side scattered light. SSC gives information about the granularity of the cell. The combination of FSC and SSC help to identify different type of cells.

Fluorescence is detected by several optical detectors, the so-called photomultiplier tubes (PMT). They read the fluorochromes excited by the light emitted from the cell crossing the laser beams. Different fluorochromes emit light at different wavelengths and are then split into specific colours by optical filters. The PMTs convert received light into an electrical pulse that is digitalised and read by a computer, which can generate histograms and dot plots.

The cell sorter Moflo XDP (Beckman Coulter, California) was used to sort cells in this study. It is equipped with 3 air cooled lasers: a 150 mW 488 nm Coherent Sapphire blue laser, a 100 mW 643 nm Coherent Cube red laser, and a 100 mW JDSU Xcyte 355 nm UV laser. Only the blue laser was used in these experiments. A 100 nm nozzle tip was used with 20 PSI sheath pressure. Yellow fluorescent protein (YFP) signal was collected in FL1 channel through a 530/40 band pass filter and FL3 channel with a 613/20 band pass filter was used to separate true YFP+ cells from auto-fluorescence background. A light scatter gate was drawn in the FSC versus SSC plot to exclude debris and big clumps and include viable cells. Cells in this gate were displayed in an SSC versus SSC-W to further target single cells. Single and viable cells were then analysed in a FL3-Log versus FL1-Log plot and a final gate was drawn on green/yellow cells for cell sorting (Han and Gu, 2016).

Preparation of all samples for flow sorting was performed by me. However, hands on use of the FACS machine was provided as a service performed by Dr Ayad Eddaoudi at the UCL Great Ormond Street Institute of Child Health Flow Cytometry Core Facility, supported by the Great Ormond Street Children's Charity, grant reference U09822 (October 2007), and UCL Capital Equipment Funding, School of Life and Medical Sciences (September 2012).

II. 15. Preparation of RNA from cells for RNA-Seq

RNA was extracted from flow sorted mouse embryonic palatal shelf cells using the RNeasy Micro Kit (Qiagen, #74004). The kit allows purification of up to 45 µg RNA from small cell and tissue samples. RNA was extracted from 3 replicate E13.5 males in each of the mutant (experimental) and WT (control) groups and submitted for RNA-Seq to identify global gene expression changes.

II. 16. RNA-Seq technology

RNA-Seq is a method of analysing a highly complex mix of transcripts using deep sequencing technologies. The chosen population of RNA is first converted to a library of cDNA fragments which will have short adaptors attached to one or both ends. The library is then sequenced to obtain short sequences from one or both ends. Sequence reads are either aligned to a reference genome or reference set of transcripts or assembled *de novo,* without the genomic sequence in order to produce a transcription map that reveals the transcriptional structure and/or level of expression of each gene (Wang et al., 2009).

RNA quantification and sample integrity check, cDNA library preparation, alignment, running on the sequencing platform (Marioni et al., 2008) and basic analysis was performed by the UCL Genomics Service (www.ucl.ac.uk/child-health/research/genetics-and-genomic-medicine-programme/ucl-genomics).

II. 17. Preparation of RNA from tissue for RTqPCR

RNA from tissue was extracted using the TRIzol method. Tissues (mouse embryo heads) were collected into 1.5 mL Eppendorf tubes and kept on ice. Then 1 mL of TRIzol (ThermoFisher, #15596026) was added to each sample and pulverized with a homogenizer. The tubes were kept for 5 min at room temperature and then 250 µL of chloroform (ThermoFisher, #10102190) was added and shaken vigorously for 15 sec. The samples were incubated at room temperature for 5 min and centrifuged at 9300 x g for 5 min. Three layers in each tube were identified and

the aqueous phase carefully removed using a pipette to a new 1.5 mL Eppendorf. At this stage 550 µL of isopropanol (ThermoFisher, #10284250) was added to the aqueous phase and mixed gently then kept at room temperature for 5 min. The tubes were centrifuged at 16100 x g for 20 min. The samples with obvious pellets at the base of each tube were placed on ice. The isopropanol was poured off and 2 mL of 75% EtOH in DEPC-treated water was added. EtOH was poured off and the pellets were air dried, then resuspended in 20 µL of DEPC-treated water. The concentration and absorbance at 260 nm were measured. A 260/280 ratio greater than 1.8 was considered as acceptable. The samples were stored at -80°C until further use.

II. 18. Reverse transcription PCR

In order to synthesise cDNA for real-time expression analysis, reverse transcription PCR (RT-PCR) was performed. In the first step, RT-PCR uses reverse transcriptase to generate cDNA from an RNA template. A first strand of cDNA was synthesised by reverse transcription of the total RNA extracted using the TRIzol method from E13.5 mouse embryo heads. Each RNA sample (100 ng) was diluted with DEPC-treated water to a total volume of 10.25 µL. The mix was initially heated at 72°C for 5 min to melt any secondary structure of the single-stranded RNA (ssRNA) and cooled to 37°C in a thermal cycler. The mixture (Table II. 10) was added for reverse transcription.

Table II. 10. Standard reverse transcription reaction mix.

Reagent	Volume (µL) per reaction
M-MLV RT buffer (5x)	4
dNTPs (10 mM)	2
Random primers (500 µg/mL)	1
M-MLV reverse transcriptase (200 units/µL)	0.5
RNasin RNase inhibitor (40 units/µL)	0.25
DEPC-treated water	2

RT reaction mix (9.75 µL) was added to each sample followed by incubation at 37°C for 1 hour before heating at 80°C for 10 min to stop the reaction by denaturing the enzyme. A negative control was used in each run, where water was used instead of RNA. To confirm the conversion of RNA to cDNA, 1 µL of cDNA samples were used performing PCR with *ACTB* primers. The primers (Table II. 11) were designed to amplify both genomic DNA by flanking a relatively short intron (134 bp) in order to detect any genomic contamination in the RNA samples, as well as to confirm the conversion of RNA to cDNA.

Table II. 11. Control primers designed for PCR to check the integrity of cDNA.

Gene	Primer sequence 5' to 3'	t (°C)	Product size (bp)	Accession number	Notes
ACTB	F: tcgtgcgtgacattaaggag R: gtcaggcagctcgtagctct	60	110	NM_001101	for cDNA

PCR products were electrophoresed to check quality and to prove absence of genomic contamination. cDNA samples were then stored at -20°C for future use.

II. 19. Reverse transcription, RNA library preparation and sequencing

First strand cDNA synthesis and RNA-Seq library construction were performed using the Ovation® SoLo RNA-Seq System (NuGEN). Twelve samples were run on the NextSeq500 (Illumina), using single-end 75 bp reads with 8 bp index and 8 bp unique molecular identifier (UMI). Barcoding individual transcripts with UMI minimises the PCR amplification bias in low input RNA-Seq protocol. Three RNA samples from each of the following biological groups were used: CM WT and *Tbx22*$^{-/Y}$; CNC WT and *Tbx22*$^{-/Y}$.

II. 20. RNA-Seq read alignment and counting

Raw sequencing reads were converted to FASTQ files using Illumina's FastQ generation application and run quality was checked. Adaptor trimming was performed using Trimmomatic 0.36.5, FastQ files were aligned to the mm10 (GRCm38) reference mouse genome using STAR FastQC aligner (v 0.71). Deduplication was performed with markdupes tool of Je suite 1.2.1 (Girardot et al., 2016). To measure gene expression FeatureCounts 1.6.0.2 tool was used.

II. 21. RNA-Seq quality check

RNA-Seq data were analysed using the standard quality control (QC) methods STAR alignment scores and Picard gene coverage (MultiQC v1.5).

II. 22. RNA-Seq differential gene expression

Differential gene expression analysis was performed with DESeq2 package (Love et al., 2014) in R (v3.5.1). Genes with mean normalised counts of <10 were excluded from the multiple testing correction. Significant threshold of Benjamini adjusted *p*-value of 5% was used. Correlations between the biological replicates were visualised by plotting the regularised log transformed gene counts. Principal component analysis (PCA) was carried out to detect any outliers.

II. 23. Gene set enrichment analysis

RNA-Seq data was analysed for differential expression against gene sets. All genes were included and ranked by Log_2 fold change (Log_2FC). For input mouse genes were used, as them converting to human orthologues, generated identical gene set enrichment result. The conversion was done using online tool at BiodbNet (biodbnet-abcc.ncifcrf.gov/db/dbOrtho.php). The ranked lists were imported into gene set enrichment analysis software (GSEA 3.0) (Mootha et al., 2003, Subramanian et al., 2005) and analysis was run under default parameters using

Hallmark, C2, C3, C5 and gene ontology (GO) palate development gene sets (Liberzon et al., 2011).

II. 23. 1. Hallmark gene set

Initial analysis was run using the 'Hallmark' curated gene sets from the molecular signature database (Liberzon et al., 2011). The Hallmark gene sets include 50 separate curated sets that represent a range of biological processes, signalling pathways and some cellular components. The Hallmark gene sets have been experimentally validated previously and commonly used in an initial analysis. The gene expression data was also run using additional C2, C3, C5 databases and GO Palate Development pathway as briefly described below. A false discovery rate (FDR) threshold of <0.25 was used throughout.

II. 23. 2. C2 gene set

The C2 gene sets include 4762 gene sets that are curated from various sources including online pathway databases, the biomedical literature, and contributions from domain experts. The C2 collection is divided into two sub-collections: chemical and genetic perturbations (CGP) and canonical pathways (CanP). Most of the CGP sets are extracted from the biomedical literature and represent signatures from several important biological and clinical states. CanP gene sets are curated from the various online databases (e.g. BioCarta; KEGG; Pathway Interaction Database; Reactome; Signalling Gateway).

II. 23. 3. C3 gene set

The C3 gene sets represent potential targets of regulation by transcription factors or microRNAs. These include 836 sets that consist of genes grouped by the short sequence motifs that they share in their non-protein coding regions. These motifs are thought to represent known or likely cis-regulatory elements in promoters and

3'-UTRs. The C3 collection is divided into two sub-collections: MIR and TFT (Xie et al., 2005).

II. 23. 4. C5 gene set

The C5 gene sets (N=5917) are derived from GO annotation. A GO annotation consists of a GO term associated with a specific reference that describes the work or analysis upon which the association is based. GO terms describe an ontological system designed to provide a biologically meaningful annotation of genes and their products. Gene products can be associated with one or more GO terms. Each annotation includes an indication as to how the annotation to a particular term is supported (geneontology.org/page/guide-go-evidence-codes).

II. 23. 5. GO palate development gene set

The GO palate development gene set is found within the biological process ontology subgroup. It includes a number of genes previously demonstrated to be involved in palate development including: *ACVR2B; ALX1; ALX4; ANP32B; ARID5B; ASPH; BBS7; BCOR; BMPR1A; BNC2; C5orf42; CHD7; CLDN5; COL11A2; COL2A1; CSRNP1; DHRS3; DLG1; DLX5; DLX6; EPHB2; EPHB3; FOXE1; FOXF2; FRAS1; FZD1; FZD2; GABRB3; GDF11; GLI3; HAND2; IFT172; INHBA; INSIG1; INSIG2; JAG2; LEF1; LRP6; MEF2C; MEOX2; MMP25; MSC; MSX1; NPRL3; OSR1; OSR2; PAK1IP1; PKDCC; PLEKHA1; PRDM16; PRRX1; PYGO2; SATB2; SGPL1; SHH; SKI; SMAD2; SMAD4; SNAI1; SNAI2; SOS1; SOX11; SUMO1; TBX1; TBX2; TBX3; TCF21; TFAP2A; TGFB3; TGFBR1; TGFBR2; TGFBR3; TIPARP; TSHZ1; TWIST1; VAX1; WDPCP; WFIKKN1; WFIKKN2; WNT11; WNT3A; WNT5A; WNT7A; WNT8A; WNT9B*.

II. 24. Functional annotation of differentially expressed genes, the database for annotation, visualization and integrated discovery

Significantly differentially expressed genes were analysed using functional annotation tool based on the database for annotation, visualization and integrated discovery (DAVID) (david.ncifcrf.gov/summary.jsp). Input of lists of genes was entered and analysed using mouse background.

II. 25. *Tbx22*^{tm1Sta} targeted allele detail and nomenclature

---

MGI: 4361266

Symbol: *Tbx22*^{tm1Sta}

Synonyms: *Tbx22*^{flox}, *Tbx22tm1*$^{(flox/exon0-2/NEO)Sta}$

Gene: *Tbx22*

Location: ChrX:107667964-107688978 bp, + strand

Genetic Position: ChrX, 47.59 cM

Disease ortholog: X-linked CP with or without ankyloglossia

In this thesis floxed allele-carrying mice are denoted ***Tbx22***^{flox}, males as ***Tbx22***$^{flox/Y}$ and females as ***Tbx22***$^{flox/flox}$ or ***Tbx22***$^{flox/+}$ while *Tbx22* knockout mice are denoted ***Tbx22***^{null}, males as ***Tbx22***$^{-/Y}$ and females as ***Tbx22***$^{-/+}$. Tissue specificity of the knockout is designated either by *Mesp1*-Cre (CM) or *Wnt1*-Cre (CNC). Wild type animals are indicated as **WT**.

II. 26. Patient samples

Genomic DNA from members of the family shown in Figure II. 12, was extracted from saliva samples obtained with Oragene^{TM} DNA Self-Collection Kits (Genotek, #OG-250) according to the manufacturer's instructions. DNA samples were

extracted from whole blood taken at the time of surgery from a cohort of 312 individuals with either NS CP or SMCP, selected from more than 750 patients with CL/P collected from the North Thames Cleft Lip and Palate Service, GOSH. Informed consent was obtained from all participants and research studies were approved by the GOSH Research Ethics Committee (REC No 08/H0713/46). DNA extraction from saliva or blood was performed in the laboratories of the North East Thames Regional Genetics Service Laboratories, GOSH, Barclay House.

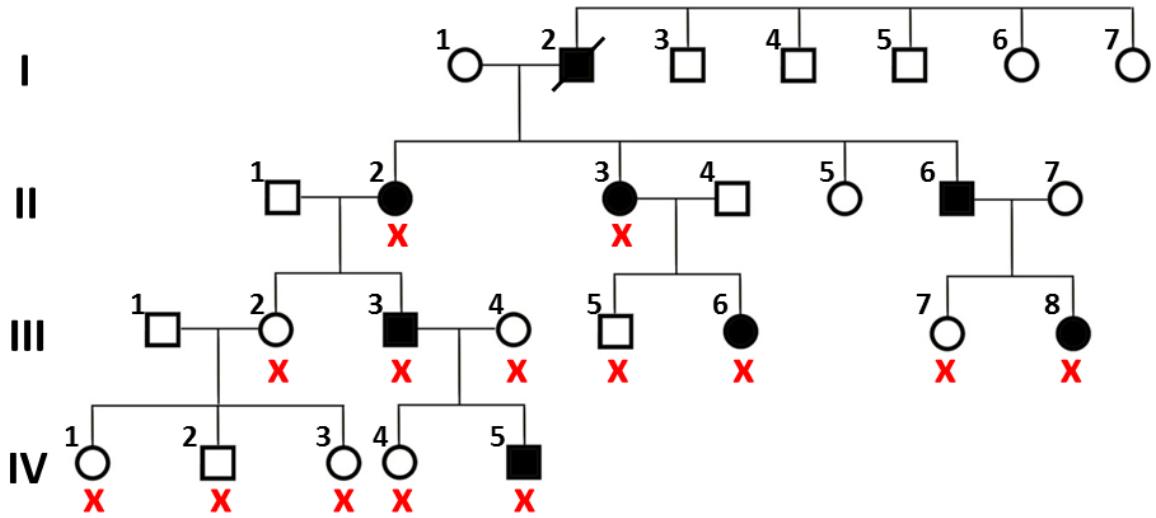

Figure II. 12. Family pedigree showing autosomal dominant inheritance of absent uvula and hypernasality.

Saliva samples were obtained from 14 individuals (**x**).

II. 27. Clinical evaluation

A diagnosis of VPI for IV.5 was made based on specialist speech and language therapy assessment, which was undertaken by Dr Debbie Sell (Sell et al., 1999) and by lateral videofluoroscopy which was carried out in the radiology department, GOSH (the method is described in more detail under III. 1. 6. Videofluoroscopy and nasendoscopy). II.2, II.3, III.3, III.4, III.5, III.6, III.8 family members' speech was assessed by Mr Brian Sommerlad.

II. 28. Cytogenetic analysis

Chromosomal microarray analysis of the proband's DNA was conducted by the North East Thames Regional Genetics Service Laboratories, GOSH, Barclay House, using the Affymetrix CytoScan 750K array. Initial interpretation following comparison to control databases and the GOSH data set was done by Ms Deborah Morrogh (principal scientist). This was followed by a qPCR assay for *FOXC1* (routinely conducted as follow up) to confirm the presence of the copy number variant (CNV) in 6p25.3 in the proband (IV.5) and to investigate inheritance from both parents (III.3, III.4) and the paternal grandmother (II.2).

II. 29. Linkage analysis

Genome wide SNP genotypes were generated by UCL Genomics from 11 members of the family (Figure II. 13) using the Infinium Human CoreExome-24 BeadChip (Illumina). III.5, III.7 and III.8 were not included at this time as samples from these individuals were not collected until a later date. Resulting data was used for linkage analysis (courtesy of Prof Martin Farrall, Wellcome Trust Centre for Human Genetics, Oxford) where a subset of informative SNPs were selected and used for parametric linkage analysis using the MERLIN program.

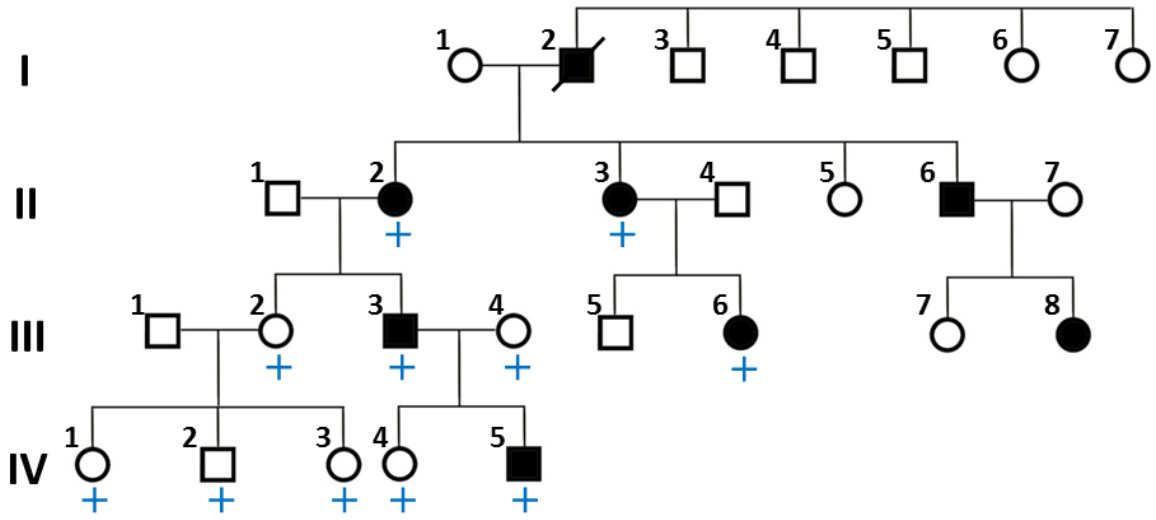

Figure II. 13. Family pedigree. Linkage analysis.

Eleven family members were genotyped for linkage analysis (+). III.5, III.7 and III.8 were not included at this time as samples from these individuals were not collected until a later date.

II. 30. Sequencing

Genomic DNAs from two affected (IV.5 and III.6) and one unaffected female (III.2) were subjected to exome sequencing, which was performed at the Next Generation Sequencing Service at the UCL Institute of Neurology. The SureSelect Human Exon Kit v.4 (Agilent Technologies) was used for sequencing according to the manufacturer's instructions. Adapters were ligated, and paired-end sequencing was performed on an Illumina HiSeq 2000, which generated 2x 50 bp reads. The mean exome coverage was 81 to 91 fold, and 98% and 86% of the target sequence was covered at least 10 to 30 times, respectively. Sequencing reads were aligned to the reference human genome (GRCh37/hg19) with the BWA consensus, variant bases were called with GATK and variants were annotated with ANNOVAR. Confirmation of all variants of interest, segregation analysis and *FOXF2* sequencing in additional patient cohorts, were all performed using Sanger sequencing according to standard methods and resulting sequence files were analysed on the Sequencher™ v5.4.6 (Gene Codes Corporation) platform (Figure II. 14).

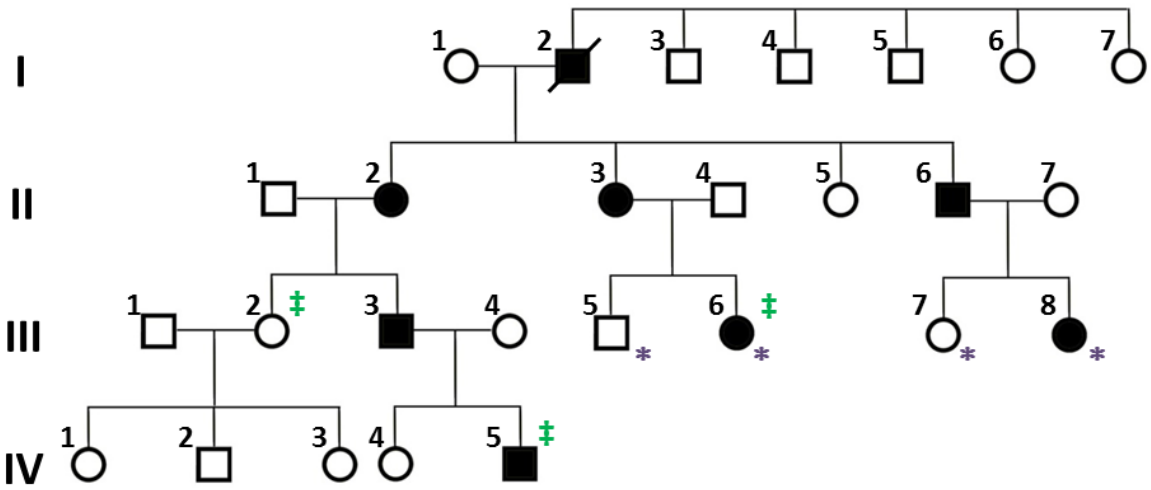

Figure II. 14. Family pedigree. Exome sequencing analysis.

Exome sequencing analysis was performed on 3 individuals (‡) and Sanger sequencing (*) was used to assess segregation of candidate gene variants in additional individuals.

II. 31. Exome sequencing analysis

Exome sequencing data was analysed under a dominant inheritance model with Ingenuity Variant Analysis software (Qiagen Bioinformatics) using the following parameters:

- **Confidence filter:** keep variants with a call quality of at least 20 in any case or control and with read depths of at least 10.
- **Common variants filter:** excluded variants with an allele frequency of at least 3% in the 1000 Genomes Project, 3% in the public Complete Genomics genomes and are present in dbSNP.
- **Genetic analysis filter:** keep variants that are associated with gain of function or are heterozygous, compound heterozygous, haploinsufficient, homozygous, het-ambiguous and occur in the case sample. It excludes variants that occur in at least 1 of the control samples.

- **Predicted deleterious filter:** keep variants that are experimentally observed/predicted to be associated with a phenotype (pathogenic, likely pathogenic, listed in HGMD), or are associated with loss of function of a gene (frameshift, in-frame indel, or start/stop codon change, missense, splice site loss up to 2 bases into intron or as predicted by MaxEntScan). Variants were investigated using the Ensembl Variant Effect Predictor, which includes a variety of *in silico* tools. The likely pathogenicity of missense variants and their effects on protein function were predicted using tools such as PolyPhen-2, SIFT, and v.1.3 CADD (with a threshold score of >15). Gene tolerance to variation was calculated for all variants using the residual variation intolerance score and then combined with the PROVEAN scores for missense variants, which combines Grantham and conservation scores. Population control databases accessed included the 1000 Genomes database, Exome Variant Server database, The Exome Aggregation Consortium (ExAC) and gnomAD as previously described (Ishida et al., 2018, McGrath et al., 1999, Hellqvist et al., 1996).

II. 32. Sanger sequencing

DNA sequencing of PCR products was performed using the Sanger dideoxy chain termination method (Sanger et al., 1992). In a Thermo-Fast® 96-well PCR plate 3-4 µL of PCR products were purified and precipitated by adding an equal volume of microCLEAN (Microzone, ref: 2MCL5). The plate was covered with MicroAmp® clear adhesive film (ThermoFisher, #4306311), vortexed and left for 5 min at room temperature, followed by centrifugation step at 1216 x g for 40 min at room temperature. MicroCLEAN was removed by centrifugation of the plate set upside down on a tissue at 27 x g for 1 min. The sequencing mixture was then added to the precipitate (Table II. 12).

Table II. 12. Standard Big Dye Terminator sequencing reaction mix.

Reagent	Volume (µL) per reaction
BigDye® Terminator v1.1	1
BigDye® Terminator v1.1 buffer (5x)	2
Betaine (5 M)	2
Forward or reverse primer (50 ng/µL)	0.5
DEPC-treated water	4.5

The sequencing program consisted of an initial incubation step at 96°C for 1 min, and 34 cycles of: incubation at 96°C for 30 sec, 53°C for 15 sec, 60°C for 4 min and at 20°C for 2 min. The sequencing products were then precipitated by adding 50 µL of the precipitation mix (5 mL of 3 M NaAc (sodium acetate) at pH 5.2, 125 mL of 100% EtOH and 40 mL of Milli-Q water) in each sample. The plate was left at room temperature for 20 min and it was then centrifuged at 684 x g for 40 min at 10°C. The solution was removed and the pellets were washed with 50 µL of 70% EtOH and spun at 684 x g for 10 min at 10°C. The EtOH was removed by spinning the plate upside-down at 7 x g for 1 min and the resulting pellets were resuspended in 10 µL of 1:10 1x TE (Tris and EDTA) buffer. The plate was then run on an ABI 3730xl DNA analyser by arrangement with staff in the North East Thames Regional Genetics Service Laboratories, GOSH, Barclay House.

II. 33. Bioinformatics analysis of candidate genes

The candidate genes were analysed by following tools:

- **SIFT** predicts whether an amino acid substitution affects protein function. The prediction is based on the degree of amino acid conservation in sequence alignments derived from closely related sequences that are collected through PSI-BLAST (Vaser et al., 2016): http://sift.jcvi.org.

- **PolyPhen-2** (Polymorphism Phenotyping v2) is a tool used to predict the possible impact of an amino acid substitution on the structure and function of a human protein using both physical and comparative considerations (Adzhubei et al., 2013): http://genetics.bwh.harvard.edu/pph2.

- **MutationTaster** evaluates disease causing potential of sequence alterations (Schwarz et al., 2010): http://www.mutationtaster.org.

- **Provean** predicts whether a protein sequence variation affects protein function (Choi and Chan, 2015): http://provean.jcvi.org/about.php.

- **Condel** (CONsensus DELeteriousness score of missense single nucleotide variants (SNVs)) - combines various tools (MutationAssessor, FATHMM) to assess the outcome of non-synonymous SNVs using a consensus deleteriousness score (Yuan et al., 2018): https://omictools.com/consensus deleteriousness-score-of-missense-snvs-tool.

- **LoFtool** provides a gene intolerance score. This provides an estimate of the consequent susceptibility to disease based on the ratio of loss-of-function to synonymous mutations for each gene in 60,706 individuals from ExAC. The score is adjusted for the gene *de novo* mutation rate and evolutionary protein conservation (Fadista et al., 2017): http://www.ensembl.org/info/docs/tools/vep/index.html.

- **FATHMM** is a high-throughput web-server capable of predicting the functional consequences of both non-synonymous SNVs and non-coding variants (Rogers et al., 2018): http://fathmm.biocompute.org.uk.

- **Mutation assessor** is used to predict the functional impact of an amino acid substitution in a protein, e.g. mutations discovered in cancer or missense polymorphisms. The functional impact is based on evolutionary conservation of the affected amino acid in protein homologs: http://mutationassessor.org/r3.

- **Meta LR** is a logistic regression based method, which incorporated 10 scores (SIFT, PolyPhen-2 HDIV, PolyPhen-2 HVAR, GERP++, MutationTaster, Mutation Assessor, FATHMM, LRT, SiPhy, PhyloP) and the maximum

frequency observed in the 1000 genomes populations. The larger value of a SNV, the more likely it is to be damaging. Scores range from 0 to 1: http://www.ensembl.org/info/docs/tools/vep/index.html.

- **Meta SVM** is a support vector, machine-based ensemble prediction score that incorporated 10 scores (SIFT, PolyPhen-2 HDIV, PolyPhen-2 HVAR, GERP++, MutationTaster, Mutation Assessor, FATHMM, LRT, SiPhy, PhyloP) and the maximum frequency observed in the 1000 genomes populations. The larger value of a SNV, the more likely it is to be damaging. Scores range from -2 to 3 in dbNSFP: http://www.ensembl.org/info/docs/tools/vep/index.html.
- **GERP** is a site conservation score. The larger the score, the more conserved the site is. Scores range from -12.3 to 6.17: http://www.ensembl.org/info/docs/tools/vep/index.html.
- **CADD** is a tool for scoring the deleteriousness of SNVs as well as insertion/deletion variants in the human genome: http://www.ensembl.org/info/docs/tools/vep/index.html.

II. 34. Collagen coated substrate

Tissue culture 60 mm dishes were coated with collagen (Life Technologies, #A10483-01) overnight at 37ºC. On the day of cell seeding, collagen was removed and the cells were seeded immediately.

II. 35. Cell culture

HeLa and HepG2 cells were cultured in 10% fetal bovine serum (FBS) (ThermoFisher, #10500064) prepared in DMEM (ThermoFisher, #41966052) supplemented with penicillin and streptomycin (ThermoFisher, #15140122). Both cell lines were passaged with 0.25% trypsin-EDTA (ThermoFisher, #25200056) when they approached 80% confluency.

II. 36. Constructs

A full length (1-447aa) *FOXF2* cDNA (pCMV6-XL4-*FOXF2*) and matching 'empty' vector were purchased from OriGene (Figure II. 15). The p.Q433P variant was introduced using site-directed mutagenesis (GeneArt®, Invitrogen). Sequence integrity was confirmed by Sanger sequencing. A Firefly luciferase reporter construct containing 4 copies of the FOXF2 binding site CAACGTAAACAATCCGA (Hellqvist et al., 1996) was synthesized by GeneScript (Figure II. 16). Cells were co-transfected with the reporter *Renilla* luciferase construct (Promega) for normalization.

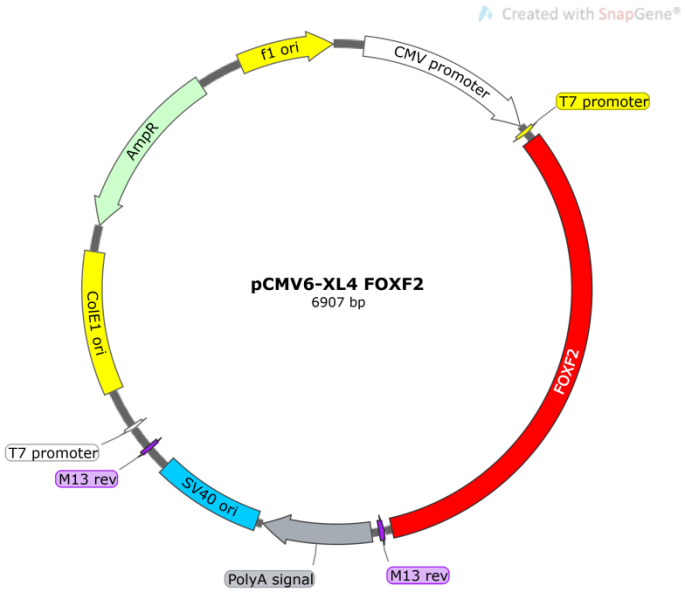

Figure II. 15. Human full length *FOXF2* cDNA clone.

The 2.2 kb *FOXF2* cDNA insert is cloned into the ampicillin resistant pCMV6-XL4 vector (size ~4.7 Kb). The diagram was created with SnapGene®.

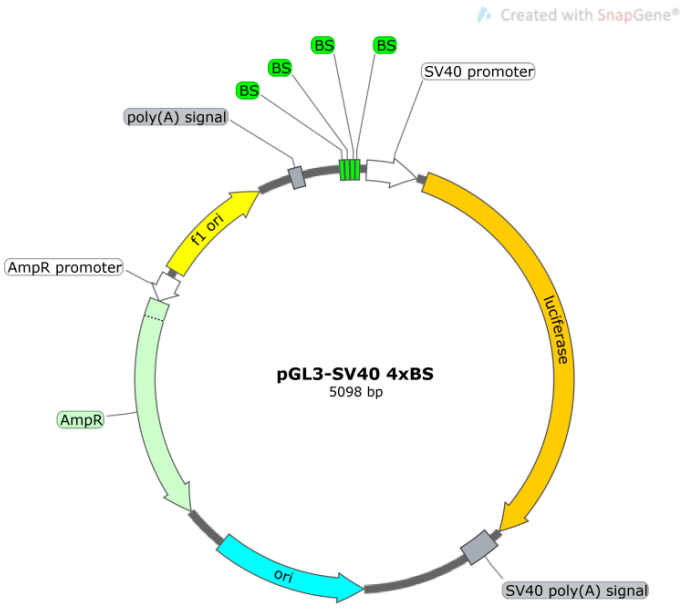

Figure II. 16. Firefly luciferase FOXF2 reporter construct.

Four copies of the FOXF2 binding site CAACGTAAACAATCCGA were cloned in front of the SV40 promoter in the luciferase containing vector pGL3-SV40. The diagram was created with SnapGene®.

II. 37. FuGENE® 6 transfection

HeLa or HepG2 cells used for transfection were centrifuged for 5 min at 200 x g to pellet. The cell pellet was then suspended in culture medium and plated one day before transfection at two different densities ($1x10^4$ and $2x10^4$ cells in 100 µL per well of a 96-well plate, growth area 0.32 cm^2). On the day of transfection, the wells with 80% confluent cells were chosen. The volumes of medium, DNA and FuGENE® 6 (Promega, # E2691) transfection reagent added per 10 wells of a 96-well plate are represented in Table II. 13, with a total volume of 100 µL per well. The time required to perform the FuGENE® 6 transfection reagent/DNA complex was 15 min at room temperature. The transfected cells were then incubated for 24 or 48 hours before assaying to allow time to express the transfected DNA.

Table II. 13. The medium, DNA and FuGENE® 6 transfection reagent added per 10 wells of a 96-well plate.

	FOXF2 cDNA	FOXF2 Q433P	FOXF2 A25G	FOXF2 A41S	Vector	Control
DNA	112 ng	112 ng	112 ng	112 ng	0	0
Luc-Rep	561 ng	561 ng	561 ng	561 ng	561 ng	0
Renilla	56 ng	56 ng	56 ng	56 ng	56 ng	0
Vector	112 ng	112 ng	112 ng	112 ng	224 ng	0
Optimem	84.21 µL	84.21 µL	84.21 µL	84.21 µL	84.21 µL	0
FuGENE® 6	2.53 µL	2.53 µL	2.53 µL	2.53 µL	2.53 µL	0
Medium	1 mL	1 mL	1 mL	1 mL	1 mL	1.1 mL

II. 38. Luciferase reporter assay

Firefly and *Renilla* luciferase activities were measured at two days post transfection using the Dual-Luciferase Reporter Assay System (Promega) in Nunc F96 MicroWell White plates on a FLUOstar Optima plate reader (BMG Labtech, UK) following manufacturer's instructions. Each sample was normalized by dividing the test reporter activity (Firefly) by the control reporter activity (*Renilla*). All reporter assay experiments were performed in triplicate and each construct was analysed in at least three independent experiments in two cell lines (HeLa and HepG2). Statistical comparisons were performed using Student's t-test. All graphs are represented as the mean ± standard deviation. $p<0.05$ was considered statistically significant.

II. 39. Protein extraction and loading buffer preparation

Following lysis, all extraction steps were carried out on ice. Samples were lysed in protein extraction KCl buffer composed of 50 mM Tris HCl pH 8.0, 10% glycerol (ThermoFisher, #15514011), 5 mM EDTA, 150 mM KCl, phenylmethanesulfonyl fluoride (Sigma-Aldrich, #93482), 1x complete protease inhibitor cocktail (Roche, #11836153001) in deionised water cooled to 4°C. Lysates were centrifuged at 10000 x g for 30 min at 4°C. The supernatant was transferred into a new tube and centrifuged at 10000 x g for 20 min at 4°C. The lysate was then stored at -80°C for further experiments.

Then lysates were prepared using 4x Laemmli buffer containing 250 mM Tris HCl pH 6.8, 4% SDS, 0.06% (w/v) bromphenol blue, 20% glycerol, 10% beta-mercaptoethanol. Finally the Laemmli buffered protein lysates were denaturated at 75°C for 10 min.

II. 40. Protein expression assays

Western blotting was performed as previously described (Bryant et al., 2018). The resolving gel was formulated using 4X Protogel® Resolving Buffer (National Diagnostics, #EC-892) and Protogel® (National Diagnostics, #EC-890) to a concentration appropriate for each assay (Table II. 14). Ammonium persulfate (ThermoFisher, #A/P470/46) and TEMED (Sigma-Aldrich, #T-8133) was added to set the gel to induce polymerisation while butanol was spread along the top to keep the surface level. After the resolving gel had set, the butanol was washed away and the stacking gel, containing Protogel® Stacking Buffer (National Diagnostics, #EC-893), Protogel®, ammonium persulfate and TEMED (Table II. 14) was added, along with a comb to structure the loading wells.

Table II. 14. Reagents and details for casting two gels for western blot assays.

Reagent	Resolving gel*			Stacking gel
	10%	12%	15%	
Protogel® (National Diagnostics, #EC-890)	3.33 mL	4 mL	5 mL	0.65 mL
4X Protogel® resolving buffer (National Diagnostics, #EC-892)	2.6 mL	2.6 mL	2.6 mL	None
Protogel® stacking buffer (National Diagnostics, #EC-893)	None	None	None	1.25 mL
Double distilled water	3.96 mL	3.29 mL	2.39 mL	3.05 mL
10% Ammonium persulfate** (ThermoFisher, #A/P470/46)	100 µL	100 µL	100 µL	50 µL
TEMED (Sigma-Aldrich, #T-8133)	10 µL	10 µL	10 µL	10 µL

*The amount of Protogel® in the resolving gel was based on the size of the target protein.

**10% Ammonium persulfate was made in double distilled water.

The gel was inserted into an electrophoresis tank filled with electrophoresis grade 25 mM Tris, 192 mM glycine and 0.1% SDS prepared from a 10x running buffer solution (Flowgen Bioscience, #EC-870). Protein samples prepared in Laemmli buffer (II. 39. Protein extraction and loading buffer preparation) were loaded into the wells along with ColorPlus Prestained Protein Marker, Broad Range, 7-175 kDa (New England Biolabs, #P7709S) for reference. The gel was run for a time appropriate to achieve optimal resolution of the target protein.

The resolved proteins were transferred to 0.45 µm nitrocellulose membrane (BIO-RAD, #162-0115) by semi-dry transfer. The transfer was carried out in a buffer composed of 15.4 g/L glycine, 3 g/L Tris and 20% methanol in deionised water for 30 min. On completion of the transfer, the membranes were treated with 3% milk in PBS on a shaker for 60 min. Following 3 washes in PBS, the

membranes were incubated overnight at 4°C in 1% milk-PBST solution containing the primary antibody (Table II. 15).

The next day, the membranes were treated with 6 PBST washes before a 1 hour secondary antibody incubation period (Table II. 15). After the membranes were treated with 6 more PBS washes they were ready to be developed. The membranes were developed using an Amersham ECLTM Western Blotting Kit (GE Lifesciences, #RPN2109) and Amersham Hyperfilm ECLTM (GE Lifesciences, #28906837). Following imaging with the ChemiDoc system (Bio-Rad), relative protein expression was analysed in Image J software.

Table II. 15. Antibody incubation details for western blot assay.

Antibody	Milk	Dilution	Tween*	Time
Human anti-FoxF2 IgG AF 6988 (R&D Systems, #Q12947)	1%	1:2000	0.1%	15 hours**
Mouse anti-GAPDH (Merck, MAB374)	1%	1:4000	0.1%	15 hours**
Rabbit anti-Sheep IgG HRP (Invitrogen, #31480)	None	1:2000	0.1%	1 hour
Goat anti-Mouse IgG HRP (Invitrogen, #31326)	None	1:2000	0.1%	1 hour

* Tween 20® (Sigma-Aldrich, #P7949). ** Timed incubation at 4°C, otherwise incubations were done at room temperature.

II. 41. Image analysis

Images to be quantified were exported as TIF files and analysed using Image J software (http://imagej.nih.gov/ij/index.html) using the 'Gels analysis tool' (Schneider and d'Adda di Fagagna, 2012). Band density peaks were analysed using the 'Wand tool' to select an area beneath the peak and the data was

exported to ROI manager. The density of the protein band of interest was normalized to that of reference protein. Data was analysed using one-way ANOVA.

II. 42. Tissue *in situ* hybridization

Preparation and *in situ* hybridization of wax embedded, coronal sections from human embryonic Carnegie stage (CS) 22 and CS23 and fetal material from 8th post conception week (L8pcw) was performed using samples collected by the Medical Research Council, Wellcome Trust Human Developmental Biology Resource (HDBR) with full ethical approval from the National Research Ethics Service, Grant #099175/Z/12/Z (Gerrelli et al., 2015, McGrath et al., 1999). All the relevant sections were selected by me and I assisted by generating the *in situ* probe. *In situ* experiments were performed by Ms Nadjeda Moreno of the HDBR. Resulting images were provided to me for interpretation.

Paraffin sections were dewaxed in two changes of histoclear and gradually hydrated in decreasing EtOH concentrations (100%, 75%, 50%, 25% - each stage 2 min). Sections were washed twice in PBS and fixed for 20 min in PFA. Then sections were washed twice in PBS, incubated with 20 µL/mL proteinase K (Sigma-Aldrich, #P2308) for 8 min and post-fixed in 4% PFA:PBS at room temperature for 5 min. After two washes in PBS, sections were treated with 0.1 M tetraethylammonium/0.25% acetic anhydride for 10 min, washed again twice in PBS. Dehydrated and air-dried slides were covered with 300 ng DIG-labelled riboprobe, hybridisation mix (50% formamide, 0.3 M NaCl, 20 mM Tris pH 8.5, 5 mM EDTA pH 8.0, 1x Denharts solution, 10% dextran sulphate), tRNA (0.5 mg/mL) and RNAse inhibitor (1 µL/mL), cover slipped and the mixture was incubated overnight at 65°C to allow hybridisation of probes to the tissue mRNA. Post-hybridisation washes were performed [2x standard sodium citrate (StSC), 65°C; 0.2x StSC, 65°C; 2x formamide wash (350 mL formamide, 70 mL 20x StSC, 280 mL dH_2O)], and slides were incubated for 1 hour in 150 mM NaCl and 100 mM Tris HCl, pH 7.5, containing 10% fetal calf serum followed by incubation with anti-DIG:alkaline phosphatase and expression was visualised using NBT/BCIP

(Sigma-Aldrich, #11681451001), sections mounted using Vectamount (Vector Laboratories, #H-5000) (Harkin et al., 2016).

FOXF2 in situ probes were generated from a 650 bp PCR fragment from the 3' UTR of the gene (RefSeq: NM_001452), which was cloned into pGEM®-T Easy (Promega, #A1360). Sense and antisense probes were synthesized using T7 or Sp6 primers respectively (Ghafoory et al., 2012).

Chapter III: Histological study of palate muscles: comparison between submucous cleft palate, normal and other cleft types

III. 1. Introduction

III. 1. 1. Velopharyngeal mechanism

The velopharyngeal mechanism consists of a muscular valve that extends from the posterior surface of the hard palate to the posterior pharyngeal wall and includes the velum, lateral pharyngeal walls and the posterior pharyngeal wall (Perry, 2011). Adequate velopharyngeal closure is essential during the activities of swallowing and speaking. These functions are complex motor skills that are achieved by synchronised coordination of several upper aerodigestive tract muscle groups that can collectively be described as the velopharyngeal port musculature (Figure III. 1, Table III. 1).

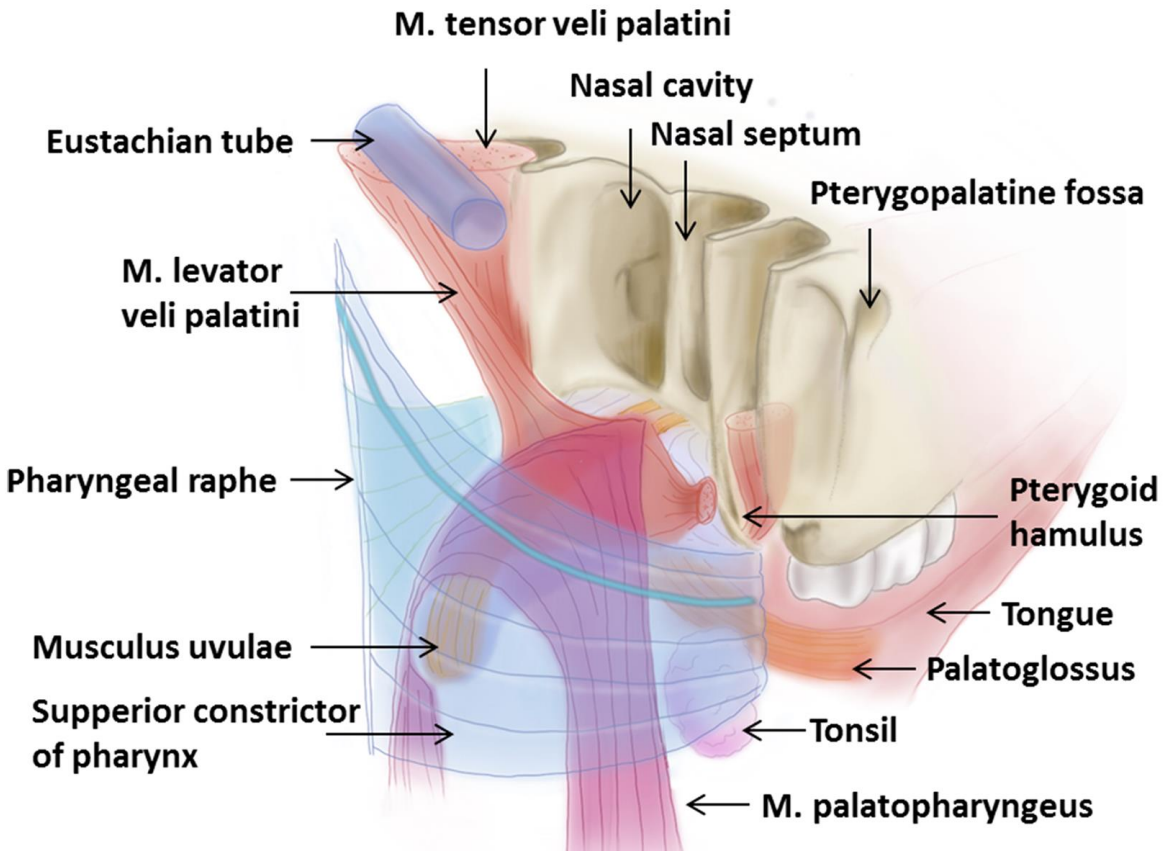

Figure III. 1. Velum and surrounding structures.

Adapted from (Carstens, 2017).

Table III. 1. Velopharyngeal port musculature.

Muscle	Position	Innervation	Function
Levator veli palatini (Figure III. 2, 1)	▪ Arises from the petrous apex and cartilaginous portion of the Eustachian tube. ▪ Inserts in the middle third of the soft palate and blends with the contralateral levator.	Pharyngeal plexus from CN IX and X.	▪ Pulls the velum in a posterosuperior direction. ▪ The major elevator for the velum.
Palatoglossus (Figure III. 2, 2)	▪ Arises from the anterior surface of the soft palate. ▪ Inserts into the lateral aspect of the tongue base.	Pharyngeal plexus.	▪ Simultaneously lowers the velum and elevates the tongue upwards and backwards.
Palatopharyngeus (Figure III. 2, 3)	▪ Arises from the soft palate. ▪ Part passes downwards and inserts into the posterior border of the thyroid cartilage. ▪ A transverse component passes around the pharynx.	Pharyngeal plexus.	▪ Positions the velum. ▪ Raises the larynx and lowers the pharynx. ▪ Narrows the velopharyngeal orifice by adducting the posterior pillars and constricting the pharyngeal isthmus.

Table III. 1. (continued).

Tensor veli palatini (Figure III. 2, 4)	▪ Arises from the scaphoid fossa, spine of the sphenoid, and the cartilaginous portion of the Eustachian tube. ▪ It inserts into a tendon which passes around the hamular process and forms the palatal aponeurosis of the anterior third of the soft palate.	Mandibular branch of CN V.	▪ Tenses the soft palate. ▪ Opens the Eustachian tube during swallowing.
Musculus uvulae (Figure III. 2, 5)	▪ Starts from the palatal aponeurosis posterior to the hard palate. ▪ Inserts into the uvula mucosa.	Pharyngeal plexus.	▪ Ads bulk to the dorsal aspect of the uvula.
Superior constrictor	▪ Arises from the lower portion of the pterygoid plate and the hamular process. ▪ Inserts into the median raphe.	Pharyngeal plexus.	▪ Produces medial movement of the pharyngeal walls. ▪ Assists in drawing the velum posteriorly.

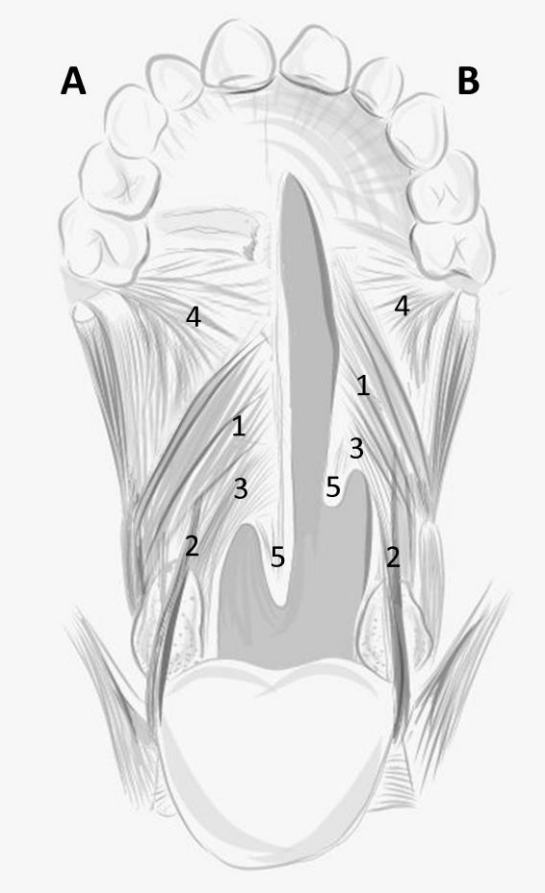

Figure III. 2. Soft palate anatomy.

A) Normal palate; **B)** cleft palate. **1** - Levator veli palatine; **2** - palatoglossus; **3** - palatopharyngeus; **4** - tensor veli palatine; **5** - musculus uvulae.

VPD is a condition where the velopharyngeal valve fails to close consistently or completely (Abduelmula et al., 2016). VPI describes an anatomical or structural defect that prevents adequate velopharyngeal closure. VPI is the most common type of VPD, usually resulting from a short or abnormal velum, which often occurs in CP or SMCP patients. Velopharyngeal incompetence refers to a neuromotor or physiological disorder, which results in poor movement of the velopharyngeal structures (Kummer et al., 2015). This is common in individuals suffering dysarthria due to cortical damage or velar paresis due to cranial nerve (CN) damage. The term velopharyngeal mislearning is also sometimes used and refers to inadequate velopharyngeal closure when attempting certain sounds due to learned misarticulations.

Velopharyngeal closure in phonation is quite distinct from the closure required for swallowing, although in patients with VPD, both aspects can be affected together or separately. In clinical practice, it has been observed that adequate velopharyngeal closure achieved when swallowing, does not necessarily lead to an adequate closure that is required for speaking (Swibel Rosenthal et al., 2018).

A column of air pressure passing from the lungs through the subglottis into the upper airway is described as phonation (Kummer, 2011b). Inadequacy of the velopharyngeal sphincter allows air to escape through the nose during the generation of consonants that normally require a high oral pressure. In such circumstances speech production is compromised by inappropriate nasal resonance and this will affect speech intelligibility (Kummer, 2011a).

In the English language, velopharyngeal closure is required for all phonemes (these are distinct units of sound in a given language that distinguish one word from another) with the exception of three, /m/, /n/, /ng/. These are produced with a nasal resonance while the velopharyngeal portal is open. Oral resonance is extremely important for the production of intelligible speech, particularly in languages which use many phonemes such as English, Danish, Finnish and others (Maddieson, 1984). As a consequence, VPI remains a challenging clinical problem (Chen et al., 1994).

III. 1. 2. Organization of intravelar structures

The anterior soft palate consists of mucous-secreting glands, as well as an abundance of adipose tissue (Kuehn and Moon, 2005). The tensor veli palatini (TVP) tendon is close to the nasal surface and is prominent in the most anterior region, just posterior to the hard palate. The middle one third of the soft palate consists of muscle tissue. There are LVP fibres coursing transversely across the midline to meet the contralateral levator. Musculus uvulae fibres are encapsulated in a sheath on the nasal side of the levator and course longitudinally, perpendicular to and cradled by the levator sling and PP fibres located laterally and not approaching the midline. The musculus uvulae is variable across and within

specimens in terms of its paired versus unpaired nature. It is the only longitudinal structure in the soft palate and lies on the nasal surface of the other muscles (Figure III. 1).

III. 1. 3. Soft palate function

The soft palate is a muscular structure attached to the posterior edge of the bony palate by its aponeurotic structure (Podvinec, 1952). The posterior edge of the soft palate forms a free and easily moving arch. In the normal soft palate, the muscles enter from the lateral aspect and each pair of muscles form a sling which moves the velum either superiorly or inferiorly. The levator pulls the palate upwards and backwards. The descending part of palatopharyngeus (and perhaps the palatoglossus) pulls the palate downwards and backwards. The transverse component of palatopharyngeus creates part of the sphincteric function of the velopharyngeal mechanism and is thought to be responsible for a muscular structure known as Passavant's ridge which develops on the posterior pharyngeal wall in some individuals. The hamulus is rounded by the tendon of the tensor which helps to form the soft palate aponeurosis (Figure III. 2). The uvula has been shown to produce and secrete thin saliva (Back et al., 2004).

III. 1. 4. Aetiology of velopharyngeal dysfunction

VPD is characterised by hypernasality and/or nasal emission/turbulence. Hypernasality is a speech disorder that is characterized by excessive sound resonating in the nasal cavity during non-nasal sounds (Tardif et al., 2018). Nasal emission and turbulence are the audible escape of air, particularly with consonants. Hypernasality and VPD may be caused by different reasons. They range from structural abnormalities (e.g. cleft palate, craniofacial disorders, tumours) to neurological and/or muscular problems such as neuromuscular syndromes, 22q11.2 deletion syndrome (22q11.2 DS) and stroke. The aetiological factors could be divided into two major groups: anatomical abnormalities of the palate and functional abnormalities unassociated with anatomical palatal defects.

CP is the most common cause of VPD (Sullivan et al., 2011). A link between VPD and CP is obvious as it has been reported to occur in 5% to 66.5% of patients following CP repair (de Blacam et al., 2018, Ha et al., 2015, Hosseinabad et al., 2015, Mapar et al., 2019). Less commonly the nasopharynx can be too large (e.g. in 22q11.2 DS patients) or VPD can develop after adenoidectomy and/or tonsillectomy or after tonsils and adenoids involute in a child, often around the age of 10 years.

Structural and neuromuscular causes of VPD are distinguished from developmental or mislearning errors. In clinical practice the velopharyngeal function (VF) is determined by perceptual assessment as well as using instrumental investigations such as lateral videofluoroscopy and nasendoscopy (Hodgins et al., 2015). Real time magnetic resonance imaging (MRI) of VF has also been described thus leading to the possibility of normative three-dimensional data sets. Real time information may also help one to better understand physiological causes such as muscle hypotonia or poor co-ordination rather than just anatomical causes of VPD (Park et al., 2015, Wylezinska et al., 2015).

III. 1. 5. Clinical representation of velopharyngeal dysfunction

Nasal regurgitation during feeding may be a precursor of VPD. Inadequate closure of the velopharyngeal port during speech may lead to hypernasal resonance, nasal emission (either nasal friction or turbulence) and reduced pressure for oral pressure consonants (de Blacam et al., 2018). Inability to produce oral pressure consonants may result in faulty adaptation. Compensatory mechanisms include speaking with a soft intensity in order to decrease the airflow through the nasal cavity, or the opposite, speaking with a loud intensity or trying to project the voice. This can result in hoarseness and even nodules on the vocal cords. Compensatory articulation can be developed such as glottal stops and pharyngeal fricatives and substituting correct phonemes with those requiring less airflow. VPI also causes the speaker to use the posterior part of his tongue and hypopharynx to produce sounds known as backing or glottal speech. A facial grimace may also be seen, a compensatory mechanism trying to close anterior nares to restrict the nasal airflow.

III. 1. 6. Videofluoroscopy and nasendoscopy

Assessment of the structure, movement, extent of closure, and timing of the velopharyngeal mechanism can be very helpful in clinical management of patients with VPD. The most common methods to visualize the velopharyngeal mechanism in action are videofluoroscopy and nasendoscopy, which significantly add to a patient's assessment (Abduelmula et al., 2016). Videofluoroscopy uses ionizing radiation during movements of the structures of the velopharynx from different imaging planes (Ysunza et al., 2016) and gives information about velar length, size of gap and the position of the levator insertion. The disadvantages of the study are: it only provides a two-dimensional view, does not display the closure pattern and the patient is exposed to radiation. However, in many cases this examination is preferred by specialists as it is less invasive and more child friendly compared to nasendoscopy or MRI study. Nasendoscopy provides a dynamic direct visualization and *in vivo* imaging of the vocal tract during articulation (Golding-Kushner et al., 1990). It is useful for closure pattern assessment, but requires more cooperation from the patient. However, it may be contraindicated in certain cases such as unusual or narrow nasal airways or bleeding disorders. Nasendoscopy is a standard visualization tool, but does not provide objective values, while videofluoroscopy provides measurements and ratios as well as objective and comparable VPI assessment outcomes. Therefore, combining videofluoroscopy and nasendoscopy has become the best approach for assessing VF (Ysunza et al., 2015).

III. 1. 7. MRI for velopharyngeal function evaluation

MRI is an imaging method that is noninvasive and does not require radiation exposure. It is easily repeatable and allows for static and dynamic views of underlying musculature and velopharyngeal structures (Perry et al., 2017, Naran et al., 2017). To date, MRI investigations in children have been limited to tasks where simple, prolonged singular sound production are recorded (Sagar and Nimkin, 2015). This is partly due to the difficulties associated with MRI imaging of children at the young age for monitoring their early speech. Also, the capture rate of the

technology in terms of frames per second has been relatively slow to properly analyse the complexity of dynamic speech, although this aspect of the technology is improving. Nevertheless, a clinical tool for assessing velopharyngeal structure and muscle function would be of benefit (Silver et al., 2011). For example, a fast oblique coronal MRI view would allow assessment of the levator muscle function in a way that is not possible using traditional imaging methods. Dynamic imaging of the vocal tract with MRI is therefore still developing field for research. There is as yet no consensus in such areas as preferred sequences, reconstruction methods and choice of parameters (Lingala et al., 2016).

III. 1. 8. Palate muscle histology

There have been only a limited number of studies performed to investigate the histological structure of palate muscles and these have limitations, such as small sample numbers, age variation, lack of controls for comparison, diverse biopsy location and most of them use post-mortem tissue. Moon et al. (1998) report LVP muscle fibre analysis in 12 adult non-cleft cadavers and suggested their findings act as a baseline against which to relate CP fibre type data. The study showed an average of 59.8% type I (slow twitch) muscle fibres across all specimens with 67.4% in males and 54.4% in females. In a comparison of LVP in ICP infants with non-cleft adult cadavers, type I muscle percentage was 37% and 75% respectively (Lindman et al., 2001). It has been suggested that different palate muscles have specialized functional roles such that the PP and uvula muscles are involved in quick movements whereas the LVP and TVP muscles perform slower contractions (Stal and Lindman, 2000). It is also known that velar musculature generally has a high aerobic sufficiency, special proprioceptive control, whilst each muscle has only one skeletal insertion and is required to work at low load and tension (Stal and Lindman, 2000). These reasons may ultimately influence the organisation of individual velar muscles that determine the palate's functional capacity. Therefore, further detailed study of specific palate muscles is still required, particularly in relation to function, and also for SMCP as a novel study group. This could provide a better understanding of the differences between ICP and SMCP in terms of

clinical outcomes and may influence decision making to plan surgical procedures as well as managing expectations.

III. 1. 9. Clinical significance of 22q11.2 deletion syndrome

22q11.2 DS (OMIM 611867), also known as velocardiofacial (OMIM 192430) or DiGeorge syndrome (OMIM 188400) is an autosomal dominant condition that affects both males and females equally with an approximate incidence of 1:4000 (Murphy and Scambler, 2005). The clinical findings associated with 22q11.2 DS vary widely between patients and include CP, SMCP, VPI without CP, cardiac abnormalities, musculoskeletal disorders, thymic aplasia or hypoplasia, T-cell abnormalities and dysmorphic facial appearance (McDonald-McGinn et al., 1997, Kirschner and Baylis, 2014). The causes of VPI include recognizable anatomical anomalies such as CP, SMCP, hypoplasia and asymmetry of the LVP (Filip et al., 2017), and a large pharynx, as well as physiological problems related to neuromuscular dysfunction. The anatomical and physiological anomalies that lead to VPD in patients with 22q11.2 DS make the surgical management challenging and results unpredictable. Various protocols exist to address the abnormalities in the velum, pharynx or both in a synchronous or staged manner (Mehendale et al., 2004, Bohm et al., 2019). However, by making surgical decisions based on velopharyngeal anatomy and function, velar muscles abnormalities should be taken into consideration.

III. 1. 10. Clinical significance of Robin sequence

RS is defined as micro- and/or retrognathia, glossoptosis, airway compromise and CP (Jones et al., 2013). RS is not a syndrome but rather describes a sequence of disorders, where one abnormality results in the next. Nevertheless, it is related to several craniofacial anomalies and often appears in conjunction with a syndromic diagnosis. In fact, approximately 50% of RS cases are reported to be syndromic (Caouette-Laberge et al., 1994, Evans et al., 2006, Izumi et al., 2012). The three most common syndromes are Stickler (types I-V OMIM 108300, 604841, 609508,

614134, 614284), 22q11.2 DS and Treacher-Collins (OMIM 154500) accounting for 65% of the syndromic cases (Van den Elzen et al., 2001, Gangopadhyay et al., 2012, Caouette-Laberge et al., 1994). More than 50 syndromes have been described in association with RS (Tan et al., 2013). The incidence of RS in UK is 1:8500 (Bush and Williams, 1983) but varies in publications because of the different methods used to collect data from different time periods (Vatlach et al., 2014, Printzlau and Andersen, 2004) and difficulties in defining the condition.

The management of infants with RS is complex and many improvements still need to be made. MDT care is essential to address the different pathologies encountered throughout infancy, childhood and adulthood. It is common for a wide U-shaped CP to be associated with RS and is reported in 73-90% of cases (Caouette-Laberge et al., 1994, Butow et al., 2009, Maas and Poets, 2014). CP repair may be done later than other CP patients and is usually left until breathing and feeding difficulties have been dealt with. Also the choice of surgical technique to close the usually wide CP is challenging and may include a staged approach (Morice et al., 2018). Patients with RS CP have been shown to have worse speech outcomes than patients with ICP (Hardwicke et al., 2016, Stransky et al., 2013). They also have higher oronasal fistula rates (Witt et al., 1997), a higher risk of secondary surgery for VPI (Witt et al., 1997) and the possibility of later pharyngeal surgery in order to manage obstructive sleep apnoea (Thieme et al., 2005).

III. 2. Aims

While surgery used to repair palate defects is relatively successful, a subset of patients can remain problematic. As such there is still a clinical need to improve surgical outcomes in these patients. The objective of this study therefore represents an attempt to better characterise the muscle architecture and histology in a range of cleft palate disorders. Improving our understanding of the underlying muscle pathology will help to provide a more logical rationale according to diagnosis for the most appropriate surgical treatment.

The aims are:

- To identify the surgical management pathway for patients with SMCP operated at the North Thames Cleft Service at GOSH and St Andrew's Centre, Broomfield Hospital, MEHT over 23 years.
- To identify the histological structure of the PP and LVP muscles in patients with SMCP and ICP in comparison to UCLP and controls.

III. 3. Results

III. 3. 1. The surgical management pathway of submucous cleft palate

Patients with SMCP are known to be among the most challenging in terms of management and to achieve a favourable outcome (Sommerlad et al., 2004). To explore the surgical management pathway of patients with SMCP an audit was carried out at the North Thames Cleft Service at GOSH and St Andrew's Centre, Broomfield Hospital, MEHT (Audit number 2693). The audit included NS SMCP cases and patients with 22q11.2 DS but excluded patients with other clinical findings suggestive of a syndrome. Follow up of audit patients was at least 6 months ending December 2018.

III. 3. 2. Audit results

Audit of the case load during the period between 20 June 1995 and 20 June 2018 (23 years) showed that 4876 patients underwent surgery at the North Thames Cleft Service (1790 with CP, 1372 with UCLP, 526 with bilateral CL/P and 1188 with non-cleft VPI).

A total of 222 (4.6%) patients, who matched the inclusion criteria, were operated on in order to manage their SMCP. Of these, 95 (42.8%) were diagnosed with 22q11.2 DS and 127 (57.2%) presented with no additional diagnosis (Figure III. 3). Mutation screening in the *TBX22* gene was performed in 42 (18.4%) patients and 3 (1.3%) were found to have a likely causal mutation leading to a positive CPX diagnosis. The 1st operation for all of the 222 patients was SMCP repair, except for one patient who underwent Hynes pharyngoplasty (Mehendale et al., 2013) as the first choice. The age distribution was 0.5-15 years, with a median of 6 years.

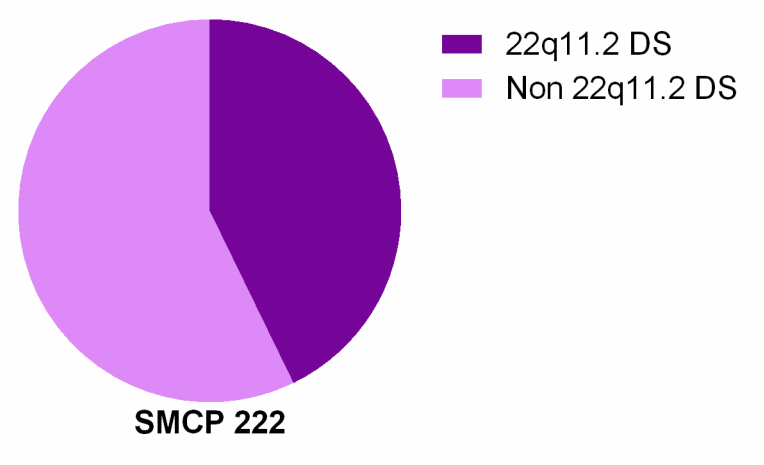

Figure III. 3. Distribution of 22q11.2 deletion syndrome in the submucous cleft palate cohort.

Ninety-five patients (42.8%) were diagnosed with 22q11.2 DS and 127 (57.2%) presented with no additional diagnosis.

A second operation was done on 103 (46.4%) patients. Of those, 53 (51.5%) were 22q11.2 DS. Most of the secondary operations involved Hynes pharyngoplasty, SMCP re-repair and buccinator flaps palate lengthening (Figure III. 4). The age distribution at this operation was 2-18 years, with a median of 8 years.

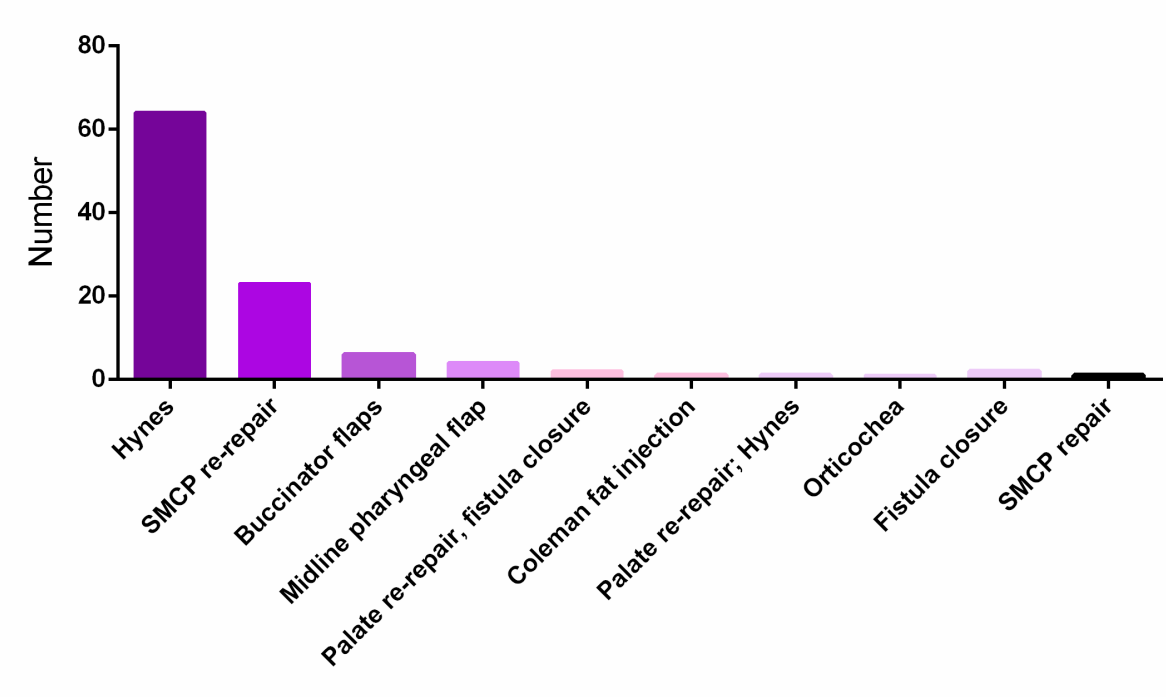

Figure III. 4. Second operation type.

Hynes pharyngoplasty was done in 62.1% cases, SMCP re-repair in 22.3% and buccinator flaps palate lengthening in 5.8%.

Subsequently 13 (5.9%) patients required 3rd operation and 7 (53.8%) of them were 22q11.2 DS. The age ranged between 6-15 years (median 10). The 3rd operation types are presented in Figure III. 5.

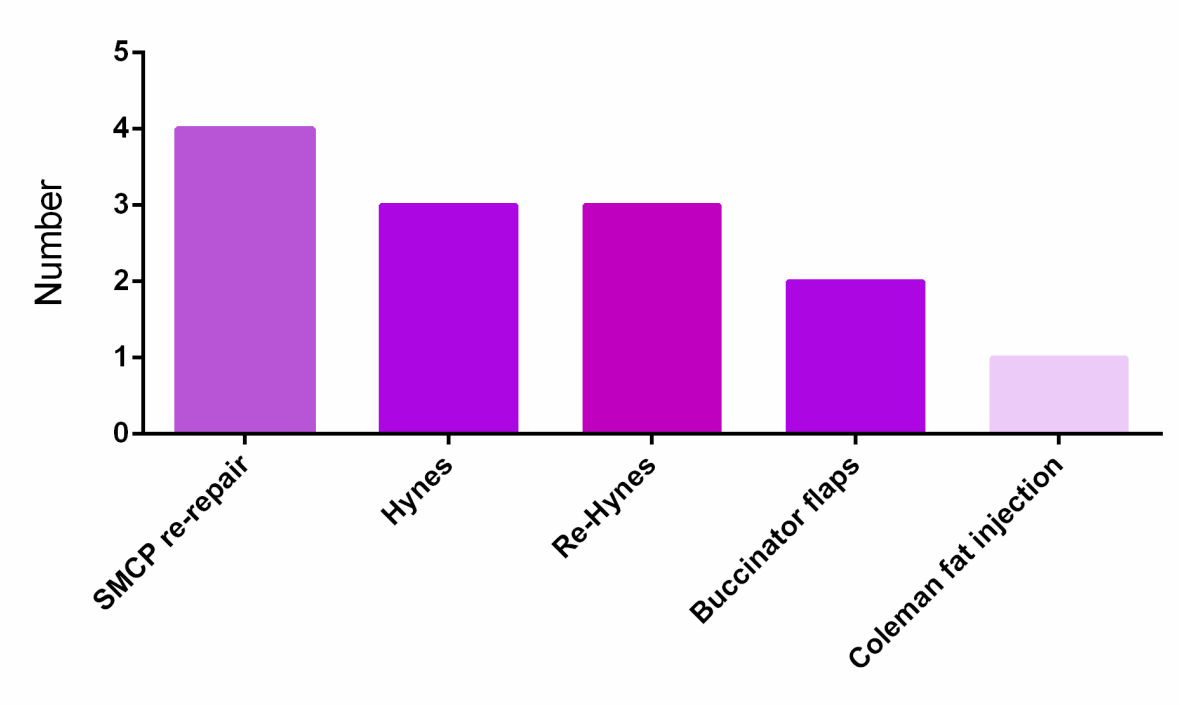

Figure III. 5. Third operation type.

SMCP re-repair was done in 30.8% cases, Hynes and redo Hynes pharyngoplasty in 23.1%.

In conclusion, over 23 years at the North Thames Cleft Service, 222 patients underwent operations to manage SMCP. Nearly half of them (42.8%) were diagnosed with 22q11.2 DS. Apart from one, the first operation was always SMCP repair, and this was followed by the 2nd intervention in nearly half of patients. About 6% of patients underwent a 3rd procedure for VPI management (Figure III. 6). The most common choices for 2nd and 3rd operations were: Hynes pharyngoplasty, SMCP re-repair and buccinators flaps palate lengthening.

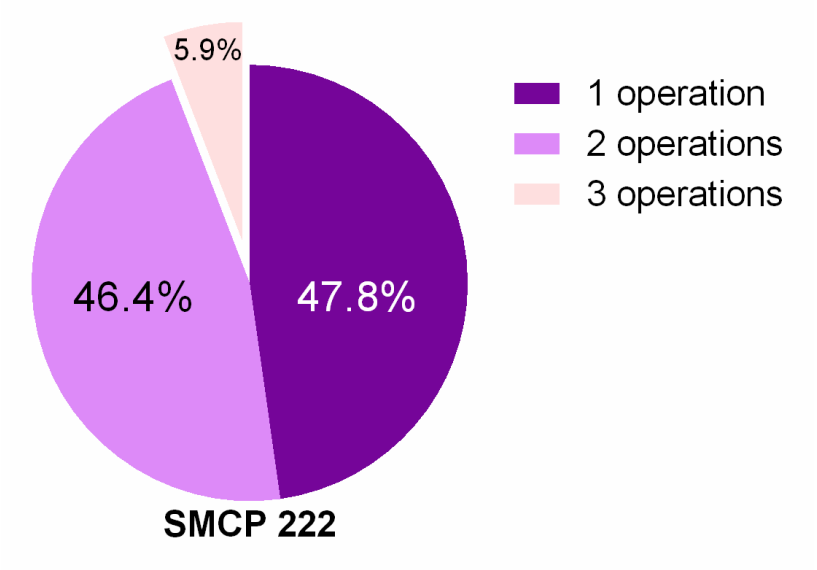

Figure III. 6. Number of operations required for VPI management in patients with SMCP.

SMCP - submucous cleft palate.

III. 3. 3. Results of histological structure of palatal muscles

III. 3. 3. 1. Patients

Muscle biopsies were taken from 99 patients. Fourteen patients (14.1%) were excluded because of the inadequate quality of specimens or insufficient documentation data. In total 103 biopsy samples were available for analysis for the remaining 85 patients (Table III. 2). All patients who underwent a tonsillectomy operation were otherwise healthy, with a normal palate appearance and with no signs of VPD. The muscle histology analysis was carried out for the following groups: UCLP, ICP, ICP in RS, SMCP, SMCP in 22q11.2 DS patients and healthy controls. Although the numbers in each SMCP group were small, especially with 22q11.2 DS, they were all considered important and nevertheless analysed.

Table III. 2. Characterisation of patients.

		No	%
Sex	M	48	56.5
	F	37	43.5
Diagnosis	ICP	41	48
	SMCP*	17	20
	UCLP	15	18
	BCLP	3	3
	Control PP	9	11
Additional diagnosis	Robin sequence	15	18
	22q11.2 DS	5	6
	Achondroplasia	1	1.2
	Apert syndrome	1	1.2
	Cornelia de Lange syndrome	1	1.2
	Kabuki syndrome	1	1.2
	1q21 deletion	1	1.2
	Chr4 deletion	1	1.2
	Ehlers-Danlos syndrome	1	1.2
	Goldenhar syndrome	1	1.2
	Stickler syndrome	1	1.2
	Tessier facial cleft	1	1.2

*One patient was diagnosed with CPX.

III. 3. 3. 2. Samples

The age of patients in the UCLP, ICP, ICP in RS groups (N=57) varied between 10 months and 15 months (Figure III. 7). In the control group (N=5), the mean age was 3 years and 1 month. The SMCP group (N=16) involved patients between 5 to 9 years of age.

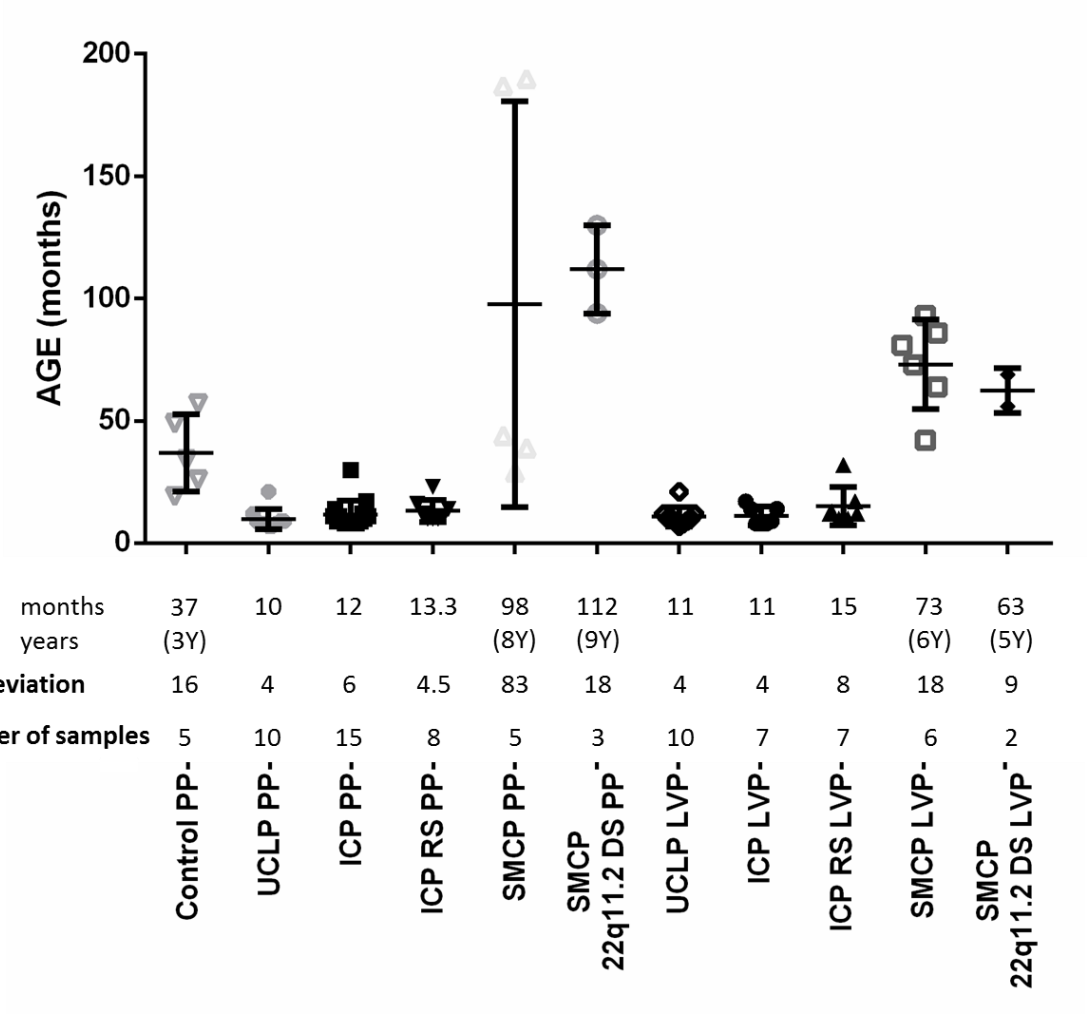

		Control PP-	UCLP PP-	ICP PP-	ICP RS PP-	SMCP PP-	SMCP 22q11.2 DS PP-	UCLP LVP-	ICP LVP-	ICP RS LVP-	SMCP LVP-	SMCP 22q11.2 DS LVP-
Mean	months	37	10	12	13.3	98	112	11	11	15	73	63
	years	(3Y)				(8Y)	(9Y)				(6Y)	(5Y)
Std. deviation		16	4	6	4.5	83	18	4	4	8	18	9
Number of samples		5	10	15	8	5	3	10	7	7	6	2

Figure III. 7. Age distribution and number of samples in each cleft or control group. Each patient is represented by an individual symbol. Error bars = standard deviation. **Y** - years; **PP** - palatopharyngeus; **LVP** - levator veli palatini; **UCLP** - unilateral cleft lip and palate; **ICP** - isolated cleft palate; **RS** - Robin sequence.

III. 3. 3. 3. Fast and slow fibre analysis

The fast and slow fibre distribution was assessed in 5 controls, 12 UCLP, 15 ICP, 5 SMCP, 8 ICP in RS and 3 SMCP in 22q11.2 DS patients in the PP group and 10 UCLP, 7 ICP, 6 SMCP, 7 ICP in RS and 2 SMCP in 22q11.2 DS patients in the LVP group (Figure III. 8). Overall, the fast fibres number varied from 0.09/10,000 μm^2 to 11.73/10,000 μm^2. For slow fibre numbers, a similar cohort was investigated (except N=12 fast vs. N=10 slow UCLP in the PP group) and these varied from 0.33/10,000 μm^2 to 6.38/10,000 μm^2 (Table III. 3 and Table III. 4).

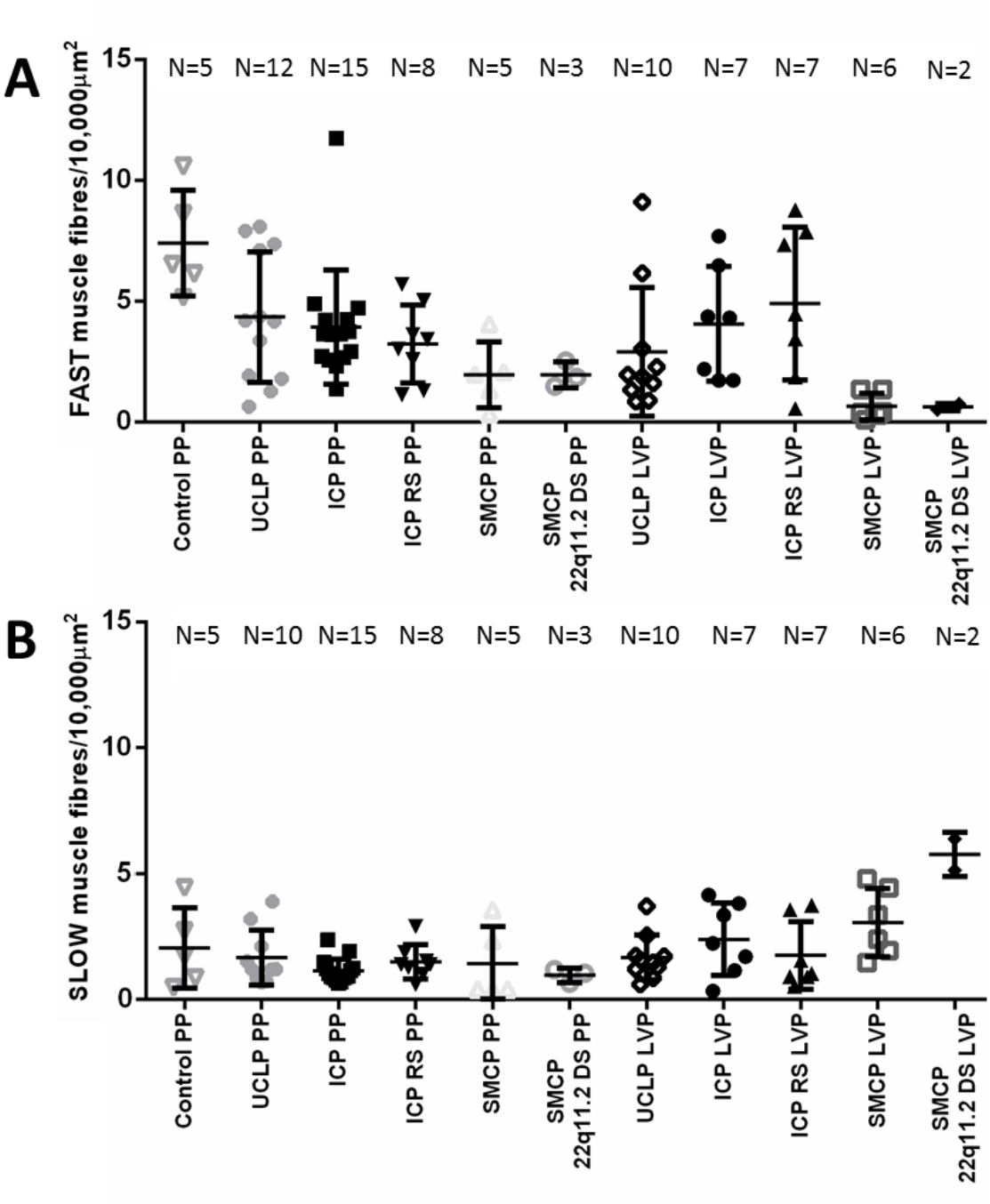

Figure III. 8. Fast and slow fibre samples and fibre number distribution.

A) Fast fibres. **B)** Slow fibres. The number (N) of patients in each group is given and each patient is represented by an individual symbol. Error bars = standard deviation.

PP - palatopharyngeus; **LVP** - levator veli palatini; **UCLP** - unilateral cleft lip and palate; **ICP** - isolated cleft palate; **RS** - Robin sequence.

Table III. 3. Fast and slow fibres/10,000µm^2 in palatopharyngeus muscle.

Diagnosis	FAST fibres/10,000µm^2	SLOW fibres/10,000µm^2
Control	8.60	1.73
	10.58	4.43
	5.14	0.46
	6.13	0.86
	6.51	2.72
Mean±SD	7.39±2.18	2.04±1.59
UCLP	1.92	1.20
	0.63	2.10
	7.10	0.71
	4.20	0.67
	1.79	1.19
	4.16	1.18
	3.36	0.84
	1.27	-
	7.36	1.51
	7.90	3.19
	8.08	3.89
	4.37	-
Mean±SD	4.35±2.70	1.65±1.10

Table III. 3. (continued).

ICP	3.73	1.90
	4.71	0.84
	3.63	0.75
	4.22	1.01
	4.24	0.91
	3.61	0.69
	2.90	0.91
	2.57	0.63
	2.65	0.85
	2.30	1.47
	1.35	0.93
	2.72	1.22
	4.88	1.14
	3.65	2.36
	11.73	1.23
Mean±SD	3.93±2.36	1.12±0.47
ICP RS	2.58	1.39
	1.13	1.26
	1.29	0.59
	3.02	1.52
	5.70	1.86
	3.62	1.39
	3.42	1.00
	5.04	2.90
Mean±SD	3.23±1.61	1.49±0.68

Table III. 3. (continued).

SMCP	2.08	0.38
	1.98	0.40
	0.33	0.40
	1.34	2.34
	4.06	3.56
Mean±SD	1.96±1.37	1.42±1.47
SMCP 22q11.2 DS	1.48	0.64
	2.52	1.18
	1.84	1.04
Mean±SD	1.95±0.53	0.95±0.28

Table III. 4. Fast and slow fibres/10,000µm^2 in levator veli palatini muscle.

Diagnosis	FAST fibres/10,000µm^2	SLOW fibres/10,000µm^2
UCLP	1.61	1.21
	3.03	1.47
	1.32	0.85
	2.26	0.60
	0.88	1.71
	0.84	2.54
	9.10	1.57
	1.96	1.28
	1.88	1.74
	6.15	3.71
Mean±SD	2.90±2.67	1.67±0.89

Table III. 4. (continued).

ICP	6.47	4.15
	2.18	1.14
	4.30	2.23
	1.71	0.33
	7.68	3.81
	1.72	3.34
	4.36	1.70
Mean±SD	4.06±2.37	2.39±1.43
ICP RS	3.45	0.52
	0.55	3.74
	7.87	0.91
	8.77	1.03
	4.47	1.55
	1.86	0.90
	7.33	3.56
Mean±SD	4.90±3.17	1.74±1.34
SMCP	0.09	3.35
	0.38	1.94
	0.30	1.46
	0.42	4.78
	1.34	2.38
	1.34	4.44
Mean±SD	0.65±0.55	3.06±1.36
SMCP 22q11.2 DS	0.73	6.38
	0.51	5.13
Mean±SD	0.62±0.16	5.76±0.88

When examining the LVP, there were significantly fewer fast fibres in SMCP compared to ICP or ICP in RS patients (Figure III. 9, A). When comparing PP fast muscle fibres, there was significantly more fast fibres in control samples compared to ICP, ICP in RS patients, SMCP and SMCP in 22q11.2 DS patients. There was no difference when comparing controls to UCLP PP samples (Figure III. 9, B). In the analysis of LVP slow muscle fibres, there were significantly more of these fibres in SMCP in 22q11.2 DS patients than in UCLP, ICP or ICP in RS patients (Figure III. 9, C). There were no statistically significant differences for PP slow fibre numbers between any groups (Figure III. 9, D).

Interestingly, in all groups of cleft and muscle type there were significantly more fast fibres compared to slow, with the exception of LVP in SMCP and SMCP in 22q11.2 DS patients. Here, a significant increase in slow fibre numbers was observed (Figure III. 9, E).

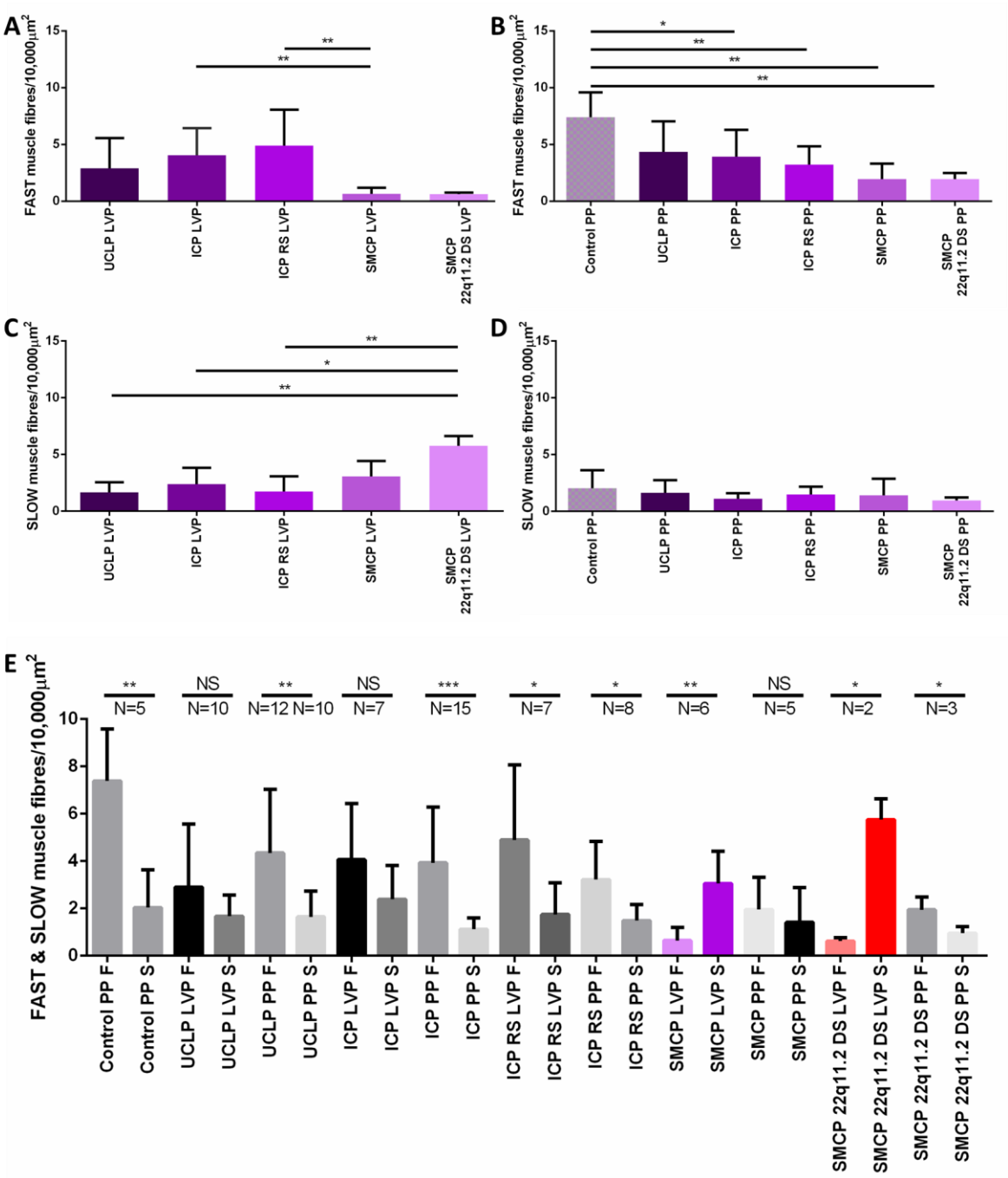

Figure III. 9. Number of fast and slow muscle fibres present in different cleft groups.
A) Fast fibre numbers in LVP; **B)** in PP muscle; **C)** Slow fibre numbers in LVP; **D)** in PP muscle; **E)** Comparison between fast and slow fibre numbers between different cleft types. The number (N) of patients in each group is given. Error bars = standard deviation.
S - slow fibres; **F** - fast fibres; **PP** - palatopharyngeus; **LVP** - levator veli palatini; **UCLP** - unilateral cleft lip and palate; **ICP** - isolated cleft palate; **RS** - Robin sequence. **p*<0.05; ***p*<0.01; ****p*<0.001; **NS** - not statistically significant, p≥0.05.

For samples where both fast and slow fibre staining was available, a fast/slow fibre ratio was calculated. The only significant finding was for LVP muscle when comparing SMCP and ICP in RS groups. All fibre distributions are presented in Figure III. 10, while the fast and slow fibres % in different cleft type groups is presented in Table III. 5.

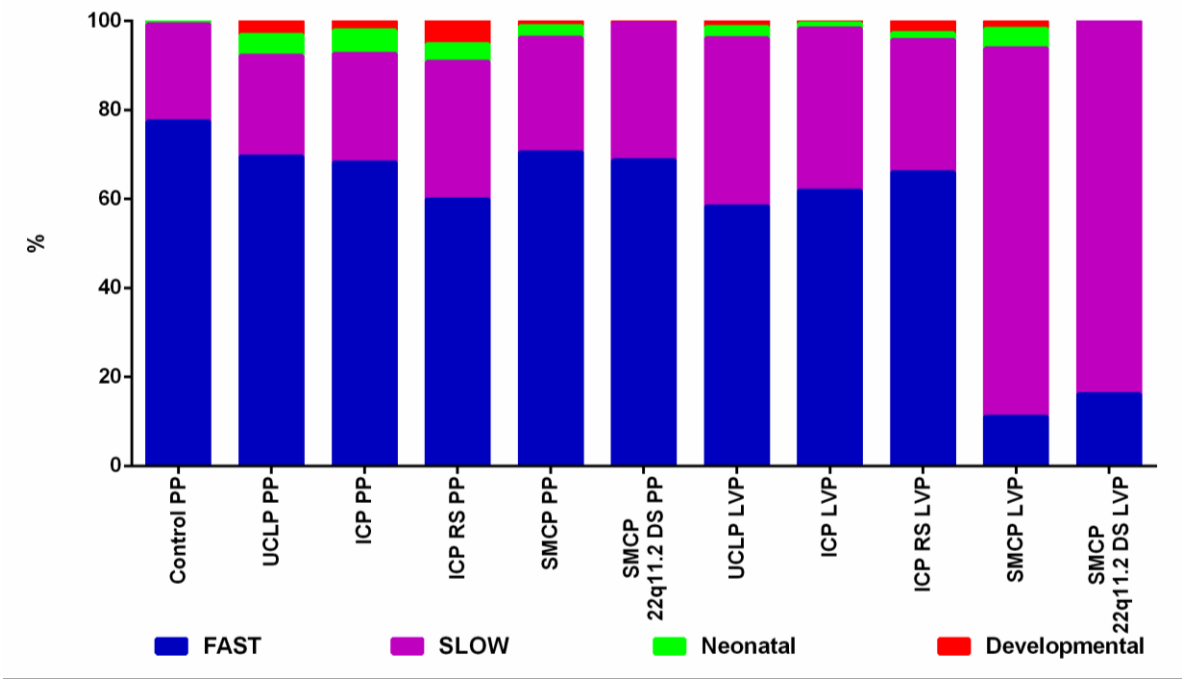

Figure III. 10. Muscle fibre distribution.

PP - palatopharyngeus; **LVP** - levator veli palatini; **UCLP** - unilateral cleft lip and palate; **ICP** - isolated cleft palate; **RS** - Robin sequence.

Table III. 5. Fast, slow, neonatal and developmental fibre frequency (%) in palatopharyngeus and levator veli palatini muscles.

Muscle	No of samples	Cleft type	%FAST	%SLOW	%NEO	%DEV
PP	4	**Control**	77.4	21.8	0.7	0.1
	9	**UCLP**	69.5	22.6	4.8	3.1
	13	**ICP**	68.2	24.4	5.2	2.2
	6	**ICP RS**	59.9	30.9	4.0	5.2
	3	**SMCP**	70.5	25.7	2.6	1.2
	2	**SMCP 22q11.2 DS**	68.7	30.8	0	0.5
LVP	8	**UCLP**	58.3	37.8	2.6	1.3
	6	**ICP**	61.9	36.4	1.1	0.6
	4	**ICP RS**	66.0	29.7	1.5	2.8
	3	**SMCP**	11.1	82.7	4.4	1.8
	2	**SMCP 22q11.2 DS**	16.1	83.9	0	0

III. 3. 3. 4. Neonatal and developmental fibre analysis

Developing skeletal muscles express unique myosin isoforms such as embryonic and neonatal myosin heavy chains. These myosin isoforms are observed during embryonic and fetal development and disappear shortly after birth when fast and slow myosins become more prevalent. In our study few samples were available for neonatal and developmental muscle fibre analysis. However, the number of muscle fibres did vary depending on age group (Figure III. 11, A). The numbers of neonatal muscle fibres were higher when the biopsies were taken in UCL, ICP and ICP in RS children (median 10 months), lower in the control group (median 2 years 6 months) and none in the 22q11.2 DS group (median 6 years). Although both groups (PP and LVP in 22q11.2 DS) had two samples each, none of them had neonatal muscle fibres. Interestingly when compared PP vs. LVP there were significantly more neonatal muscle fibres in PP group in ICP (p=0.0039) and in UCLP (p=0.0178). The developmental myosin stain did not reveal any obvious prevalence for these fibres in either PP or LVP muscles at the time of surgery (Figure III. 11, B).

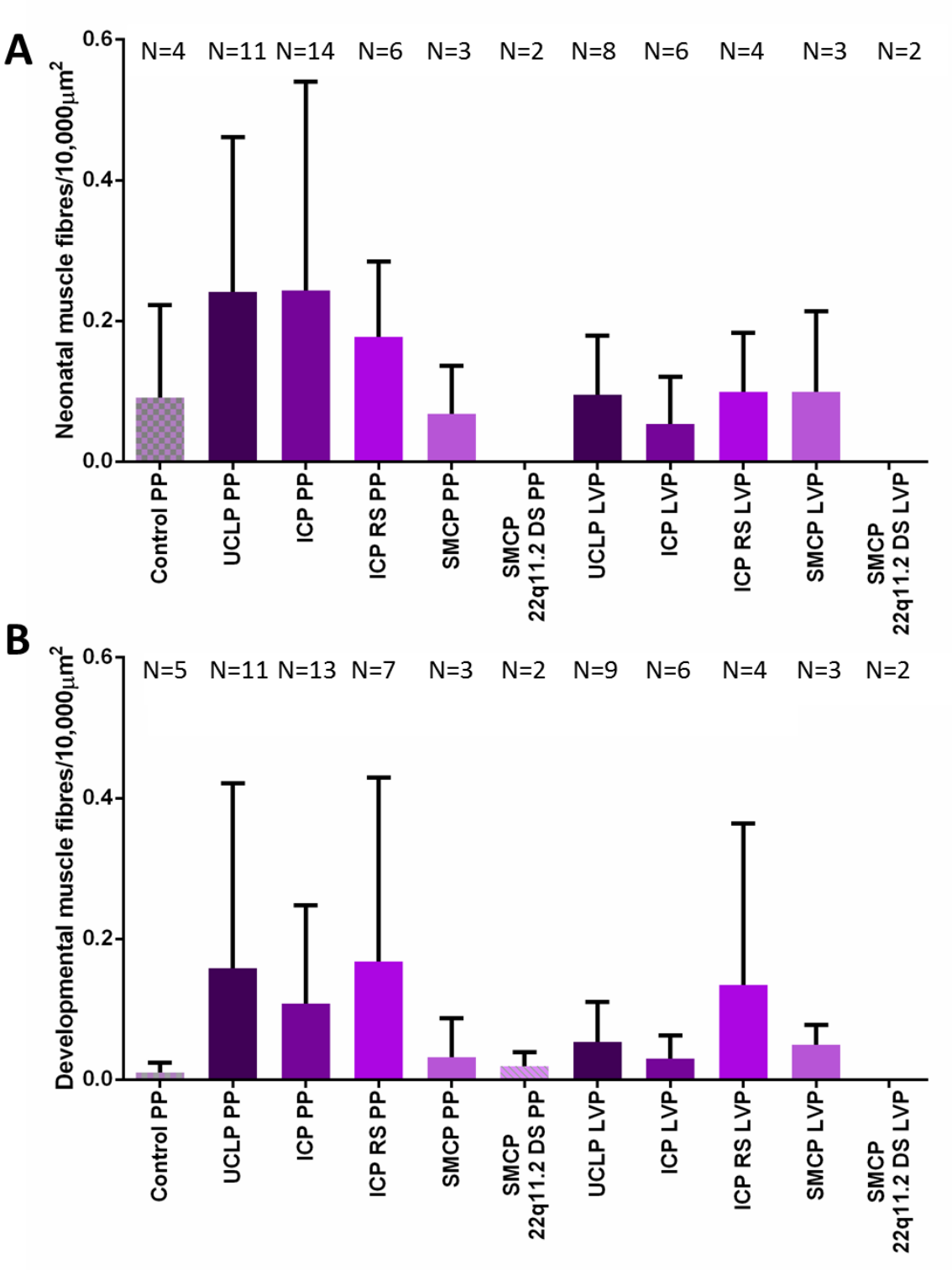

Figure III. 11. Neonatal and developmental myosin stain.

A) Neonatal muscle fibre density, **B)** Developmental muscle fibre density. No statistically significant difference was detected between groups. The number (N) of patients in each group is given. Error bars = standard deviation. **PP** - palatopharyngeus; **LVP** - levator veli palatini; **UCLP** - unilateral cleft lip and palate; **ICP** - isolated cleft palate; **RS** - Robin sequence.

III. 3. 3. 5. Mitochondrial activity analysis

Oxidative enzyme activity is predominantly located in the mitochondria. Skeletal muscle mitochondrial function is reduced with aging, metabolic diseases associated with insulin resistance and physical activity (Lanza and Sreekumaran Nair, 2010). In our study COX, SDH, NADH-TR and Gomori trichrome stains were performed on PP and LVP muscle samples. However, there was no visible mitochondrial pathology seen or any clear differences between the various cleft groups studied.

III. 3. 3. 6. Fat accumulation analysis

To score fat accumulation, the samples were grouped according to whether fat was either not detectable, detectable, apparent or significant. Combining the variability with the low number of samples in each group, limited the overall interpretation and no definitive conclusions could be drawn. Nevertheless, there did appear to be more fat in the SMCP PP muscle when compared to other cleft and muscle types (Figure III. 12). This finding would ideally need to be investigated in a larger sample number to confirm.

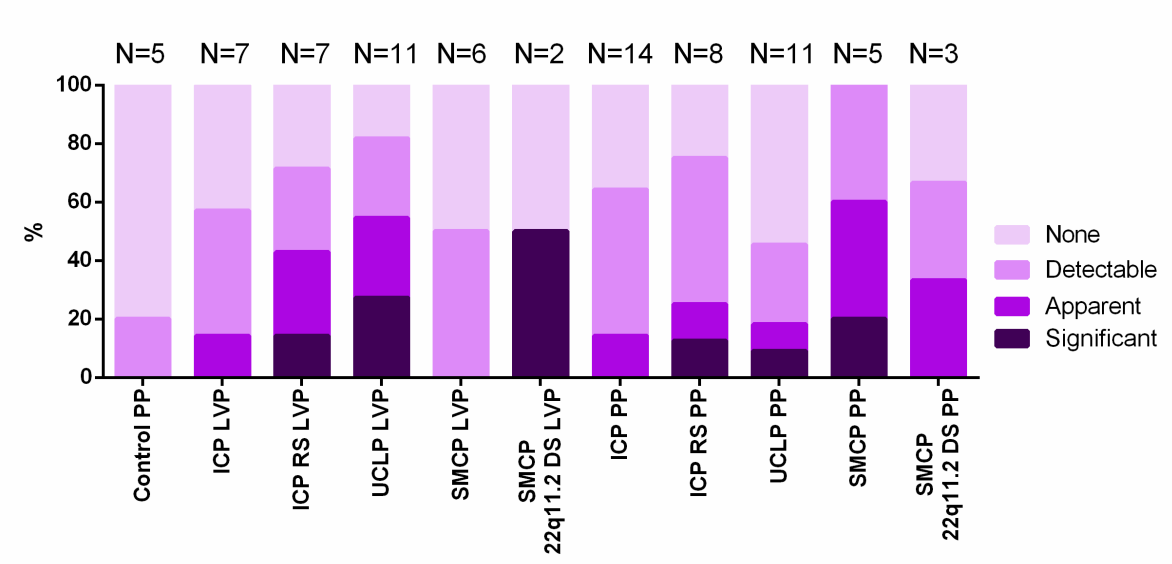

Figure III. 12. Evaluation of fat accumulation in different cleft and muscle types.
PP - palatopharyngeus; **LVP** - levator veli palatini; **UCLP** - unilateral cleft lip and palate; **ICP** - isolated cleft palate; **RS** - Robin sequence.

III. 3. 3. 7. Connective tissue in muscle analysis

Connective tissue in each muscle was analysed using the picrosirius stain. No statistically significant differences were observed either between cleft or muscle type (Figure III. 13).

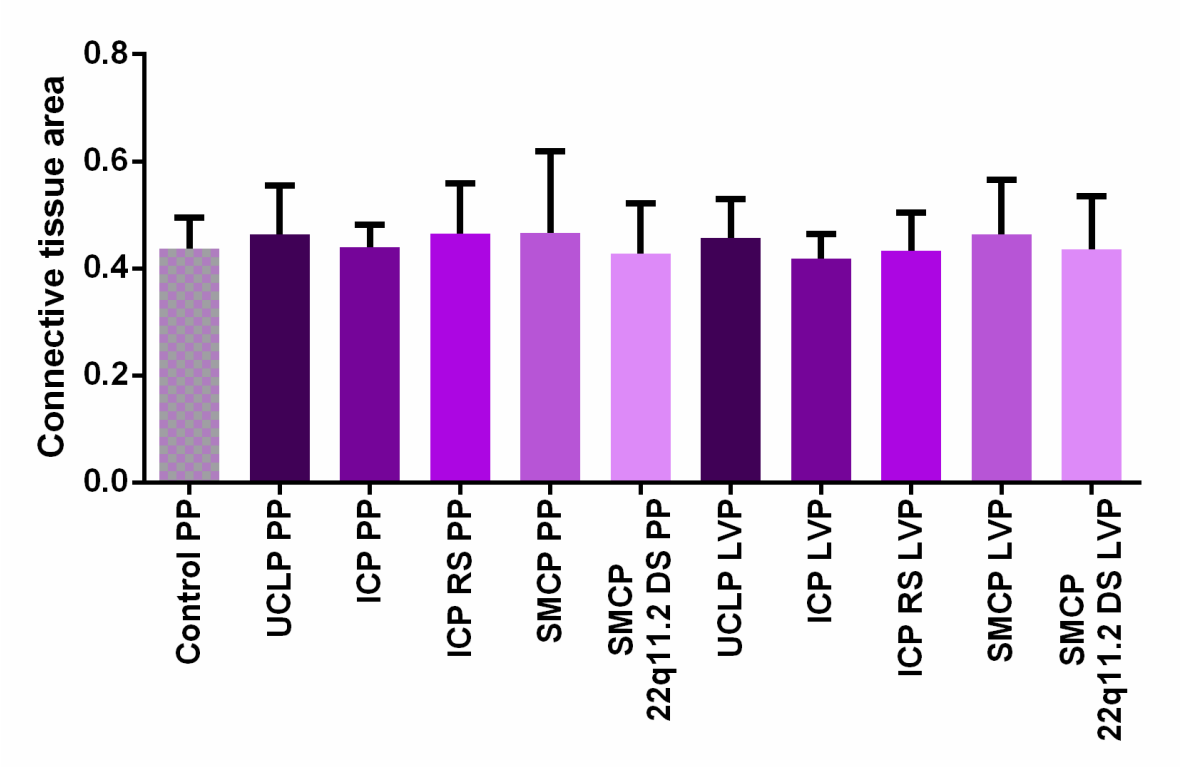

Figure III. 13. Connective tissue in different cleft and muscle types.
No statistical significance was detected. Error bars = standard deviation.
PP - palatopharyngeus; **LVP** - levator veli palatini; **UCLP** - unilateral cleft lip and palate; **ICP** - isolated cleft palate; **RS** - Robin sequence.

III. 3. 3. 8. Muscle biopsy histology in cleft syndromes

There were complete single sets of stained samples available for analysis in patients with achondroplasia, Apert, Cornelia de Lange and Kabuki syndromes.

Achondroplasia is caused by mutations in the *FGFR3* gene (Daugherty, 2017). It is a disorder of bone growth that prevents ossification (the cartilage changing to bone) particularly in the long bones of the arms and legs. A single biopsy was taken from the PP muscle in a boy with achondroplasia and ICP, age 1 year and 9 months. Fast and slow muscle fibre number was compared to the average PP muscle fibre number in ICP and controls. No obvious difference in fast fibres number was detected (Figure III. 14). There were more slow fibres compared with the average number of slow fibres in ICP but the number did not differ compared to controls (Figure III. 15). The fast and slow fibres ratio was consequently lower, due to relatively higher number of slow fibres compared to fast (Figure III. 16). There were no developmental fibres in the biopsy sample, but there were more neonatal muscle fibres compared to ICP and controls. Mitochondrial activity analysis revealed no obvious mitochondrial pathology in muscle. There was no fat in the sample, corresponding with findings in the PP muscle in ICP and controls. The measurement of connective tissue in the sample showed no difference compared to ICP and control samples (Figure III. 17).

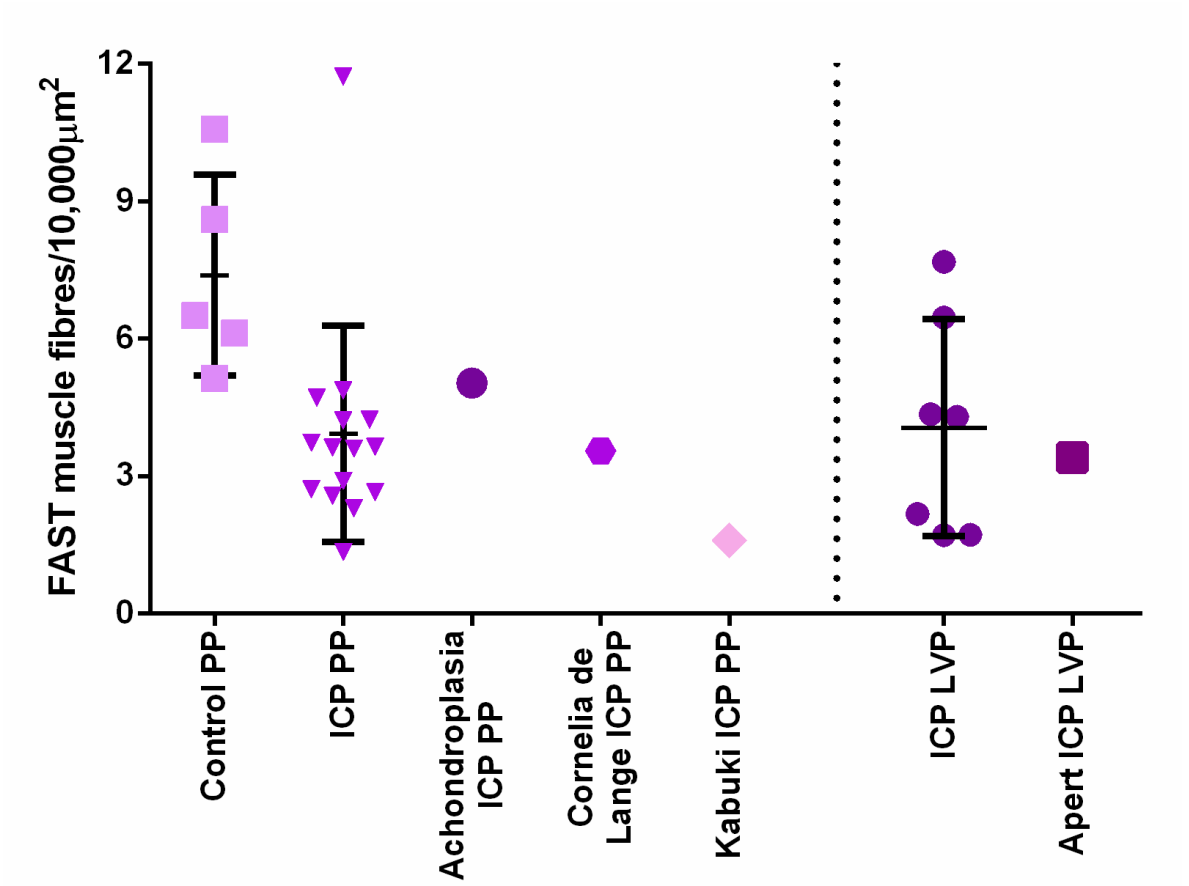

Figure III. 14. Syndromic muscle biopsy analysis for fast fibres.

Comparison of fast fibre number between PP muscle in control, ICP, achondroplasia ICP, Cornelia de Lange ICP and Kabuki ICP PP. To the right of a dotted line comparison between ICP LVP and Apert ICP LVP is presented. Each patient is represented by an individual symbol. Error bars = standard deviation. **PP** - palatopharyngeus; **LVP** - levator veli palatini; **UCLP** - unilateral cleft lip and palate; **ICP** - isolated cleft palate; **RS** - Robin sequence.

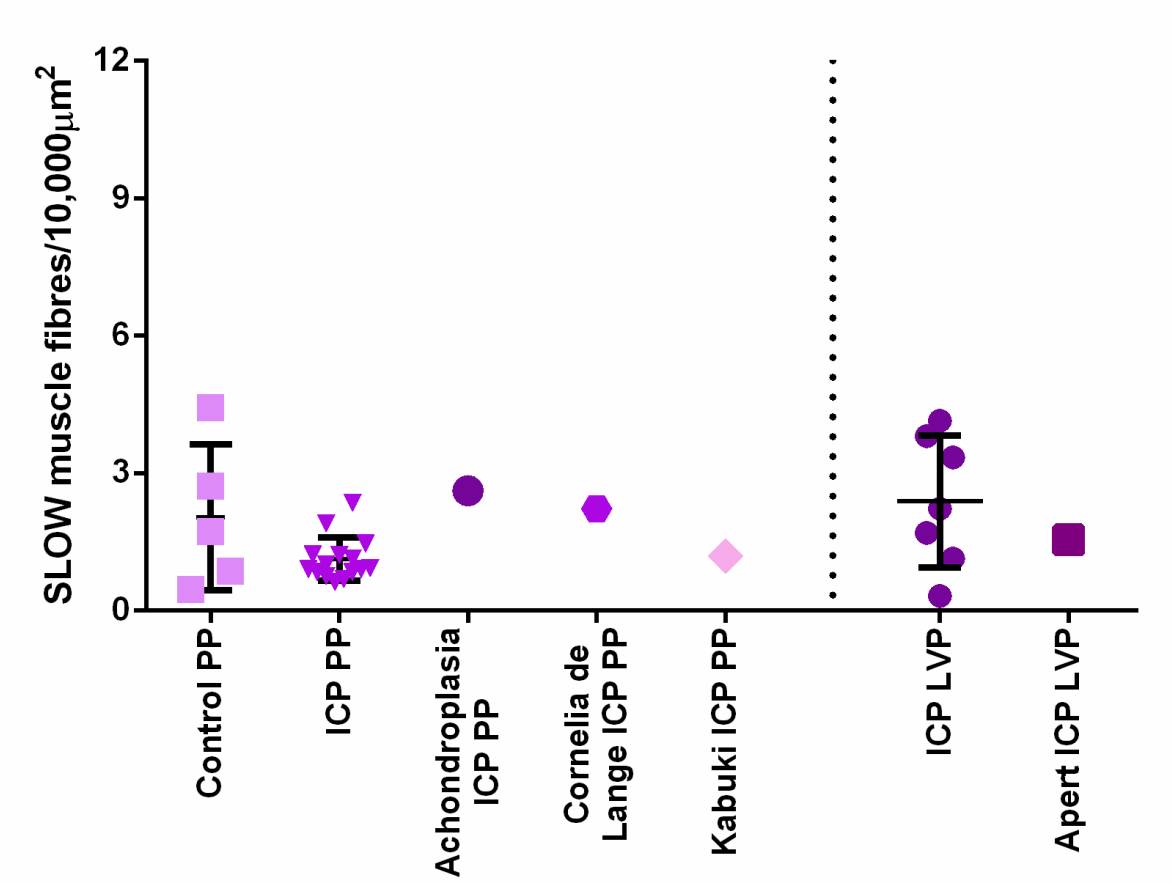

Figure III. 15. Syndromic muscle biopsy analysis for slow fibres.

Comparison of slow fibres between PP muscle in control, ICP, achondroplasia ICP, Cornelia de Lange ICP and Kabuki ICP. To the right of a dotted line comparison between ICP LVP and Apert ICP LVP is presented. Each patient is represented by an individual symbol. Error bars = standard deviation. **PP** - palatopharyngeus; **LVP** - levator veli palatini; **UCLP** - unilateral cleft lip and palate; **ICP** - isolated cleft palate; **RS** - Robin sequence.

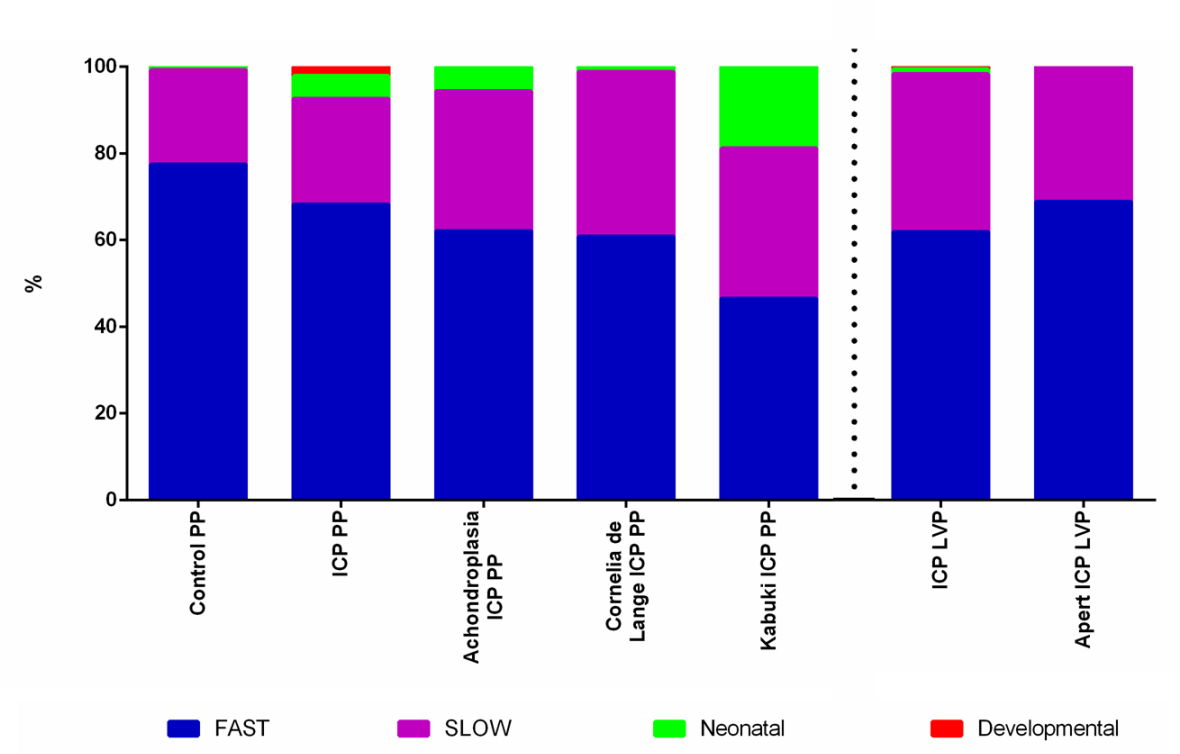

Figure III. 16. Ratio of different muscle fibres in syndromic muscle biopsy.
Fast, slow, neonatal and developmental fibre ratios compared between PP muscle in control, ICP, achondroplasia ICP, Cornelia de Lange ICP and Kabuki ICP. To the right of the dotted line a comparison between ICP LVP and Apert ICP LVP is presented.
PP - palatopharyngeus; **LVP** - levator veli palatini; **UCLP** - unilateral cleft lip and palate; **ICP** - isolated cleft palate; **RS** - Robin sequence.

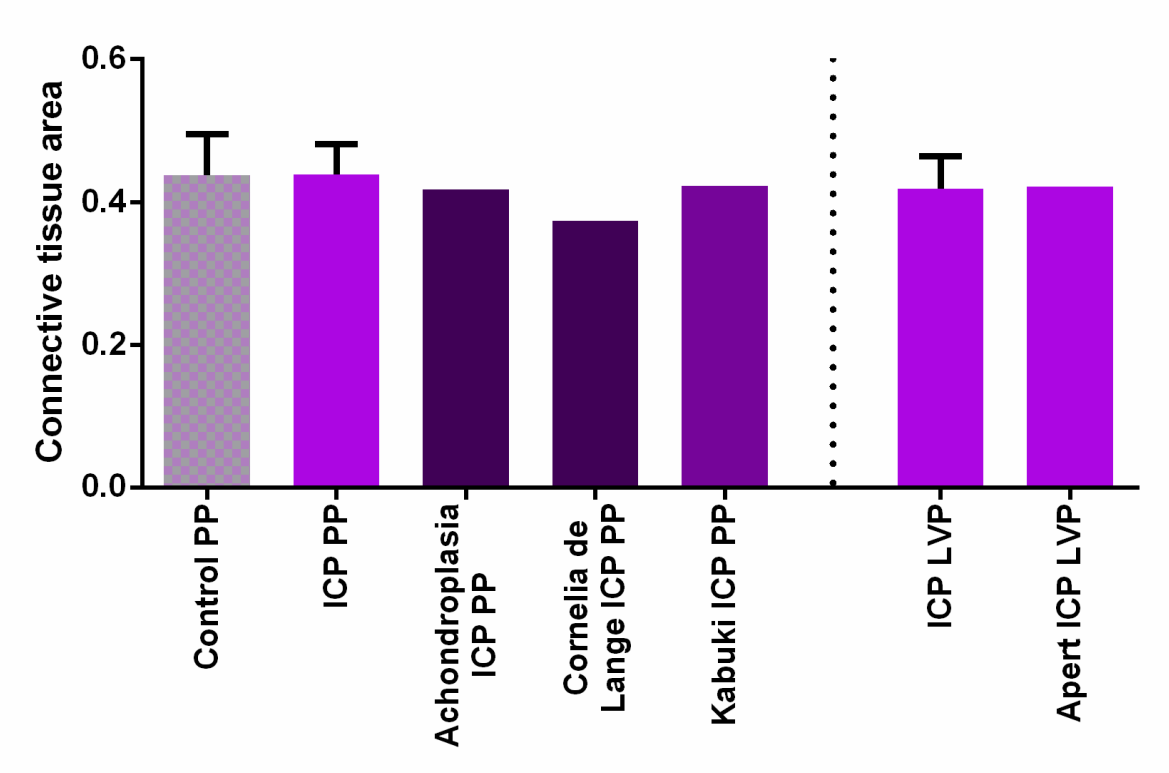

Figure III. 17. Connective tissue analysis in syndromic muscle biopsy.
Connective tissue area comparison between PP muscle in control, ICP, achondroplasia ICP, Cornelia de Lange ICP and Kabuki ICP. To the right of the dotted line, a comparison between ICP LVP and Apert ICP LVP is presented. Error bars = standard deviation.
PP - palatopharyngeus; **LVP** - levator veli palatini; **UCLP** - unilateral cleft lip and palate; **ICP** - isolated cleft palate; **RS** - Robin sequence.

Apert syndrome is characterized by craniosynostosis, the premature fusion of cranial bones and syndactyly of fingers and toes (Das and Munshi, 2018). The early fusion prevents the brain from growing normally and affects the shape of the skull, including the face. A single biopsy of LVP muscle was available from a 4 years and 8 months old female with Apert syndrome who had ICP.

Slow and fast fibre analysis did not show any difference when compared to ICP LVP muscles (Figure III. 14, Figure III. 15). There were no developmental or neonatal muscle fibres in the biopsy sample and no mitochondrial pathology was noted (Figure III. 16). There was significant fat infiltration observed in the sample. The area of connective tissue did not differ compared to ICP LVP samples

(Figure III. 17). In conclusion, the LVP muscle in the Apert syndrome patient was infiltrated with fat, but otherwise no obvious significant differences were observed when compared to ICP LVP muscle.

Cornelia de Lange syndrome is a developmental disorder that affects many parts of the body. It is characterized by slow growth and short stature, intellectual disability, distinctive facial features, low-set ears, small nose and small teeth (Xing et al., 2019). One female patient with this syndrome undergoing CP repair at age 2 years and 6 months had a PP muscle biopsy taken and the slides were available for analysis. Fast muscle fibre analysis showed no difference compared to the average for ICP PP fast muscle fibres and less when compared to controls (Figure III. 14). There were slightly more slow muscle fibres compared to ICP PP (Figure III. 15) and decreased fast and slow muscle fibre ratio when compared to ICP and control PP (Figure III. 16). There was roughly similar number of neonatal muscle fibres compared to control PP (similar age group), but less compared to ICP PP. No developmental muscle fibres were noted. Mitochondrial activity stain did not reveal any obvious abnormality. There was detectable amount of fat in biopsy sample. Connective tissue area again did not show any difference when compared to ICP and controls (Figure III. 17).

Kabuki syndrome is a genetic disorder. The name comes from the resemblance of its characteristic facial appearance to the stage makeup used in traditional Japanese Kabuki theatre. It is characterized by distinctive facial features, mild to severe intellectual disability and developmental delay, microcephaly, short stature and skeletal abnormalities (Adam et al., 1993). A single female patient with Kabuki syndrome and ICP had a biopsy taken from the PP muscle at an age of 2 years and 7 months. There were a lower number of fast muscle fibres in the sample compared to control PP muscle (Figure III. 14). The slow fibre number did not differ (Figure III. 15). Fast and slow fibre ratio was on the lower side (Figure III. 16). There were no neonatal fibres detected, although developmental muscle fibres were obviously higher in number that developmental muscle fibres in ICP and controls. Mitochondrial activity staining did not reveal any obvious abnormality. Fat infiltration was graded as apparent. Connective tissue assessment did not reveal any obvious difference compared to ICP or controls (Figure III. 17).

III. 4. Discussion

In this study, a basic histology screen was performed on palate muscle biopsies in children who underwent CP repair. Muscle histological structure was compared between ICP, UCLP and SMCP. Breaking these groups down further was possible by identifying those with RS related ICP and SMCP with a molecular diagnosis of 22q11.2 DS. To our knowledge, this represents the first study involving samples from different cleft types and using descending PP muscle fibres as controls from healthy children who underwent tonsillectomy operation for obstructive sleep apnoea or recurrent chronic tonsillitis. Single muscle biopsy sets were also analysed for achondroplasia, Apert, Cornelia de Lange and Kabuki syndromes.

In the literature, the function of the PP muscle seems to be controversial. Based on its anatomy, its primary actions are reported to be velar depression and retrodisplacement (Fara and Dvorak, 1970, Huang et al., 1998). There is also evidence that palatopharyngeal function occurs during velar elevation and this complements levator function (Podvinec, 1952, Bosma, 1953). On the other hand there is an assumption that the PP muscle is a natural antagonist of the LVP and it should not be contracting simultaneously, therefore it would have no active role in speech (Dickson, 1972, Dickson, 1975). Electromyographic studies suggest that PP activity does occur in speech, particularly in relation to LVP activity (Moon et al., 1994). This functional study is supported by anatomical findings that the PP occupies the posterior part of the velum lateral and inferior to the LVP, suggesting that it has a significant effect on the velum, independently of the LVP (Huang et al., 1998). The wide distribution of the PP muscle suggests that it acts not only to elevate the pharynx or depress the soft palate, but may also function as a nasopharyngeal sphincter when closing the pharyngeal isthmus (Ezzat and El-Shenawy, 2015). Our study shows that the PP muscle fibre type distribution does not differ dramatically when compared to the LVP muscle. This finding may support the idea, that PP is also a speech muscle. Based on published data and the histological PP structure, it seems that the PP muscle may be more significant during palate repair than previously thought and may require more attention during surgery. However, this hypothesis will require further investigation.

Passavant's ridge was first described in 1869 by a German surgeon Gustav Passavant. He reported the existence of a transverse forward projection on the posterior pharyngeal wall during speech in CP patients and concluded that the ridge was an essential structure for normal velopharyngeal closure (Passavant, 1869). The concept has created a lot of controversy for many years. It is, however, widely agreed that the ridge is not present in all individuals (with or without CP) and is not essential for velopharyngeal closure (Glaser et al., 1979, Mardini et al., 2016). Passavant's ridge is made of the fused fibres of the PP muscle and pterygopharyngeal portion of the superior constrictor (Zemlin, 1964) leading to a sphincter like function (Amelot et al., 2003) which tends to occur below the level of velopharyngeal closure (Calnan, 1957) where the fibres of the PP are more abundant (Huang et al., 1998). Historically the idea of Passavant's ridge as being import for speech has varied between being crucial to being of no significance at all. Nevertheless, a potential role for this structure should not be forgotten. The fact that Passavant's ridge is composed of the PP muscle supports the idea of a possible involvement in speech. Speech requires precise timing and co-ordination of the velum, lateral and posterior pharyngeal walls to be effective. It is possible that at least in some individuals, their Passavant's ridge may play a significant and major role to assist in VP closure. For this reason, studies investigating precise timing of the co-ordinated movements of Passavant's ridge and the velum are still required.

LVP muscle is considered the most important muscle for velum elevation and retraction (Huang et al., 1998). It occupies the middle 40% of the soft palate and is essential for normal velopharyngeal closure (Boorman and Sommerlad, 1985, Maue-Dickson, 1979).

Extensive interest in understanding velopharyngeal structures from both anatomical and physiological perspectives shows their significance in speech, swallowing and hearing (Ettema et al., 2002, Hamlet and Momiyama, 1992, Huang et al., 1997). Acquired knowledge allows better understanding and ultimately management of dysfunction, although further studies are required. As such, recent attention has been directed to velopharyngeal anatomy in MRI studies. Dynamic MRI is being used to better understand the muscular structure of the velopharynx,

and this method has been proposed as a novel tool for clinical examination, that may assist in CP patients management (Perry et al., 2017), see also III. 1. 7. MRI for velopharyngeal function evaluation.

There is limited literature describing the precise function of velopharyngeal structures and how they coordinate timing to achieve velopharyngeal closure (velum, pharyngeal sphincter and Passavant's ridge). A general assumption could be that abnormal muscle action, either through incoordination or miss-timing could be a key factor causing VPD. This study therefore focused on the histological integrity of the LVP and PP muscles, whilst a more detailed investigation of their overall structure would need to be tested by videofluoroscopy or MRI in future studies. Furthermore there is evidence in the literature for disturbance to swallowing due to shifts in the timing of muscle motions, although functional coordination between the soft palate and the pharynx is necessary during deglutition process (Kahrilas, 1993, Logemann et al., 2000).

In a much earlier study, using 12 adult non-cleft cadavers, Moon et al. (1998) reported 59.8% type I (slow twitch) LVP muscle fibres (Moon et al., 1998). Meanwhile, Lindeman et al. (2001) reported 36.9% type I fibres in ICP LVP (8 patients) and 74.9% in LVP muscle in non-cleft 5 adult cadavers (Lindman et al., 2001). Findings from our study largely agreed, since there were 36.4% slow muscle fibres in the LVP muscle in ICP and 37.8% in UCLP. The most dramatic finding was increase of slow fibres in SMCP (82.7%). When evaluating type II (fast twitch) fibres in LVP, Moon et al. (1998) reported 40.2% in 12 non-cleft cadavers while Lindman et al. (2001) reported 63.1% in 8 infant cleft patients, while just 25.1% in 5 non-cleft adult cadavers. In our study there were 61.9% fast muscle fibres in the LVP muscle in ICP and 58.3% in UCLP (Table III. 6). The fast fibre numbers were similar to previous reported, but SMCP muscle fibre distribution analysis (11.1%) again appeared to contradict the ratio reported previously and was clearly different to other cleft types analysed in our study. Whilst the numbers are different, the interpretation should be cautious since the SMCP patients were generally older than the other cleft patients (since their operation is usually performed at an older age). It will be important to determine how muscle fibre type distribution alters with age, and potentially the length of time they remain inactive.

Stal and Lindman (2000) examined PP, the uvula, the levator and TVP for comparison with human limb (the first interosseus and biceps brachii) and facial muscles (zygomaticus major) using enzyme-histochemical, immunohistochemical and biochemical methods (Stal and Lindman, 2000). Specimens were taken post-mortem from two adult males and three females (mean age 54.4 years). They found that the fibre type including fetal myosin heavy chain isoform (MyHC) composition, indicated that the PP and uvula muscles functioned in quick movements while the LVP and TVP muscles represented slower and continuous contractions. The authors also state that palate muscles are fatigue resistant, based on higher aerobic capacity and the richer capillary net. Moreover palate muscles differ from limb muscles but were more similar to facial muscles in respect of morphology, capillary density and content of muscle spindles (Stal et al., 1996). In our study we did not investigate the uvula muscle (which may not exist in cleft palates) but did find that fast fibres were prevalent in the PP muscle in all cleft groups as well as in the PP controls.

Stal and Hicks (1998) examined the histopathologic structure of the musculus uvulae and the levator muscle bundle from SMCP or OSMCP patients in comparison with normal soft palate tissue at autopsy from 12 children from each year of life up to 11 years of age. The study involved 28 patients (12 SMCP and 16 OSMCP) with a mean age of 33.6 months (Stal and Hicks, 1998). The study showed myocyte fascicular disorganization, myocytes atrophy and the presence of dense, mature collagen deposition in SMCP samples. In our study we have not graded SMCP severity and there were smaller numbers of SMCP samples compared to other cleft groups as well as muscle evaluation method differed significantly.

Lindman et al. (2001) examined the LVP muscle in children born with CP (8 males and 3 females, age mean 19.5 months) morphologically and biochemically (Lindman et al., 2001). No muscle tissue was present in 3 biopsies. For reference, samples were obtained from the non-cleft adults post-mortem: the LVP muscle and the biceps brachii [the samples were obtained from the corresponding area as the cleft LVP samples and were identical with those used by Stal and Lindman (2000)]. The main finding was a difference in fibre size, fibre type, MyHC compositions and

capillary supply when compared the LVP in CP children with normal adults. In our study the age also varied depending on cleft diagnosis, but we did not see the same variation that Lindman et al. (2001) described, when the samples were compared to adults.

Stal et al. (2000) report 13.8% type I (slow twitch) and 86.2% type II (fast twitch) in PP muscle fibres in 5 non-cleft cadavers. In our study there were 24.4% in ICP, 25.7% in SMCP and 22.6% in UCLP when evaluating slow muscle fibres in PP muscle and fast fibres analysis showed 68.2% in ICP, 70.5% in SMCP and 69.5% in UCLP. There were more slow fibres in PP muscle and relatively fewer fast fibres comparing our study of cleft children to the adult cadavers in Stal et al. (2000), Table III. 6.

Table III. 6. The comparison between muscle fibre frequency (%) with previously reported results.

Samples		No of samples	%FAST	%SLOW
LVP	**ICP**[I]	10	61.9	36.4
	SMCP[II]	5	11.1	82.7
	UCLP[III]	8	58.3	37.8
Infant cleft LVP[*]		8	63.1	36.9
Adult LVP[**] (non-cleft)		5†	25.1	74.9
Adult LVP[***] (non-cleft)		12†	40.2	59.8
PP	**ICP**[1]	19	68.2	24.4
	SMCP[2]	5	70.5	25.7
	UCLP[3]	9	69.5	22.6
Adult PP[**]		5†	86.2	13.8

[*](Lindman et al., 2001). [**](Stal and Lindman, 2000). [***](Moon et al., 1998). † Cadavers. [I] Neonatal fibres 1.1%; developmental fibres 0.6%. [II] Neonatal 4.4%; developmental 1.8%. [III] Neonatal 2.6%; developmental 1.3%. [1] Neonatal 5.2%; developmental 2.2%. [2] Neonatal 2.6%; developmental 1.2%. [3] Neonatal 4.8%; developmental 3.1%.

VPI in the presence of SMCP may be related to fatigue of the soft palate caused by abnormal insertion of the LVP muscles (Weatherley-White et al., 1972) which are also operating at a mechanical disadvantage. A palatoplasty with LVP repositioning should help solve the problem, but studies show that attempted repair of the palatal defect has often given less good results (Park et al., 2000, Abyholm, 1976, Sommerlad et al., 2004) compared to other cleft types (Bicknell et al., 2002, Ysunza et al., 2002, Wong et al., 2019). It is possible that the intrinsic muscle morphological abnormality remains after repair and adds to the reasons for VPI. Our study demonstrated that there was indeed a different fibres distribution, with slow fibres prevalence, in SMCP LVP compared to other cleft types and this might be significant finding in terms of persistent VPI.

Ageing is important when considering muscle function. Studies on muscle morphology and electrophysiology show that during ageing, a shift in fibre type occurs. This is likely due to degeneration of motor neurons in limb (Trappe et al., 1995) and masticatory muscles (Monemi et al., 1996). In limb muscles, atrophy and fibre loss is primarily with the fast type II fibre population, while in masseter (a human jaw muscle) degeneration is mainly affecting the type I fibres (Stal and Lindman, 2000). It is difficult to tell how much fibre type population is affected by age in cleft patients. Routine CP palate repair is usually done in the first year of life, however, SMCP patients generally present later and therefore surgery is also performed when the child is older (Chen et al., 1996). In our study muscle biopsy samples were collected in CP patients from ages between 10 to 15 months, in control (tonsillectomy) group from 1 year 7 months to 4 years 2 months, while the SMCP group ranged from 5 to 9 years. Muscle structures are known to mature through childhood and this could be seen in the shift from developmental and neonatal fibres. Another factor to be taken into consideration is the abnormal cleft muscle anatomical position is present for longer because of later correction in SMCP. This may affect normal muscle functional development, and therefore, not all the changes described may simply be due to aging. There are studies investigating aging especially in physical performance of athletes (Doherty et al., 1993) but there is much less known about aging of velar structures and their performance.

There has long been a discussion in literature about the most efficient palate repair method from anatomical, physiological and outcome measures perspectives. Although many techniques are described, none of them seem to provide the ideal option. One of the most widely used techniques to repair CP as well as SMCP is intravelar veloplasty (IVVP) (Sommerlad, 2006). This technique is advocated widely since the velar muscles are initially orientated in the wrong direction and demonstrate abnormal attachment (Kriens, 1969, Kriens, 1970). Therefore detaching the muscles from their abnormal insertion and repositioning in more normal anatomical position should restore velar function (Sommerlad et al., 2004). IVVP indeed recreates the levator sling mechanism, also restoring PP muscle position. Reconstruction of the PP muscle enables the sphincter mechanism to be restored which, in theory at least, improves pharyngeal wall function.

Another widely used technique for palate repair is Furlow palatoplasty (Furlow, 1986). From an anatomical point of view, the aim is to reorientate the velar muscles to the correct transverse position, whilst at the same time, lengthening the velum to reduce the distance between palate and posterior pharyngeal wall. Although lengthening of the velum in itself is not necessarily advantageous, a functional lengthening of the soft palate is a desirable outcome (Huang et al., 1999). The oral and nasal myomucosal flap repositioning enables the LVP and PP muscle to overlap, which is not morphologically normal since it has been shown that the LVP fibres do not overlap significantly across the midline (Huang et al., 1998). The muscle overlap result in thickening of the velum and this asymmetrical design is responsible for an occasionally observed asymmetrical velar movement (Huang et al., 1999).

The pharyngeal flap is relatively unphysiological and disrupts the anatomical integrity of the pharyngeal wall. It often depends on the low sphincteric action of pharyngeal muscles (superior constrictor and the transverse fibres of palatopharyngeus) to achieve closure against the midline flap. If these muscles are not primarily speech muscles, the timing of their movement may intrinsically be too slow to avoid nasal emission of air.

The sphincter pharyngoplasty theoretically relies on transposed palatopharyngeus muscles to achieve active sphincteric closure. It may do less damage to the normal anatomy and tends to correct coronal and circular VPI patterns (Cole et al., 2008). It seems that IVVP and the Furlow procedure do correct LVP and PP position and are appropriate techniques for primary as well as secondary palatoplasty (Mapar et al., 2019, Taib et al., 2015, Bruneel et al., 2018, Chen et al., 1996, Chen et al., 1994).

Our study showed that in the limited, single case analysis of achondroplasia, Apert, Cornelia de Lange and Kabuki syndrome patients, palate muscles did not differ from CP cases. Currently syndromic CP care does not differ for these syndromes from a general cleft management point of view but does require certain treatment adjustments according to the specific medical needs of the individual.

From personal observation and discussion with experts in cleft patient management (personal communication with several of the North Thames Cleft Team surgeons), it has been noticed that during SMCP repair, the LVP appears to be less robust and has the appearance of being more fatty. Our study did not find an obvious difference in term of fat content for the LVP albeit looking at a very small sample number, however, the PP muscle showed a higher tendency for fat accumulation in SMCP patients. This finding will need to be further investigated in future studies using a larger number of patients. Whilst there has been little previous work done on this topic, there has been some evidence to suggest that palate muscles has a higher content of connective tissue within the velum muscles (Stal and Lindman, 2000) compared to limb. However, in our study a significant difference for connective tissue levels in LVP and PP muscles in different cleft types was not observed.

III. 7. Conclusion

In the present study to investigate velum LVP and PP muscles histology, we have identified the fast and slow fibre distribution in ICP, ICP in RS, UCLP, SMCP, SMCP in 22q11.2 DS and normal controls. The results show that in all groups, fast fibres were prevalent with the exception of SMCP LVP, where the number of slow fibres was greater than fast fibres. Analysis of fat accumulation showed a tendency for the SMCP PP muscles to be more fatty. Contrary to the literature, connective tissue within LVP and PP muscle did not show significant differences. Analysis of single samples from the CP syndromes achondroplasia, Apert, Cornelia de Lange and Kabuki did not reveal significant differences.

Our study suggests that SMCP may be a special group amongst cleft types with an essentially different pathology to CP. An intrinsic deficit in the morphology of the velum musculature could possibly explain certain difficulties in SMCP patient management and the less favourable surgery outcomes that often occur. However, the biopsies were from older subjects and we did not have other specimens from older CP patients for comparison. Further studies are therefore required.

III. 8. Future work

In a project such as this, much time and effort is required to collect a suitable and biologically significant sized sample collection. The numbers collected are dependent on many factors, not least the willingness of the patients and their families to participate and the compliance of the surgical team, who will perform the biopsies. Another restricting factor is the number of cases seen by the given team. There is a good case for collaboration with cleft teams at other centres, in order to obtain sufficient numbers. However, as the number of participating surgeons increase, this would require good management since there are more opportunities for variability in the sample collection, from documentation, to muscle type as well as non-uniform site of a biopsy. It is therefore important to identify a project such as this as early as possible and to try to have patient recruitment into the research project and sample collection occur as part of the routine ethos. Only by actively pursuing sample collection over an extended period will it be possible to generate sufficient sample numbers, particularly for the more rare CP syndromes of interest, particularly 22q11.2 DS, RS and other.

As is often the case when embarking upon a study such as this, significant methodological advances can occur over the duration of the project. At the inception of this project, it was decided to collect muscle biopsies and process them for routine histology. However, more recent technologies have been developed which have the potential to both increase ease of analysing data and improve the information content obtained. One such method uses immunofluorescence analysis, often with dual markers assisting quantification of transverse sections using and automated scanning system and an image processing script (e.g. Definiens Architect software) (Sardone et al., 2018). Unfortunately, it was not possible to adapt the biopsies taken in the present study to this technology since they were sectioned and processed by routine stains piecemeal over the course of the project. However, for future palate muscle histology studies, I would recommend use of this type of approach.

Stem cell therapy in human and animal studies is now becoming ever more widely discussed in the literature, particularly over the last decade (Mazzetti et al., 2018,

Tanikawa et al., 2013, Li et al., 2019c, Schreurs et al., 2019). One of the future proposals would be to investigate the effect of stem cells on palatal muscle and bone development. The stem cells, usually derived from adipose tissue, amniotic fluid or muscle satellite cells from the individual to be treated, would be used to first test whether they have the capacity to colonise and affect tissues that are involved in the palate defect. This could potentially be by injecting straight into the blood stream, more directly into the soft palate tissue or applied with a biological scaffold during surgery. Some functional evidence for the applicability of this type of project has been described for satellite cells, the muscle stem cells (MSCs) (Abou-Khalil et al., 2015). However, the development of a reliable embryonic MSCs differentiation protocol is required and first introducing MSCs into a palate shelf culture model (Shiota et al., 1990) might be a useful approach. This could be followed by stem cell based tissue engineering strategies applied to an *in vivo* model such as *Tbx22*^{null} mice in order to investigate effects on the features of SMCP (Carvajal Monroy et al., 2013). Successful stem cell based tissue engineering strategies could be then translated into clinical practice and would potentially improve CP repair outcomes. A detailed understanding of palate muscle histology would therefore be very helpful to inform and guide stem cell based tissue engineering studies to achieve the best result.

Chapter IV: Investigation of transcriptional changes downstream of *Tbx22* during mouse palate development

IV. 1. Introduction

IV. 1. 1. *TBX22*

The TBX22 transcription factor has been demonstrated to play a major role in human palatogenesis (Braybrook et al., 2001, Braybrook et al., 2002, Marcano et al., 2004, Andreou et al., 2007). The *TBX22* gene encodes a member of a family of proteins that were identified and named due to sharing a common DNA-binding sequence, the so called T-box domain (Naiche et al., 2005). The original T-box protein, simply called T (Tailless), was first identified as the mutated gene present at the *T* locus of the *Brachyury* mouse (Wilkinson et al., 1990). *T* was found to encode a transcription factor, which was characterized by the T-box DNA-binding domain. Subsequent discovery of other proteins containing similar DNA-binding motifs gave rise to the T-box protein family. In mammals 17 T-box genes are present. They are grouped into five subfamilies: Tbx1, Tbx2, Tbx6, Brachyury/T and T-brain (Tbr1) (Naiche et al., 2005). TBX22 belongs to the TBX1 subfamily, along with TBX10, TBX15, TBX18 and TBX20 (Naiche et al., 2005) where TBX22, TBX15 and TBX18 are most closely related, each sharing a single ancestral progenitor sequence in the primitive chordate, *Amphioxus* (Ruvinsky et al., 2000). T-box containing proteins are all transcription factors that are involved in the regulation of many different developmental processes (Papaioannou and Silver, 1998, Papaioannou, 2014). T-box proteins were found to bind directly to DNA via a conserved sequence of ~180 amino acids (Muller and Herrmann, 1997). Oligonucleotide binding site selection assays identified a 20 base pair palindromic sequence T(G/C) ACACCTAGGTGTGAAATT or a portion of this sequence called the T-half site AGGTGTGAAATT as the common consensus sequence that T binds to, either as a dimer or as a monomer (Kispert and Hermann, 1993). Other T-box genes that have been tested, also bind to a similar sequence, this includes TBX22 that was found to bind to the imperfect palindrome AGGTGTG AAATTGTCACCT (Andreou et al., 2007).

T-box family members differ through divergent sequences in the N- and C-terminal domains that flank the T-box domain. Generally, the C-terminus acts as the transcriptional activator and/or repressor domain, while N-terminus interacts with cofactors. It is known, that T and TBX5 proteins hold two C-terminal activation

domains and two repression domains (Zaragoza et al., 2004). Reporter gene expression assays in T showed that the two activation domains work additively (Kispert and Hermann, 1993). In contrast, TBX2 and TBX3 are considered as transcriptional repressors (Carreira et al., 1998). Reporter studies of TBX22 revealed that it was primarily a transcriptional repressor although there was also evidence of a weak activation domain (Andreou et al., 2007).

Several co-factors that interact with T-box proteins have been identified and these include homeodomain proteins (Bruneau et al., 2001), GATA zinc finger proteins (Stennard et al., 2003) and LIM domain proteins (Krause et al., 2004). These are thought to play significant roles in T-box proteins transcriptional regulation. Some target genes are thought to be regulated by T-box proteins without cofactor help (Kusch et al., 2002).

Mutations in *TBX22* were found to underlie the inherited X-linked disorder, CP with ankyloglossia (CPX; OMIM 303400) (Braybrook et al., 2001). Mutations were originally found in several large X-linked families but broader studies of CP revealed mutations in about 4% of CP cases, often including sporadic individuals or small families where X-linked inheritance could not be determined (Marcano et al., 2004, Suphapeetiporn et al., 2007). This makes mutation in *TBX22* as one of the most common genetic causes of CP. As an X-linked condition, CPX was found to affect predominantly male patients but also approximately one-third of female carriers are affected with a cleft (Braybrook et al., 2002). Ankyloglossia without CP is present in many carrier females and occasionally in males who show partial penetrance (Marcano et al., 2004). In general there is high phenotypic variation associated with *TBX22* mutations (Figure IV. 1), including ankyloglossia alone, CP or SMCP each with or without ankyloglossia, hypodontia and even the CHARGE-like/Abbruzzo-Erickson syndrome (Pauws et al., 2009b, Suphapeetiporn et al., 2007). These genetic findings indicate that it must play a major role in normal human palatogenesis. This is supported by various further studies including expression analysis. Temporal and spatial expression analysis in human and mouse using *in situ* hybridization showed that *TBX22/Tbx22* is expressed primarily in the palatal shelves and developing tongue during the period of palatogenesis, indicating an important role in palatal and tongue development (Marcano et al.,

2004, Bush et al., 2002). Knockout of *Tbx22* in the mouse also supports this although it results primarily in a SMCP with high penetrance, and only occasionally overt CP has been observed (Pauws et al., 2009a).

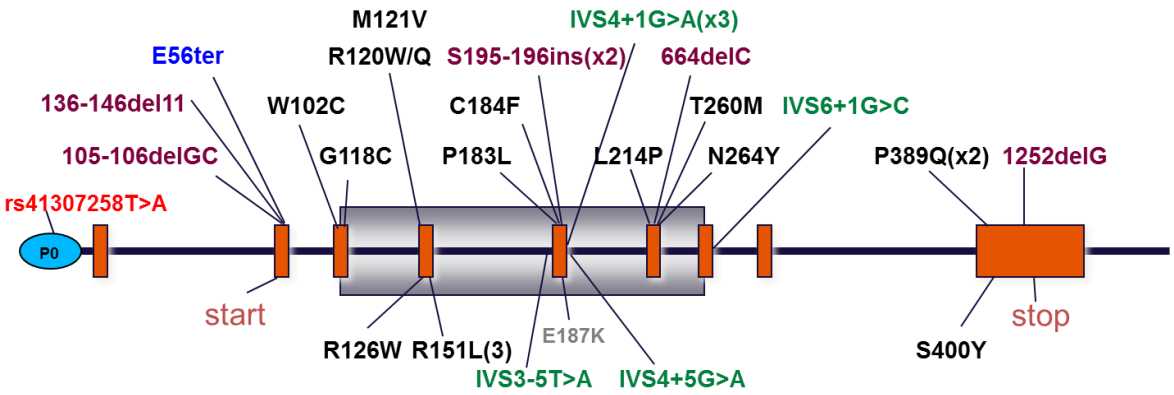

Figure IV. 1. Mutational spectrum found in *TBX22*.

Promoter, missense, nonsense, in/del and splice site mutations in *TBX22* cause syndromic and NS CPX with a broad range of phenotypes (SMCP, CLP, ankyloglossia, hypodontia and Abbruzzo-Erickson syndrome). Data from Stanier et al. (Stanier et al., 2018).
Red - non-coding SNP; purple - indel; blue - gain of stop; black - missense; green - splice site; P0 – promoter; orange boxes – exons; grey box – T-box domain encoding exons; start and stop codons are indicated.

IV. 1. 2. *TBX22* regulation and function

The majority of TBX22 missense mutations have been identified within the DNA binding T-box domain (Braybrook et al., 2002, Marcano et al., 2004, Suphapeetiporn et al., 2007, Chaabouni et al., 2005). This suggests that resulting loss of transcription factor binding is a possible mechanism. Evidence for this was provided by electrophoretic mobility shift assay (EMSA) studies, which showed complete or partial loss of binding to the T-box binding element consensus sequence (Andreou et al., 2007). It is interesting to note that the precise binding sequence does not occur as a linear sequence in the human genome, rather, it is more likely that TBX22 (along with other T-box genes) more naturally binds to single T-half sites, or pairs that are brought into apposition by DNA looping. In terms of regulation of *TBX22*, investigation of the genomic sequence first revealed

a putative promoter sequence upstream of a noncoding exon, which was approximately 10 kb away from the first coding exon that contained the translation start site (Braybrook et al., 2002). Using reporter assays to test these sequences, significant promoter activity was identified for a minimal 300 bp sequence, upstream of the start of transcription and adjacent to the distant exon. This sequence also contained a putative T-half site (Andreou et al., 2007). Investigating a series of different cell lines revealed that promoter activity could only be detected in those cell lines that did not express *TBX22*. With the hypothesis that this might indicate auto-regulation, it was then demonstrated *in vitro* that TBX22 functioned as a transcriptional repressor and could repress its own transcriptional activity. Analysis of patient mutations demonstrated that they had a significant effect on abrogating DNA binding and affected TBX22 transcriptional repression (Andreou et al., 2007). Another important factor in the regulation of transcriptional activity was transient post-translational modification by the small ubiquitin-related modifier SUMO-1. TBX22 was shown to require sumoylation at amino acid residue p.K63 for repression activity, whilst in the absence of this SUMO modification, TBX22 remained transcriptionally inactive (Andreou et al., 2007).

TBX22 was investigated for potential transcriptional targets using comparative array analysis of RNA extracted from mouse embryonic palatal shelves in WT and *Tbx22*$^{-/Y}$ animals (Hoshino, 2011). Mutant embryonic palates were found to be enriched mainly for muscle precursors, which included the myogenic transcription factor *MyoD*. The latter was confirmed when the *MyoD* promoter was shown to physically bind to TBX22 using a CoIP method (Kantaputra et al., 2011).

The transcription factor *Mn1* was shown to play an important role in the regulation of posterior palatal growth and development (Liu et al., 2008). In these studies, *Mn1* was shown not only to have a similar AP expression distribution in the developing palate as *Tbx22*, but was also shown to drive expression of *Tbx22* promoter constructs. In fact, overexpression of *Mn1* in NIH3T3 cells increased endogenous *Tbx22* expression in a dose dependent manner, which provided evidence that *Mn1* may play an important role in regulating *Tbx22* during mammalian palate development (Liu et al., 2008). Regulation of *Tbx22* in the chick has also been investigated. Both Higashihori et al. (2010) and Fuchs et al. (2010)

demonstrated that FGF induces and maintains *Tbx22* expression, while BMP has the effect of restricting *Tbx22* expression. Overexpression of *Tbx22* led to decreased cell proliferation and reduced expression of the craniofacial transcription factors *Msx2* and *Dlx5* (Higashihori et al., 2010, Fuchs et al., 2010).

IV. 1. 3. Cleft palate animal models

Nine animal species are described in the literature for CLP research, although use of the cat, pig, sheep and guinea pig animal models are rare. The chick has been widely used by developmental biologists, even for craniofacial development; however, birds have a natural CP, clearly limiting their use in this regard. If research requires surgical or more complex manipulations, dogs are found to be the most suitable for that purpose (Jänicke and Huber, 1996). Because of difficulties in keeping and obtaining permission to work with larger species of animal model, use of smaller animals has gained increasing importance. The most frequently used animal model to study CP is mouse (Gritli-Linde, 2012) and rat (Poswillo and Roy, 1965). The mouse is a particularly good model for CP as it shares many anatomical and molecular similarities with human palate development and is amenable to experimental and genetic manipulation in a cost effective manner. Although CP is a lethal condition to new born pups because of breathing and feeding incompetence, study of palate development in the mouse embryo has provided many clues to various genetic, cellular and molecular events important in the aetiology of orofacial clefts. CP results from disruptions affecting cell migration, proliferation, apoptosis, ECM deposition and morphogenetic movements (Fan et al., 2016, Nakajima et al., 2018, Nik et al., 2016, Fuchs et al., 2010). During early embryo development the mouse and human palates are largely similar and essentially of very similar size. Mice and humans share over 99% of their genes and many causative genes in human CP have the same effect in mice (Li et al., 2017a).

There are many genetically altered mice which provide good models for CP. Most clefting phenotypes in mice are recessive with the cleft phenotype only being expressed in mice that are homozygous for the given ablated gene (Gritli-Linde,

2012). One example is haploinsufficiency of *TBX1* causing CP in humans which most commonly results in the 22q11.2 DS, whilst the full phenotype in mice, which also includes CP, is only present in homozygous null animals. Interestingly, as one of the only other T-box genes that when mutated reproducibly results in CP, TBX1 is structurally highly similar to TBX22 and is in the same phylogenetic subfamily (Papaioannou and Silver, 1998).

Other mouse models which replicate cleft syndromes found in humans include various fibroblast growth factor receptor (FGFR) mutations. FGF signalling has a number of important roles during lip and palate development and both activating and loss-of-function mutations can result in CP (Stanier and Pauws, 2012). An activating mutation in FGF receptor 2 (*Fgfr2*) is used as a model of Cruzon's syndrome in humans. Other mutations in either *Fgfr1* and *Fgfr2* are associated with Kallman (OMIM 308700), Pfeiffer (OMIM 101600) an Apert (OMIM 101200) syndromes where CP is part of a broad craniofacial phenotype (Lee et al., 2018).

IV. 1. 4. *Tbx22* knockout mouse

Mice lacking *Tbx22* were generated (Figure IV. 2) by introducing loxP sites flanking the first 2 exons of the *Tbx22* gene (Pauws et al., 2009a). The first 2 exons were subsequently removed using a *βactin*-Cre loxP deleter strain to create the $Tbx22^{null}$ allele. The original allele was introduced into 129/Sv embryonic stem cells but was later bred onto either C57Bl/6 or CD1 backgrounds for further experiments.

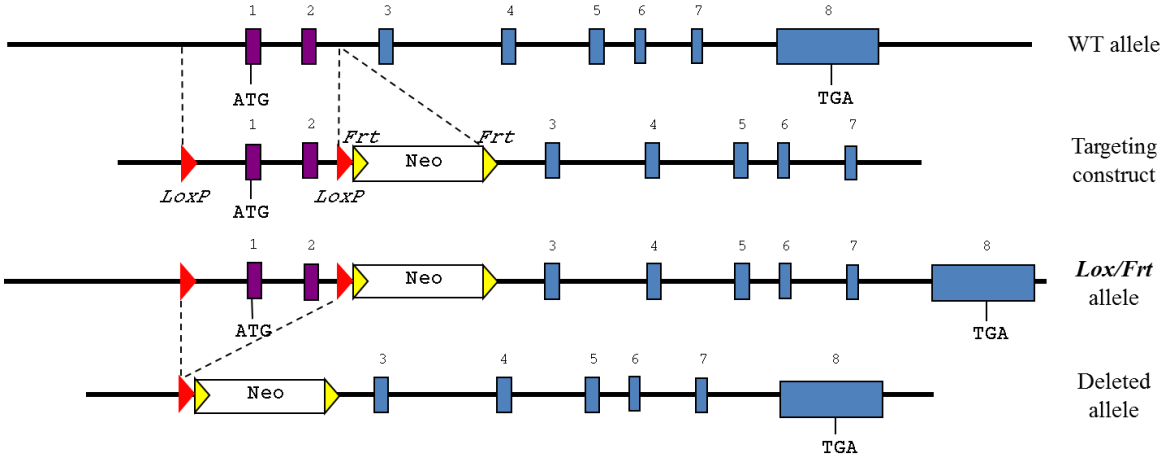

Figure IV. 2. Mouse *Tbx22* knockout.

Schematic diagram of the mouse *Tbx22* gene and the targeting construct. After recombination, *LoxP* sites along with a *Frt*-flanked Neo^R cassette are inserted creating a floxed mutant allele ($Tbx22^{flox}$). Then a $Tbx22^{null}$ allele was created crossing with *βactin*-Cre loxP delete strain. It was reported that even after removing Neo^R cassette from $Tbx22^{null}$ allele using *Flp*-deleter *in vivo*, the identical phenotype in mutants was observed (Pauws et al., 2009b).

In the *Tbx22* knockout mouse, overt CP was reported only in a small proportion (<5%) of male null animals (Pauws et al., 2009a). The remainder exhibited a notch in the posterior edge of the hard palate. Analysis of the craniofacial skeleton showed that this corresponded with reduced formation of the intramembranous palatine bones, which constitute the posterior region of the hard palate. This finding is equivalent to the phenotype of a SMCP, similar to that seen in many CPX patients. A number of animals were also found to have either bilateral or unilateral choanal atresia. The bilateral form was believed to contribute to postnatal lethality since surviving male null animals with a SMCP often had unilateral choanal atresia but never bilateral choanal atresia, although this was frequently seen at embryonic stages. Isolated SMCP (with or without unilateral choanal atresia) did not appear to affect survival or longevity as opposed to an overt cleft which was early postnatal lethal. The marked effect on palatal bone formation indicated that *Tbx22* plays an important role in osteogenic patterning, with mutant animals exhibiting delayed maturation to the osteoblasts in the palatine bones (Pauws et al., 2009a).

In humans, ankyloglossia is considered a characteristic phenotype of CPX. In *Tbx22* knockout mouse embryos, a highly penetrant, more anterior caudal attachment of the tongue to the mandible was described (Pauws et al., 2009a). This was equivalent to the shortened frenulum (ankyloglossia), although in these mice, the attachment was never seen reaching the tip of the tongue, and was considered only a very mild form of ankyloglossia.

IV. 1. 5. *TBX22* and *Tbx22* expression

In the human, *TBX22* expression is first detected by *in situ* hybridisation at CS16 with a signal in the first pharyngeal arch. By CS17 a strong signal is detected in the mesenchyme of the lateral and medial nasal processes, the lateral palatal processes and at the base of the tongue (Braybrook et al., 2002, Bush et al., 2002). There is also expression in the mesenchyme of the developing face and base of the brain. At CS19 the expression is observed in the developing nose, primary palate, base of the tongue and in the developing facial mesenchyme. At the same stage, a strong signal is detected in the oronasal membrane, which ruptures to form the anterior connection between the nasal and pharyngeal cavities. At CS19 lateral palatal processes have not as yet begun to grow downwards as lateral palatal shelves, yet clear expression is still detected. Palatal shelves grow vertically at CS20 and CS21 where there is strong expression of *TBX22*, Figure IV. 3. Expression in the palatal shelves appears stronger medially than laterally. This observation is supported by the expression pattern in the developing mouse palate. Expression analysis of E12.5-E17.5 mouse embryos showed that the location of mRNA expression closely correlates between mouse and human (Hoshino, 2011). At later stages, *Tbx22* expression was also detected in mouse lung and whisker follicles (Braybrook et al., 2002, Bush et al., 2002). The expression of *TBX22* is entirely consistent with the CPX phenotype and as such the mouse provides a useful model for craniofacial development research.

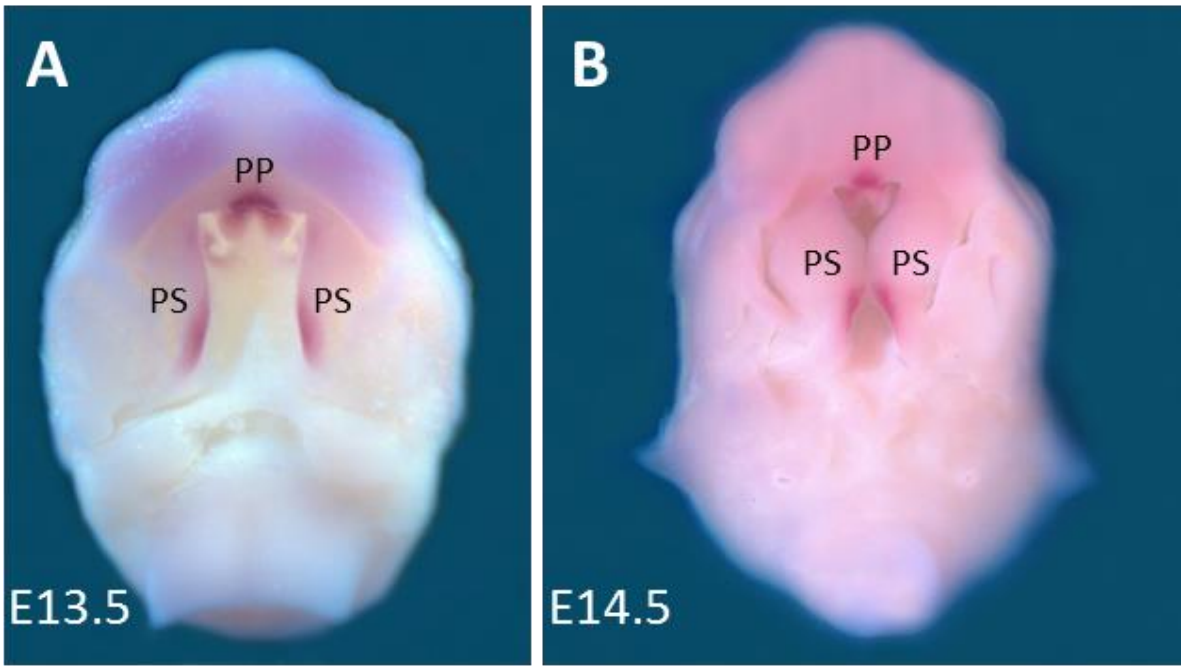

Figure IV. 3. *Tbx22* expression pattern in mouse embryo.

Tbx22 expression in the developing palatal shelves as detected by whole mount in situ hybridisation using a *Tbx22* antisense probe at **A)** E13.5 and **B)** E14.5. **PP** - primary palate; **PS** - palatal shelf (Hoshino, 2011).

IV. 1. 6. Cranial neural crest and cranial mesoderm

Craniofacial development is a complex three-dimensional process. Cartilage and bone of face, jaws, palate and skull are formed from cells that differentiate from CNC and CM derived progenitors. CNC cells generate most of the peripheral nervous system, cartilages, bones and loose connective tissues in the vertebrate facial and branchial regions. CM is known as a precursor tissue for the muscles as well as endothelial cells including the vasculature and connective tissue (Noden and Trainor, 2005). Both phenotype and transcriptome studies in conditional knockout mice for differentially enriched genes in the CM and CNC show that cross-talk between the two tissues is crucially important (Fan et al., 2016).

The precise role and contribution of specific cell lineages have traditionally been studied using cell lineage tracing, where marking a specific cell type allows it to be followed during development. In earlier days, these studies relied on externally applied tracers or inter-embryonic transplantation (Yoshida et al., 2008). In mice,

extrinsic cell labelling or transplantation approaches have been restricted either by the time period during which the embryos are accessible *in vitro* or by the duration of a label injected *in vivo*. Therefore, little information is gained as to interactions between tissue origins and cell fates (Chai et al., 2000). A more recent tool added to the developmental biologist's armoury came with the introduction of transgenic animals. This included mice modified at the *Rosa26* (R26) locus (Soriano, 1999). R26 was identified in 1991, during an experiment to introduce a promoter-free retrovirus carrying the β-Galactosidase (β-Gal) reporter randomly into the mouse genome. The R26 line 'trapped' a mouse gene that showed ubiquitous expression of the reporter, while the mice were free of abnormalities and remained fertile (Friedrich and Soriano, 1991). Subsequent tools could be generated to investigate tissue specific lineages without some of the earlier limitations. An example of this uses the *Cre*-loxP reporter system (Liu et al., 2018) where the expression of Cre-recombinase results in recombination between two loxP sites engineered into a genome. Cre itself is usually driven by a single gene promoter in order to target a particular cell population during development and by using a single-coloured loxP reporter system, *Cre*-loxP recombination can be used to label Cre-expressing cells (Madisen et al., 2010). As an example, it was possible to generate a *Wnt1*-Cre/R26 line with a permanent molecular marker for NC cells, allowing the tracing of NC migration from early embryos to adults following *LacZ* expression (Yoshida et al., 2008, Chai et al., 2000). A further refinement was to swap β-Gal for a fluorescent marker such as YFP e.g. R26-Fl-stop-Fl-YFP, so that specific cells can be viewed under UV or used in fluorescence cell sorting experiments.

IV. 1. 7. Intramembranous and endochondral ossification

Ossification (osteogenesis) in human embryo begins by the 6th or 7th week of embryonic life. Beforehand, in the early stages, the embryo's skeleton consists of fibrous membranes and hyaline cartilage (O'Rahilly and Gardner, 1972). Intramembranous ossification and endochondral ossification are two osteogenic pathways which both produce bone tissue, despite using a different mechanism (Breeland and Menezes, 2019).

Endochondral bone can be considered a replacement tissue and it replaces cartilage which is the most common template (Ortega et al., 2004). A framework determines where bones will form during fetal development. This framework consists of HA, chondroitin sulphate, collagen fibres, and water and is produced by chondroblasts. Chondrocytes are chondroblasts surrounded and isolated by matrix. Cartilage has no blood vessel support unlike most connective tissue and functions instead by diffusion through the matrix. During fetal development and childhood growth, bone is formed on the cartilaginous matrix. Most cartilage has been replaced with bone by the time of birth (Ortega et al., 2004). The skull base and long bones are formed by endochondral ossification. It is a much longer process than intramembranous bone formation (Rauch and Glorieux, 2004). Hyaline cartilage serves as template and is replaced by bone completely. At 6 to 8 weeks of gestational age chondrocytes differentiate from mesenchymal cells to form the cartilaginous skeletal precursor of the bones. Afterwards perichondrium appears. Production of matrix makes the chondrocytes grow in size. Matrix calcifies and this process causes chondrocytes to die and the surrounding cartilage to disintegrate. The spaces formed are invaded by blood vessels, bringing osteogenic cells which will become osteoblasts. These spaces combine to form the medullary cavity. Capillary penetration then initiates bone producing periosteum formation from perichondrium while osteoblasts form a periosteal collar of compact bone around the cartilage of the diaphysis. Ossification begins deep in the periosteal collar from the primary ossification centre usually around the 2nd or 3rd month of fetal life. While this is in progress, chondrocytes and cartilage continue to grow at the future epiphyses. Cartilage remains at the joint surface and as an epiphyseal plate which is responsible for the longitudinal growth once the fetal skeleton is fully formed. After birth, matrix mineralization continues along with death of chondrocytes and invasion of blood vessels from the periosteum. The epiphyseal regions are seeded with osteogenic cells that become osteoblasts, which at this stage are called secondary ossification centres (Rauch and Glorieux, 2004).

In contrast, the flat bones of the face, most of the cranial bones, and the clavicles are formed by intramembranous ossification. In this case, compact and spongy bone develops directly from sheets of undifferentiated mesenchymal connective tissue (Jin et al., 2016). The process starts when mesenchymal cells begin to

differentiate into capillaries, osteogenic precursor cells and then osteoblasts. Early in development, osteoblasts first appear in clusters, described as ossification centres, which spread out and fuse to form bone tissue. The bone matrix is then produced by osteoblasts which secrete an unmineralized, organic glue-like substance called osteoid, composed principally of collagen and mucopolysaccharides. Inorganic minerals are then laid down and the osteoid calcifies to produce the primitive trabecular bone matrix. During this process some osteoblasts remain trapped within the matrix and become terminally differentiated osteocytes. These cells connect with one another and remain in the bone where they are long lived and function in bone maintenance and adaptation to bone stresses, load changes or damage. Whilst osteoid forms the trabecular matrix, osteoblasts at the spongy bone surface create periosteum. Periosteum plays a protective role of compact bone superficial to the trabecular bone. Red marrow is formed by condensation of trabecular bone surrounding nearby blood vessels. Intramembranous ossification begins *in utero* and ends at the end of the adolescent growth spurt. At birth, the skull and clavicles are not yet fully ossified and the skull sutures still remain open, which facilitates the skull to deform during birth and allows for post-natal growth of the brain (Jin et al., 2016).

IV. 2. Aims and rationale of the study

As described above, previous studies of mice with constitutively deleted *Tbx22* revealed a phenotype of SMCP in the majority of animals (Pauws et al., 2009a). This was best observed by staining cranial skeletal preparations at E15.5 or older with alcian blue and alizarin red. This technique revealed a clear deficiency in the pair of developing palatal bones. In the present study, an important aim was to gain a better understanding of cell lineage-specific function of *Tbx22* in palatal bone formation by dissecting the contribution of the CM and CNC in *Tbx22*-dependent palatogenesis. As an initial step, this was first looked at in stained cranial skeletal preparations, following tissue specific ablation of *Tbx22* using the *Cre*-loxP system. Following this, a more precise investigation would be carried out into *Tbx22*-dependant tissue specific gene expression differences that occur immediately prior to palatal shelf fusion.

Tbx22 was already known to be expressed most highly in the posterior region of the elevating palatal shelves at E13.5 (Braybrook et al., 2002, Bush et al., 2002). Hoshino (2011) previously investigated *Tbx22*-dependent palatal gene expression analysis using whole, dissected E13.5 palatal shelves examined with a microarray-based technology. This analysis would now be considered somewhat crude, since it included the entire palatal shelf including all cell types therein, even those that do not express *Tbx22.* The microarray platform itself has various limitations since it was based on hybridization technology, relied on fluorescence detection for quantitation and by design only looked at a defined set of targets that inefficiently represent the transcriptome. These methodologies have more recently been superseded both by RNA-Seq technology and the ability to more precisely isolate palatal tissue in a cell-type specific way.

The current study therefore planned to improve the resolution of previous analysis at the tissue specific level by adopting the *Cre*-loxP system to introduce fluorescence cell sorting to separate and recover *Tbx22*-expressing cells and to use RNA-Seq to improve the coverage of the cell type-specific transcriptome. It will be possible to compare gene expression in flow sorted palatal shelf tissue specific cells between WT and *Tbx22*$^{-/Y}$. This would facilitate the identification of relevant

downstream transcriptional targets in both CM and CNC derived tissue. These transcripts would potentially highlight genes and pathways that are important for normal palate development and those that are defective in *Tbx22* mutants.

IV. 3. Results

IV. 3. 1. Tissue specific ablation of *Tbx22* using the *Cre*-loxP system

The SMCP phenotype with reduced development of palatal bones is characteristic of the *Tbx22*$^{-/Y}$ mouse (Pauws et al., 2009a). To interrogate the tissue specific origin of this, *Tbx22* was selectively deleted in either CNC (using *Wnt1*-Cre) or pre-somitic CM (using *Mesp1*-Cre). Four crosses (females *Tbx22*$^{flox/+}$ with males *Wnt1*-Cre or *Mesp1*-Cre) were set up and 31 embryos at stage E17.5 were recovered for analysis (19 in *Wnt1*-Cre and 12 in *Mesp1*-Cre cross). The heads of each of these animals were separated from their bodies and dissected for visual evaluation. After genotyping, a total of 8 males were identified. These were visually inspected and the SMCP palate phenotype was clearly observed in all animals in which the gene was deleted. This included both the CM (N=3) and CNC (N=1) deleted mice, while the phenotype was not seen in WT controls (N=4). The phenotypes were confirmed following the alcian blue and alizarin red skeletal staining protocol (Figure IV. 4) (Nagy et al., 2009) as described in the Section II. 11. Alcian blue and alizarin red skeletal staining.

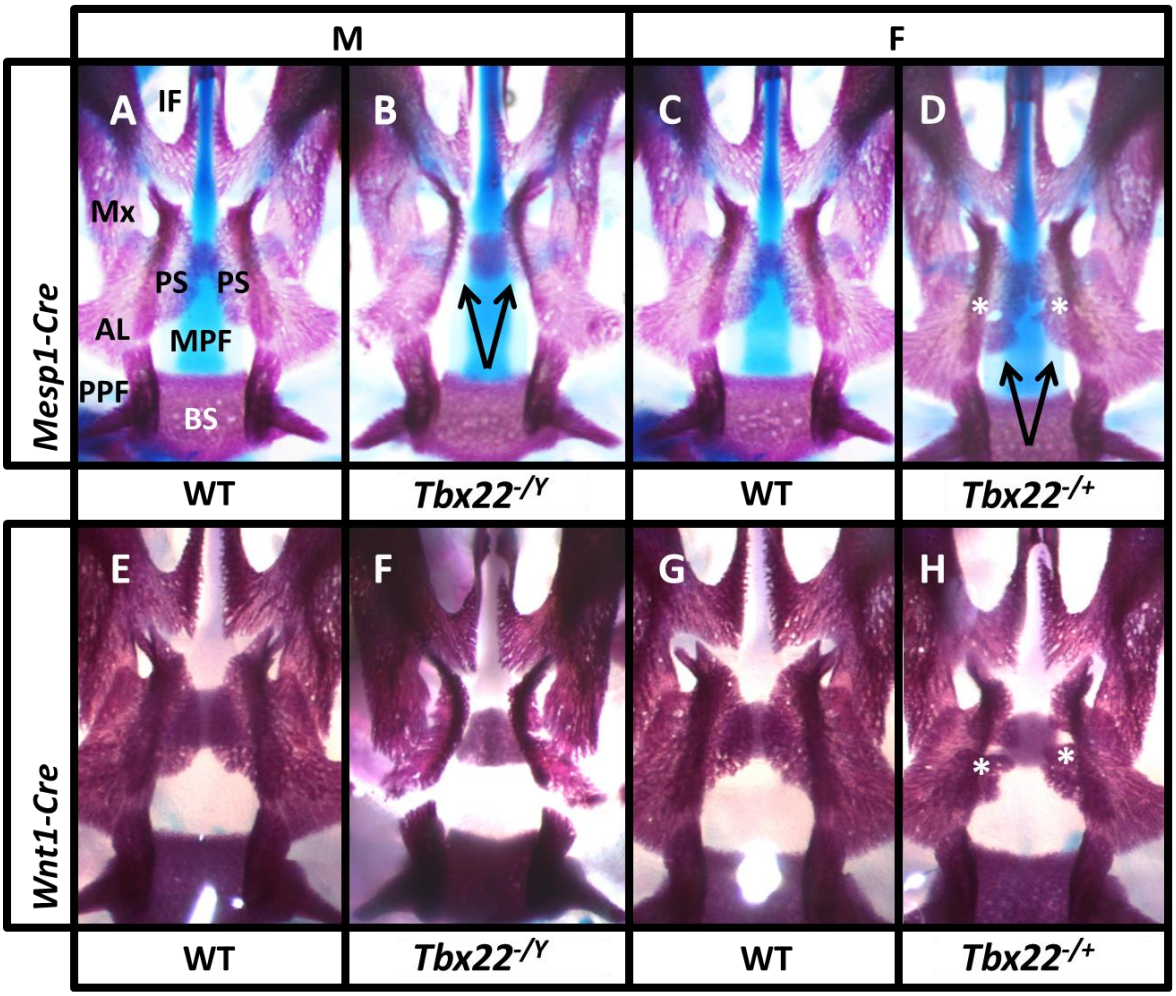

Figure IV. 4. Palate phenotype in E17.5 WT and null (*Tbx22*$^{-/Y}$) male and heterozygous female embryos.

A, E) WT male and **C, G)** WT females have palatal shelf bones that appear normal. **B)** *Mesp1*-Cre positive male and **F)** *Wnt1*-Cre positive males lack equivalent bone structure in the palatal shelves (SMCP phenotype). **D)** *Mesp1*-Cre positive female and **H)** *Wnt1*-Cre positive female both exhibit a bone deficit affecting the palatal shelf margins (indicated with ∗). Arrows indicate structural changes. **PS** - palate shelf; **IF** - incisive foramina; **PPF** - parapterygoid fossa; **AL** – alisphenoid; **BS** – basisphenoid; **Mx** – maxilla; **MPF** - mesopterygoid fossa (Missagia and Perini, 2018).

Interestingly, *Mesp1*-Cre (N=2) and *Wnt1*-Cre (N=1) positive heterozygous females also developed a visible bone deficit phenotype affecting palatal shelves margins. This phenotype was not as severe as in males and was only noticed after staining rather than during preliminary examination of the gross anatomy. More surprisingly, not only CM or CNC specific *Tbx22*-deleted animals exhibited SMCP (or females

with the affected palate shelves margin phenotype), but also *Tbx22*$^{flox/Y}$ males (N=6) and *Tbx22*$^{flox/+}$ females (N=3), while WT controls (M=4; F=11) were normal. To investigate this unexpected finding further, confirmation was performed by further palatal phenotype assessments, made after crossing CD1 males with *Tbx22*$^{flox/+}$ females (2 crosses, N=14). CD1 mice were chosen for this purpose since they are known to have large litters and a previous study already showed that the phenotype on the CD1 background was similar to both 129/Sv and C57Bl/6 (Pauws et al., 2009a). Therefore, to investigate the development of their palatal bones, WT and floxed male embryos recovered at E17.5 were subjected to the alcian blue and alizarin red skeletal staining protocol (II. 11. Alcian blue and alizarin red skeletal staining). This confirmed that *Tbx22*$^{flox/Y}$ animals do have a visible deficit (M=6) in palatal bone formation that was similar to that previously described in *Tbx22*$^{-/Y}$ mice (Pauws et al., 2009a). Also, female *Tbx22*$^{flox/+}$ (F=2) mice developed a bone deficit phenotype affecting palatal shelves margins, Figure IV. 5.

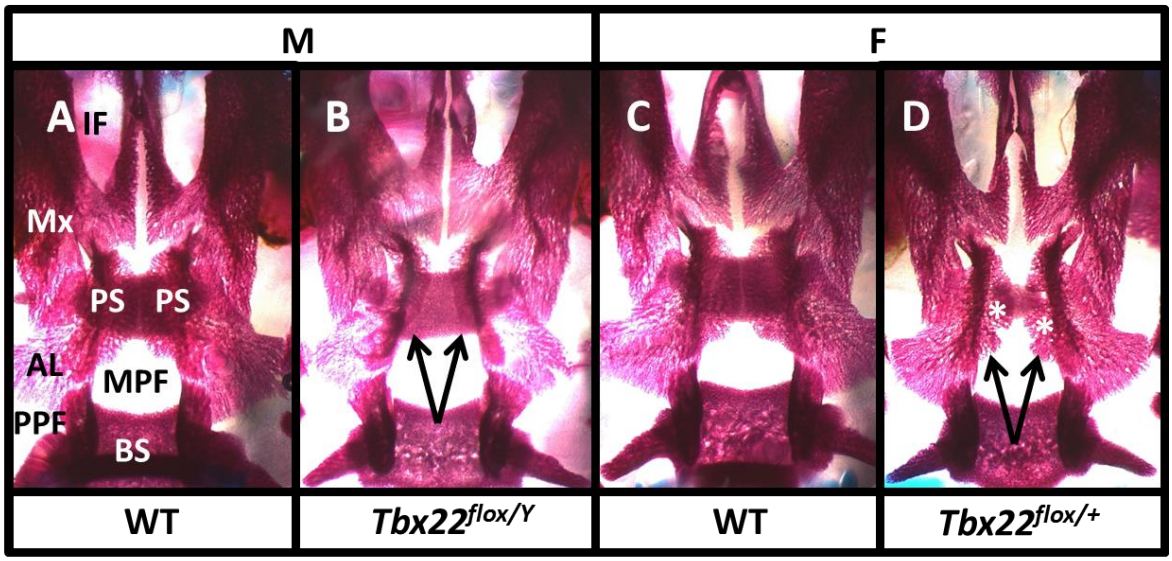

Figure IV. 5. The palate phenotype in *Tbx22*^{flox} animals compared to WT.
A) WT male with a normal palate; **B)** *Tbx22*$^{flox/Y}$; shows a lack of bone structure in the palatal shelves (SMCP phenotype); **C)** WT female with a normal palate; **D)** *Tbx22*$^{flox/+}$, shows a bone deficit at the palatal shelf margins (indicated with ⁎). Arrows indicate structural changes. **PS** - palate shelf; **IF** - incisive foramina; **PPF** - parapterygoid fossa; **AL** – alisphenoid; **BS** – basisphenoid; **Mx** – maxilla; **MPF** - mesopterygoid fossa (Missagia and Perini, 2018).

In earlier studies, it was noted that the majority of constitutive null *Tbx22*$^{-/Y}$ mice that were generated by crossing floxed mice with *βactin*-Cre survived with sufficient health to allow these mice to be maintained as a colony for use without always crossing to a Cre-deleter strain. As a consequence, all of the published experiments (Pauws et al., 2009a) used these constitutively null mice exclusively and the floxed allele remained uninvestigated for any phenotype. However, the overall health and wellbeing of these null animals was slightly compromised compared to WT and animals carrying the floxed allele. The constitutive null males tended to be smaller, less active and with poor overall appearance, whilst the floxed animals are visually indistinguishable from WT littermates. It was also reported that removing the intragenic *Neo*^{R} cassette that was retained in the *Tbx22*^{null} allele using *Flp*-deleter *in vivo*, had no obvious effect on the mutant phenotype (Pauws et al., 2009b). However, this new finding of a palatal bone phenotype in the floxed allele raised the possibility that it may indeed represent a deleterious allele. Should the *Tbx22 loxP sites and FLP-flanked Neo*^{R} cassette

potentially affects *Tbx22* expression, this might be considered a hypomorph, where expression is reduced, although not to the same extent as the complete null.

It was therefore decided to investigate *Tbx22* transcripts in floxed mice to see if this allele did indeed result in reduced or abrogated expression of *Tbx22*. To do this a TaqMan® Gene Expression assay was carried out (II. 9. 2. TaqMan® gene expression assay). RNA was extracted from three biological replicates of E13.5 WT, $Tbx22^{flox/Y}$ and $Tbx22^{-/Y}$ males heads (II. 17. Preparation of RNA from tissue for RTqPCR). Averaged *Tbx22* expression (Figure IV. 6) showed, at least at the resolution of this assay, that the level was very similar between $Tbx22^{flox/Y}$ and $Tbx22^{-/Y}$ but significantly lower when compared to WT. With expression levels reduced to that of a null, this provided a plausible explanation for why the SMCP phenotype was observed in $Tbx22^{flox/Y}$ animals. However, it does not support the idea of being a hypomorphic allele in terms of the general wellbeing of the animals. An explanation for the difference may need to be investigated by testing *Tbx22* expression at earlier developmental stages or potentially by dissecting different tissues or even cell types.

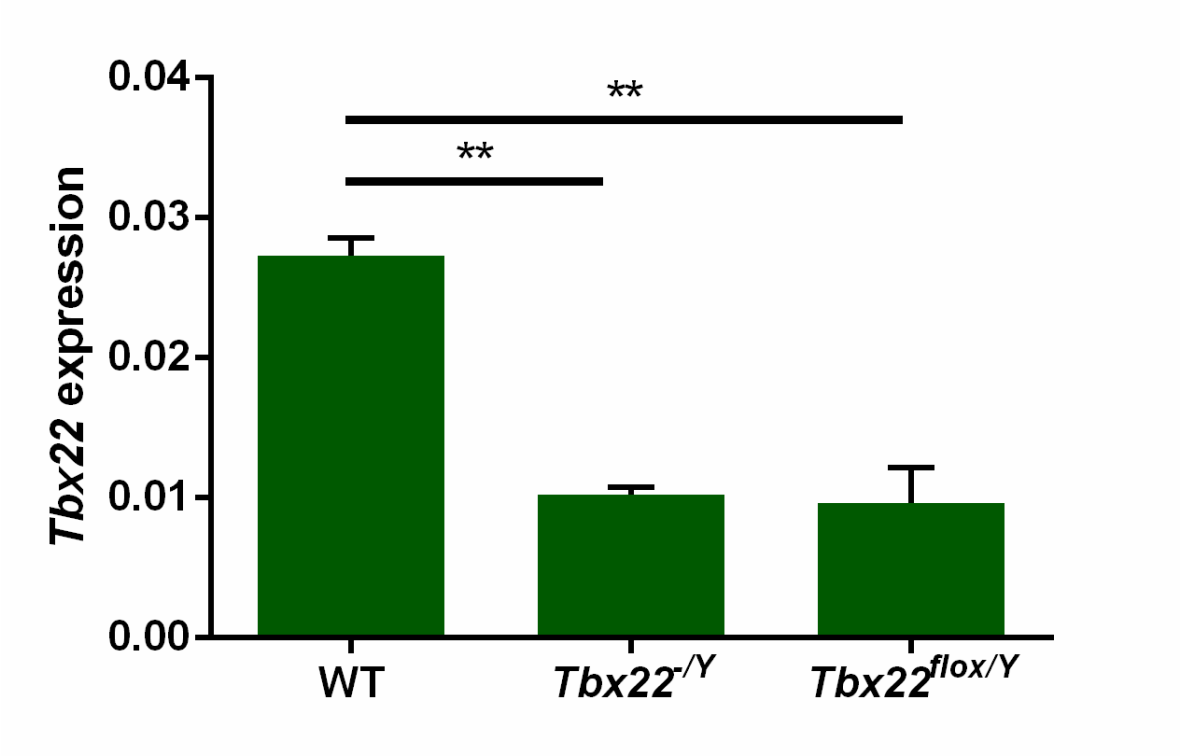

Figure IV. 6. *Tbx22* expression in male WT, null and floxed craniofacial tissues. Statistical comparisons between *Tbx22*$^{-/Y}$ and *Tbx22*$^{flox/Y}$ compared to WT. Error bars = standard deviation. ***p*<0.01.

Next, to provide a more detailed examination of the role of the TBX22 transcription factor in palatal shelf development, it was decided to investigate gene expression changes in the two most predominant cell types, CM and CNC. By specifically isolating palatal cells from each of these cell types, it was expected to gain more fundamental insights into the contribution of each embryonic tissue to palate development.

Previous work investigating the functional role of TBX22 using the *Tbx22*^{null} mouse model was performed by Hoshino (2011). In her thesis, she described microarray analysis of E13.5 palatal shelves dissected from WT and *Tbx22*$^{-/Y}$ mice showing a global upregulation of muscle genes (myosin and muscle actin). This corresponded with a moderate upregulation in *MyoD* and *myogenin,* while reduced expression of *Cyclin D2* was noted in the null palatal shelves. Another key transcription factor of myogenesis *Myf5* also showed a trend towards increased expression in the null palatal shelves but failed to achieve a statistical significance. This work indicated

that TBX22 played a role in the regulation of cell proliferation as well as a previously identified role in osteoblast differentiation and maturation in palate development. The experiments were based on the hypothesis that TBX22 mainly acts as a transcriptional repressor and down regulated genes were not followed up in this particular project. Although it was earlier reported that TBX22 has both repression and activation domains (Andreou et al., 2007).

IV. 3. 2. Use of a conditional mouse line to generate a palatal shelf phenotype and cell-type specific transcription profile

To investigate transcriptional changes that occur downstream of TBX22, a conditional mouse line was first generated by crossing several transgenic strains. This first step involved introducing a fluorescent marker, R26-Fl-stop-Fl-YFP, on to the *Tbx22*^{flox} strain. Then, when crossed with either *Mesp1*-Cre (Yoshida et al., 2008) or *Wnt1*-Cre (Chai et al., 2000) lines, it was possible to use FACS to isolate cells derived from either CM or CNC respectively. Flow sorted labelled cells could then be used for RNA isolation and subsequent RNA-Seq.

A female *Tbx22*$^{flox/flox}$ mouse with target exons flanked by loxP sites was crossed with an R26-YFP male and the resulting female *Tbx22*$^{flox/+}$*/R26* offspring were then used for all subsequent experiments. Female *Tbx22*$^{flox/+}$*/R26* mice were then crossed with males which have the Cre gene linked either to the CM cell-specific promoter, *Mesp1*-Cre, or to a CNC cell-specific promoter, *Wnt1*-Cre. Embryos were recovered at E13.5 and used for palatal shelf dissection. The resulting tissues were treated (II. 13. Palate shelf dissection and cells preparation for flow sorting) to dissociate the cells and used for flow sorting. Fluorescently labelled cells were recovered from either WT *Tbx22*$^{+/Y}$ males or from Cre positive *Tbx22*$^{flox/Y}$ males (which become *Tbx22*$^{-/Y}$). A schematic diagram depicting how the conditional mouse line was generated is presented in Figure IV. 7.

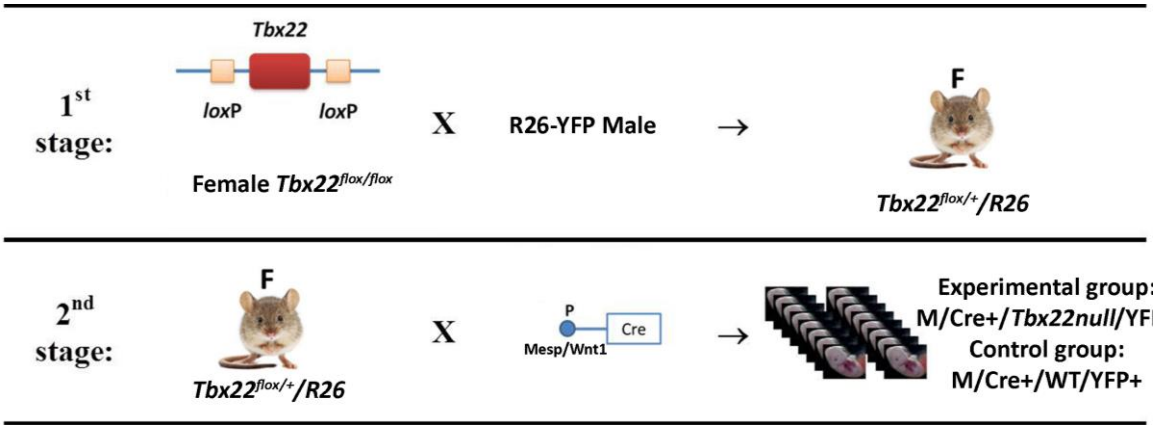

Figure IV. 7. Conditional mouse line generation.

The 1st stage involved introduction of the fluorescent marker R26-Fl-stop-Fl-YFP on to the *Tbx22*^{flox} strain. The 2nd stage involved crossing either with *Mesp1*-Cre or *Wnt1*-Cre lines to produce mutant (Males, *Tbx22*^{null}, Cre+ and YFP+) and WT (Males, WT, Cre+ and YFP+) embryos for flow sorting.

IV. 3. 3. Optimization of palate shelf tissue dissociation into single cells for flow sorting

To identify the best method to dissociate palatal shelf tissue to allow flow sorting of single cells, four methods were used, including the use of trypsin, accutase, dispase/collagenase/$CaCl_2$ solution or mechanical dissociation (II. 12. Methods to dissociate palate shelf tissue into cells) were tested (Figure IV. 8). The mechanical dissociation method was found to be quite aggressive and caused the most cell death. The impact of trypsin was less damaging, resulting in a good yield of single cells but also resulted in a significant number of dead cells as well as a large number of undissociated aggregates. Accutase generally had a low impact on cell dissociation of the palate tissue. The dispase/collagenase/$CaCl_2$ solution had a good yield of single cells whilst giving the lowest number of aggregates and dead cells and was chosen as optimal method for cell preparation prior to flow sorting.

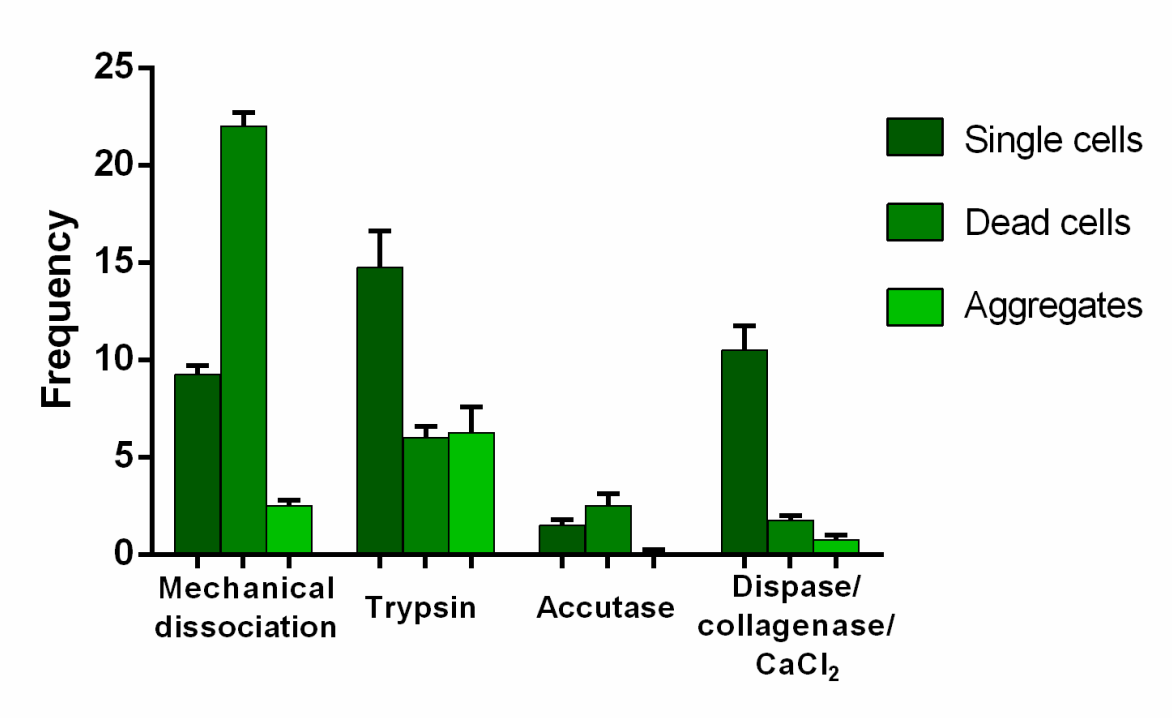

Figure IV. 8. Optimization of methods to dissociate palatal shelf tissue into its constitutive single cells.

Each of the four methods were assessed by counting viable single cells, dead cells or cell aggregates. Error bars = standard deviation.

IV. 3. 4. Isolation and analysis of cranial mesoderm and cranial neural crest populations in the palatal shelf

As previously described, conditional gene targeting using the *Cre*-loxP system depends on the generation of mice that express Cre-recombinase in a cell type specific pattern. To better understand embryogenesis in Cre expressing mice, reporter constructs can be used where expression of the reporter gene is activated only after Cre-mediated excision of a stop codon (Mao et al., 2001, Tsien et al., 1996).

In this experiment we were interested in investigating the role of TBX22 in palatal development, principally in the most relevant tissues likely to be involved in the observed phenotype, mainly bone and muscle. Therefore, excision was mediated in CNC using *Wnt1*-Cre and CM using *Mesp1*-Cre. The experimental animals were all males since they have been reproducibly shown to have the more severe bone

phenotype (Pauws et al., 2009a). All experimental embryos were collected in triplicate at E13.5 from crosses of female *Tbx22*$^{flox/+}$*/R26* with either male *Mesp1*-Cre (N=13) or *Wnt1*-Cre (N=8). *Tbx22*^{null} cells were recovered from *Tbx22*$^{-/Y}$ males that were positive for Cre and R26. The control (WT) group consisted of cells from WT male littermates, also positive for Cre and R26. Palatal shelves were dissected (Figure II. 11) and cells were dissociated and prepared for cell sorting (II. 13. Palate shelf dissection and cells preparation for flow sorting). Each sample yielded 3000-7760 (*Mesp1*) and 39000-97000 (*Wnt1*) YFP+ cells, which were stored frozen at -80°C.

The number of embryos collected is given in Table IV. 1 and the total number of cells recovered is presented in Table IV. 2. For the *Mesp1*-Cre cross, in all animals subjected to FACS (i.e. both sexes and all genotypes), a total of 2,430,242 cells were collected, of which 8% were YFP+. For the *Wnt1*-Cre cross, 3,201,390 cells were recovered, of which 38% were YFP+. Specifically in experimental males, the ratio of YFP+ CM to CNC cells corresponded to 1:3.8 in WT and 1:5.6 in null embryos (Figure IV. 9). Other cell types present in the palate, such as epithelia and endothelial cells, were expected to be collected in the YFP- fraction.

Table IV. 1. Collection and analysis of YFP+ E13.5 embryos.

Embryos were collected from 21 litters.

Embryos	*Mesp1*	%	*Wnt1*	%	Total	%
F*	12	40%	13	54%	25	46%
M	18 (null 10 / WT 8)	60%	1 (null 4) / 1 (WT 7)	46%	29	54%
Total embryos number	121	100%	89	100%	210	100%
Total YFP+	30	25%	24	21%	56	26%

*Females were not investigated further for genotype.

Table IV. 2. Number of YFP+/- cells sorted.

Mesp1-Cre					*Wnt1*-Cre				
		YFP +/-	Cell No	Embryo No			YFP +/-	Cell No	Embryo No
M	WT	YFP+	87710	10	M	WT	YFP+	417290	7
		YFP-	793000				YFP-	683540	
		Total	880710				Total	1100830	
	null	YFP+	35329	8		null	YFP+	211000	4
		YFP-	541000				YFP-	403000	
		Total	576329				Total	614000	
F*		YFP+	78503	12	F*		YFP+	583200	13
		YFP-	894700				YFP-	903360	
		Total	973203				Total	1486560	
Total cells number			**2430242**		**Total cells number**			**3201390**	
Total YFP+ number			**201542 (8%)**		**Total YFP+ number**			**1211490 (38%)**	

*Females were not investigated further for genotype.

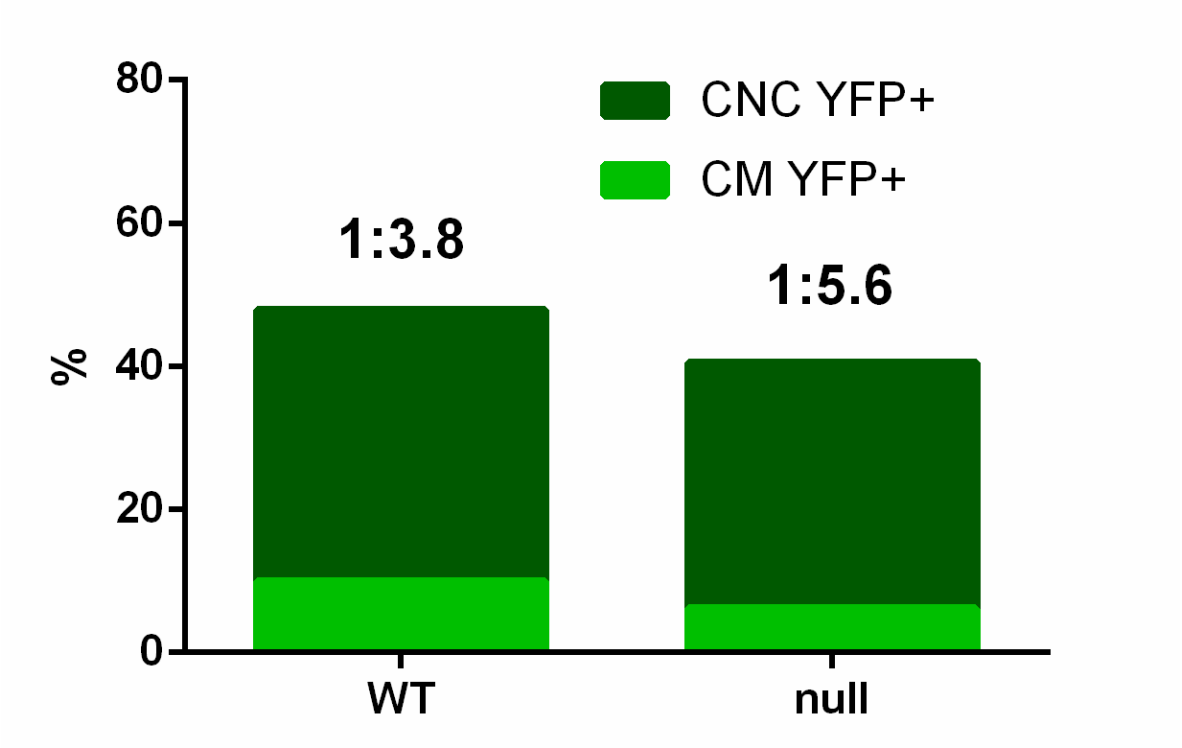

Figure IV. 9. Graphic representation of YFP+ cell ratio of CM and CNC origin in WT and null male embryos.

The ratio of CM:CNC cells in WT and null palatal shelves was 1:3.8 and 1:5.6 respectively.

IV. 3. 5. RNA sequencing

RNA samples were sent to UCL Genomics for RNA quality check and RNA sequencing (https://www.ucl.ac.uk/child-health/research/genetics-and-genomic-medicine-programme/ucl-genomics/technology). Figures IV. 10 to IV. 12 represent quality control data provided by UCL Genomics.

IV. 3. 6. RNA quality check

High Sensitivity D1000 RNA ScreenTape® was used in the Agilent 2200 TapeStation system to determine RNA quality to ensure that there was sufficient RNA of suitable quality to use for sequencing. The readout was analysed by the TapeStation Analysis Software (A.02.02). The RNA quality is indicated by the RNA integrity number (RIN), which is estimated from the 28S to 18S ribosomal RNA (rRNA) ratio. A RIN number of 10 represent the highest quality. All of the RNA samples passed the QC (Figure IV. 10, Figure IV. 11 and Table IV. 3) and were used for sequencing.

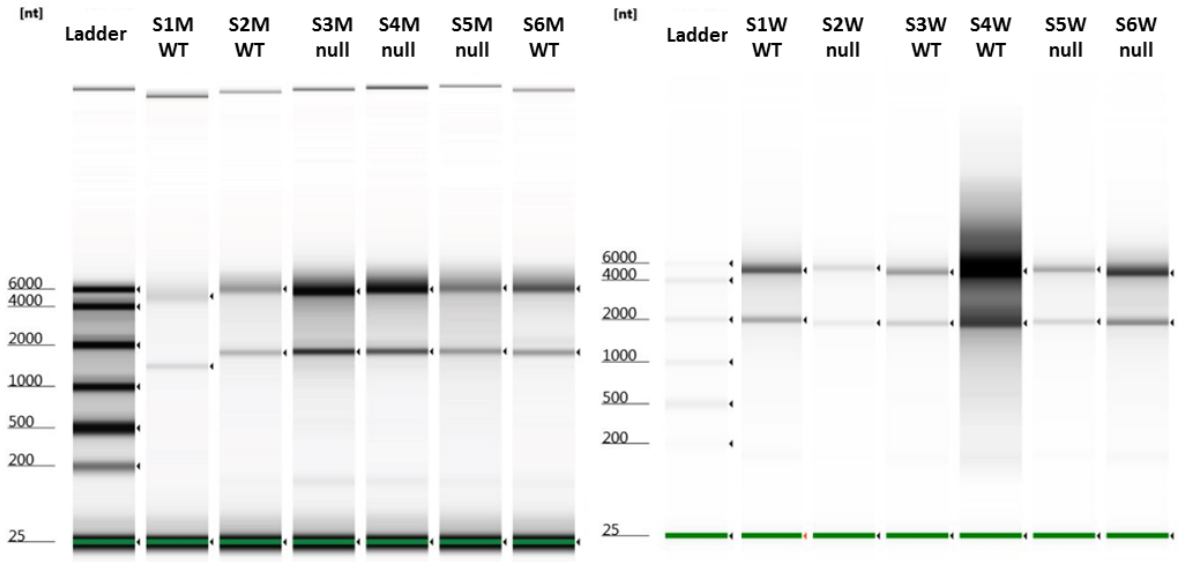

Figure IV. 10. Quality control for each RNA sample by TapeStation.
Automated gel electrophoresis readout of the Agilent 2200 TapeStation system. The double bands in each lane represent 28S and 18S rRNA. **S** - sample; **1-6** - number of sample; **M** - *Mesp1*-Cre cross; **W** - *Wnt1*-Cre cross; **WT** - control group; **null** - experimental group.

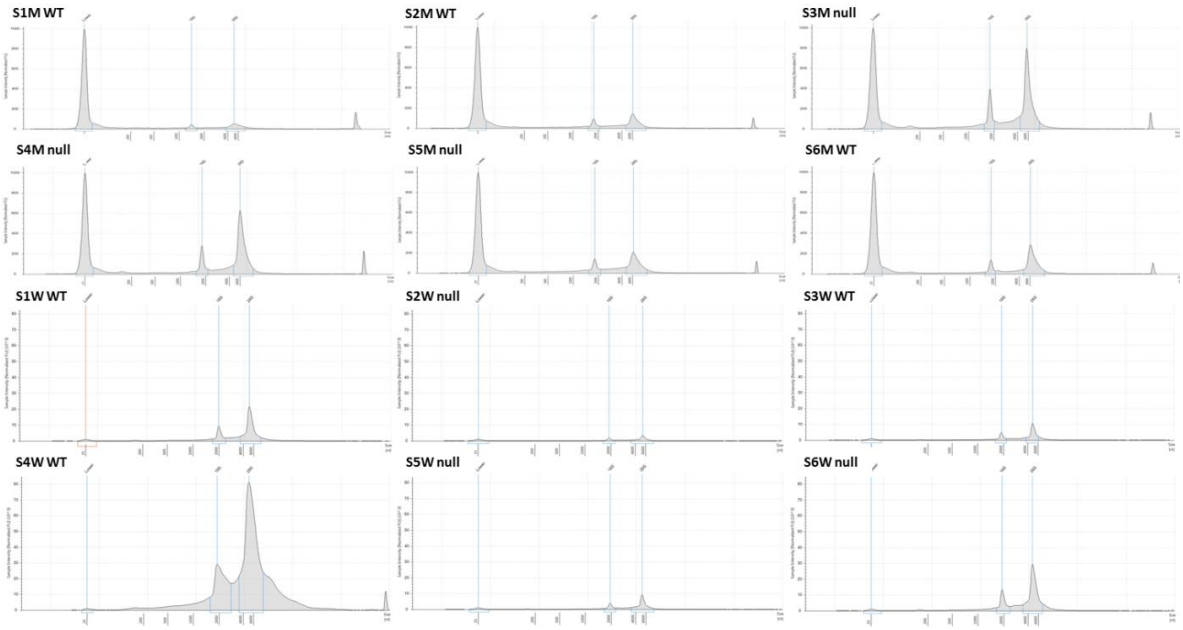

Figure IV. 11. Quality control of each RNA sample by electrophoresis.

Electropherograms of the RNA samples with sample intensity and 28S and 18S rRNA indicated by the double peaks relative to the ladder. **S** - sample; **1-6** - number of sample; **M** - *Mesp1*-Cre cross; **W** - *Wnt1*-Cre cross; **WT** - control group; **null** - experimental group.

Table IV. 3. RNA quality control summary.

Summary table of the RIN values and RNA concentrations of each sample. **S** - sample; **1-6** - number of sample; **M** - *Mesp1*-Cre cross; **W** - *Wnt1*-Cre cross; **WT** - control group; **null** - experimental group.

Well	Cells No	RINe	28S/18S (Area)	Conc. [pg/µL]
Ladder		-	-	1580
S1M WT	3120	6.9	2.6	213
S2M WT	3560	7.7	2.6	268
S3M null	7760	9.0	3.3	734
S4M null	5600	9.2	3.8	641
S5M null	4600	7.7	2.7	388
S6M WT	3000	8.7	4.1	336
Ladder		-	-	3000
S1W WT	82000	8.9	3.2	16200

Table IV. 3. (continued).

S2W null	39000	8.6	2.7	2820
S3W WT	56000	8.9	2.6	7490
S4W WT	82000	7.4	2.7	165000
S5W null	45000	8.8	3.2	6590
S6W null	97000	9.0	3.1	24100

IV. 3. 7. RNA-Seq quality control

RNA-Seq data were analysed using the standard quality control methods STAR alignment scores and Picard gene coverage (Figure IV. 12). These showed that all samples were of good quality and that the majority of reads aligning to coding regions or UTRs of known genes.

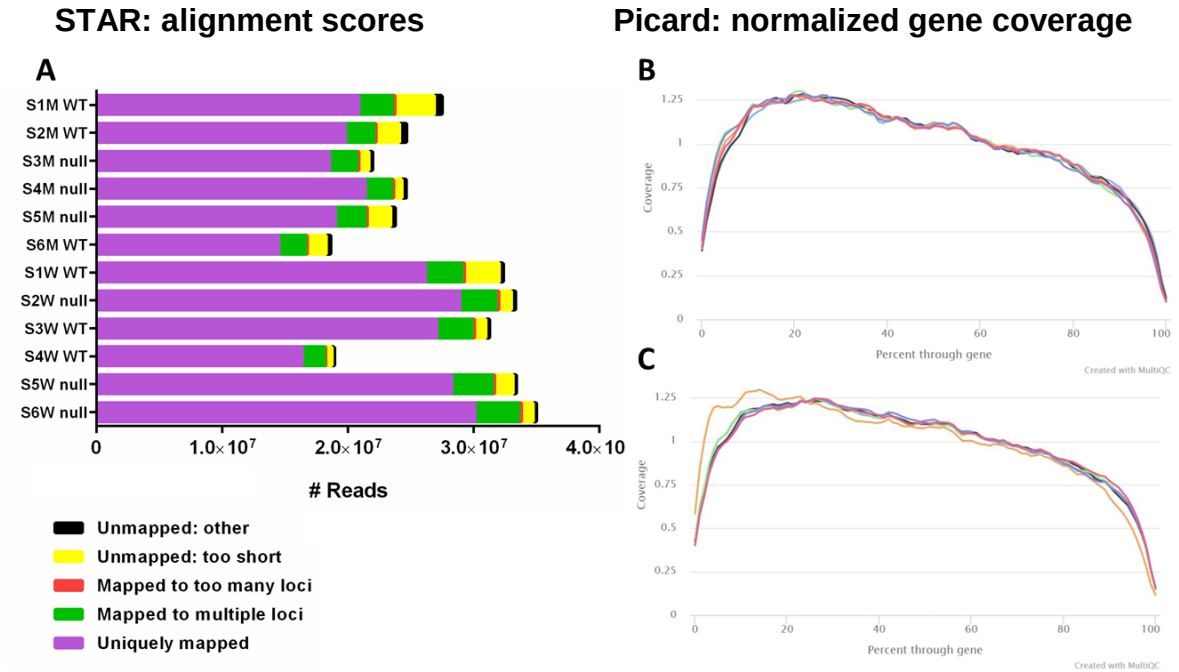

Figure IV. 12. STAR alignment scores and Picard gene coverage.

A) RNA-Seq STAR alignment scores (percentage) of the samples; Picard gene coverage in CM and **C)** in CNC derived cells. RNA-Seq quality control analysis showed good quality of all samples.

IV. 3. 8. Differential expression analysis

Differential expression analysis (Owen and Moosajee, 2019, Shu et al., 2019, Costa-Silva et al., 2017) was used to investigate changes in gene expression in FACS sorted CM or CNC derived cells isolated from E13.5 WT or *Tbx22*$^{-/Y}$ mouse palatal shelves. Overall 4 different analyses were performed: a) *Tbx22*$^{-/Y}$ were compared to WT in CM derived cells *(Mesp1*-Cre); b) *Tbx22*$^{-/Y}$ samples were compared to WT in CNC derived cells *(Wnt1*-Cre); c) WT were compared between *Mesp1*-Cre and *Wnt1*-Cre isolated cells; d) *Tbx22*$^{-/Y}$ samples were compared between *Mesp1*-Cre and *Wnt1*-Cre isolated cells. For descriptive purposes in each comparison, those genes that had differentially higher expression (increased read count) were referred to as 'up regulated' and those that had lower expression (lower read count) as 'down regulated'. These terms do not refer to the absolute expression levels of the genes.

As RNA-Seq data was generated from 3 separate embryos for each group as biological replicates (Schurch et al., 2016), the DESeq2 algorithm was used to normalise counts (rlog normalization) (Love et al., 2014). This was followed by a PCA to determine the overall similarity of the replicate samples (Anders and Huber, 2010). The PCA plot (Figure IV. 13, A) shows the distribution of the sample groups. Clear separation can be seen between *Mesp1*-Cre and *Wnt1*-Cre derived samples. While *Tbx22*$^{-/Y}$ and WT samples were less well defined within the *Wnt1*-Cre cluster compared to that derived from CM. Differential gene expression between groups is also presented in volcano plots (Figure IV. 13, B, C). As could be expected, the most significant down regulated gene in CNC cells (Figure IV. 13, C) was *Tbx22,* although it was not the most significant down regulated gene in CM (Figure IV. 13, B).

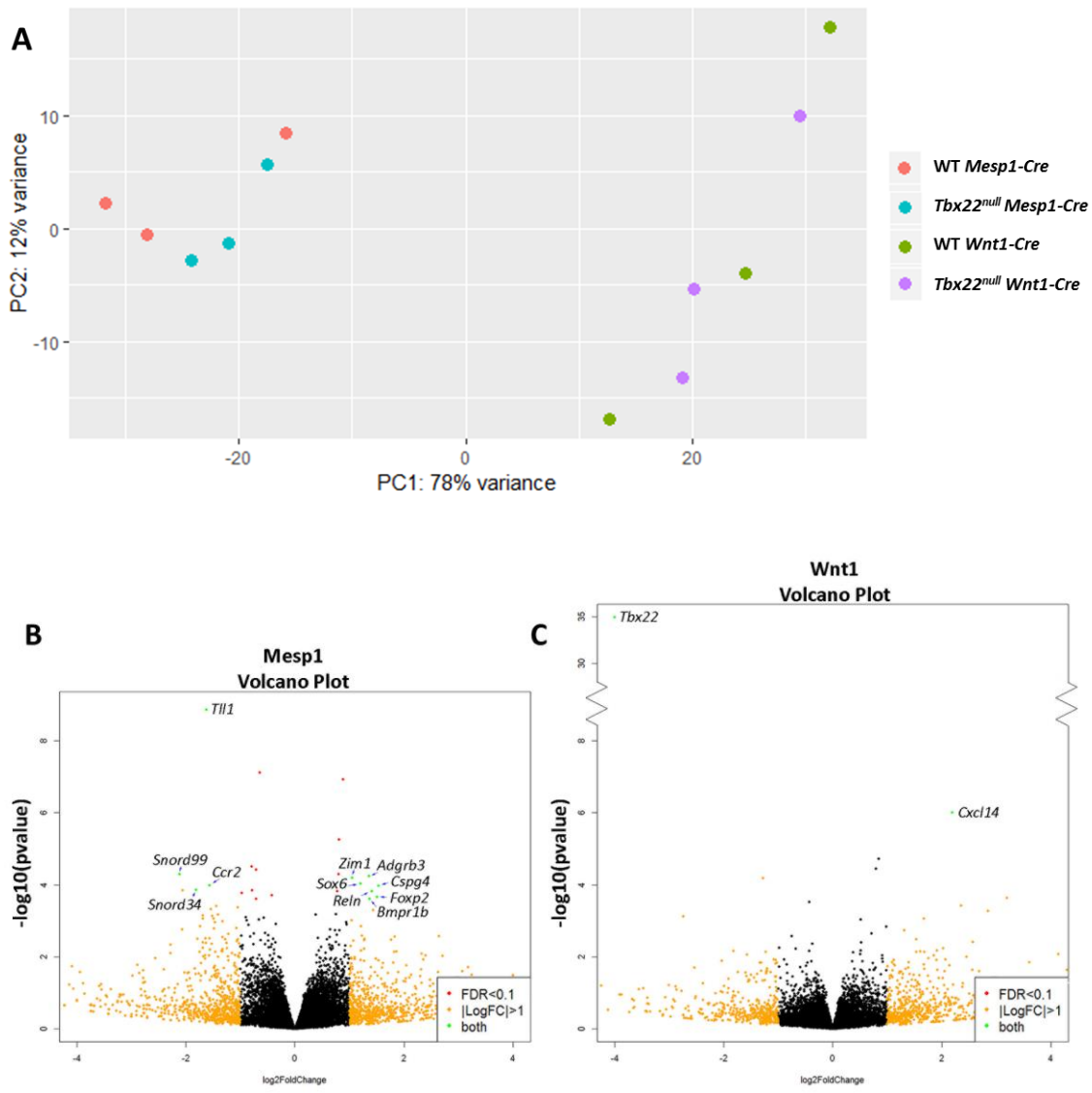

Figure IV. 13. Principal component analysis and volcano plots depicting differential expression.

A) PCA plot of WT cells samples and *Tbx22*$^{-/Y}$ cells samples, compared between CNC and CM origin; **B)** volcano plot represents differential expression of genes in mesoderm derived cells (*Tbx22*$^{-/Y}$ vs. WT) and **C)** CNC derived cells (*Tbx22*$^{-/Y}$ vs. WT). *p*adj significance cut-offs are: red dot (•) - FDR<0.1; yellow dot (•) - $Log_2FC>1$; green dot (•) - FDR<0.1 and $Log_2FC>1$.

The DESeq2 algorithm with default settings was used to calculate a fold change (FC) and perform statistical test for differential expression between *Tbx22*$^{-/Y}$ and WT samples in CM and CNC derived cells as well as to compare WT *Mesp1*-Cre vs. WT *Wnt1*-Cre and *Tbx22*$^{-/Y}$ *Mesp1*-Cre vs. *Tbx22*$^{-/Y}$ *Wnt1*-Cre. A significance threshold of adjusted *p*-value <0.1, *p*-value <0.05 and a -1>Log_2FC<1 (0.5>FC<2) was used to determine significantly up and down regulated genes.

At *p*adj value <0.1, 11 genes were up regulated in CM derived cells when comparing *Tbx22*$^{-/Y}$ and WT samples and 11 genes that were down regulated in the same group. Comparing *Tbx22*$^{-/Y}$ and WT in CNC derived cells, only 1 gene was up and 1 gene was down regulated at *p*adj value <0.1, Table IV. 4. These findings were surprising since *Tbx22* is much more highly expressed in CNC at this developmental stage and one might have anticipated that resulting downstream genes would be most affected in this tissue.

Table IV. 4. WT vs. *Tbx22*$^{-/Y}$ differentially expressed genes in CM (*Mesp1*-Cre) and CNC (*Wnt1*-Cre) derived cells.

The list of genes with *p*adj value <0.1 between groups (WT compared to *Tbx22*$^{-/Y}$) in CM (*Mesp1*-Cre) and CNC (*Wnt1*-Cre) derived cells ranked by FC. **Av exp** - average normalised read count.

WT vs. *Tbx22*$^{-/Y}$ in *Mesp1*-Cre				
Up regulated				
Gene	**Log_2FC**	***p*adj**	**Av exp WT**	**Av exp *Tbx22*$^{-/Y}$**
Cspg4	1.53	0.07	52.02	150.65
Foxp2	1.51	0.09	213.27	609.60
Reln	1.41	0.08	88.40	234.50
Bmpr1b	1.37	0.09	47.41	122.79
Adgrb3	1.36	0.06	46.92	120.59
Sox6	1.20	0.07	138.24	318.14
Zim1	1.05	0.06	153.33	316.87

Table IV. 4. (continued).

Scarna13	0.89	0.00	202.84	374.11
Fat1	0.81	0.01	1844.66	3233.13
Notch3	0.80	0.06	319.74	556.22
Peg3	0.78	0.08	2236.25	3829.47
Down regulated				
Gene	**Log_2FC**	***padj***	**Av exp WT**	**Av exp *Tbx22*$^{-/Y}$**
Nr2f2	-0.42	0.09	1228.61	916.45
Lars2	-0.65	0.00	18194.99	11613.01
Ahr	-0.71	0.06	554.52	338.91
Aplnr	-0.71	0.09	2046.92	1249.31
Emcn	-0.78	0.08	1873.73	1087.52
Npnt	-0.79	0.06	307.96	178.00
Apln	-0.97	0.08	389.79	198.78
Ccr2	-1.56	0.07	91.62	30.96
Tll1	-1.63	0.00	449.50	145.60
Snord34	-1.81	0.08	340.19	96.78
Snord99	-2.12	0.06	210.62	48.37
WT vs. *Tbx22*$^{-/Y}$ in *Wnt1*-Cre				
Up regulated				
Gene	**Log_2FC**	***padj***	**Av exp WT**	**Av exp *Tbx22*$^{-/Y}$**
Cxcl14	2.19	0.01	12.89	57.50
Down regulated				
Gene	**Log_2FC**	***padj***	**Av exp WT**	**Av exp *Tbx22*$^{-/Y}$**
Tbx22	-4.04	0.00	448.95	27.57

To consider direct interaction between CNC and CM derived tissues, it was interesting to look at genes that were significantly up or down regulated in CM derived tissue in the *Wnt1*-Cre data. In most cases there was no clear concordance observed, reflecting the independant nature of those two embryonic cell lineages with respect to *Tbx22* genotype. However, two genes that were significantly down regulated in CM derived tissue and significantly up regulated in CNC derived tissue were *Npnt* (*p*=0.000019, average expression (av exp)=455.55 [$Tbx22^{null}$], av exp=252.21 [WT]) and *Ccr2* (*p*=0.049, av exp=9.498 [$Tbx22^{null}$], av exp=2.94 [WT]). Overall *Ccr2* expression was at a very low level in this comparison and not considered biologically significant. Genes differentially expressed in CNC derived cells presented in Table IV. 5.

Table IV. 5. Performance in CNC (*Wnt1*-Cre) of the significantly (*p*adj) differentially expressed genes found in CM (*Mesp1*-Cre) cells.

Av exp - average normalised read count; **NS** - not statistically significant, p≥0.05. Light green colour rows - up regulated, darker green colour rows - down regulated genes.

WT vs. $Tbx22^{-/Y}$ in *Wnt1*-Cre					
Gene	**Log_2FC**	***Up/Down***	***p***	**Av exp WT**	**Av exp $Tbx22^{-/Y}$**
Npnt	0.85	↑	0.000019	252.21	455.55
Ccr2	1.79	↑	0.049	2.94	9.498
Snord99	0.39	↑	NS	97.61	129.43
Snord34	0.39	↑	NS	111.80	147.02
Lars2	-0.14	↓	NS	20887.81	18908.94
Aplnr	-0.35	↓	NS	221.44	174.39
Tll1	0.22	↑	NS	59.18	70.26
Nr2f2	-0.15	↓	NS	1582.31	1419.34
Ahr	0.08	↑	NS	625.56	660.31
Emcn	-0.08	↓	NS	167.46	159.61

Table IV. 5. (continued).

Apln	-0.04	↓	NS	53.90	52.21
Scarna13	-0.47	↓	NS	975.66	700.50
Zim1	0.31	↑	NS	569.57	708.60
Fat1	0.20	↑	NS	8643.72	9967.19
Peg3	0.19	↑	NS	8242.25	9379.53
Sox6	0.15	↑	NS	1156.54	1289.61
Bmpr1b	0.16	↑	NS	142.91	161.49
Notch3	-0.05	↓	NS	1174.25	1134.18
Adgrb3	-0.06	↓	NS	404.86	390.00
Cspg4	0.09	↑	NS	306.58	329.42
Reln	0.09	↑	NS	171.63	184.69
Foxp2	-0.01	↓	NS	1337.77	1329.64

Tbx22 was, as expected, down regulated both in CNC (Table IV. 4) and in CM derived tissue (*p*=0.0014, av exp=11.97 [$Tbx22^{null}$], av exp=40.15 [WT]). It was the only significant (*p*adj value <0.1) down regulated gene in CNC.

Cxcl14 was the only up regulated gene (*p*adj<0.1) in CNC tissue. It is described as an antimicrobial gene which belongs to the cytokine family that encodes secreted proteins involved in immunoregulatory and inflammatory processes (Hromas et al., 1999). *CXCL14* is expressed in skin, kidneys and other tissue, such as brain, colon, duodenum and oesophagus. There is a reported role of CXCL14 as critical mediator in endogenous anti-inflammatory mechanisms in ischemic brain (Lee et al., 2017). Also CXCL14 is known for its significance in proliferation and metastasis of tumours (Lin et al., 2014). There is currently no clearly identified role for this gene in palatogenesis, although in chick embryo studies, there is indication that CXCL14 may regulate craniofacial tissue growth during embryonic development (Gordon et al., 2011). STRING was used to investigate the known interaction network of CXCL14 protein, Figure IV. 14 (Szklarczyk et al., 2015).

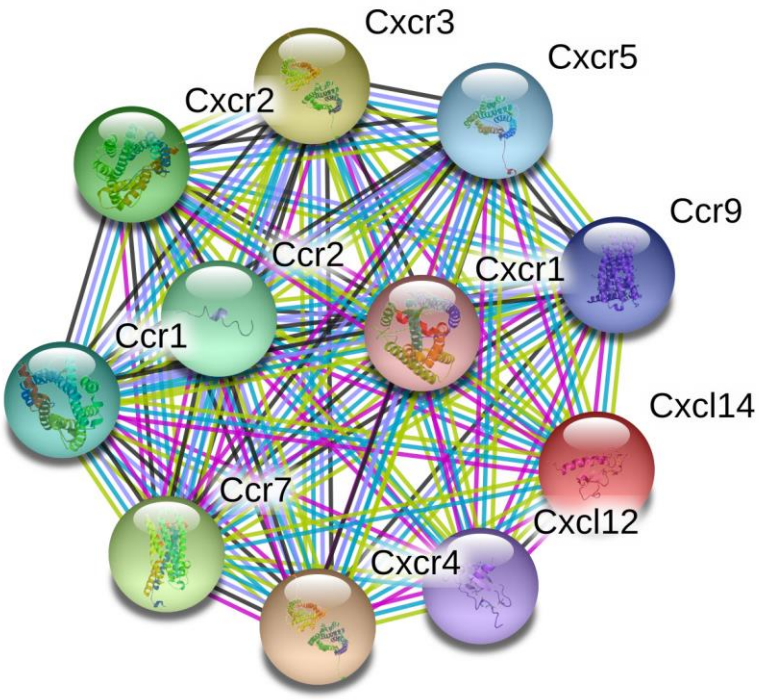

Figure IV. 14. CXCL14 protein interaction network visualized by STRING.
Network nodes represent the proteins produced by a single, protein-coding gene locus. Edges represent protein-protein interactions.

Looking at the dataset prior to statistical adjustment for multiple testing, 254 genes were found to be significantly (p<0.05) up regulated and 301 genes were significantly down regulated in CM derived cells when comparing *Tbx22*$^{-/Y}$ to WT samples. For CNC derived cells, 104 genes were significantly up regulated and 72 down regulated in *Tbx22*$^{-/Y}$ compared to WT cells. The 30 genes with the largest FC and the lowest p value (up and down regulated) are presented in Table IV. 6.

Table IV. 6. The list of genes ranked according to the largest fold change and then lowest *p* value between groups (*Tbx22*$^{-/Y}$ compared to WT) in CM (*Mesp1*-Cre) and CNC (*Wnt1*-Cre) derived cells.

The genes were selected by *p* value and then were ranked by highest FC (1st column) and lowest *p* (2nd). Genes in red indicate those with the highest significance/fold change.

Tbx22$^{-/Y}$ vs. WT in *Mesp1*-Cre							
Up regulated				Down regulated			
1st column		2nd column		1st column		2nd column	
Biggest FC	Log_2 FC	Lowest *p* value	Log_2 FC	Biggest FC	Log_2 FC	Lowest *p* value	Log_2FC
Matn3	6.21	*Scarna13*	0.88	*Hbb-bh1*	-5.12	*Tll1*	-1.63
Ecel1	5.12	*Fat1*	0.81	*Atp6v0d2*	-4.93	*Lars2*	-0.65
Masp2	4.66	*Notch3*	0.80	*Acsbg1*	-4.81	*Npnt*	-0.79
Mir140	4.61	*Adgrb3*	1.36	*Gjb6*	-4.09	*Ahr*	-0.71
Entpd3	4.43	*Zim1*	1.05	*H2-DMb1*	-3.94	*Snord99*	-2.12
Adgrf2	4.09	*Sox6*	1.20	*Ccr9*	-2.98	*Ccr2*	-1.56
S100b	4.00	*Cspg4*	1.53	*Cd300lf*	-2.89	*Snord34*	-1.81
Rbm44	3.71	*Reln*	1.41	*Apob*	-2.86	*Emcn*	-0.78
Stk33	3.24	*Peg3*	0.78	*Ehf*	-2.78	*Ifi203*	-2.06
Mfsd4	3.17	*Foxp2*	1.51	*Kynu*	-2.78	*Apln*	-0.97
Mia	3.07	*Bmpr1b*	1.37	*Slfn14*	-2.56	*Nr2f2*	-0.42
Olfr558	3.06	*Scn3a*	1.43	*H2-Eb1*	-2.41	*Aplnr*	-0.71
Scrg1	2.76	*Meox2*	0.75	*Psmb8*	-2.28	*Gm1966*	-1.44
Scn5a	2.71	*Igf1r*	0.38	*Mir677*	-2.28	*Slc39a8*	-1.05
Tc2n	2.65	*Smoc2*	1.04	*Snord99*	-2.12	*Snord100*	-1.54
Myh6	2.62	*Thbs1*	0.94	*Snord42a*	-2.07	*Snord32a*	-1.41
Susd5	2.48	*Stk26*	0.95	*Ifi203*	-2.06	*Snord12*	-1.69
Lmo3	2.40	*Lgr5*	1.21	*Lrat*	-2.03	*Snord87*	-1.52
Fam101a	2.35	*Prickle1*	0.65	*Dbx1*	-1.99	*Clec14a*	-0.90
Fam71a	2.33	*Matn3*	6.21	*Tlx1*	-1.97	*Rgs2*	-0.57

Table IV. 6. (continued).

Foxl1	2.32	***Fosb***	0.74	***Tfcp2l1***	-1.95	***Snord82***	-1.69
Slc1a1	2.29	***Barx1***	0.82	***Col28a1***	-1.93	***Cd74***	-1.50
Myh7b	2.13	***Irs2***	0.77	***Ermap***	-1.83	***St6gal1***	-0.66
Tmem178	2.10	***Tmtc1***	1.23	***Nlrp1b***	-1.82	***Ly6e***	-0.88
Kcnj8	2.04	***Tc2n***	2.65	***Snord34***	-1.81	***Snord61***	-1.33
Slc41a2	2.03	***Csmd3***	1.83	***Snord55***	-1.79	***Snord47***	-1.47
Col11a1	2.03	***Hmga2***	0.63	***Ackr2***	-1.76	***Anp32b***	-0.35
Actg2	1.99	***Plekhg2***	0.42	***Plbd1***	-1.75	***Tek***	-0.85
Vwc2	1.90	***Sim2***	1.28	***Tbx22***	-1.74	***Tbx22***	-1.74
Rspo2	1.86	***Ptprd***	0.59	***Scarna17***	-1.73	***Arhgap30***	-1.07
***Tbx22*$^{-/Y}$ vs. WT in *Wnt1*-Cre**							
Up regulated				**Down regulated**			
Biggest FC	**Log_2 FC**	**Lowest *p* value**	**Log_2 FC**	**Biggest FC**	**Log_2 FC**	**Lowest *p* value**	**Log_2FC**
Six6	8.22	***Cxcl14***	2.19	***Tbx22***	-4.04	***Tbx22***	-4.04
Tshb	5.54	***Npnt***	0.85	***Ccl28***	-2.74	***Myh3***	-1.28
Mtnr1a	5.18	***Fosl2***	0.79	***Mir3113***	-2.54	***Shisa3***	-0.44
Lhx3	4.76	***Sim1***	3.19	***Lmod3***	-2.03	***Ccl28***	-2.74
Sox14	4.76	***Krt5***	2.36	***Myot***	-1.91	***Tmem181b-ps***	-0.75
Irs4	4.44	***Irs4***	4.44	***Hist1h2ac***	-1.82	***Nr2f1***	-0.38
Plek2	4.29	***Scg2***	2.85	***Gm10037***	-1.74	***Hist1h3a***	-0.98
Six3	4.14	***Clu***	1.68	***Hist1h3b***	-1.60	***Pisd-ps1***	-0.68
Six3os1	3.61	***Col12a1***	0.51	***Hist1h3h***	-1.58	***Hist1h4b***	-0.43
Sim1	3.19	***Grm7***	0.98	***Hist1h2ad***	-1.58	***Hist1h2ac***	-1.82
Scg2	2.85	***Dsp***	1.31	***Hist1h3d***	-1.55	***Hist1h3c***	-1.23
Myo5c	2.69	***Dcn***	0.71	***Tceal7***	-1.54	***Hist1h2ad***	-1.58
Trp73	2.57	***Krt14***	1.53	***Hist1h3f***	-1.53	***Spag17***	-1.08
Ndufa4l2	2.56	***Trp73***	2.57	***Hfe2***	-1.50	***Ttn***	-0.90

Table IV. 6. (continued).

Lad1	2.45	***Nnt***	0.52	***Hist1h2an***	-1.44	***Hist1h3g***	-1.05
Krt5	2.36	***Six6***	8.22	***Tnnc2***	-1.40	***Lmod3***	-2.03
Cxcl14	2.19	***Ch25h***	2.03	***Eps8l1***	-1.39	***Ebf3***	-0.39
Pax1	2.14	***Thbd***	0.51	***Tmem8c***	-1.33	***Hist1h3i***	-1.31
Serpinb5	2.07	***Pitx2***	1.91	***Hist1h3i***	-1.31	***Hist1h4a***	-0.47
Ap1m2	2.05	***Esrp1***	1.60	***Hist1h2ai***	-1.31	***Tmem8c***	-1.33
Ch25h	2.03	***Grhl2***	1.53	***Mlph***	-1.28	***Nlrp5-ps***	-1.02
Wnt7b	2.01	***Epcam***	1.68	***Myh3***	-1.28	***Hist1h3e***	-1.04
Gm1966	1.95	***Smoc2***	0.38	***Gpr83***	-1.25	***Actc1***	-0.85
Cldn6	1.92	***Six3***	4.14	***Hist1h3c***	-1.23	***H2afx***	-0.49
Pitx2	1.91	***Ogn***	0.50	***Myl4***	-1.22	***Tnnc1***	-0.98
Igsf1	1.90	***Adgrv1***	0.91	***Hist1h2ag***	-1.22	***2310015A10Rik***	-0.59
Cfh	1.85	***Cfh***	1.85	***Mybph***	-1.22	***Mir3113***	-2.54
Ccr2	1.79	***Lad1***	2.45	***Mylpf***	-1.20	***Mylpf***	-1.20
Plch2	1.76	***Plch2***	1.76	***Myh7***	-1.20	***Myh7***	-1.20
Iigp1	1.75	***Fat2***	0.91	***Klhl31***	-1.14	***Mybph***	-1.22

Comparing all of the significant differentially expressed genes, *Npnt, Gm1966, Ccr2, Cd74, Rnu12, Snord16a, Myo6 and Gas5* were found to be down regulated in CM derived cells but up regulated in CNC cells.

These included the *Npnt* gene (Nephronectin) which was among the most significantly down regulated genes in CM derived cells and significantly up regulated in CNC derived cells. NPNT is described as a component of the core Fraser protein Complex (Kiyozumi et al., 2012). Fraser syndrome is a rare autosomal recessive multiorgan disorder which is characterized by cryptophthalmos, syndactyly, renal agenesis, and other morphogenetic defects including CL/P (Slavotinek and Tifft, 2002). In humans *NPNT* has been reported as being mutated in Fraser syndrome 1 (Saleem and Siddiqui, 2015). NPNT is also

known as being essential for kidney development and may play a role in development and function of various other tissues, as well as regulating cell adhesion spreading and survival, through the binding of several integrins, notably ITGA8 (Kiyozumi et al., 2012). In adults, *NPNT* expression was widely found in lung, kidney, brain, uterus, placenta, thyroid gland and blood vessels. Studies in zebrafish show that *Npnt* is expressed in facial tissues (Talbot et al., 2016). *Npnt* is therefore implicated in embryonic development as well as maintenance of various adult tissues (Huang and Lee, 2005, Sun et al., 2018). The NPNT protein interaction network, visualized by STRING is presented in Figure IV. 15, (Szklarczyk et al., 2015)

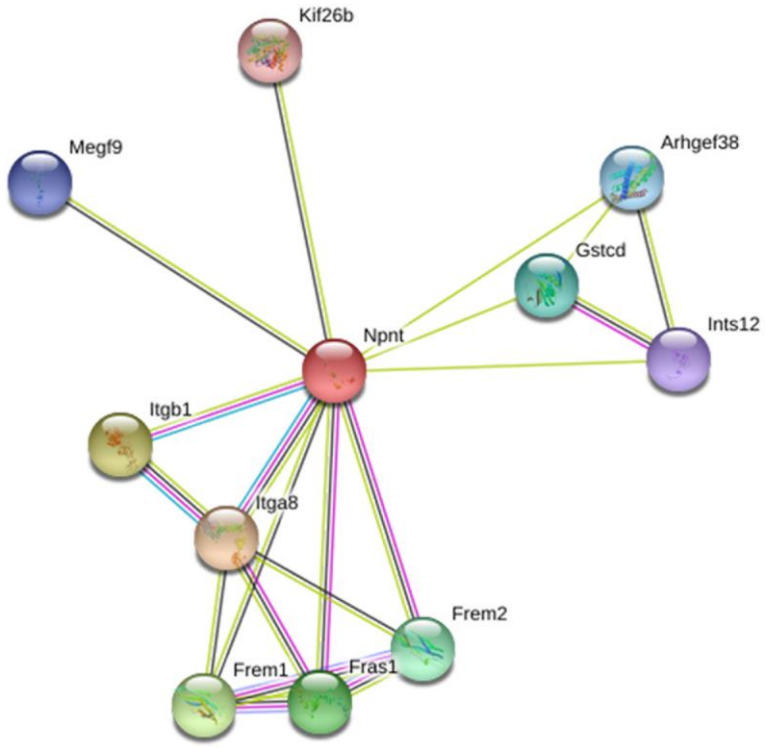

Figure IV. 15. NPNT protein interaction network visualized by STRING.
Network nodes represent the proteins produced by a single, protein-coding gene locus. Edges represent protein-protein interactions.

IV. 3. 9. Differential expression analysis comparing cranial mesoderm and cranial neural crest derived cells in WT and *Tbx22*$^{-/Y}$ mouse palatal shelves

The DESeq2 algorithm was used to calculate a FCs and perform a statistical test for differential expression between WT mice palate shelves that derived from CM and CNC cells. These genes could be considered to provide a differential signature for the respective cell types (Bronner and Simoes-Costa, 2016, Simoes-Costa et al., 2014). There were 1382 up regulated (*p*adj<0.1; $\log_2$FC>1) and 1548 down regulated (*p*adj<0.1; $\log_2$FC<-1) genes. The top 25 genes that were significantly differentially regulated with the lowest *p*adj value are presented as heat maps in Figure IV. 16. Genes *Diras2*; *Tfap2b* and *Miat* were the most up regulated and genes *Nckap1l*; *F13a1*; *Mrc1*; *Csf1r*; *Cx3cr1* and *Cfh* were the most down regulated in *Wnt1*-Cre compared to *Mesp1*-Cre.

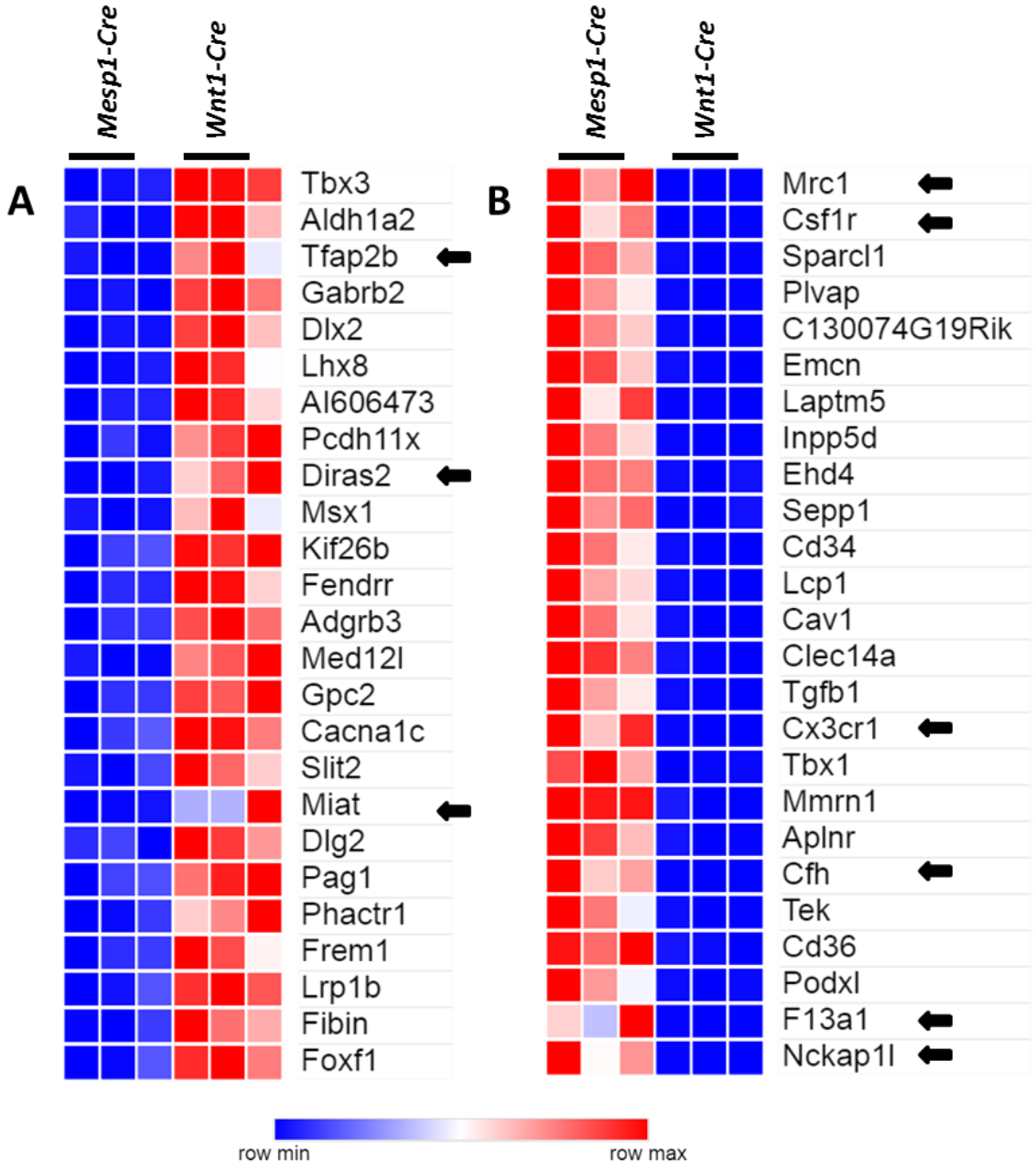

Figure IV. 16. Heat maps representing differential expression between CM and CNC derived cells in WT mice palate shelves.

A) Up regulated genes in *Wnt1*-Cre compared to *Mesp1*-Cre, arrows indicate the genes with highest FC, $log_2FC>3$. **B)** Down regulated genes in *Wnt1*-Cre compared to *Mesp1*-Cre, arrows indicate the genes with highest FC, $log_2FC<-6$. Expression values are represented as colours, where the range of colours red, pink, light blue and dark blue shows the range of expression values as high, moderate, low and lowest respectively.

A similar analysis was performed to identify genes that are differentially expressed between CM and CNC derived cells in *Tbx22*$^{-/Y}$ mice palatal shelves (Figure IV. 17). Genes *Nfasc; Cadm3; Ptprz1* and *Miat* were the most up regulated, whilst genes *Csf1r; Mrc1; Sox18; Rasgrp3*; *Pcdh12* and *Klhl4* were the most down regulated when comparing *Wnt1*-Cre to *Mesp1*-Cre transcripts.

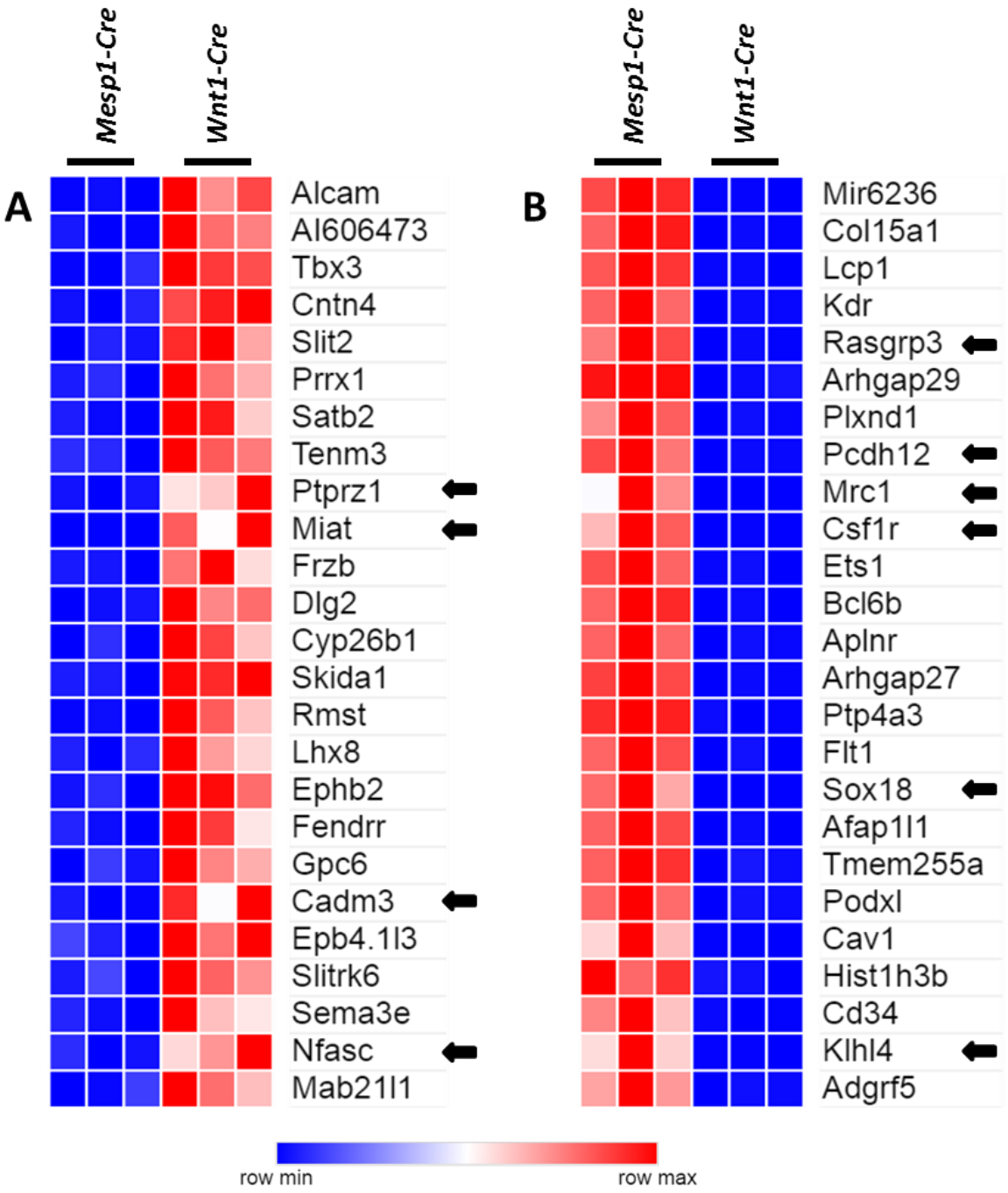

Figure IV. 17. Heat maps representing differential expression between CM and CNC derived cells in *Tbx22*$^{-/Y}$ mouse palatal shelves.

A) Up regulated genes in *Wnt1*-Cre compared to *Mesp1*-Cre. Arrows indicate the genes with highest FC, $\log_2$FC>2.7 and **B)** down regulated genes in *Wnt1*-Cre compared to *Mesp1*-Cre. Arrows indicate the genes with highest FC, $\log_2$FC<-4. Expression values are represented as colours, where the range of colours red, pink, light blue and dark blue shows the range of expression values as high, moderate, low and lowest respectively.

IV. 3. 10. Gene set enrichment analysis

IV. 3. 10. 1. Hallmark gene set

There were 9 gene sets significantly enriched for the *Tbx22*$^{-/Y}$ phenotype when comparing *Tbx22*$^{-/Y}$ to WT in CNC derived cell population at FDR < 25% (Figure IV. 18). Those included bile acid metabolism (genes involved in metabolism of bile acids and salts), **apoptosis** (genes mediating programmed cell death by activation of caspases), IL6 via STAT3 signalling (genes up-regulated by IL6 via STAT3, e.g., during acute phase response), **epithelial mesenchymal transition** (genes defining epithelial-mesenchymal transition, as in wound healing, fibrosis and metastasis), **hypoxia** (genes up regulated in response to low oxygen levels), allograft rejection (genes up regulated during transplant rejection), interferon alpha and gamma response (genes up regulated in response to alpha interferon proteins and IFNG) and P53 pathway (genes involved in p53 pathways and networks). In the apoptosis pathway, 154 genes were involved, in epithelial mesenchymal transition 185 genes and in hypoxia pathway 182 genes.

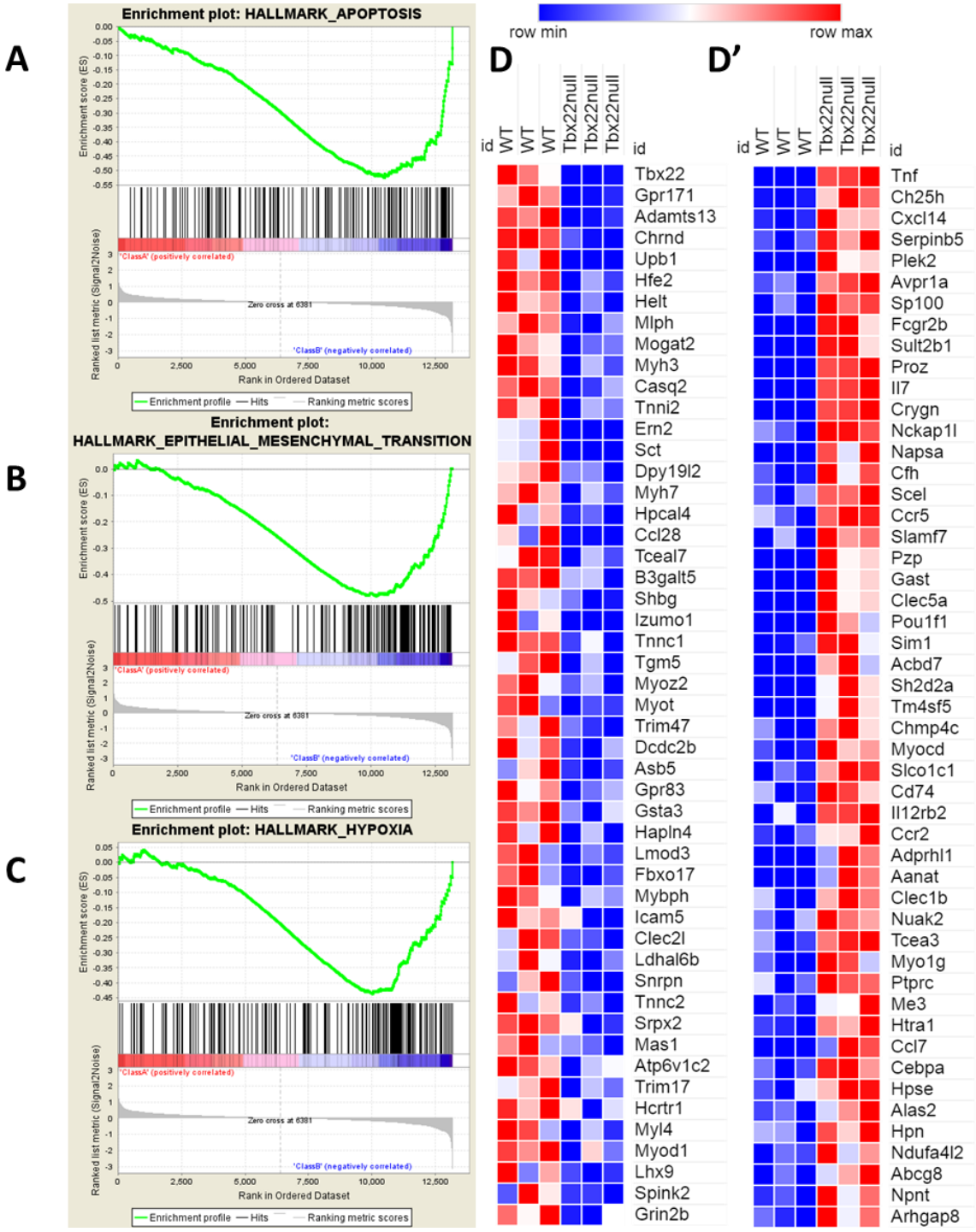

Figure IV. 18. Enrichments plots identified in the Hallmark gene set.

Enrichments plots show the distribution of genes from the **A)** Apoptosis; **B)** Epithelial mesenchymal transition and **C)** Hypoxia gene sets (Hallmark). **D)** Heat Map of top 50 genes down regulated and **D')** up regulated for each phenotype in *Wnt1*-Cre group. Expression values are represented as colours, where the range of colours red, pink, light blue and dark blue shows the range of expression values as high, moderate, low and lowest respectively.

There were 26 gene sets significantly enriched in *Tbx22*$^{-/Y}$ CM derived cells when compared to *Tbx22*$^{-/Y}$ CNC derived cells at FDR < 25%. The same gene sets and an additional 10 (in total 36) were enriched in WT CM derived cells compared to WT CNC derived cell population. Those 10 included: xenobiotic metabolism (genes encoding proteins involved in processing of drugs and other xenobiotics), protein secretion (genes involved in protein secretion pathway), oxidative phosphorylation (genes encoding proteins involved in oxidative phosphorylation), UV response (genes down regulated in response to UV radiation), myogenesis (genes involved in development of skeletal muscle), haem metabolism (genes involved in metabolism of haem (a cofactor consisting of iron and porphyrin) and erythroblast differentiation), MYC targets V2 (A subgroup of genes regulated by MYC - version 2), apical surface (genes encoding proteins over-represented on the apical surface of epithelial cells, e.g., important for cell polarity), WNT beta catenin signalling (genes up-regulated by activation of WNT signalling through accumulation of beta catenin CTNNB1), E2F targets (genes encoding cell cycle related targets of E2F transcription factors) were 10 pathways which were significantly enriched in WT CM derived tissue group and haven't reached significance in *Tbx22*$^{-/Y}$ phenotype. One of these, enrichment of the myogenesis pathway in WT CM derived tissue expressed genes may be of particular interest to help to explain certain gene expression changes in the mutant phenotype that might lead to insufficient palate development.

IV. 3. 10. 2. C2 gene set

In this set, Jiang Hypoxia Via VHL pathway was significantly enriched in the WT phenotype at FDR < 25% when comparing *Tbx22*$^{-/Y}$ vs. WT in CM derived cells. The Jiang Hypoxia Via VHL pathway is one of the best characterized hypoxia signalling pathways in tumour cells. Although this pathway correlates significantly, there were just 29 genes involved, and it is not clear regarding the importance of this finding in palate development.

There were 2 significantly enriched pathways in WT phenotype when comparing *Tbx22*$^{-/Y}$ vs. WT in CNC derived cells. These were the Holleman Prednisolone

Resistance B All Up pathway, which involved 18 genes and the Dairkee Cancer Prone Response BPA pathway involved 45 genes.

At FDR < 25%, 2010 gene sets were significantly enriched in WT *Mesp1*-Cre, when comparing WT in CM vs. CNC derived cells. This is expected finding showing the difference between CM and CNC derived WT tissue.

At FDR < 25%, 1847 gene sets were significantly enriched in *Tbx22*$^{-/Y}$ *Mesp1*-Cre when comparing *Tbx22*$^{-/Y}$ in CM vs. CNC derived cells. This finding shows the difference in gene expression in CM and CNC derived cells when *Tbx22* is disrupted.

IV. 3. 10. 3. C3 gene set

There were 64 gene sets significantly enriched in WT CM derived cells when comparing WT in CM vs. CNC derived cells and 72 gene sets in *Tbx22*$^{-/Y}$ CM derived cells when comparing *Tbx22*$^{-/Y}$ in CM vs. CNC derived cells at FDR < 25%.

IV. 3. 10. 4. C5 gene set

There were 357 gene sets significantly enriched in WT CM derived cells when compared WT in CM vs. CNC derived cells and 340 gene sets in *Tbx22*$^{-/Y}$ CM derived cells when comparing *Tbx22*$^{-/Y}$ in CM vs. CNC derived cells at FDR < 25%.

IV. 3. 10. 5. GO palate development gene set

This gene set was enriched in *Tbx22*$^{-/Y}$ phenotype when comparing *Tbx22*$^{-/Y}$ vs. WT at FDR < 25% in CM derived cells. It was enriched in WT CNC derived cells when comparing WT CM vs. CNC at FDR < 25%. It was also enriched in *Tbx22*$^{-/Y}$ CNC derived cells when comparing *Tbx22*$^{-/Y}$ in CM vs. CNC at FDR < 25%. (Figure IV. 19).

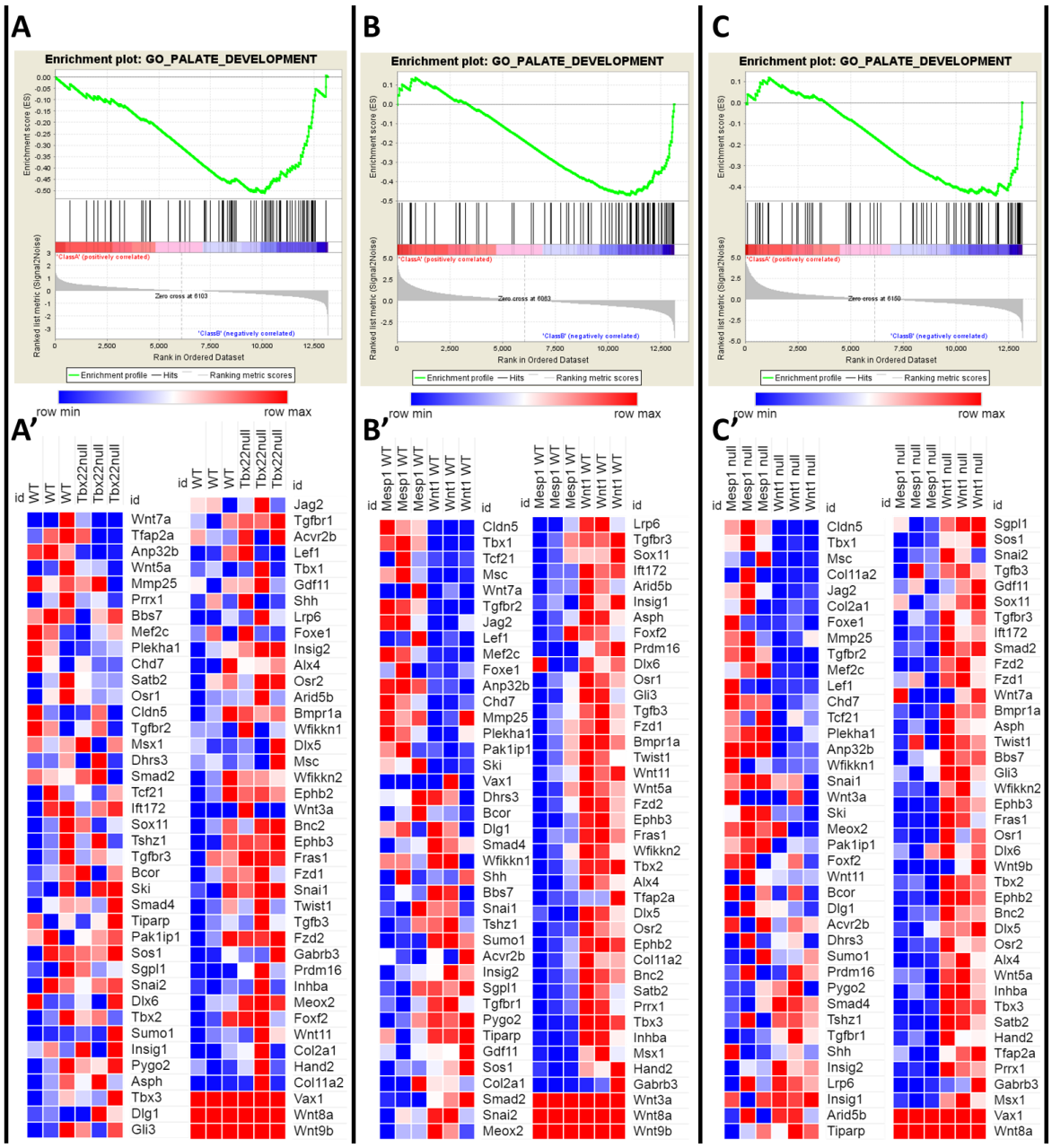

Figure IV. 19. Palate development gene set enrichment plots and heat maps comparing different groups.

A), A') Comparison of WT and *Tbx22*$^{-/Y}$ transcripts in CM derived cells using GSEA show that the *Tbx22*$^{-/Y}$ phenotype was significantly enriched in the GO Palate Development pathway. **A)** Enrichment plot; **A')** enriched genes heat map. **B), B')** Comparison of WT transcripts between CM and CNC derived cells showing significant enrichment in CNC derived tissue in the GO Palate Development pathway. **B)** Enrichment plot; **B')** enriched genes heat map. **C), C')** Comparison of *Tbx22*$^{-/Y}$ between CM and in CNC derived cells show that the *Tbx22*$^{-/Y}$ phenotype in CNC derived tissue was significantly enriched in the GO Palate Development pathway. **C)** Enrichment plot; **C')** enriched genes heat map. Expression values are represented as colours, where the range of colours red, pink, light blue and dark blue shows the range of expression values as high, moderate, low and lowest respectively.

IV. 3. 11. Differentially expressed genes analysis using the DAVID functional annotation tool

DAVID provides a comprehensive set of functional annotation tools to better understand the biological context within a large and complex list of genes (Abduelmula et al., 2016).

Gene Ontology (GO) analysis was used to explore the significantly differentially expressed genes (p<0.05). Biological Process and Cellular Component terms significantly (adjusted p<0.05) over represented in the group of differentially expressed genes are summarized in Table IV. 7. The number of GO terms significantly enriched in groups of genes was variable. The Biological Process terms included ones relevant to palatal development and the palatal shelf closure process with such terms as cell and focal adhesion as well as known developmental pathways including Wnt and calcium signalling. Some terms appear in comparison groups and are highlighted in red together with the most important pathways in palate development (Table IV. 7).

Table IV. 7. Functional annotation of significantly differentially expressed genes.
The table represents the GO Biological Process and Cellular Component terms enriched in the groups of significantly differentially expressed genes. Red colour indicates the most relative terms occur in palate development. ◄ indicates the same term or pathway in different comparison groups. ◄ and underlined indicate unique terms to specific comparison group.

GO Biological Process terms			
	Terms		**Benjamini – Hochberg corrected *p* value**
***Tbx22*$^{-/Y}$ vs. WT *Mesp1*-Cre**	Axon guidance	◄	2.9E-03
	Focal adhesion	◄	3.5E-02
	B cell receptor signalling pathway	◄	4.4E-02
***Tbx22*$^{-/Y}$ vs. WT *Wnt1*-Cre**	**ECM-receptor interaction**	◄	1.5E-02

Table IV. 7. (continued).

WT *Mesp1*-Cre vs. WT *Wnt1*-Cre	Rap1 signalling pathway	◄	1.0E-14
	Axon guidance	◄	3.1E-14
	Leukocyte transendothelial migration	◄	2.2E-12
	Focal adhesion	◄	8.5E-11
	Regulation of actin cytoskeleton	◄	1.1E-10
	Fc gamma R-mediated phagocytosis	◄	3.5E-09
	Platelet activation	◄	6.7E-09
	Chemokine signalling pathway	◄	1.4E-08
	MAPK signalling pathway	◄	4.0E-08
	Ras signalling pathway	◄	9.9E-08
	Osteoclast differentiation	◄	1.0E-07
	Oxytocin signalling pathway	◄	2.3E-07
	Circadian entrainment	◄	2.9E-06
	PI3K-Akt signalling pathway	◄	2.9E-06
	Cell adhesion molecules (CAMs)	◄	7.0E-06
	cAMP signalling pathway	◄	1.2E-05
	B cell receptor signalling pathway	◄	2.6E-05
	Cholinergic synapse	◄	3.7E-05
	Toll-like receptor signalling pathway	◄	4.2E-05
	Adherens junction	◄	1.2E-04
	Fc epsilon RI signalling pathway	◄	1.2E-04
	Glutamatergic synapse	◄	1.2E-04
	Arrhythmogenic right ventricular cardiomyopathy	◄	2.6E-04
	NF-kappa B signalling pathway	◄	2.7E-04
	Endocytosis	◄	3.1E-04
	NOD-like receptor signalling pathway	◄	4.6E-04
	Calcium signalling pathway	◄	5.0E-04

Table IV. 7. (continued).

WT *Mesp1*-Cre vs. WT *Wnt1*-Cre (continued)	Natural killer cell mediated cytotoxicity	◀	5.3E-04
	TNF signalling pathway	◀	1.1E-03
	cGMP-PKG signalling pathway	◀	1.3E-03
	Phagosome	◀	2.0E-03
	Adrenergic signalling in cardiomyocytes	◀	2.1E-03
	Sphingolipid signalling pathway	◀	2.6E-03
	GABAergic synapse	◀	2.8E-03
	T cell receptor signalling pathway	◀	2.8E-03
	HIF-1 signalling pathway	◀	3.3E-03
	Neurotrophin signalling pathway	◀	3.6E-03
	Other types of O-glycan biosynthesis	◀	4.2E-03
	Cytokine-cytokine receptor interaction	◀	5.1E-03
	GnRH signalling pathway	◀	6.6E-03
	Estrogen signalling pathway	◀	7.1E-03
	Regulation of lipolysis in adipocytes	◀	7.9E-03
	Gap junction	◀	1.0E-02
	Lysosome	◀	1.3E-02
	VEGF signalling pathway	◀	1.4E-02
	Dopaminergic synapse	◀	1.5E-02
	ErbB signalling pathway	◀	2.2E-02
	ECM-receptor interaction	◀	2.5E-02
	Apoptosis	◀	2.7E-02
	Dorso-ventral axis formation	◀	3.2E-02
	Vascular smooth muscle contraction	◀	3.4E-02
	Antigen processing and presentation	◀	3.8E-02
	Jak-STAT signalling pathway	◀	4.1E-02
	Notch signalling pathway	◀	4.4E-02
	Rap1 signalling pathway	◀	1.0E-14

Table IV. 7. (continued).

***Tbx22*$^{-/Y}$ *Mesp1*-Cre vs. *Tbx22*$^{-/Y}$ *Wnt1*-Cre**	Axon guidance	◄	2.2E-16
	Rap1 signalling pathway	◄	1.7E-11
	Focal adhesion	◄	4.7E-11
	Chemokine signalling pathway	◄	1.4E-10
	Leukocyte transendothelial migration	◄	7.2E-10
	Platelet activation	◄	1.1E-09
	Fc gamma R-mediated phagocytosis	◄	1.2E-08
	Regulation of actin cytoskeleton	◄	1.4E-08
	PI3K-Akt signalling pathway	◄	1.7E-08
	Osteoclast differentiation	◄	5.2E-08
	MAPK signalling pathway	◄	1.3E-07
	Ras signalling pathway	◄	6.1E-07
	Arrhythmogenic right ventricular cardiomyopathy	◄	2.1E-06
	Toll-like receptor signalling pathway	◄	6.4E-06
	Circadian entrainment	◄	8.1E-06
	Cell adhesion molecules (CAMs)	◄	2.7E-05
	ECM-receptor interaction	◄	3.8E-05
	Cholinergic synapse	◄	4.2E-05
	cAMP signalling pathway	◄	4.7E-05
	B cell receptor signalling pathway	◄	5.5E-05
	Oxytocin signalling pathway	◄	6.8E-05
	Dopaminergic synapse	◄	8.7E-05
	Adherens junction	◄	9.0E-05
	NOD-like receptor signalling pathway	◄	9.6E-05
	NF-kappa B signalling pathway	◄	1.1E-04
	Glutamatergic synapse	◄	1.3E-04
	Fc epsilon RI signalling pathway	◄	6.9E-04
	Adrenergic signalling in cardiomyocytes	◄	7.0E-04

Table IV. 7. (continued).

Tbx22$^{-/Y}$ *Mesp1*-Cre vs. *Tbx22*$^{-/Y}$ *Wnt1*-Cre (continued)	HIF-1 signalling pathway	◄	7.1E-04
	cGMP-PKG signalling pathway	◄	1.0E-03
	Sphingolipid signalling pathway	◄	1.5E-03
	Wnt signalling pathway	◄	2.4E-03
	GABAergic synapse	◄	2.5E-03
	Phagosome	◄	2.8E-03
	T cell receptor signalling pathway	◄	2.8E-03
	TNF signalling pathway	◄	5.0E-03
	Natural killer cell mediated cytotoxicity	◄	5.4E-03
	Calcium signalling pathway	◄	1.4E-02
	Endocytosis	◄	1.4E-02
	Cytokine-cytokine receptor interaction	◄	1.5E-02
	Neurotrophin signalling pathway	◄	1.5E-02
	Vascular smooth muscle contraction	◄	2.6E-02
	Notch signalling pathway	◄	3.5E-02
	VEGF signalling pathway	◄	4.7E-02

IV. 3. 12. Genes with consensus T-box binding sites

The most significant differentially expressed genes (Table IV. 4) were investigated for the possible presence of a consensus T-box binding half site. Text searching was carried out for AGGTGTGA or its complimentary sequence (TCACACCT) and included incomplete putative half sites. This search was carried out in a 1000 bp upstream sequence that was identified from the start of transcription of each gene based on the RefSeq annotation in the UCSC browser. The search was based on several assumptions: that this region approximately represented the gene's promoter and that the T-box binding site, if present, would be in the chosen portion of the promoter. Out of 23 genes investigated in this way, 8 were identified as containing putative binding sequences and therefore potential direct binding

targets. However, further analysis would need to be done to confirm these theoretical findings. For example, promoter studies and EMSA as previously described in Andreou et al. (2007) would provide functional evidence. Nevertheless, this crude search could be used as an indication and provide guidance for which genes could be prioritized for further studies.

Cxcl14 up regulated in *Wnt1*-Cre (*p*adj=0.0095, av exp=57.50 [*Tbx22*^{null}], av exp=12.89 [WT]). Not significant in *Mesp1*-Cre. Sequence with T-box binding sites (in capital letters and underlined):

[tcaaagcaacagagtggtccagggacaggagtcccagttctgcagccgtatatactgaggaccctcctggcctagtcacctgcttcctagc
tctgtgaccttggacaagttatttcttctctcagagcatgtttcCACACCTgtcaaataaagaaattaaaagtaccaacttggaagaaaagt
accaattggtaagaatcaaagtaatagataaattagacataaaacgatggtgccaataagtaacatttcctgggtactgacaacatgtatga
tttctatagttctcacagccaccctatcagaaacactgtgatgatctgcactttacagatgatgaaacaaaagctgagagcggtaaagtcactt
gtgctggaaagtagtgaggagggaatttctgccactatggctgggcTCACACCactatacctcgcattctggcacaatgtctagaacat
gggaaggccttcatccagatggttaccactgtcatcgctctccactagggctctctacctggctttggagagtagtgtgagagtgaggactc]

Fosl2 up regulated in *Wnt1*-Cre (*p*=0.000036, av exp=306.47 *[Tbx22*^{null}*]*, av exp=178.11 [WT]). Not significant in *Mesp1*-Cre. Sequence with T-box binding sites:

[ctcccgcccgtgccaccgcctggcttcctcgcgcggggtgcgcggttggcgtcagcgcggccgggagccggggctgggaggggagag
ctgcgcccgcctcctcccctcccgcgcctcttcctcctccgcggcctcctccccccgcctcctcgtgcgctcctccctgcaAGGTGGAgtct
ggggttgacgtgagtgaatccacatggtacagggctggagaataaagAGTGTGAGttgaactcgtgccattgtagtgactcatctcgg
gcagagcgctagggctccgagcgaaccagcgag]

Myh3 down regulated in *Wnt1*-Cre (*p*=0.000066, av exp=220.13 [*Tbx22*^{null}], av exp=531.63 [WT]). Not significant in *Mesp1*-Cre. Sequence with T-box binding sites:

[taagagaaagaaggagaggagtagaaggaggagaagggagaagagggcaagggggaggggaattattgctattaattattattatt
attaattattcctggcacaggttttgcaaTCACAACCcaaggttgtgataaaatcttgctcaaaattcaaaaaggatttcaacttttcactctc
agtcttattcacttttccatatgatgagatttctaagtaagccacccgacttcagtccttggtgcccaatagctaggggctcacgccgcgttcag
GGTGTGAtgagcgcctgagaacggaggtggctgcccccgcaactcctcctggagtgaggccatcccatcccatcaggggagggag
caccggccccaagttcagagaaaggcatcccaagctcct]

Shisa3 down regulated in *Wnt1*-Cre (*p*=0.00031, av exp=443.91 [*Tbx22*^{null}], av exp=598.94 [WT]). Not significant in *Mesp1*-Cre. Sequence with T-box binding sites:

[tgcgagctggccttggctggcagaggtgaccggcaatccttcagccggcggaaaaagtgcgagtgtgtgtgtgtgtgcttgtgaaaatgt
gccgttcctcccagaaaaagtggaaacgtAGGTGGAaagctcagcacatgttggcgacacctaaaaaccatgttctcggtcctgaac
ctttagaagcggtatcccaggaacgagtctgagtctgtgcaacagggcacagatgattcgacaaacttcaatgactgcaccgcattcatgc
attatatccattgaaaagtaaatccagcgt]

Krt5 up regulated in *Wnt1*-Cre (*p*=0.00038, av exp=65.84 [*Tbx22*^{null}], av exp=12.69 [WT]). Not significant in *Mesp1*-Cre. Sequence with T-box binding sites:

[acaggccgtcagactctcaacatgttcctgatgagattagaagctcctgcaggtatgtgtttgtggcggccttcagcctgtatcaacacatac
gatgactcatttcttccctagtggaatagagcttgctggaaCACACCTgggggggctggggaaccggcagagtagctacccccaaaga
gagacgctatagcccatgagtctcagggttttttttaagggattgcatgggatccccgggtttcctaaa]

Tll1 down regulated in *Mesp1*-Cre (*p*adj=0.000012, av exp=145.60 [*Tbx22*^{null}], av exp=449.50 [WT]). Not significant in *Wnt1*-Cre. Sequence with T-box binding sites:

[gtgattgggttagatggtgcgaatatttttttttttcaagttaggaagagggtaaaaagacaggctggcgggggggaaggcaaacagtgcatc
cccaaatccTCACACTtttgctctcttgcagtcagttgctttgctggcttctgcaggc]

Lars2 down regulated in *Mesp1*-Cre (*p*adj=0.00034, av exp=11613.01 [*Tbx22*^{null}], av exp=18194.99 [WT]). Not significant in *Wnt1*-Cre. Sequence with T-box binding sites:

[gttgatttattacaagcatgaaacacttgccgggtgtgtggcagtgggggcatgggatatacaaactcctcgaggaaagggaaggcatca
tgctttcctgactcccagcacacttgccAGGTGAGAaaagtaccttaccccaaacctattcttggccaggtaattccacccccccgcccca
gggctagaggattacgcaatatggtggaagaaggtgcctcactcatcatgcagtcaattaggaatcaaga]

Scarna13 up regulated in *Mesp1*-Cre (*p*adj=0.00035, av exp=374.11 [*Tbx22*^{null}], av exp=202.84 [WT]). Not significant in *Wnt1*-Cre. Sequence with T-box binding sites:

[ctgtatcctcagtgcctaggacgatgcttggaacgtggtaagtgctcctattggcgggaagaataaatccggaagagcaggaccagtgga
cttgctacataatctgtagtcttggagccgcacagggttggtggtaccctcgagCACACC]

IV. 4. Discussion

Construction of a mouse knockout model for *Tbx22* has allowed a more detailed understanding of the developmental processes that lead to a SMCP phenotype (Pauws et al., 2009a). Whilst previous studies reported on the constitutive *Tbx22*^{null}, in this Chapter IV, it was intended to harness the *Cre*-loxP system to look more closely at the cell-type specific contribution of *Tbx22* in the developing palate. Given the previous implication of disturbed muscle gene expression profiles (Hoshino, 2011) and palatal bone loss (Pauws et al., 2009a) leading to a SMCP phenotype, studies were focused on *Mesp1*-expressing CM and *Wnt1*-expressing CNC derived cells.

Correct development of both bone and muscle are inter-reliant on each other and are closely related to the clinical presentation of palatal defects in the human population. It is therefore essential to distinguish the roles of CNC and paraxial mesoderm as different cells lineages in order to better understand the importance of interaction between them (Grenier et al., 2009, Trainor and Tam, 1995). The respective contributions of CNC and CM to craniofacial development can be investigated in cell lineage tracing experiments (Yoshida et al., 2008). However, it is not known whether myogenic CM and skeletogenic CNC cells interact while at the development stage or later when the musculoskeletal morphogenesis is completed, especially in palate development.

For this experiment we have used a conditional mouse line using homozygous floxed females crossed with R26-YFP to introduce a *Cre* activated fluorescent marker. Therefore, subsequent crossing of YFP+ offspring with tissue specific *Cre* will mark the CM derived cell lineage (*Mesp1*-Cre) or the CNC derived cell lineage (*Wnt1*-Cre). Our experiment differed from similar cell lineage tracing studies due to the earlier finding that *Tbx22* expression in floxed animals was already compromised and similar to that observed in null animals. Normally, a tissue specific knockout would only ablate the gene in the desired cells whilst it would continue to be expressed normally in all other cells. In this case, the CM or CNC derived *Tbx22*^{null} cells were knocked out in an environment where all of the rest of the cells also had *Tbx22* expression close to null levels. This does have the

advantage of excluding *Tbx22* expression-related factors from surrounding cells e.g. CM-CNC cross talk, which might affect gene expression in the desired null cells.

The CNC is an embryonic stem cell population that gives rise to the facial skeleton and also includes the palate shelves (Bush and Jiang, 2012). Defects in CNC development significantly contribute to congenital birth defects (Wu et al., 2017, Rogers et al., 2012). For this reason the CNC transcriptome has been widely analysed in gene regulatory networks (Rogers et al., 2012, Wu et al., 2017). To validate our data set quality, we looked for expression of well-known NC-specific transcription factors such as *Tfap2A* (av exp=140.44), *Pax7* (av exp=25.18), *Sox8* (av exp=30.73), *Sox10* (av exp=287.25), *Ets1* (av exp=295.20) and *Foxd3* (av exp=47.15) (Simoes-Costa et al., 2014). All were present in our experimentally generated data set.

Apart from CNC derived tissue, another robust cell population in embryonic head formation is paraxial mesoderm. An understanding of CM development is important given its contribution to the craniofacial skeleton, muscles, its influence on CNC migration and the likely role as a supportive tissue for cranial neural tube morphogenesis (Sambasivan et al., 2011). There are few studies that focus on gene function in CM and its role in craniofacial development (Sambasivan et al., 2009). The main myogenic network consists of the basic helix-loop-helix (bHLH) myogenic regulatory factors (MRFs), which identify muscle and/or promotes muscle differentiation: *Myf5, Mrf4; Myf6; MyoD* (*MyoD1* and *myogenin*), as well as mesoderm markers: *Pax3, Pax7, Pitx2, Tbx1, Msc* (also known as *MyoR*), *Tcf21, Six1, Six4, Meox1; Meox2; Eya1* and *Eya2* (Weintraub et al., 1991). All were present in our experimentally generated data when analysing gene expression in CM derived tissue (*Pax3* av exp=11.22, *Pax7* av exp=95.74, *Pitx2* av exp=37.45, *Tbx1* av exp=238.05, *Msc* av exp=39.70, *Tcf21* av exp=3.46, *Six1* av exp=450.38, *Six4* av exp=280.73, *Meox1* av exp=40.52; *Meox2* av exp=202.15; *Eya1* av exp=285.32 and *Eya2* av exp=90.19).

In our study, finding significant down regulation of *Tbx22* in CNC derived cells (*p*adj<0.1) validated the data set and confirmed the effective knock out in these

cells. There was also significant down regulation of *Tbx22* in CM derived tissue but the initial expression level in WT cells was already much lower. This result therefore questioned whether *Tbx22* expression in CM derived cells has functional significance, at least when compared to the higher levels in CNC derived tissue. It was also notable that *Mesp1* was not expressed in CNC nor *Wnt1* expression in CM derived tissues (both counts were = 0). This indicated that they were specific for the cell types stated and that there would not be significant overlap.

In the PCA, as expected, there was clearly much more difference in gene expression between CM and CNC derived populations than between WT and null cells for each cell population. This mirrored the differences between cell lineages, whilst *Tbx22* as a transcriptional factor was only likely to affect a relatively small number of downstream targets.

In terms of cell numbers, we found that when analysing the CM derived tissues, overall 8% of cells were YFP+ compared to 38% YFP+ cells when analysing CNC derived tissue. When looking specifically at the experimental male WT and null embryos, the ratio of YFP+ cells per WT embryo between CM and CNC derived tissue was 1:3.8 in favour of CNC and even more skewed, 1:5.6 in null palatal shelves. This increase suggests that *TBX22* may play an important role in the distribution and numbers of these cell types in the developing palate. Cell proliferation in palatal shelves was previously investigated using phospho-histone H3 (Ser10) in an immunological assay to assess mitotic index (Hoshino, 2011). For the purpose of that analysis, the palatal shelves were designated into the anterior, middle and posterior regions. The results suggest that loss of *Tbx22* lead to reduced cell proliferation rates especially in the middle to posterior palatal mesenchyme (*Tbx22* expression zones) at E13.5. There was no statistically significant difference in the proliferation rate in the palatal epithelium along the anterior to posterior regions. This was expected as *Tbx22* is known to be expressed almost exclusively in the palatal mesenchyme but not in the epithelium (Braybrook et al., 2002, Bush et al., 2002). Therefore, TBX22 may play a significant role in cell proliferation in the palatal mesenchyme at E13.5, in addition to previously suggested roles in osteoblast differentiation and maturation at later stages.

It was noticed in our study that the overall number of cells collected in CM derived tissue was smaller compared to CNC derived tissue in both WT and null embryos (~75,000). One explanation might be related to the sequence of experiments leading to an improvement in dissection technique (*Mesp1*-Cre cross was followed by *Wnt1*-Cre cross) or more efficient tissue dissociation occurred when changing to fresh reagents. However, this numbers were consistent across each sample set and variability in technique or reagents are thought unlikely to be the main reason. More likely, other explanations such as the overall size of the embryo being smaller or that there are *Tbx22*-distinct effects on CM and CNC derived tissue. Both of these are feasible, but require further studies to draw firm conclusions. Other palatal cells present are likely to include epithelial, blood vessels and connective tissue such as fibroblasts, adipocytes or immune cells, all of which would be expected to be YFP-. In terms of absolute total numbers of cells, it is likely that Cre-excision efficiency was not 100%, which might result in a lower number of YFP+ cells captured than theoretically possible, whilst there will be also, almost certainly, some level of contamination of fluorescent and non-fluorescent cells that occurs due to miss-sorting. However, since the methodology of the experimental set up is to differentiate both cell lineages including mouse breeding, dissection, tissue processing and flow sorting was essentially the same, we can conclude that the dissected E13.5 palatal shelf tissues consist of nearly 5x more CNC derived cells compared to CM cells.

Several studies that are similar to the *Tbx22* study reported in this thesis have looked at *Tbx1* expression and its relation to palate development. It was well described that loss of *Tbx1* function in mouse causes a clinical picture similar to that seen in 22q11.2 DS patients (Morrow et al., 2018). Microdeletion of chromosome 22q11.2 (OMIM 188400) is associated with significant developmental anomalies, including cardiac anomalies, thymus aplasia/hypoplasia, craniofacial dysmorphism and CP (Van et al., 2019). Also *TBX1* mutations were identified in both sporadic and familial cases of patients who had the 22q11.2 DS phenotype but no detectable deletion (Yagi et al., 2003, Paylor et al., 2006, Zweier et al., 2007). Interestingly, Van et al. (Van et al., 2019) in their study reasoned that TBX1 was responsible for a number of the phenotypic features of 22q11.2 DS but not the

intellectual disability, which is a common feature of the deletion syndrome. Subsequently Zoupa et al. (2018) carried out a microarray analysis to investigate potential transcriptional target genes of TBX1, using cDNA transcribed from total RNA derived from the dissected secondary palatal shelves of E13.5 *Tbx1*$^{+/+}$; *Tbx1*$^{+/-}$ and *Tbx1*$^{-/-}$ embryos (N=3 for each group). In this study WEB-based Gene Set Analysis Toolkit (WebGestalt, http://www.webgestalt.org/option.php, version 05/20/2014) was used. Comparison between mutant embryos and WT, heterozygous and WT and mutant versus heterozygous were performed. The authors validated the results performing RTqPCR using gene-specific primers. In the Zoupa et al. (2018) study when comparing mutant embryos and WT, 89 genes were identified as differentially expressed in mutant compared to WT (3 genes were upregulated and 86 were downregulated). There were no statistically significant changes when comparing heterozygous and WT embryos. However, when comparing homozygous (mutant) vs. heterozygous animals, 88 genes were identified, of which 11 genes were upregulated and 77 were downregulated. When analysing differential expressed gene pathways with KEGG, the most significant were those associated with cardiac muscle physiology in both groups (mutant vs. WT and mutant vs. heterozygous). Other pathways included phagosome and focal adhesion, tight junction and calcium signalling pathways and Alzheimer's disease in mutant vs. WT group and tight junction, calcium signalling, focal adhesion, neuroactive ligand-receptor interaction, phagosome and Alzheimer's disease pathways in mutant vs. heterozygous group (Zoupa et al., 2018).

Another study also analysing *Tbx1* expression was performed by Funato et al. (2018). As in the Zoupa et al. (2018) study, the authors carried out microarray analysis to investigate potential transcriptional target genes of *Tbx1* using cDNA transcribed from total RNA derived from the dissected secondary palatal shelves of E13.5 from eight wild type or *Tbx1* knockout embryos. The authors used the PANTHER (protein annotation through evolutionary relationship; http://www.pantherdb.org/) classification system for pathway analysis of the expression results (Mi et al., 2013) and the Reactome pathway database (http://www.reactome.org). Using a 2 FC cut-off, the study found that more than 150 genes what were dysregulated, including *Tbx1*. These genes were involved in pathways associated

with striated muscle contraction and transmission across chemical synapses. The authors concluded that dysregulated genes in *Tbx1* knockout palatal shelves were specific to the development and differentiation of neurons, muscles, and bones, and included mouse homologs of several disease genes of oral cleft in humans (Funato and Yanagisawa, 2018).

In our study, RNA sequencing was carried out on flow sorted palate shelves tissue specific cells (CM and CNC derived) of E13.5 *Tbx22*^{null} and WT embryos (N=3 for each group). Unlike the TBX1 studies described above, our results were specific to the particular cell lineages they were derived from. There were 22 differentially expressed genes (11 genes were upregulated and 11 were downregulated) when compared mutants vs. WT in *Mesp1*-Cre group and just two genes (one upregulated and one downregulated) when comparing mutants vs. WT in the *Wnt1*-Cre group (*p*adj<0.1). Differentially expressed genes were investigated for common pathways using the GSEA and DAVID functional annotation tools. Focal adhesion (mutant vs. WT in *Mesp1*-Cre group; WT in *Mesp1*-Cre vs. WT in *Wnt1*-Cre; mutant in *Mesp1*-Cre vs. mutant in *Wnt1*-Cre) and calcium signalling (WT in *Mesp1*-Cre vs. WT in *Wnt1*-Cre; mutant in *Mesp1*-Cre vs. mutant in *Wnt1*-Cre) pathways were enriched in our analysis, similar to Tbx1 study by Zoupa et al. (2018).

In Hoshino's earlier study (Hoshino, 2011), an attempt was made to identify downstream targets under the transcriptional control of TBX22 at E13.5. This was performed more similarly to the methods employed by Zoupa et al. (2018) and Funato et al. (2018). Hoshino (2011) dissected whole E13.5 palatal shelves from WT and *Tbx22*^{null} animals. It was thought that the use of whole palatal shelves could have contributed to the relatively low FCs identified since the samples would have contained a complex mix of cell types, of which only a fraction would express *Tbx22*. In our study, specific knockdown of *Tbx22* in CM and CNC derived cell lineages is a substantial change in target and has clarified specific transcriptional effects that *Tbx22* has on each cell type. Hoshino (2011) identified and described a number of interesting up or downregulated genes, some of which were experimentally validated using RTqPCR and in the case of *MyoD*, shown to involve direct promoter binding using a CHiP-PCR assay (Kantaputra et al., 2011).

Therefore, it was of great interest to compare the new results from cell lineage specific palatal cells to RNA extracted from whole palate, albeit using different analytical platforms. It was immediately striking that none of the top differentially expressed genes (by *p* value or FC) were common to the two studies. Hoshino (2011) highlighted the importance of GABAergic inhibitory neurotransmission in the normal palate and developing CP phenotype in mice lacking *Gabrb3* or *Gad1.* In her study, the FCs for *Gabrb3* (FC=1.04, *p*=0.54) and *Gad1* (FC=1.03, *p*=0.48) in the *Tbx22*^{null} palatal shelves were close to 1.0 and downregulation of *Gabrb2* by 1.24 fold (*p*=0.000024) was noted. Also were *Gabra1* (FC=1.22, *p*=0.15) and *Gria4* (FC=1.21, *p*=0.13) genes identified. These latter genes did not reach statistical significance but were discussed as interesting to follow up further. In our study, *Gabrb3* was not significantly expressed in either cell lineage studied with low expression in CM derived cells (FC=1.59, *p*=0.33, av exp=18.95 [*Tbx22*^{null}], av exp=11.79 [WT]) and higher expression in CNC derived cells (FC=0.75 [$\log_2$FC=-0.42], *p*=0.70, av exp=301.43 [*Tbx22*^{null}], av exp=404.40 [WT]). *Gad1* was not expressed at all in either *Mesp1*-Cre or *Wnt1*-Cre cells. Not significant and low expression was noted of *Gabrb2* in *Mesp1*-Cre (FC=1.52, *p*=0.25, av exp=24.97 [*Tbx22*^{null}], av exp=16.39 [WT]) and in *Wnt1*-Cre not significant but slightly higher expression (FC=1.16, *p*=0.37, av exp=319.20 [*Tbx22*^{null}], av exp=274.06 [WT]). *Gabra1* was not highly expressed in CM (FC=1.09, *p*=0.84, av exp=24.93 [*Tbx22*^{null}], av exp=22.63 [WT]) with higher although not significant expression in CNC derived cells (FC=1.28, *p*=0.19, av exp=307.78 [*Tbx22*^{null}], av exp=239.69 [WT]) as well as *Gria4* in CM (FC=1.87, *p*=0.10, av exp=42.77 [*Tbx22*^{null}], av exp=22.56 [WT]) and in CNC (FC=1.06, *p*=0.75, av exp=272.35 [*Tbx22*^{null}], av exp=257.59 [WT]). Therefore, our study as well as previous work did not identify any obvious significance for *Tbx22* regulation in GABAergic inhibitory neurotransmission.

Another gene found to be downregulated in null palatal shelves in Hoshino (2011) was *Pax3* (FC=1.21, *p*=0.40). In our study, *Pax3* was not expressed in CM derived cells and more surprisingly showed low expression in CNC derived cells (FC=0.90 [$\log_2$FC=-0.15], *p*=0.80, av exp=55.33 [*Tbx22*^{null}], av exp=60.78 [WT]), note that significance was not reached in either case.

Retinoic acid (RA) is synthesised from retinol (vitamin A) via retinal as the intermediate and its association with the development of CP is discussed in Hoshino (2011). *In vivo* gene disruption of *Adh1* in mice leads to a reduction in retinoid metabolism and the microarray data revealed a reduced expression of *Adh1* (FC=1.27, *p*=0.27) in the *Tbx22*^{null} palatal shelves. In our study there was no *Adh1* expression in CM or CNC derived tissue and it was not considered important to palate development at stage E13.5.

Some of genes which were upregulated in Hoshino (2011) were followed up by RTqPCR based on the fact that TBX22 was demonstrated to act as a transcriptional repressor *in vitro* (Andreou et al., 2007). Due to the less efficient methodology using microarray often generating false positive results, an alternative methodology of RTqPCR was necessary to provide verification of the results. *Ctsk* (FC=1.62, *p*=0.074) was the only known gene related to osteogenesis. However, the microarray data for *Ctsk* was a false positive after RTqPCR verification. In our study *Ctsk* was very low expressed in CM (FC=1.45, *p*=0.50, av exp=36.12 [*Tbx22*^{null}], av exp=24.72 [WT]) and slightly higher in CNC derived tissue (FC=1.29, *p*=0.07, av exp=141.37 [*Tbx22*^{null}], av exp=108.79 [WT]) with no statistical significance. Other genes related to osteogenesis or ossification such as *Runx2*, *Osterix*, *Osteopontin (Opn)*, *Alkaline phosphatase (Alpl)*, *type I collagen* and others were checked for differential expression. None of them were considered important and no change in bone markers suggests that at least at this stage E13.5, bone development is not significantly altered to cause palate development pathology.

Interestingly in Hoshino (2011), there was a general upregulation of muscle related genes (20 out of all 43 upregulated genes) in the *Tbx22*^{null} palatal shelves. They belonged to myosin, actin, actinin, titin, troponin and calsequestrin gene families. Their functions were muscle metabolism, contraction and filament assembly. *Myh3, Acta1, Casq2* were chosen for RTqPCR validation. The microarray data showed increased expression of *Myh3* (FC=1.57, *p*=0.061), *Acta1* (FC=1.35, *p*=0.12) and *Casq2* (FC=1.30, *p*=0.21). The RTqPCR results also indicated upregulation for *Myh3* (FC=2.44, *p*=0.030), *Acta1* (FC=2.16, *p*=0.030) and *Casq2* (FC=2.32, *p*=0.035) validating the microarrays results. In our study *Myh3* was upregulated in *Mesp1*-Cre (FC=1.18, *p*=0.82, av exp=1359.67 [*Tbx22*^{null}], av exp=1152.70 [WT])

and significantly downregulated in *Wnt1*-Cre (FC=0.41 [log_2FC=-1.28], *p*=0.000066, av exp=220.13 [*Tbx22*^{null}], av exp=531.63 [WT]) with lower expression compared to CM derived cells. The same tendency was observed in *Acta1* expression, with lower expression levels: *Mesp1*-Cre (FC=1.35, *p*=0.51, av exp=120.10 [*Tbx22*^{null}], av exp=88.96 [WT]) and *Wnt1*-Cre (FC=0.55, [log_2FC=-0.85], *p*=0.097, av exp=27.09 [*Tbx22*^{null}], av exp=48.34 [WT]). Low expression was observed of *Casq2,* in *Mesp1*-Cre (FC=1.32, *p*=0.59, av exp=52.17 [*Tbx22*^{null}], av exp=39.65 [WT]) and in *Wnt1*-Cre (FC=0.49, [log_2FC=-1.04], *p*=0.035, av exp=11.99 [*Tbx22*^{null}], av exp=24.37 [WT]).

The initial process of muscle differentiation or myogenesis involves the determination of mesodermal cells to myoblasts that are embryonic progenitor cells of myocytes. Then the mononucleated myoblasts align, fuse with each other and form multinucleated myotubes or skeletal muscles. This process is largely controlled by myogenic regulatory factors *MyoD*, *Myf5*, *myogenin* and *Mrf4* (Arnold and Braun, 1996). Hoshino (2011) in her study investigated *MyoD*, *Myf5* and *myogenin* while *Mrf4* was not followed up as it was suggested not to be involved in the development of head muscles. There was a trend towards upregulation for *MyoD* (FC=1.17, *p*=0.27), *myogenin* (FC=1.09, *p*=0.70) and *Myf5* (FC=1.19, *p*=0.13) in the *Tbx22*^{null} palatal shelves. RTqPCR showed increase in statistical significance and validated the microarray result for *MyoD* (FC=1.73, *p*=0.017) and *myogenin* (FC=1.69, *p*=0.038). *P21*, the known target of MyoD, was also increased as measured by RTqPCR (FC=1.62, *p*=0.031). *Myf5* expression detected by RTqPCR was also increased on average although it was not statistically significant (FC=1.75, *p*=0.10). In our study *MyoD* was not significantly upregulated in CM (FC=1.55, *p*=0.25, av exp=237.59 [*Tbx22*^{null}], av exp=153.03 [WT]) but significantly downregulated in CNC derived cells (FC=0.56, [log_2FC=-0.83], *p*=0.028, av exp=41.33 [*Tbx22*^{null}], av exp=73.97 [WT]). There was no significance in *Myf5* expression, but the upregulation tendency was observed in CM cells (FC=1.32, *p*=0.57, av exp=68.34 [*Tbx22*^{null}], av exp=51.81 [WT]) and downregulation in CNC (FC=0.62, [log_2FC=-0.69], *p*=0.29, av exp=13.38 [*Tbx22*^{null}], av exp=20.83 [WT]). On both occasions low expression was noted. *Myogenin* and *Mrf4* did not appear on differential expression genes list in our study.

Zoupa et al. (2018), Funato et al. (2018) and Hoshino (2011) all carried out microarray analysis on whole palatal shelves. Dissection of palatal shelves provides mixed cell population and requires accurate dissection. For flow sorting palatal shelves tissue requires less accuracy in dissection, but uses a complex protocol for dissociation. Although microarrays still remain popular for transcript profiling they have a number of limitations. These include limited accuracy of quantitative expression measurements due to background hybridization, probes differ considerably in their hybridization properties, and arrays are limited to interrogating only those genes for which probes are designed (Zhao et al., 2014). RNA-Seq describes the direct sequencing of transcripts and the method has been seen as a gold standard, which is replacing microarray analysis for whole genome transcriptome profiling (Mortazavi et al., 2008). RNA-Seq allows the detection of novel transcripts, can show allele-specific expression and the effects of different splice junctions. RNA-Seq avoids the related biases introduced during hybridization of microarrays and does not depend on genome annotation for prior probe selection (Zhao et al., 2014). Whether using microarray or RNA-Seq, it is recommended to use at least biological triplicates. Microarray analysis is thought to be even more reliable at identifying true differences when analysing six replicate samples for each condition (Pan et al., 2002). Schurch et al. (2016a) claim that three biological replicates are sufficient in RNA-Seq studies, although a higher replicate number may also allow for more significant results to be achieved (Schurch et al., 2016). Another confounder may be the genetic background of the samples. For example, in the Hoshino (2011) study the comparison was done between mice (WT and mutant) who were essentially all on the same CD1 genetic background (bred from the same colony), while the current RNA-Seq study may be more heterogeneous due to the 2 stage cross, firstly to introduce fluorescent marker (R26-YFP) and secondly performing Cre recombination (*Mesp1*-Cre and *Wnt1*-Cre). All of the strains used were C57Bl/6, but each has been maintained separately, originally by different groups so some differences may exist.

Cxcl14 was the only upregulated gene identified in CNC derived palate cells. CXCL14 is expressed in skin, kidneys, skeletal muscle and other tissue, such as brain, colon, duodenum and oesophagus. It was previously shown that B-cells,

monocytes, THP-1, monocyte derived immature dendritic cells (iDC), fibroblasts, keratinocytes and endothelial cells express or release CXCL14 constitutively following inflammatory cues (Lu et al., 2016). The target cells of CXCL14-chemotactic activity are natural killer, monocytes, THP-1, neutrophils, monocyte derived iDC, endothelial cells and microbes (Lu et al., 2016). The molecular mechanisms governing expression of *CXCL14* and CXCL14-mediated functions are not yet clear. However, the work in this thesis suggests a possibility that the processes described are involved in embryonic palate development. There is already evidence that *CXCL14* is expressed in skeletal muscle in both mice and human (Sleeman et al., 2000, Cao et al., 2000). Further evidence is suggested by studies in the chick that showed that *Cxcl14* displays a complex pattern of expression in the branchial arches, trigeminal placode and ganglion, inner ear, dorsal midline of the brain, somites, trunk neural tube and limb bud (Gordon et al., 2011). At Hamburger Hamilton stage 30, *Cxcl14* continued to be expressed in limited domains of the upper and lower jaws, including the maxillary mesenchyme. Gordon et al. (2011) suggest that this expression pattern raises the possibility that CXCL14 may be involved in some of the same developmental events during which CXCL12-CXCR4 signalling is known to play a role. They go on to speculate that CXCL14 may serve to regulate tissue growth during embryonic development. In our study, *Cxcl14* was upregulated in CNC derived cells but not in CM derived cells when analysing differential expression. It remains to be determined if this gene contributes to palate development directly or to the regulation of biological processes that might lead to developmental palate pathology.

In our study *Bmpr1b* was significantly upregulated in CM derived tissue (FC=2.59, *p*=0.00025, *p*adj= 0.099, av exp=122.79 [$Tbx22^{null}$], av exp=47.41 [WT]) with no significance observed in CNC derived cells. There has previously been a *BMPR1B* mutation identified as a cause of RS (MIM: 261800) (Yang et al., 2017). RS is a congenital sequence of disorders involving micrognathia, glossoptosis and CP, therefore *Bmpr1b* upregulation here might suggest a significant involvement in Tbx22-mediated palate development.

Our RNA-Seq results showed that *Tgfbr2* was significantly upregulated in CNC derived cells (FC=1.14, *p*=0.04, av exp=851.66 [$Tbx22^{null}$], av exp=743.30 [WT]).

Mice with a conditional *Tgfbr2* deletion in the CNC were shown to exhibit complete cleft secondary palate, calvaria agenesis, and other skull defects with complete phenotype penetrance (Ito et al., 2003).

Foxp2 was significantly upregulated in CM derived cells (FC=2.85, *p*=0.00022, *p*adj=0.097, av exp=609.60 [*Tbx22*^{null}], av exp=213.27 [WT]) with not statistically significant differential expression in CNC derived tissue, although high expression overall in *Tbx22*^{null} (av exp=1329.64) as well as in WT controls (av exp=1337.77). *FOXP2* has been proposed as a NS CLP candidate in a GWAS study (Mohamad Shah et al., 2016). It is also better known for its proposed involvement in sequential learning processes and language production (Onnis et al., 2018). Interestingly a mouse knockout for the *Foxp2* gene vocalized less, produced shorter syllables and displayed an arrhythmic vocalizations' structure compared with their typical developing littermates but was not reported to have a CP (Castellucci et al., 2016).

Npnt gene (Nephronectin) was noted for its significant differential expression. In CM derived cells it was downregulated (FC=0.58, [$\log_2$FC=-0.79], *p*=0.000031, av exp=178.00 [*Tbx22*^{null}], av exp=307.96 [WT]), while in CNC derived cells it was upregulated (FC=1.80, *p*=0.000019, av exp=455.55 [*Tbx22*^{null}], av exp=252.21 [WT]). NPNT has been reported as being involved in the clinical presentation of Fraser syndrome 1 (Kiyozumi et al., 2012). NPNT is thought to be important in cell adhesion, differentiation, spreading, and survival (Ikehata et al., 2017). The NPNT protein belongs to the epidermal growth factor (EGF)-like superfamily and exhibits several common structural determinants. NPNT has been shown to be involved in kidney development, renal injury repair, atrioventricular canal differentiation, pulmonary function, and muscle cell niche maintenance (Sun et al., 2018, Soler Artigas et al., 2015). Also NPNT regulates osteoblast differentiation and mineralization, as well as osteogenic angiogenesis (Sun et al., 2018). These latter findings are interesting and corresponds to deficient osteogenesis of the secondary hard palate in *Tbx22*^{null} mice, where loss of *Tbx22* function causes reduction in ossification after condensation of the palatal mesenchyme and delay in the maturation of osteoblasts (Pauws et al., 2009a). This *Tbx22* knock out effect could be related to interaction with *Npnt* leading to *Tbx22*^{null} mice palatal phenotype. From our study results it is obvious that knocking out *Tbx22* in palate tissue affect

Npnt expression but it is not clear why it goes down in CM and up in CNC. Interestingly, knockout of *Npnt* in the mouse were largely normal although hair follicles were mildly affected (Fujiwara et al., 2011). However, no studies have reported the effect of overexpression. This may result in a TBX22-CNC-mediated, palatal tissue-specific effect resulting in isolated SMCP while constitutive miss-expression of *Npnt* might impact Fraser syndrome 1, with its greater range of clinical symptoms. It would therefore be of interest to look more closely at *Npnt* function in future studies.

None of the genes in our study reaching adjusted significance were reported previously as candidate genes in syndromic or NS CLP (Seto-Salvia and Stanier, 2014, Thieme and Ludwig, 2017). However, analysis of some of the top genes listed in the unadjusted list (Table IV. 6) are considered as cleft candidates or significantly contribute to regulation of genes directly involved in palate development, Table IV. 8.

Table IV. 8. Analysis of top genes listed in the unadjusted list.

		Evidence for a role in CLP
Matn3		*Matn3* expression is involved in the EGF pathway in *Irf6*^{null} mice salivary gland and pancreas. *IRF6* controls cell differentiation in ectodermal and craniofacial tissues by regulating expression of target genes. Haploinsufficiency of *IRF6* causes syndromic forms of CLP, VWS and popliteal pterygium syndrome (Metwalli et al., 2018).
↓↑	↑CM	
FC	73.87	
p	0.0018	
Av exp [*Tbx22*^{null}]	15.86	
Av exp [WT]	0.00	
Notch3		A heterozygous pathogenic variant in *NOTCH3* was found in a proband with consistent clinical findings of lateral meningocele syndrome (LMS). LMS is characterized by multiple lateral spinal meningoceles, distinctive facial features, joint hyperextensibility, hypotonia and skeletal, cardiac, urogenital anomalies. Additional findings of LMS include hearing loss and CP (Ejaz et al., 1993).
↓↑	↑CM	
FC	1.74	
p	0.000051	
Av exp [*Tbx22*^{null}]	556.22	
Av exp [WT]	319.74	
Sox6		Osteogenic pathway gene *Sox6* together with *Bmp3*, *Bmp5*, *Bmp7*, *Mef2c* and *Sp7* was noted to exhibit significantly increased and expanded expression in *Osr2*$^{-/-}$ embryos palatal mesenchyme (Fu et al., 2017). Previous studies showed that *Osr2* transcription factor is an intrinsic regulator of palatal shelf growth and morphogenesis (Lan et al., 2004).
↓↑	↑CM	
FC	2.30	
p	0.000092	
Av exp [*Tbx22*^{null}]	318.14	
Av exp [WT]	138.24	

Table IV. 8. (continued).

Reln		A case was described where ultrasound examination of 29 years old, primigravid woman revealed facial cleft, ambiguous external genitalia and hypogenitalism in the fetus. Amniocentesis was carried out and whole genome aCGH analysis on uncultured amniocytes detected a 13.45 Mb deletion at chromosome 7q22.1-7q31.1, or arr cgh 7q22.1q31.1 (98,423,469-111,872,943) x 1 (NCBI build 37). The deleted region encompasses 220 genes and 96 OMIM genes including *ZKSCAN5*, *ARPC1A*, *CYP3A43*, *RELN*, *LAMB1*, *IMMP2L* and *DOCK4* (Chen et al., 2013). The *RELN* gene is important for brain development and is described in neuronal migration disorders (Spalice et al., 2009).
↓↑	↑CM	
FC	2.66	
p	0.00015	
Av exp [*Tbx22*^{null}]	234.50	
Av exp [WT]	88.40	
Gjb6		RA receptor knockout studies illustrated the importance of RA signalling in palate development causing orofacial clefts and malformation of other craniofacial structures (Mark et al., 2009). When comparing cleft and non-cleft keratinocytes in culture, P63 was downregulated by RA only in cleft keratinocytes. The further analysis of P63 target genes *IRF6, CDH3, GJB6,* and *DLX5* was carried out. It showed that the expression of both *GJB6* and *DLX5* was significantly reduced by RA in cleft as well as non-cleft keratinocytes (Mammadova et al., 2014). However, in our study, the overall expression was very low and any functional interpretation should be considered with caution.
↓↑	↓CM	
FC	0.06	
p	0.018	
Av exp [*Tbx22*^{null}]	1.154	
Av exp [WT]	19.46	

Table IV. 8. (continued).

Ahr		
↓↑	↓CM	Copy number changes of potential significance corresponding to the genes *AHR* as well as *ADH7* (formerly referred to as *ADH3*) and *CRYZ* were identified for NS CLP using WES technology. *ADH7* and *AHR*, share involvement in biological pathways linked to environmental factors known to influence NS CLP (Cai et al., 2017).
FC	0.61	
p	0.000038	
Av exp [*Tbx22*^{null}]	338.91	
Av exp [WT]	554.52	
Six6		
↓↑	↑CNC	There are reported cases when haploinsufficiency of *BMP4*, *OTX2* and possibly *SIX6* are thought to contribute to the malformations of the eye, limbs, CP, brain with developmental and growth delay associated with deletions in chromosome 14q22-23 (Lumaka et al., 2012, Thienpont et al., 2007).
FC	297.77	
p	0.0042	
Av exp [*Tbx22*^{null}]	66.05	
Av exp [WT]	0	
Six3		
↓↑	↑CNC	There were 8 genes identified *Chrng*, *Foxc2*, *H19*, *Kcnj13*, *Lhx8*, *Meox2*, *Shh* and *Six3* within *TGFβ*$^{-/-}$ mice, which may function as the primary contributors to the development of CP (Ozturk et al., 2013).
FC	17.66	
p	0.0084	
Av exp [*Tbx22*^{null}]	29.79	
Av exp [WT]	1.55	

Table IV. 8. (continued).

Myh3		
↓↑	↓CNC	*Myh3* is a gene associated with human CP and has been shown to be downregulated in *Tbx1*$^{-/-}$ palatal shelves (Funato and Yanagisawa, 2018, Grefte et al., 2012).
FC	0.41	
p	0.000066	
Av exp [*Tbx22*^{null}]	220.13	
Av exp [WT]	531.63	
Foxl1		*Foxl1* is the direct transcriptional target one of several Fox transcription factors which are upregulated by Hh-Smo signalling. There was shown that ectopic Hh-Smo signalling results in fully penetrant CP and defective palatine bone formation using a gain-of-function mouse model to activate Smoothened (*Smo*) signalling in the palatal mesenchyme (*Osr2-IresCre; Smo*$^{+/M2}$) (Hammond et al., 2018).
↓↑	↑CM	
FC	4.98	
p	0.023	
Av exp [*Tbx22*^{null}]	22.08	
Av exp [WT]	4.35	
Ptprd		*PTPRD* is one of the three members (PTPRF, PTPRD and PTPRS) of leukocyte antigen related (LAR) family of receptor-like protein tyrosine phosphatases in humans. They are known for implication of diverse processes of inhibition of cell growth, embryonic development and axonal guidance. Mutations in the LAR family are associated with developmental defects such as CP as well as various cancers including breast, neck, lung, colon and brain (Mitchell et al., 2016).
↓↑	↑CM	
FC	1.51	
p	0.0033	
Av exp [*Tbx22*^{null}]	1479.90	
Av exp [WT]	981.90	

Table IV. 8. (continued).

Sim2		*Sim2* is a basic bHLH PAS transcription factor and is evolutionarily related to the *Drosophila single-minded* gene, a key regulator of central nervous system midline development. *Sim2*$^{-/-}$ homozygous mice exhibit a cleft of the secondary palate and malformations of the tongue and pterygoid processes of the sphenoid bone (Shamblott et al., 2002).
↓↑	↑CM	
FC	2.43	
p	0.0032	
Av exp [*Tbx22*^{null}]	344.65	
Av exp [WT]	142.10	
Barx1		*Barx1* mesenchymal expression in the posterior region of palate control posterior mesenchymal cell proliferation. *Barx1* expression shifts anteriorly in *Pax9* mutant palatal shelves at E13.5, possibly PAX9 modulating *Barx1* expression during posterior mesenchymal proliferation (Li et al., 2019b).
↓↑	↑CM	
FC	1.76	
p	0.0019	
Av exp [*Tbx22*^{null}]	277.46	
Av exp [WT]	157.35	
Prickle1		*Prickle1* is a core component of the Wnt/PCP pathway in skull bone formation. The *Prickle1*$^{-/-}$ mutants are microcephalic and develop enlarged fontanelles between insufficient frontal bones, also develop a midline CL, incompletely penetrant CP, and decreased proximal-distal growth of the head (Wan et al., 2018). It is also known that PRICKLE1 directs palate morphogenesis in mice and humans (Yang et al., 2014).
↓↑	↑CM	
FC	1.57	
p	0.0017	
Av exp [*Tbx22*^{null}]	356.08	
Av exp [WT]	227.10	

Table IV. 8. (continued).

Lgr5		*LGR5* gene can cause ankyloglossia (OMIM 106280) associated with tooth number anomalies. *Lgr5* knockout mice with ankyloglossia died within 24 hours due to suckling defects. Histological analyses revealed fusion of the tongue to the floor of the oral cavity. Immunostaining of *Lgr5* expression in the epithelium of the tongue and in the mandible of the WT embryos, suggested a role of the Lgr5 signalling pathway in tongue development (Acevedo et al., 2010).
↓↑	↑CM	
FC	2.32	
p	0.0014	
Av exp [*Tbx22*^{null}]	164.20	
Av exp [WT]	70.81	
Thbs1		*THBS1* is reported to be associated with orofacial clefts or orofacial development together with *DGCR6, FGF2, FRZB, LETM1*, *MAPK3*, *SPRY1, TSHZ1, TTC28, TULP4, WHSC1, WHSC2* as well as *SATB2* and *MEIS2* are described as causative. The study analysed 249 genomic deletions and 226 duplications from a cohort of 312 orofacial cleft in Decipher and ECARUCA. Genomic regions deleted or duplicated in multiple patients were identified, and genes in these overlapping CNVs were prioritized based on the number of genes encompassed by the region and gene expression in embryonic mouse palate (Conte et al., 2016).
↓↑	↑CM	
FC	1.92	
p	0.0011	
Av exp [*Tbx22*^{null}]	701.64	
Av exp [WT]	365.01	

Table IV. 8. (continued).

Igf1r		A frameshift mutation in *IGF2* was identified in a single child with Silver-Russell syndrome-like phenotype. The child had also CP. Functional analyses showed that the IGF2 variant lost its ability to interact with the IGF1R due to changes in protein structure. This change led to only marginal activation of IGF1R. 3D protein structure prediction and overexpression studies demonstrated that the *IGF2* gene variation resulted in impaired ligand/receptor binding and thus prevented *IGF1R* activation (Rockstroh et al., 2019).
↓↑	↑CM	
FC	1.31	
p	0.00068	
Av exp [*Tbx22*^{null}]	1876.49	
Av exp [WT]	1437.99	
Meox2		To examine association of *MEOX2* polymorphism with NS CP in a Vietnamese population a total of 570 DNA samples, including 277 cases and 293 controls were analysed. The study findings suggest that NS CP might be influenced by variation of *MEOX2*, especially SNP rs2237493 in Vietnamese females.
↓↑	↑CM	
FC	1.68	
p	0.00065	
Av exp [*Tbx22*^{null}]	272.93	
Av exp [WT]	161.92	
Rspo2		*Rspo2* is a mesenchyme-derived factor which plays a critical role in regulating the first branchial arch patterning and morphogenesis. It affects ectodermal-mesenchymal interaction and is a novel genetic factor for CP. CP in *Rspo2*$^{-/-}$ mice is not associated with defects intrinsic to the palatal shelves but possibly caused by delayed palatal shelf elevation, small mandible and failure of lowering the tongue (Jin et al., 2011).
↓↑	↑CM	
FC	3.63	
p	0.0071	
Av exp [*Tbx22*^{null}]	46.18	
Av exp [WT]	12.55	

Table IV. 8. (continued).

Col11a1		
↓↑	↑CM	Microarray hybridization analysis was performed in 15 individuals with NS CLP. Eleven exonic CNVs affecting at least one exon of 13 selected candidate genes were identified. One of these was a CNV overlapping *COL11A1* (Jin et al., 2011).
FC	4.08	
p	0.049	
Av exp [*Tbx22*^{null}]	1391.76	
Av exp [WT]	340.73	
Scarna17		
↓↑	↓CM	*SCARNA17* SNPs rs8097060 and rs17713847 were found significantly associated with NS CLP risk together with other genes such as *LOXHD1* (rs1450425), *SKA1* (rs6507992), *SMAD7* (rs78950893), *CTIF* (rs6507872), *CTIF* (rs8091995) and *MYO5B* (rs17715416) (Mitra et al., 2016).
FC	0.30	
p	0.046	
Av exp [*Tbx22*^{null}]	5.13	
Av exp [WT]	17.30	
Pitx2		
↓↑	↑ CNC	Evidence suggests that a TGFβ-FGF9-PITX2 signalling cascade regulates CNC cell proliferation during palate formation *Fgf9* and *Pitx2* expression was significantly downregulated in the palate of *Tgfbr2*$^{fl/fl}$ *Wnt1*-Cre mice while *Fgf9* and *Pitx2* loss of function mutations resulted in CP (Iwata et al., 2012).
FC	3.76	
p	0.0067	
Av exp [*Tbx22*^{null}]	151.86	
Av exp [WT]	40.03	

Table IV. 8. (continued).

Esrp1		
↓↑	↑ CNC	Mice with ablation of *Esrp1* developed CLP. Loss of both *Esrp1* and its paralog *Esrp2* results in widespread developmental defects with broad implications to human disease (Bebee et al., 2015).
FC	3.04	
p	0.0072	
Av exp [*Tbx22*^{null}]	101.56	
Av exp [WT]	33.057	
Mlph		A study of 64 candidate genes genotyped with an average of 4.3 SNPs per gene on a sample of 58 case-parent non-syndromic oral clefts trios identified SNPs around *MLPH* gene in linkage disequilibrium. The gene was expressed in relevant embryonic tissues according to the Craniofacial and Oral Gene Expression Network (COGENE) consortium (Park et al., 2006).
↓↑	↓ CNC	
FC	0.41	
p	0.046	
Av exp [*Tbx22*^{null}]	6.44	
Av exp [WT]	15.46	

There were also certain pathways identified in our study which are thought to play important roles in palate development:

Focal adhesion pathway is important in many biological processes including cell motility, cell proliferation, cell differentiation, regulation of gene expression and cell survival (Burridge, 2017). At cell-ECM contact points, specialized structures are formed and termed focal adhesions. These consist of bundles of actin filaments which are anchored to transmembrane receptors of the integrin family through a multi-molecular complex of junctional plaque proteins. These biological processes are likely to play important roles in early palatal shelf development, including subsequent elevation and fusion.

ECM-receptor interaction pathway. The ECM consists of a complex mixture of structural and functional macromolecules and is important in tissue and organ

morphogenesis as well as in the maintenance of cell and tissue structure and function (Kerrisk et al., 2014). Specific interactions between cells and the ECM are mediated by transmembrane molecules, mainly integrins and proteoglycans. These interactions lead to the control of cellular activities such as adhesion, migration, differentiation, proliferation, and apoptosis. In addition, integrins function as mechanoreceptors and provide a force-transmitting physical link between the ECM and the cytoskeleton. The ECM-receptor interaction pathway was the only pathway significant in our analysis when comparing *Tbx22*^{null} to WT in CNC derived cells and is significant in palate development.

Osteoclast differentiation pathway. Osteoclasts are multinucleated cells from the hematopoietic monocyte-macrophage lineage and are responsible for bone resorption. Osteoclastogenesis is mainly regulated by signalling pathways activated by RANK and immune receptors, whose ligands are expressed on the surface of osteoblasts. Signalling from RANK changes gene the expression pattern through transcription factors such as NFATc1, which characterizes the active osteoclast (Chen et al., 2018). Osteogenesis is particularly important in the development of the hard palate. The osteoclast differentiation pathway was enriched in both comparisons between CM and CNC derived tissue, in *Tbx22*^{null} and WT. This indicates an importance for bone remodelling during development and possibly with a significant role even at an early stage at E13.5 just before bilateral palatal shelves fusion.

Cell adhesion molecules (CAMs) are glycoproteins expressed on the cell surface and play a critical role in a wide array of biologic processes that include haemostasis, the immune response, inflammation, embryogenesis, and development of neuronal tissue. There are four main groups: the integrin family, the immunoglobulin superfamily, selectins, and cadherins (McKeown et al., 2013). The CAMs pathway enrichment was noted in both comparisons, similar to the osteoclast differentiation pathway. It is interesting that CAMs' role in immune system and inflammation processes overlap with known *Cxcl14* gene function, which was significantly upregulated in CNC derived cells. Our data suggests that biological processes in which CAMs and *Cxcl14* are involved, most likely play a

more significant role in palate development than is currently known. This requires further investigation.

Calcium signalling pathway is important for Ca^{2+} entering the cell from the outside and being a principal source of Ca^{2+} signal. Ca^{2+} enters the cell as a result of a large electrochemical gradient across the plasma membrane. Ca^{2+} signal is essential for cell viability and although it is difficult to visualize a direct link with congenital palate abnormalities, interruption in cells homeostasis may have a distant or partial role in craniofacial developmental disorders.

Wnt signalling pathway. Wnt proteins are secreted morphogens that are required for many basic developmental processes including cell-fate specification, progenitor-cell proliferation and the control of asymmetric cell division. The main Wnt-signalling pathways include the canonical, the PCP and the Wnt/Ca^{2+} pathways (Tran and Zheng, 2017). The Wnt signalling pathway is known to play significant role in craniofacial development (Shimomura et al., 2019, Yuan et al., 2017) and was again supported in our study.

IV. 5. Conclusion

In this Chapter IV, a conditional mouse line was used to generate a palatal shelf cell-type specific phenotype to investigate transcriptional changes downstream of TBX22.

Previous reported studies investigating *Tbx22,* exclusively used constitutively *Tbx22*^{null} mice that were generated by crossing floxed mice with mice carrying *βactin*-Cre (Pauws et al., 2009a). Therefore the floxed allele had not been investigated for phenotypic consequences. While carrying out this study that was designed to investigate transcriptional changes downstream of TBX22, a palate phenotype in the floxed animals was noticed (SMCP in *Tbx22*$^{flox/Y}$ and diminished palatal shelf margins in *Tbx22*$^{flox/+}$). This raised the possibility that the floxed allele may be a hypomorph. This was investigated using a TaqMan® gene expression assay, which showed that the *Tbx22* expression level was very similar between *Tbx22*$^{flox/Y}$ and *Tbx22*$^{-/Y}$ but significantly lower when compared to WT. At this stage, the floxed allele is more akin to a null allele. However, it might be necessary to perform further investigations at earlier developmental stages or potentially by dissecting different tissues or cell types to more accurately differentiate the two alleles.

RNA sequencing was carried out on flow sorted YFP+ CM and CNC derived palatal cells at stage E13.5. Flow sorting allowed assessment of the relative cell counts for each cell type in both WT and null animals. We found that the dissected E13.5 palatal shelves consist of nearly 5x more CNC derived cells compared to CM cells. The ratio of YFP+ cells in CM and CNC was 1:3.8 in WT and 1:5.6 in null male embryos. Whilst the total number of cells was reduced in null palates, the alteration in the ratio between these important cell types may suggest a possible role for *Tbx22* that affects cell type-specific proliferation. Also it is interesting to note that the overall number of cells recovered were lower in the *Mesp1*-Cre cross compared to *Wnt1*-Cre. It may be related to improved skill acquisition, laboratory-based variables, an effect based on the relative size of the resulting embryos or even that there are Tbx22-distinct proliferative effects on CM and CNC derived tissues.

Eleven up regulated genes reached statistical significance after multiple testing correction in CM derived cells when comparing *Tbx22*$^{-/Y}$ and WT samples (*Cspg4, Foxp2, Reln, Bmpr1b, Adgrb3, Sox6, Zim1, Scarna13, Fat1, Notch3, Peg3*) and 11 genes were down regulated in the same group (*Nr2f2, Lars2, Ahr, Aplnr, Emcn, Npnt, Apln, Ccr2, Tll1, Snord34, Snord99*). Comparing *Tbx22*$^{-/Y}$ and WT in CNC derived cells, *Cxcl14* was up and *Tbx22* was down regulated. This result was surprising since *Tbx22* appeared to be more highly expressed in CNC, therefore it might have been expected that this was where more significant expression changes would have been found. However, it is important to note that the functional significance of all of the differentially expressed genes needs to be further investigated to determine if they are biologically relevant effects.

This study did not show any statistically significant changes in key bone or muscle markers with the exception of *Npnt*. Genes encoding muscle proteins and muscle transcriptional regulators such as *Myod* were most affected in the Hoshino (2011) study. This was particularly striking since poor development of intramembranous bones of the palate is the most obvious anatomical consequence of loss of TBX22 function (Pauws et al., 2009a). This may suggest that, at least at the stage E13.5, bone and/or muscle development are not the primary cause of the SMCP phenotype.

The study identified upregulation of the *Npnt* gene in CNC and downregulation in CM cells in *Tbx22*^{null} compared to WT mice. NPNT is involved in the clinical presentation of Fraser syndrome 1 as well as being described as a regulator of osteoblast differentiation/mineralization and osteogenic angiogenesis (Saleem and Siddiqui, 2015). This may correspond to deficient osteogenesis of the secondary hard palate in *Tbx22*^{null} mice, where loss of *Tbx22* function causes reduction in ossification after condensation of the palatal mesenchyme and delay in the maturation of osteoblasts (Pauws et al., 2009a). This could therefore correspond to the *Tbx22*^{null} palatal phenotype, but further work would be required to understand the cell type specific relevance of the opposite effects on differential expression.

None of the genes that reached the adjusted significance threshold were reported previously as candidate genes in syndromic and NS CLP, although several could

now be investigated further to confirm their significance. At the unadjusted significance level, a number of genes associated with clefting that were upregulated in CM were *Notch3, Sox6, Reln, Ptprd, Sim2, Barx1, Prickle1, Thbs1, Igf1R, Col11A1,* and downregulated in CM was *Ahr* and in CNC was *Myh3*. These genes (and others) might have reached a more statistically significant level if the experimental design had included an increased number of replicates. In the longer term, it may well be beneficial to introduce a second round of validation using additional animals and/or a different method of measuring RNA levels such as RTqPCR.

In terms of pathway analysis, osteoclast differentiation, calcium signalling, focal adhesion, Wnt signalling and CAMs pathways were the most enriched in the functional annotation of significantly differentially expressed genes. Each of these has potential relevance to palate development and as such these individual pathways could benefit from further study. This might take the form of interrogating individual components in more detail.

In conclusion, *Tbx22* as transcriptional factor has a significant and complex effect in palate development at E13.5. The studies presented here add to the current knowledge of the role of TBX22 in palate development, particularly at the transcriptional level. This provides an important background to better understand the development of SMCP, with a view to the future prospect of translating research outcomes into clinical practice.

IV. 6. Future work

In this study, mouse palatal shelves were dissected at E13.5. This developmental time point was largely based on previous data, which demonstrated that *Tbx22* is maximally expressed at E13.5 (Hoshino, 2011). This is also a good time to look at the developing palate since changes are very dynamic around the time of shelf elevation, immediately prior to fusion. Moreover, this time point has also been widely used in other studies, so provides the clearest opportunity for comparison. However, analysing the RNA-Seq data, it became obvious, that data from only one developmental stage is also limiting. Previous studies (Bush et al., 2002, Braybrook et al., 2002, Hoshino, 2011), have shown that *Tbx22* expression is transient in the palate, starting from around E9.5 through to E14.5, at which point it shuts down. It is therefore likely that a more complete understanding of downstream transcriptional affects could be made by studying a similar range. RNA-Seq experiments are not cheap and it can also be challenging to collect sufficient animal tissues of appropriate genotypes. Nevertheless, when planning future work, it would certainly be of interest to carry out a similar experiment but at stages E12.5 and E14.5. Earlier stages would be harder to do in the same way since the palate shelves are only just starting to emerge and accurate dissection is not feasible. This might be circumvented by disaggregating whole embryos and sorting labelled 'palatal' progenitor cells. For later stages post E14.5, the palatal shelves will be fused together and no longer show significant *Tbx22* expression, although the legacy of persistent TBX22 protein might still be obvious (Bush et al., 2002, Braybrook et al., 2002, Hoshino, 2011).

In our study we collected flow sorted, YFP+ cells with which to perform RNA-Seq analysis, whilst the remainder cells were collected into a separate fraction. It would be interesting to also carry out RNA-Seq on the YFP- cell fraction, to look at their gene expression patterns. In our study CM and CNC derived cells were a little less than 50% of the palatal shelf total cell content E13.5. These were chosen for their known biological relevance for palate development, yet it is possible that differential gene expression analysis and comparison between other YFP+ and YFP- contributing cells could give further answers in understanding the intricacies of palate development.

The study was carried out collecting and comparing different genotypes using 3 biological replicate samples in each group. There is no doubt that a larger number of samples would give more robust data, enhancing conclusions and planning further analysis. Although samples collection was time demanding and technique sensitive, I would consider at least 6 samples for further studies.

The *Cxcl14* gene was found to be significantly upregulated in CNC derived cells. Although this gene is not known as cleft gene, its potential importance must be recognised. Although there is already a knockout model (Meuter et al., 2007), in this case it would be necessary to produce an overexpression model in order to investigate a possible effect on palate development and phenotype.

Putative TBX22 binding sites were identified by a simple word search, notably in *Cxcl14, Fosl2, Myh3, Shisa3, Krt5*, *Tll1*, *Lars2* and *Scarna13*. To test their validity, it would be necessary to carry out a functional binding-site assessment, potentially using an EMSA (Tada and Smith, 2001) or a ChiP experiment as was performed for *MyoD* (Kantaputra et al., 2011). Indirect targets are less easily confirmed but could be independently verified by replication in further mouse studies or alternatively by knocking down *Tbx22* in suitable cell lines and using RTqPCR.

Earlier studies used constitutive $Tbx22^{null}$ mice and as such, the floxed allele had not been investigated for any phenotype. In this study, we have now recognized the SMCP phenotype in floxed animals and even a mild phenotype in heterozygous floxed female mice. Because it is an X-linked condition, and based on previous studies (Andreou et al., 2007), the *Tbx22* knockout is likely to result a complete loss of function in affected males. We therefore looked at *Tbx22* gene expression analysis in male mice to confirm our findings. Whilst it was possible to make inferences about transcriptional changes downstream of *Tbx22*, it might have been better to first generate a floxed line that did not affect *Tbx22* expression. This might be achievable by removing the NEO^{R} cassette from the intronic location between exon 2 and 3 by crossing with an FRT mouse. Although, this experiment was performed early on (prior to this thesis), the lack of an obvious phenotype resulted in only a superficial investigation before the line was discarded. This experiment would likely produce a useful model, contributing towards an allelic series that delivers different levels of *Tbx22* expression. This would allow greater fine tuning to study of the effect of reduced TBX22 on palate development.

Chapter V: Disruption of *FOXF2* as a likely cause of absent uvula and hypernasality in an Egyptian family

V. 1. Introduction

CL/P is a spectrum of aetiologically distinct defects which include complete or incomplete bilateral or unilateral CL, with or without CP, as well as isolated cleft of the secondary palate. This is due to different tissue lineages contribution and distinct timing of various fusion events during development (Harville et al., 2005, Stanier and Moore, 2004).

Defects of the secondary palate range from complete overt cleft of the hard and soft palate, to cleft of the soft palate only. They also include SMCP, where the palatal shelves have fused and the oral mucosa is intact (Calnan, 1954). There are also other phenotypes of the palate described such as high arch or absent uvula, but they may be part of syndrome and not necessarily the cause of palate dysfunction (Chipeta et al., 2009). However, a high arched palate for example, may cause secondary dental anomalies and can complicate intubation. The latter being a major problem for craniofacial patients who frequently require multiple surgeries during childhood (Tabler et al., 2013).

Palate appearance alone does not determine palate function. It is known, that up to 20% people with SMCP triad do not develop VPI (Boyce et al., 2018). Functional insufficiency can result in feeding difficulties, hearing loss due to otitis media and unintelligible speech characterized by hypernasality, audible nasal emission and passive and non oral articulation errors (de Blacam et al., 2018, Sell et al., 1999).

In the literature the term ‘absent uvula’ is mentioned relatively few times meaning different conditions (Chipeta et al., 2009, Chilkoti et al., 2017). The causes of absent uvula can be generally classified into congenital and acquired. Acquired causes may be secondary to surgery such as uvulopalatopharyngoplasty for obstructive sleep apnoea (Madani, 2007) or the cultural practice of removing the uvula for chronic cough in Sub-Saharan Africa (Adoga and Nimkur, 2011). The congenital absence of the uvula is very rare in the general population. On oral examination there was one case reported in a study of 2258 neonates (Jorgenson et al., 1982), although it is not clear if this finding was confirmed by follow up examination.

In this study we have investigated what we believe to be a previously undescribed palate defect, which is also associated with the clinical presentation of VPI. Affected individuals in an autosomal dominant family presented with no uvula, a short posterior border of the soft palate and an apparent absence of the anterior tonsillar pillars with rudimentary posterior pillars (Figure V. 1). Whilst there are rare descriptions of absent uvula in the literature, there are no descriptions of familial absent uvula and hypernasality or the anatomical features of the individuals in this report. To investigate the genetic basis of this condition, we report here genetic studies which identify a missense variant in *FOXF2* as the likely cause of this condition.

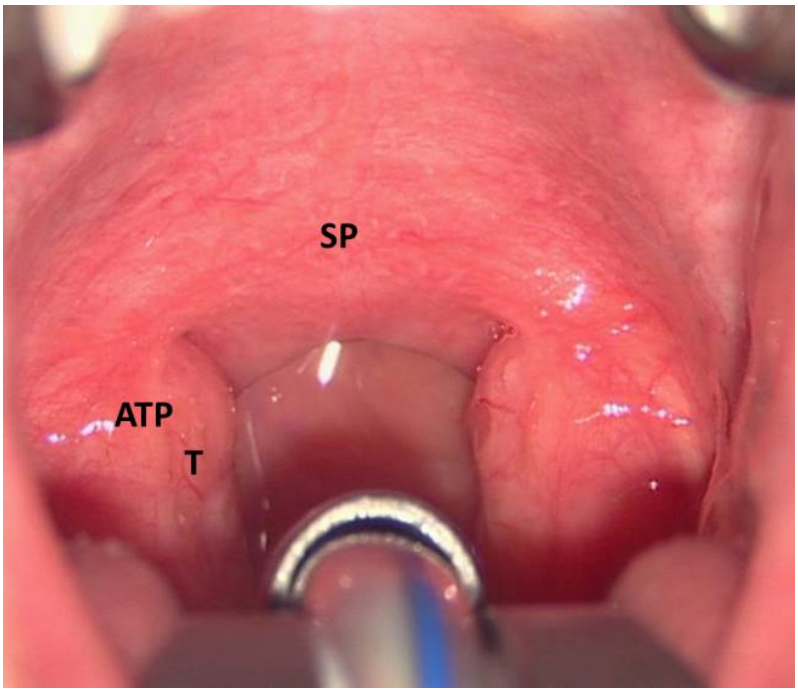

Figure V. 1. Absent uvula, a tight posterior border of the velum, no anterior pillar and rudimentary posterior pillar of the fauces.

Note the short posterior border of the soft palate where the uvula should be and the unusual structure of the pillar of fauces. **ATP** - anterior tonsillar pillar; **SP** - soft palate; **T** - tonsil.

V. 2. Gene identification strategies

The identification of genes responsible for familial diseases brings a number of important benefits for patients and their families, clinicians and researchers. A molecular diagnosis can give valuable information regarding the clinical presentation and progression as well as allowing genetic counselling for future risk and prenatal testing (Gilissen et al., 2012). For novel genes, it will often allow a better understanding of the disease pathway involved along with the biochemistry of the underlying protein, which may ultimately lead to the development of therapeutic interventions.

Since the mid-1980s, when a structured approach to disease gene identification first started, there has been many leaps in technological innovation that have streamlined the process, not least of which was publication of the human genome sequence (Leung, 2004). Prior to this point, there was only a rudimentary understanding of the position and order of genes in the genome. One early example was the identification of the gene mutated in CPX. In the 1950's and 60's, family data was starting to be assembled for a large Icelandic pedigree where male patients had CP, usually accompanied by ankyloglossia (Bjornsson et al., 1989). DNA samples were collected and with the advent of the then new linkage or positional cloning technology (Botstein et al., 1980), work eventually commenced around 1985 towards mapping the causal locus on the ChrX. This resulted in a statistically significant linkage, mapping the gene to Xq21.3 (Moore et al., 1987), which represented one of only a small handful of successfully linked disease genes at that time (along with chronic granulomatous disease, cystic fibrosis, Duchenne muscular dystrophy, and retinoblastoma). However, neither the sequence nor the gene content of that interval was known at that time and it took many years to fine map and eventually determine the causal gene. This eventually came about as a consequence of the high resolution genetic map produced from incremental studies with the Icelandic family along with several more recently acquired Brazilian and North American families, coupled to the early draft of the human genomic sequence. Together, these efforts revealed several candidate genes in the interval, all of which were sequenced using Sanger sequencing technology (Sanger, 1988). Only one gene, *TBX22* had a plausible mutation in the Icelandic

family, and importantly, further mutations were identified in each of the other putative CPX families screened, confirming it as the causal gene (Braybrook et al., 2001). Thus, a combination of technologies that were implemented over a period spanning several decades eventually contributed to the identification of *TBX22* as the gene mutated in CPX.

Sequencing technologies have since continued to advance and the process of disease gene identification has also evolved to keep pace. Next generation sequencing allows millions of genomic variants to be identified simultaneously for each individual. This is extremely efficient and cost effective, particularly as the time taken to generate this data also improved, allowing a complete set of variants to be generated in as short as 24-48 hours. A choice of technology exists regarding what fraction of the genome is to be investigated. This includes WES that selectively sequences a chosen fraction of the genome, normally all of the known exons in order to capture information of the coding fraction of the genome (Majewski et al., 2011). The current method of choice now is more often sequencing the entire genome, which is referred to as whole genome sequencing (WGS). This has the benefit of choosing to look specifically at the exome fraction (where most easily recognizable mutations are found) but also the rest of the genome where deep intronic or intragenic variants might reveal mutations in non-coding, regulatory or splicing regions (Gilissen et al., 2014). On the downside, the size and complexity of the data sets generated creates a number of challenges and it can be extremely difficult to recognize a causal variant from the vast numbers of benign variants (Holzinger et al., 2017). As a consequence, it has become necessary to carefully design an appropriate strategy and couple this to specialist bioinformatics tools to assist in the prioritization of potentially pathogenic variants. Alongside this, there is still an important role for the inclusion of traditional disease gene identification approaches, often starting with karyotyping and including linkage analysis, homozygosity mapping, copy number variation analysis, and SNP-based association analysis (Kurotaki et al., 2002, Kerem et al., 1989, Lander and Botstein, 1987, Vissers et al., 2005, Duerr et al., 2006).

Linkage studies rely on the use of large, phenotypically well-characterized families (Dixon, 2010). Ideally, 10 or more informative meiosis (i.e. transmission of an allele

from a heterozygous parent through which the disease passes) are required to trace the genomic location of an autosomal dominant disease, but far smaller families, with as few as three affected individuals can be used for recessive diseases. Family members are typed for polymorphic markers throughout the genome in order to detect which regions the affected individuals share, and are therefore most likely to contain the disease gene. Although there have been different iterations of this process, the method of choice currently is to genotype all available family members using a SNP array, containing 100's of thousands of common SNPs distributed evenly across the genome. These variants can be tracked for co-inheritance with the disease trait throughout the family pedigree using specially designed programmes such as MERLIN (Dudbridge, 2003). If a disease gene is close to a particular SNP, i.e. linked, it will almost always be inherited with it. If affected individuals all show the same genotype at a particular SNP, the disease gene may be close by. Statistical analysis is used to formalize the results and give likelihood ratios, the logarithm of the odds (LOD) score, or the location of a disease locus (Rice et al., 2001).

In our study we first used cytogenetic analysis which implicated a possible CNV. However, the associated pathology, which included a well reported duplication of the *FOXC1* gene, did not fit with this family. Then further investigations were performed starting with linkage analysis using the extended family pedigree. This identified a number of possible genomic loci where the disease gene could be located. We then chose to use the unbiased screening strategy of WES rather than looking for possible candidate genes. WES analysis results were overlaid with the linkage analysis results to generate a list of the candidate variants. To confirm their sequence validity, they were subject to Sanger sequencing. Bioinformatics screening was then used to assess the potential effects of the sequence change on protein function, although variability between programmes did not ultimately add a great deal of support for one candidate versus another. Obtaining further samples from the family provided additional segregation analysis, which was highly informative and helped to identify a single, potentially phenotype-causing gene variant. Interestingly, this was in the same vicinity as the original CNV. Therefore, in this work, a combination of disease-causing identification strategies proved to be

successful, allowing the identification of a plausible missense variant, but also in the genetic landscape of a nearby CNV as the likely cause of this rare autosomal dominant palate and velopharynx phenotype.

V. 3. Aims

- To describe the clinical representation, surgical management and outcome in a patient presenting with a rare palate phenotype causing VPD.
- Pursue gene discovery in a large multiplex family with an unusual autosomal dominant hypernasality and absent uvula palate phenotype.
    - To perform cytogenetic analysis, SNP genotyping, linkage analysis and WES to identify the likely candidate gene and causal variant.
    - Screen a cohort of patients with palate defects (NS CP and SMCP) to determine the frequency of mutations in the best candidate gene and to review the phenotypic spectrum involved.
    - Perform functional analysis of the likely causal variants.
    - Confirm appropriate developmental expression analysis of the likely causal gene.

V. 4. Results

V. 4. 1. Clinical representation

An Egyptian boy (IV.5) presented with a clinical history of occasional nasal regurgitation while breastfeeding in infancy (Figure II. 12). This was followed by speech and language delay and hypernasality. On examination at 3 years, the patient's uvula was noted as absent, and the posterior border of the soft palate appeared short. The anterior tonsillar pillars were also absent, while the posterior pillars were described as rudimentary (Figure V. 1). There was poor velar movement. There were no obvious syndromic features. The family history revealed 7 other individuals with no uvula and a tight posterior border of the velum and pillar structure (Figure II. 12). All affected family members had mild hypernasal speech.

The proband (IV.5) was first seen at the age 3 years by the speech and language therapist at GOSH. His attention and listening skills were noted to be immature. He was using single words, with some two and occasional three word utterances and used other nonverbal means to communicate including pointing, taking the adult to what he wanted and gestures. In summary, he had receptive and expressive language delay with a greater deficit in his expressive language.

Overall he was assessed as mildly hypernasal. His sound system, however, was characterized by numerous cleft speech characteristics, including backing to velar for plosives and fricatives, and glottal stops. Glottal reinforcement was also noted. There was a weakness of pressure, leading to a weak nasalized plosive for /b/, but at times, he had no oral pressure which resulted in the nasal replacements of voiced plosives e.g. /b>m/, /d>ng/. Nasal turbulence was detected as an active part of his nasal fricatives. There was also some accompany nasal emission on his correct consonants e.g. targets /p/, /b/. He also had some unusual realisations, for example velar nasals for oral plosives, and syllabic nasals, where the vowel in the syllable with a nasal was omitted. There were also some developmental immaturities including syllable elision, consonant harmony, and stopping e.g. target /f/ in word initial position. There was some variability in his productions. On a task of sound stimulability, it was possible to elicit /p/, /b/, /f/ with help /d/, /k/, /g/

suggesting potential for change with therapy even with the current structure. Another noticeable aspect of his speech was the weak and breathy quality.

On clinical examination the palate was thin and short with only small adenoids above and at the plane of attempted closure. There was some slight movement of the posterior pharyngeal wall. On lateral X-ray video, the velum appeared thin and lift was poor (better with /a/ than with /i/) (Figure V. 2). With many sounds, movement was actually produced by the tongue but there was some active velar movement when the levator knee appeared to be somewhat anterior, notably on repetition of /ba/. The palate never lifted to the plane of the hard palate and there was a consistent velopharyngeal gap with active movement.

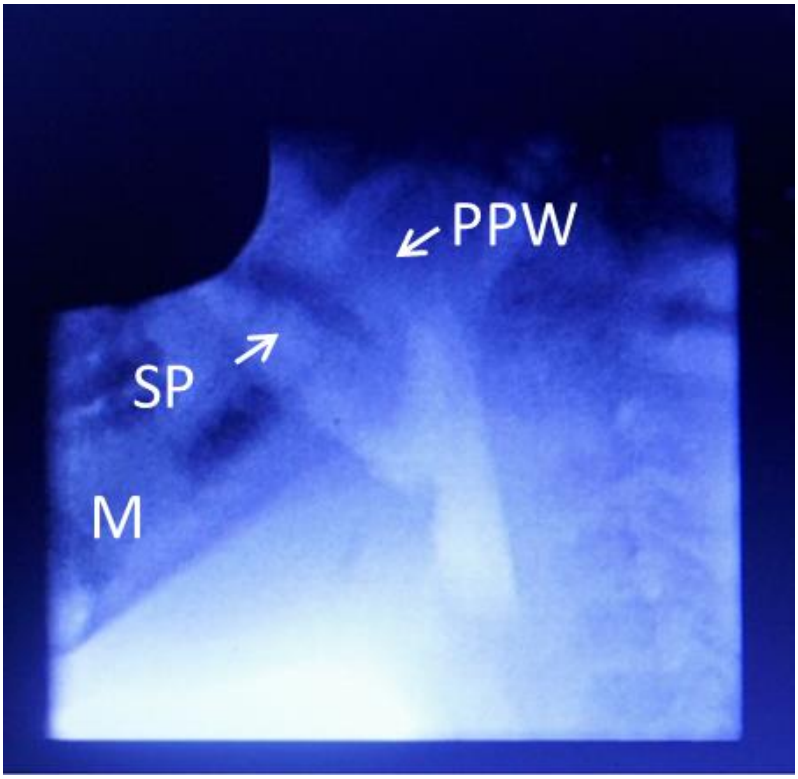

Figure V. 2. Still image from lateral X-ray video saying /i/. Preoperative view.
SP - soft palate; **PPW** - posterior pharyngeal wall; **M** - mandible.

V. 4. 2. Genetic investigations

It was first decided to investigate the proband (IV.5) for a cytogenetic abnormality. This would include examination of the 22q11.2 locus, of which, CNVs are often associated with abnormalities of the palate. Genome wide cytogenomic microarray was therefore performed on DNA from the proband. This excluded a deletion at 22q11.2 but instead highlighted the likely presence of two close together duplications on 6p25.3 (Figure V. 3). These consisted of a small gain of 227,481 bp, not interfering with any known coding gene and a nearby gain of approximately 480,000 bp, encompassing the whole of *FOXC1* and the 5' exons of *GMDS*. To validate this finding, a qPCR assay for *FOXC1* (Figure V. 4) confirmed the presence of the CNV and demonstrated inheritance from the father (III.3) and his paternal grandmother (II.2), who both had palates of similar appearance to the proband and each had mild hypernasality. The variant was not present in the proband's mother (III.4). Looking at these specific regions in the Decipher database (https://decipher.sanger.ac.uk/) revealed many (>60) individuals with either loss or gain of genetic material from this interval (Figure V. 5). These individuals suffered from a variety of clinical symptoms although disruption of *FOXC1* most frequently was associated with defects of the eye including aniridia, Rieger anomaly, glaucoma, and Peter anomaly (Ittner et al., 2005). Mainly caused by deletion but also in some cases duplication of *FOXC1*, as well as point mutations in this gene can result in a well characterized syndrome called Axenfeld-Rieger syndrome. This is primarily a defect involving the anterior segment of the eye, often causes glaucoma resulting in vision loss, but also can affect other parts of the body with distinctive facial features, seizures, micro- or oligodontia and heart defects among other less common features (Zamora and Salini, 2019). Despite the confirmed occurrence of duplication in the three tested affected individuals in the Egyptian family, none experienced any of these common symptoms, including glaucoma in the older generation.

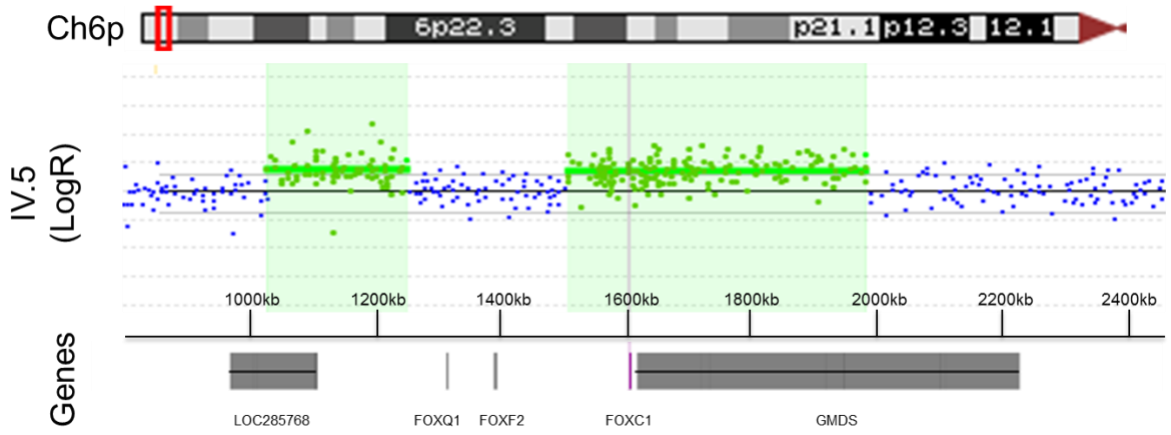

Figure V. 3. Cytogenetic analysis of the proband IV.5.

From top to bottom: The approximate chromosomal position in 6p25.3 is shown. The LogR track shows the tandem chromosomal gains in the proband IV.5. The location of genes in the interval is provided in the bottom track.

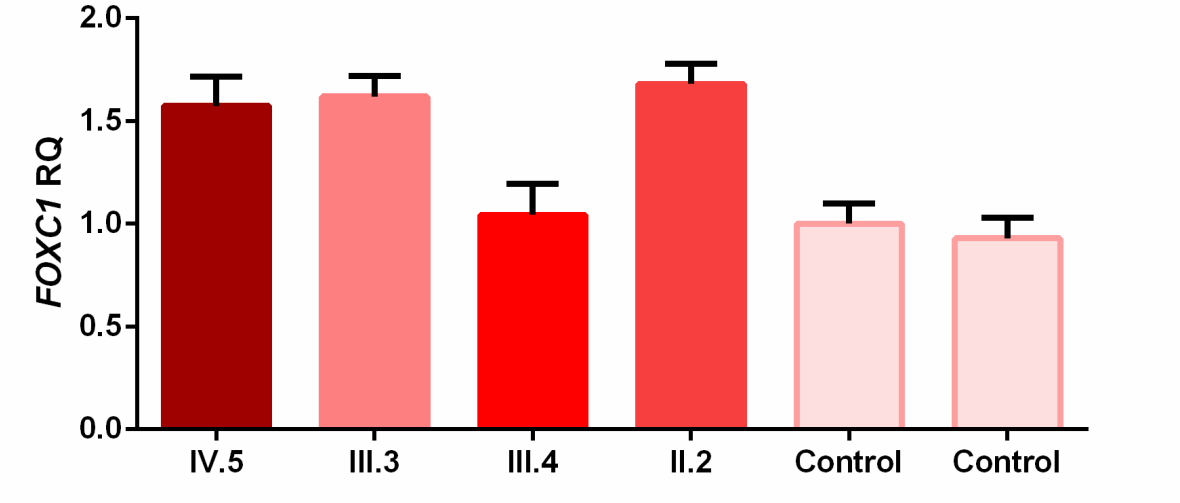

Figure V. 4. Validation of copy number variation.

A qPCR assay of *FOXC1* was performed in the proband (IV.5), father (III.3), mother (III.4), grandmother (II.2) and two unrelated controls to validate the copy number gain identified by cytogenetic array. RQ – relative quantification. Error bars = standard deviation.

Interestingly, two individuals, one with a small deletion of *FOXF2* and one with a slightly larger duplication covering *FOXQ1*, *FOXF2* and *FOXC1*, were reported to have a hypoplastic and bifid uvula respectively. The patient with the *FOXF2* deletion also co-inherited a *de novo* Chr5 duplication, which was thought more likely pathogenic, whilst the Chr6p deletion, was present in the unaffected father. However, it was not confirmed whether the father actually had his uvula examined.

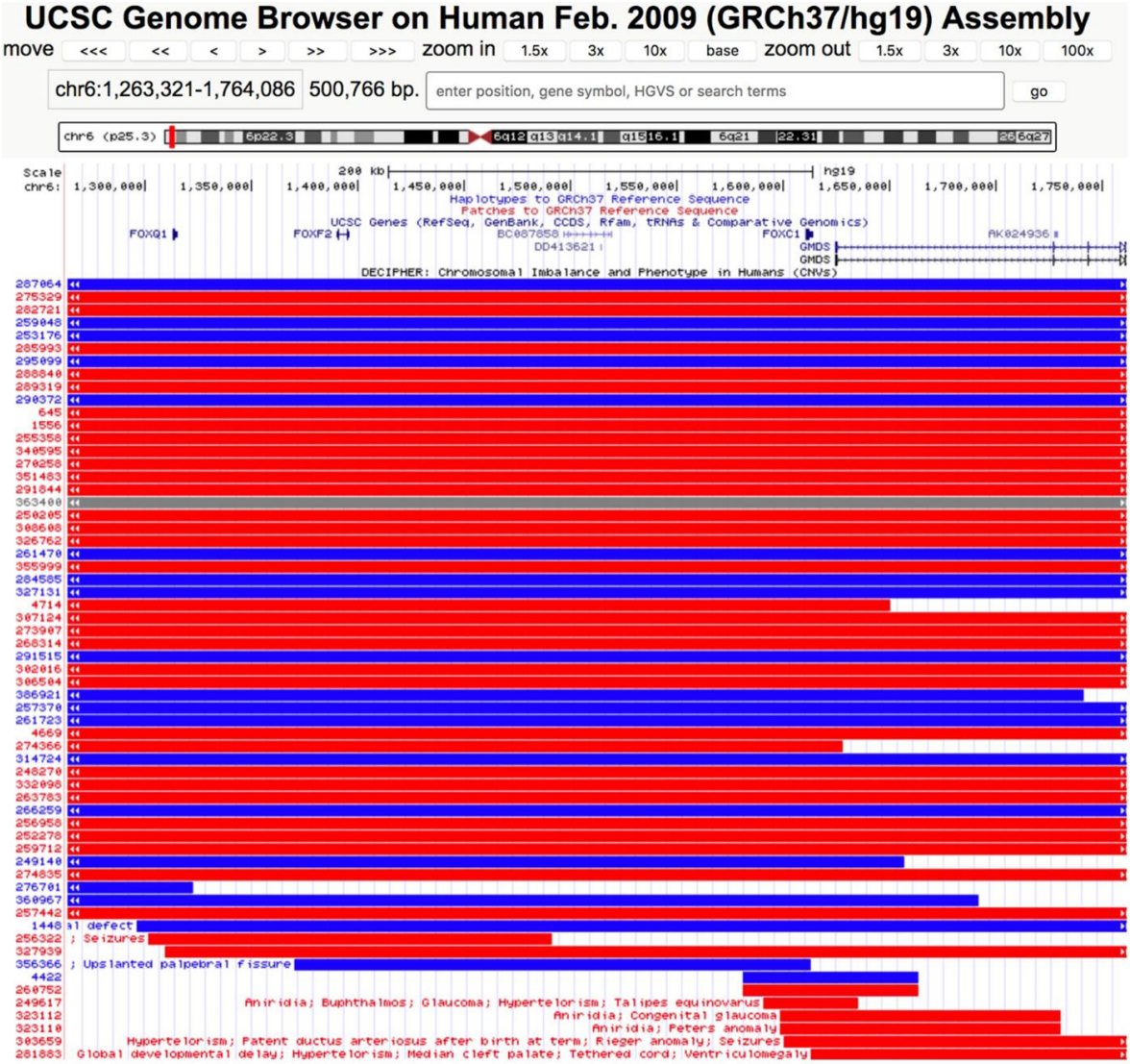

Figure V. 5. Patients with copy number gains (blue) or losses (red) of 6p25.3 in the Decipher database shown as a track on the UCSC genome browser.

Patient 256322 has aplasia/hypoplasia of the uvula and 290372 has a bifid uvula.

V. 4. 3. Linkage analysis

Since the cytogenetic analysis did not appear to reveal any conclusive results, it was decided to investigate further, this time utilizing the power of genetic resolution from the wider family that might help to pinpoint the approximate location of a causal allele. This was done by array-based SNP genotyping of all available individuals and using the resulting data for linkage analysis.

SNP based genotyping was therefore performed on 11 members of the family (Figure V. 6). Individuals III.5, III.7 and III.8 were not included at this time as DNA samples were unavailable. Genotyping was performed by UCL Genomics using the Infinium Human CoreExome-24 BeadChip. Genotypes were then sent to Prof Martin Farrall (Wellcome Trust Centre for Human Genetics, Oxford) to run linkage analysis using the MERLIN package. Samples were tested for quality control which indicated no inconsistencies between the 'inferred from ChrX genotype data' or from the recorded sex. The overall genotype missingness rate was very low (>0.003157, where a high rate of missing genotype calls can imply poor quality genotyping). The genome average identity by descent was consistent with that expected, indicating that the family structure worked appropriately. Following QC, a set of 5,497 autosomal SNPs that were informative in the family and located at approximately 0.5 cM spacing were selected for parametric linkage analysis. This set of SNPs captured 89% (SE 4.2%) of the theoretical maximal linkage information in the family. This data was then returned to us for further analysis. Linked regions were assessed based on segregation according to their LOD scores. Overall, ten regions fully segregated with affected and unaffected status to reach the maximum LOD score of ~1.5 and one small region on Chr8 which narrowly failed to reach this score (Table V. 1; Figure V. 7). Collectively, these intervals contained approximately 760 RefSeq genes and spanned a little over 100 million bases. The likely causal gene was expected to segregate with one of these intervals. Interestingly, the region of 6p25.3 which contains the tandem duplication described above, was present in one of the linked regions (Chr6: 212798-1529802) indicating that the duplications continued to segregate appropriately in other family members.

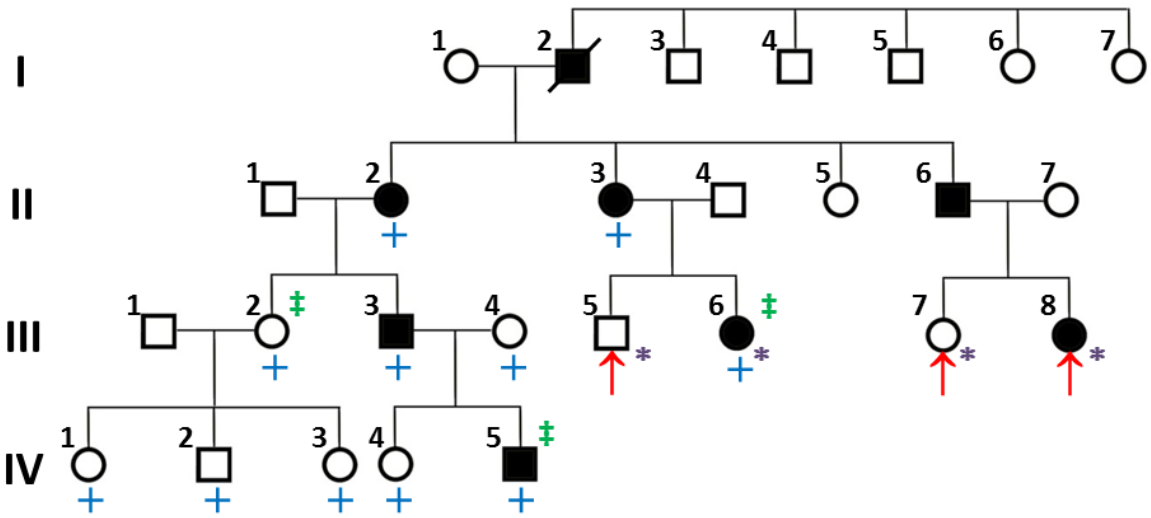

Figure V. 6. Family pedigree.

Eleven family members were genotyped for linkage analysis (+). Exome sequencing analysis was performed on 3 individuals (‡) and Sanger sequencing (*) was used to assess segregation of candidate gene variants in additional individuals (↑).

Table V. 1. Chromosomal regions identified with maximal or near maximal LOD scores.

Chromosome	Interval	Peak LOD	No of genes
2	18353520-29144214	1.5049	104
5	125184468-126823999	1.4968	7
6	212798-1529802	1.459	7
7	20053768-29473812	1.5049	64
8	24799492-26766081	1.3183	12
8	74112646-86229868	1.5049	41
9	14919291-23388822	1.5049	35
9	134749315-137892716	1.5049	98
12	20641007-23305532	1.505	21
12	66283785-83815294	1.505	68
15	54512632-86111814	1.505	100s

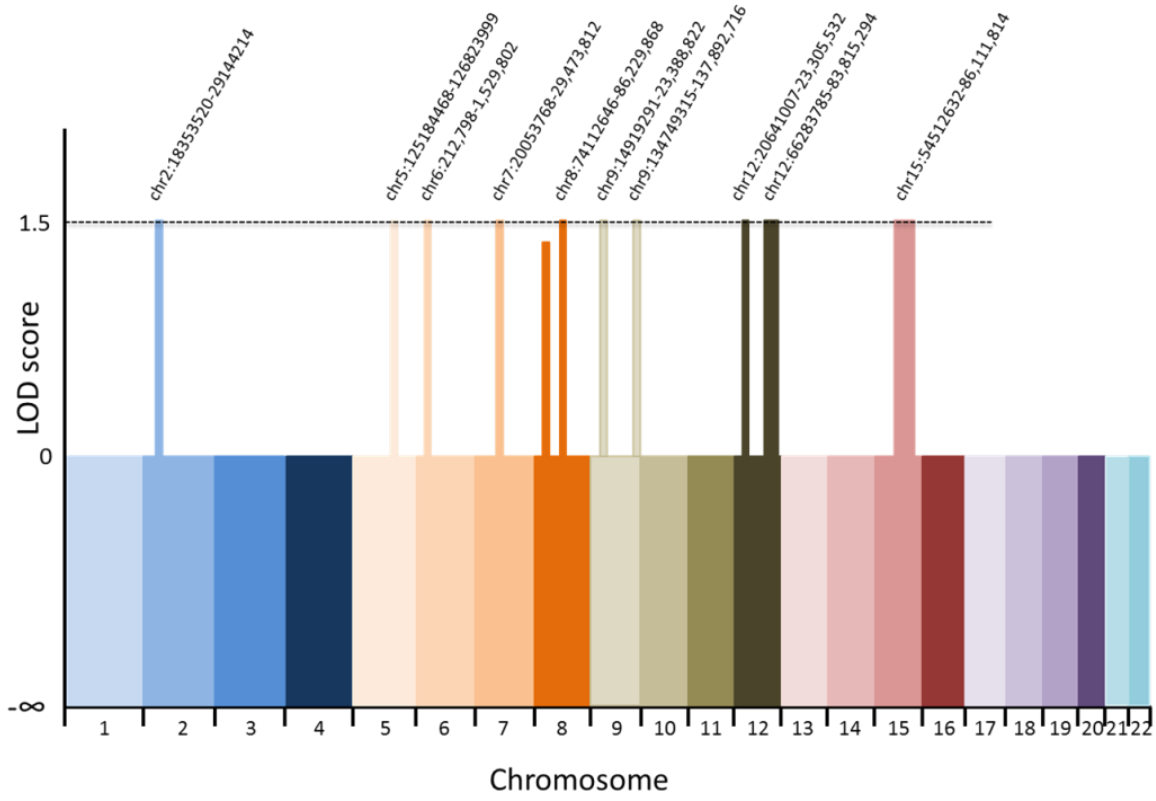

Figure V. 7. Manhattan plot depicting results of the linkage analysis.

Ten regions with the sequence intervals shown achieved the maximal LOD score of or near ~1.5.

V. 4. 4. Exome sequencing

In order to interrogate individuals for variants present in the coding fraction of the genome, it was decided to subject selected individuals to WES. This was performed on 3 individuals: two affected (IV.5 and III.6) and one unaffected female (III.2) who had 3 unaffected children (Figure V. 6), by sending DNA samples to the Next Generation Sequencing Service at the UCL Institute of Neurology. Sequencing data was analysed by uploading the aligned .bam files into the Ingenuity Variant Analysis package (Qiagen Bioinformatics). Variants were selected when present in the two affected but not the unaffected individual after filtering with the settings described in Section II. 31. Exome sequencing analysis. This resulted in a total of twenty-one candidate variants that met the appropriate criteria. The next step was to align these against the intervals identified by the

linkage analysis. Here a fully penetrant model was used, which was based on the pedigree structure which showed a high frequency of affected individuals and no evidence of loss of penetrance typically by skipping of a generation. This was particularly evident for individual III.2 who was phenotypically normal and had three unaffected children. The linkage results effectively took into account segregation across all available individuals without the need to sequence them all. Eleven variants were effectively excluded while 10 remaining variants which aligned within the linked regions were therefore considered as candidates. Each variant was visually checked using the Integrated Genome Viewer and then correctly validated by Sanger sequencing. Details of each candidate variant (*PLB1; FOXF2; SNX10; PLIN2; IGDCC3; THSD4; SEMA7A; SCAPER; SH2D7* and *IL16*) are presented in Table V. 2. To gain a better idea of the potential pathogenicity of each variant, bioinformatics analysis using a number of commonly used predictive algorithms was used (Table V. 3). At this stage none of the variants were considered stronger candidates than another, although *PLIN2* and *SCAPER* in particular scored uniformly low with most tools. Since the bioinformatics tools tended to give contradictory information, this data was not relied upon for prioritization and the next section describes how segregation analysis was more definitive to include/exclude variants of significance.

Table V. 2. Candidate genes identified by combined linkage and exome sequencing analysis (locations based on GRCh37/hg19 assembly).

Gene	Position in ExAC	Position in gene	Linkage interval
PLB1	2:28,851,473	c.3671C>T	2:18,353,520-29,144,214
FOXF2	6:1,395,057	c.1298A>C	6:212,798-1,529,802
SNX10	7:26,386,079	c.17A>C	7:20,053,768-29,473,812
PLIN2	9:19,116,484	c.1076T>C	9:14,919,291-23,388,822
IGDCC3	15:65,623,929	c.1217G>A	15:54,512,632-86,111,814
THSD4	15:72,069,606	c.2950G>A	15:54,512,632-86, 111,814

Table V. 2. (continued).

SEMA7A	15:74,710,611	c.370G>A	15:54,512,632-86,111,814
SCAPER	15:77,067,396	c.835T>C	15:54,512,632-86,111,814
SH2D7	15:78,390,321	c.317G>A	15:54,512,632-86,111,814
IL16	15:81,582,851	c.1390G>C	15:54,512,632-86,111,814

Table V. 3. Bioinformatics analysis of candidate genes.

	PLB1	***FOXF2***	***SNX10***	***PLIN2***	***IGDCC3***
Variant	c.3671C>T p.A1224V	c.1298A>C p.Q433P	c.17A>C p.Q6P	c.1076T>C p.N359S	c.1217G>A p.A406V
ExAC	N/A	2/121406	1/121404	130/121408	143/115572
SIFT	Tolerated	Deleterious	Tolerated	Tolerated	Deleterious
Polyphen2	Probably damaging (0.964)	Benign (0.055)	Benign (0.063)	Benign (0.002)	Probably damaging (0.991)
Mutation taster	Disease causing	Disease Causing	Disease causing	Polymorphism	Disease causing
Provean	Neutral	Neutral	Neutral	Neutral	Neutral
Condel	Deleterious	Deleterious	Neutral	Neutral	Deleterious
LoFtool	Benign	Unknown	Possibly damaging	Benign	Benign
FATHMM	Tolerated	Damaging	Tolerated	Tolerated	Tolerated
Mutation assessor	Medium	Medium	Neutral	Neutral	Low
Meta LR or SVM	Tolerated	Damaging	Tolerated	Tolerated	Tolerated
GERP	4.73/2.81	5.76 (Conserved)	4.93	5.75/0.549	4.92
CADD	29.4	23.9	19.02	<10	27.9

Table V. 3. (continued).

	THSD4	*SEMA7A*	*SCAPER*	*SH2D7*	*IL16*
Variant	c.2950G>A p.V984M c.1870G>A p.V624M*	c.370G>A p.R124W	c.835T>C p.T279A c.97A>G p.T33A	c.317G>A p.R106H	c.1390G>C p.G464R
ExAC	1/120762	14/120552	214/120538	1/120338	N/A
SIFT	Deleterious *tolerated	Deleterious	Tolerated	Tolerated	Tolerated
Polyphen2	Probably damaging (1.00)	Probably damaging (0.989)	Benign (0.005)	Probably damaging (0.944)	Probably damaging (0.967)
Mutation taster	Disease causing	Polymorphism	Disease causing	Polymorphism	Polymorphism
Provean	Neutral	Neutral	Neutral	Deleterious	Neutral
Condel	Deleterious	Deleterious	Neutral	Deleterious	Neutral
LoFtool	Possibly damaging	Possibly damaging	Benign	Possibly damaging	Benign
FATHMM	Tolerated	Tolerated	Tolerated	Damaging	Tolerated
Mutation assessor	Low	Low	Low	Low	Neutral
Meta LR or SVM	Tolerated	Tolerated	Tolerated	Damaging/ Tolerated	Tolerated
GERP	4.85	4.42/1.53	5.76/2.17	4.51	4.89
CADD	26.2	28.3	<10	24.2	22. 7

We had earlier made requests to the family to try to recruit several further members, who could theoretically increase the available discriminatory power. The individuals in question lived in a different part of Egypt, in the Sinai Peninsula and consequently it had been more difficult to reach them. At around this time the palate operation was planned for the proband (IV.5) by Mr Brian Sommerlad who had been the contact with the family. He had been able to visit and meet III.5, III.7 and III.8 (Figure V. 6). Following obtaining ethical consent and performing clinical assessment, saliva samples for DNA were obtained from these individuals. It was decided that, along with III.3 as a replication control, each of the 10 variants would be investigated for segregation using Sanger sequencing in these individuals (Figure V. 8 and Figure V. 9). This data was extremely useful since apart from *FOXF2*, all of the other 9 variants failed to completely segregate in the family. Eight of these were in the newly added affected individual III.8, while for *SNX10,* the putative 'mutant' allele was present in her unaffected sister III.7. In this case, it is possible that III.7 could be considered as a non-expressing carrier. However, first treating the family as fully penetrant, and secondly considering what is known about the gene, it did not appear to be a high quality functional candidate. *SNX10* has previously been reported as the causal gene in autosomal recessive osteoporosis, where patients present early in life with extreme sclerosis along with other serious clinical manifestations, while no phenotype was reported in their 'healthy' heterozygous relatives (Aker et al., 2012, Megarbane et al., 2013). *Snx10* in mice was found to be expressed in osteoclasts and in gastric epithelia (Ye et al., 2015) and knockout resulted in death at 3-4 weeks, with severe growth restriction and impaired skeletal development (Ye et al., 2015). Although the variant we detected was rare (1/121404 in gnomAD), the bioinformatics was also not compelling (Table V. 3) so we decided not to pursue this gene further.

Therefore, the only variant that fully segregated with the phenotype was c.1298A>C (p.Q433P) in the *FOXF2* transcription factor, which consequently was considered as the most likely pathogenic variant Figure V. 8. The effect of these new genotypes incorporated as additional SNPs into the linkage analysis is shown in Table V. 4 (courtesy of Prof Martin Farrall). As could be predicted, the LOD score at 6p25.3, which increased to 1.87, was the only one to increase.

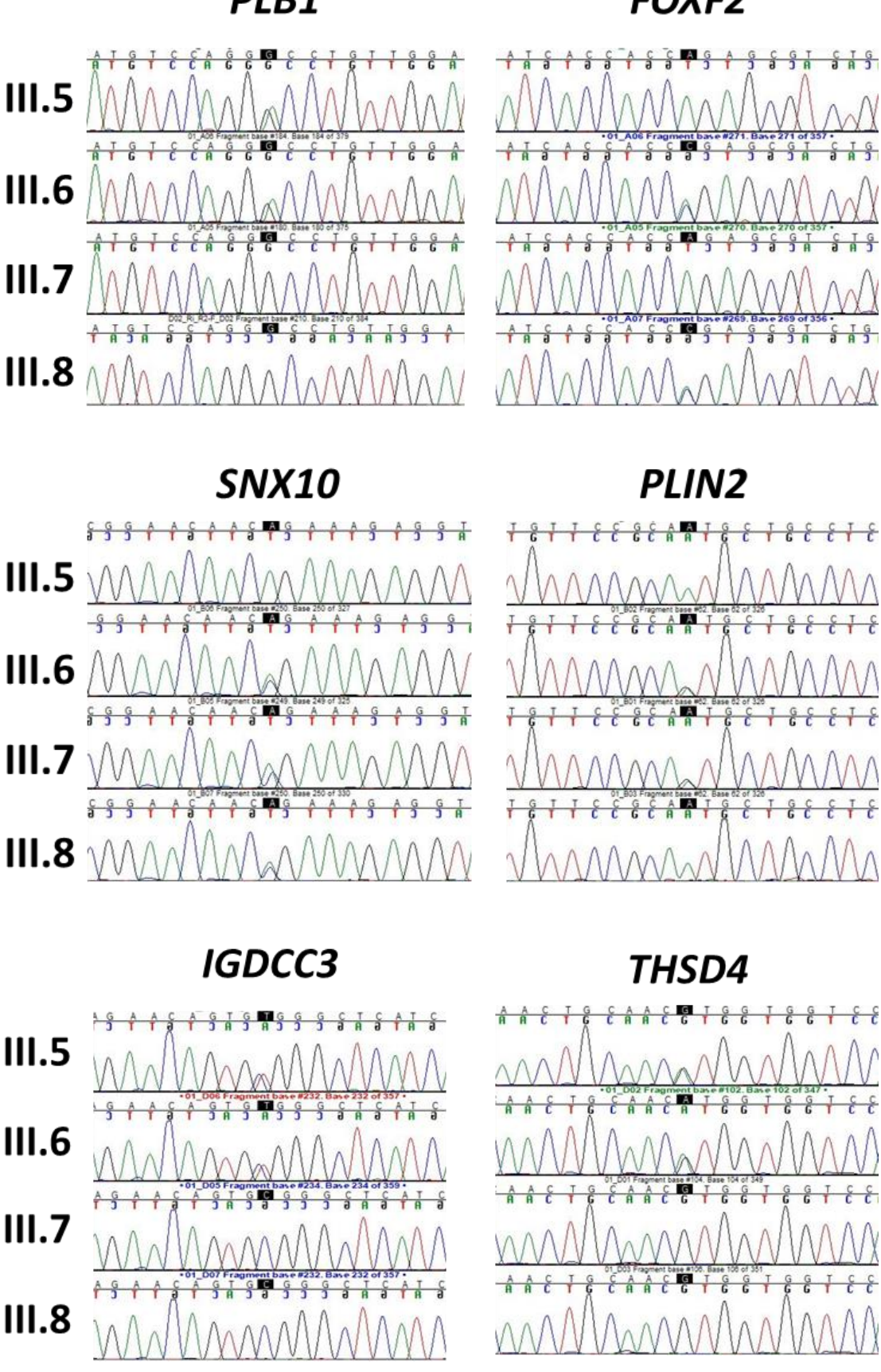
PLB1
FOXF2
III.5
III.6
III.7
III.8
SNX10
PLIN2
III.5
III.6
III.7
III.8
IGDCC3
THSD4
III.5
III.6
III.7
III.8

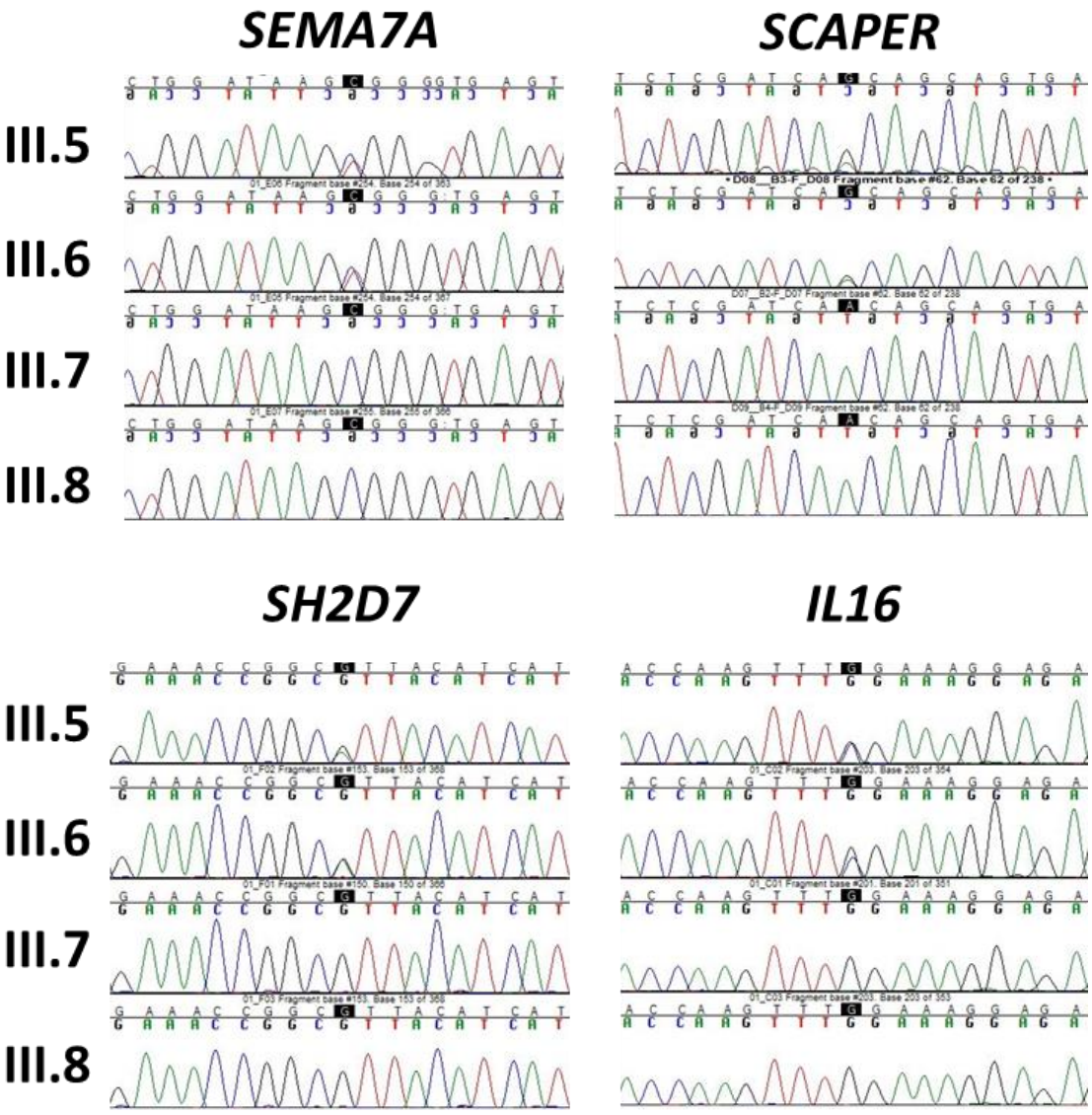

Figure V. 8. Sanger sequencing chromatograms of the 10 candidate variants showing investigation of segregation in newly acquired family members.

The only variant that fully segregated with the phenotype was c.1298A>C (p.Q433P) in the *FOXF2* transcription factor. Note that III.5 and III.7 are unaffected, while III.6 and III.8 are affected individuals.

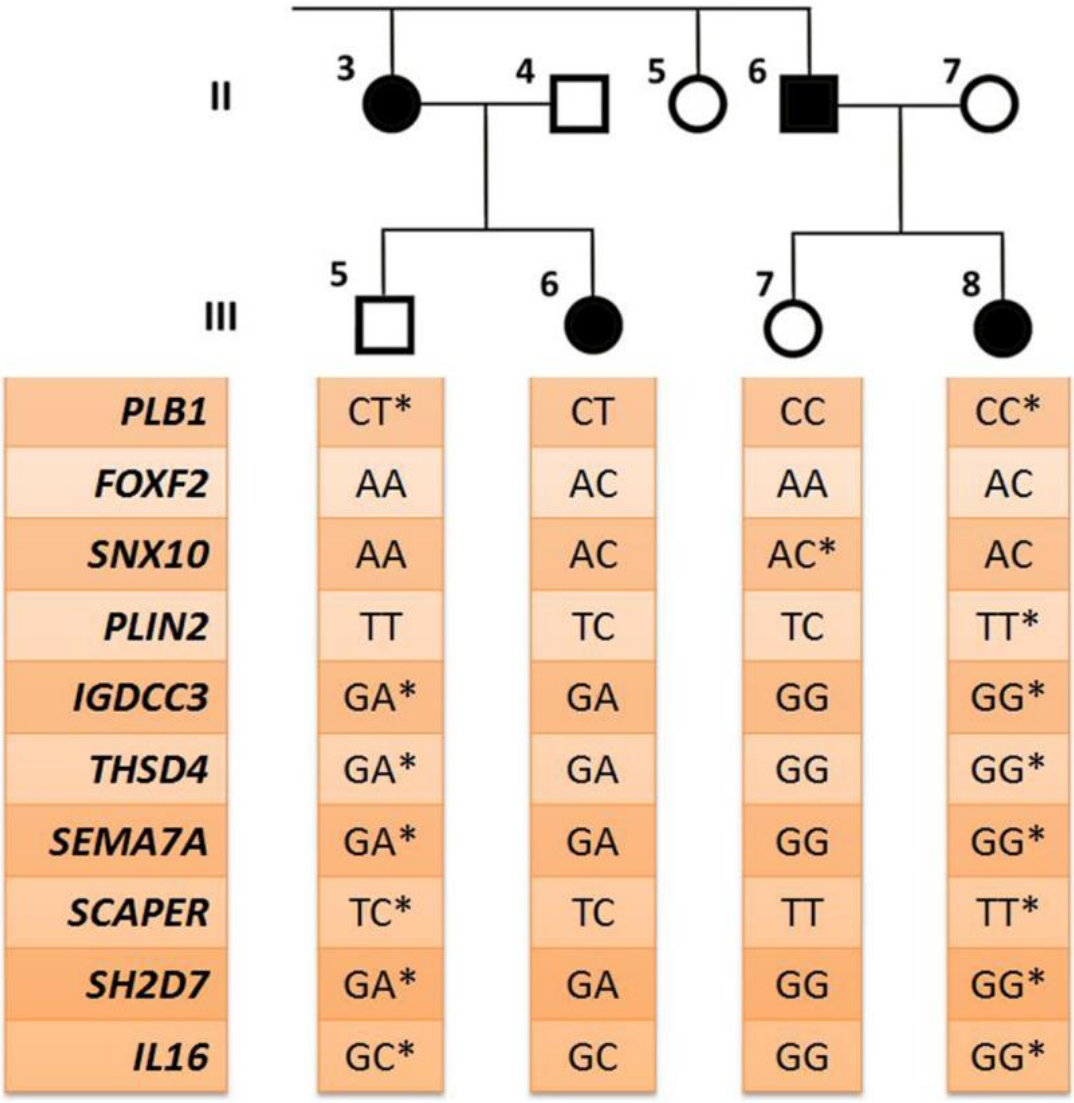

Figure V. 9. Segregation analysis of candidate variants in newly acquired family members.

Genotypes are shown for individuals III.5, III.6, III.7 and III.8. * represents recombination that serves to exclude the variant from perfect segregation in the family.

Table V. 4. Updated LOD scores including the additional 3 family members.
Included/excluded was determined by recombination in one or more affected individual apart from *SNX10*, which was a recombination in an unaffected individual (III.7).

Gene	New LOD	Old LOD	Included/Excluded
PLB1	1.2256	1.501	Excluded
FOXF2	1.8730	1.390	Included
SNX10	1.4377	1.504	Excluded
PLIN2	1.4010	1.504	Excluded
IGDCC3	0.2132	1.505	Excluded
THSD4	-0.3626	1.505	Excluded
SEMA7A	-0.4584	1.505	Excluded
SCAPER	-0.4619	1.505	Excluded
SH2D7	-0.4374	1.505	Excluded
IL16	-0.0171	1.505	Excluded

The *FOXF2* c1298A>C (p.Q433P) variant has been reported twice in 2 heterozygous European individuals of unknown phenotype in the ExAC and gnomAD databases. Two further missense substitutions are also reported to affect the same amino acid codon, c1299G>C (p.Q433H) Latino and c1297C>G (p.Q433G) East Asian, once each in a total of 246,272 alleles. In terms of amino acid conservation, the glutamine residue is well conserved across species, excluding chicken and lamprey (Figure V. 10). Interestingly, the *FOXF2* variant is very close to, and in linkage disequilibrium with the 6p25.3 tandem duplication identified by the cytogenetic analysis.

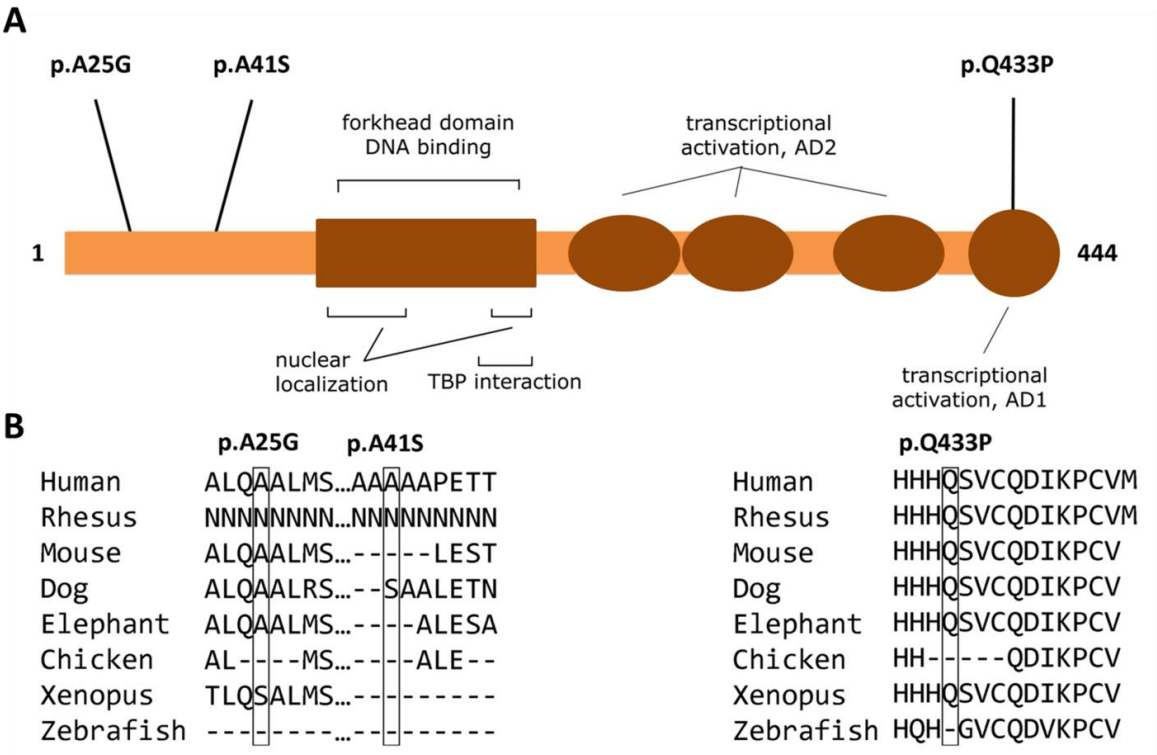

Figure V. 10. Schematic diagram showing the functional domains of *FOXF2.*

A) The location of nonsynonymous missense variants p.A25G, p.A41S and p.Q433P are given. **B)** The evolutionary conservation of each variant is indicated in the respective boxed areas.

V. 4. 5. Analysis of *FOXF2* in individuals with non-syndromic cleft palate and submucous cleft palate

Ideally, we would have chosen to investigate further individuals with absent uvula and hypernasality, however, this condition is extremely rare and no other cases were known to us, even following extensive searching. Therefore, in order to investigate whether *FOXF2* pathogenic variants might underlie other, more common forms of CP, a cohort of 240 patients with NS CP and 72 patients with SMCP was selected for sequencing from our collection of >750 CL/P patient DNA samples. This cohort included all available cases with bifid uvula and clefts affecting the soft palate. It did not include individuals with CL, since it was designed to include the most similar affected tissues as with absent uvula. *FOXF2* consists of only two exons but given the size of exon one, sequencing was performed with four primer pairs (Table II. 1) amplifying overlapping fragments to fully cover the coding regions, intronic splice sites and the majority of the UTRs.

Variants identified are listed in Table V. 5 and depicted in Figure V. 10 and Figure V. 11. Two rare/unique missense variants were identified (Figure V. 11, A, B), however, neither were predicted to be damaging by bioinformatics analysis (Table V. 5). Two other, more common missense variants were also identified (Figure V. 11, C, D). c.394G>A (p.A132T) at 6:1,390,576 was present in the gnomAD database as 170/19,842 alleles in Asian heterozygotes, while c.700C>A (p.P234T) at 6:1,390,882, was present as 182 heterozygotes and 3 homozygotes in 16,934 alleles in the African population and 28/30,890 heterozygotes in the Latino population. Since these variants were described as benign (Table V. 5), they were not studied further. The coding sequence of *FOXF2* was also investigated in available exome sequencing data generated from ~30 multiplex, NS CL with or without CP (NS CLP) families from previous genetic studies in our laboratory, but did not reveal any variants of interest.

Table V. 5. Bioinformatics analysis of *FOXF2* missense variants identified in individuals with cleft palate or submucous cleft palate.

Location	6:1,390,068	6:1,390,021	6:1,390,341	6:1,390,647
Phenotype	CP	SMCP	CP	CP
Variant	c.120G>T	c.74C>G	c.394G>A	c.700C>A
AA change	p.A41S	p.A25G	p.A132T	p.P234T
ExAC	3/10192	N/A	59/119460	70/54414
SIFT	Tolerated	Tolerated	Tolerated	Tolerated
Polyphen2	Unknown	Unknown	Benign (0.105)	Benign (0.01)
Mutation taster	Neutral	Neutral	Disease causing	Disease causing
Provean	Neutral	Neutral	Neutral	Neutral
Condel	Neutral	Neutral	Unknown	Unknown
LoFtool	Unknown	Unknown	Unknown	Unknown
FATHMM	Damaging	Damaging	Damaging	Damaging
Mutation assessor	Neutral	Neutral	Neutral	Neutral
Meta LR or SVM	Tolerated	Tolerated	Tolerated	Tolerated
GERP	2.3	2.3	4.14/3.27	4.1
CADD	1.388	9.198	2.693	2.429

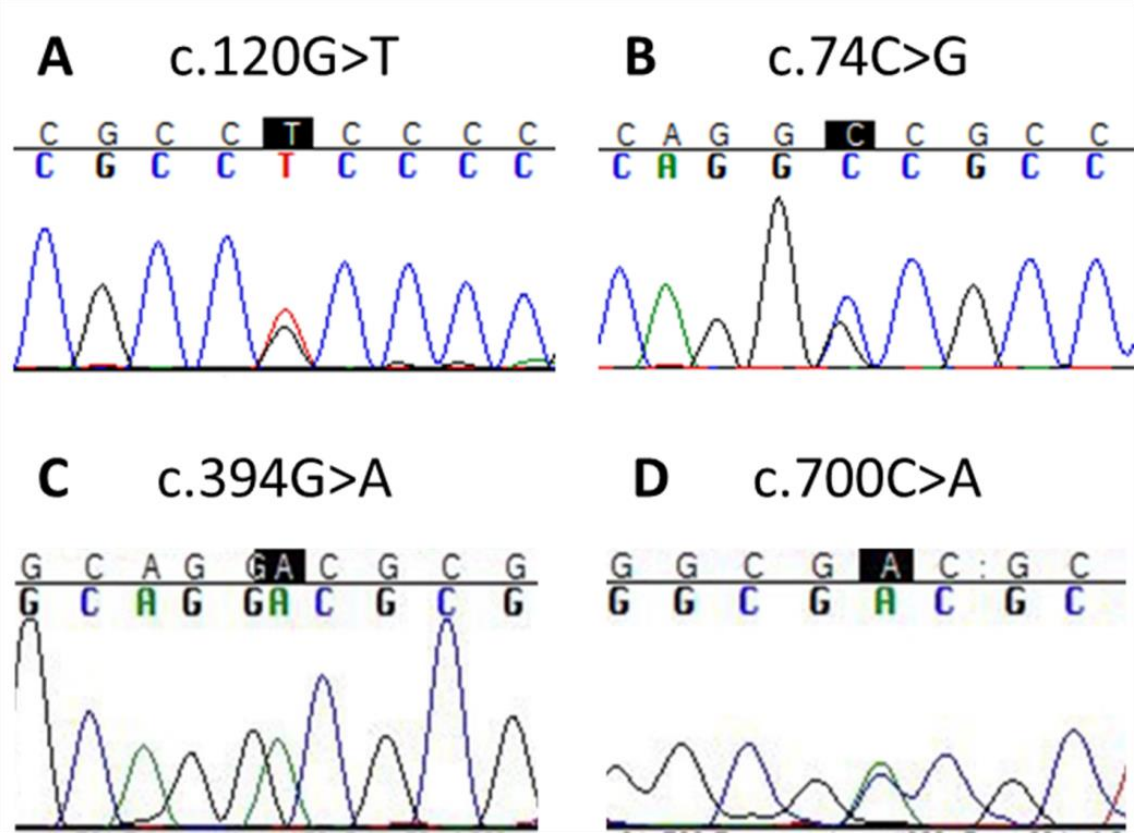

Figure V. 11. Representative *FOXF2* Sanger sequencing chromatograms from individuals in the CP cohort.

Sequences of the *FOXF2* gene in 4 individuals with NS CP or SMCP. **A)** c.120G>T (p.A41S) in an individual with CP; **B)** c.74C>G (p.A25G) in an individual with SMCP; **C)** c.394G>A (p.132T) in an individual with CP; **D)** c.700C>A (p.P234T) in and individual with CP.

V. 4. 6. Effect of the FOXF2 p.Q433P variant on transcriptional activation

The likelihood that FOXF2 may play a causal role in development of the palate and uvula was enhanced following a review of the literature, initially with a report of a mouse *Foxf2* knockout being described having a CP (Wang et al., 2003); see also V. 5. Discussion. This mouse model has been further studied more recently, where both Nik et al. (2016) and Xu et al. (2016) report detailed analysis of the palate defect along with the identification of down stream genes and pathways that are affected by *Foxf2*. CP is not the same as absent uvula, although there may be some common aspects, including during development. However, the mouse differs

from humans anatomically since it lacks an uvula (Finkelstein et al., 1992). Therefore, to further assess the possibility of a pathogenic effect caused by the p.Q433P variant, we decided to perform *in vitro* functional testing. The p.Q433P variant is located in the previously described activation domain AD1 at the C-terminal region of FOXF2 (Hellqvist et al., 1998) (Figure V. 10). This is an important domain required for FOXF2 to act as a transcriptional activator. It was therefore decided to test the effect of the variant on its ability to affect activation using a transient luciferase reporter assays. To do this, a full length *FOXF2* cDNA coupled to a CMV promoter was first obtained from OriGene (II. 36. Constructs). Then a p.Q433P variant was made using site directed *in vitro* mutagenesis. Both constructs were completely sequenced to verify their integrity and to ensure that only the sequence difference was the one introduced by design. Hellqvist et al. (1998) previously performed investigations of the FOXF2 as a transcription factor and had earlier described a preferred binding site: CAACGTAAACAATCCGA (Hellqvist et al., 1996) that functioned as a transcriptional target. We therefore synthesized (GeneScript) a similar reporter construct containing 4 tandem copies of this sequence coupled to firefly luciferase. WT and p.Q433P constructs were co-transfected with the FOXF2 reporter and a *Renilla* luciferase reporter into HeLa cells to assess the effect of the variant. Both WT and p.Q433P constructs produced significant activation compared to 'empty' vector. However, the pathogenic variant, contrary to expectation, caused a significant 1.5 fold increase in activation compared to the WT sequence (Figure V. 12). A similar result was found on multiple occasions when repeating the experiment.

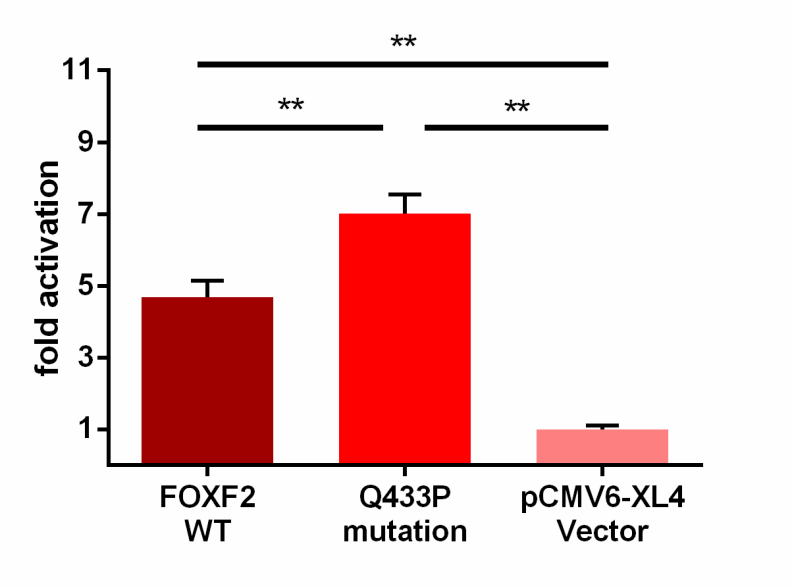

Figure V. 12. Effect of WT and p.Q433P variant FOXF2 on transcriptional activation. Transcriptional activation of FOXF2 WT and p.Q433P constructs in HeLa cells. Data represent the average ± standard deviation (error bars) of triplicate samples at 24 hours post transfection. All data presented were representative of at least 3 replicate experiments. *p<0.05; **p<0.01.

Western blotting was routinely performed in order to check loading. Interestingly, this revealed a dramatic and reproducible 11-fold increase in the quantity of the FOXF2-Q433P protein compared to WT (Figure V. 13).

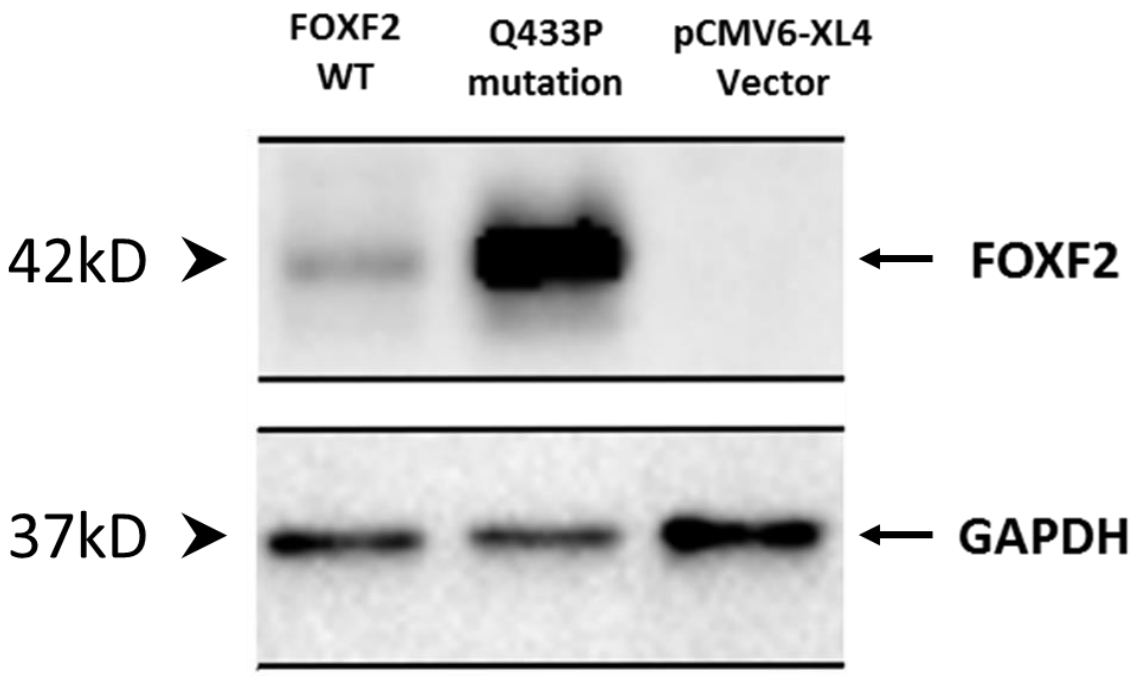

Figure V. 13. Visualization of WT and p.Q433Pvariant FOXF2 proteins following transient transfection.

Western blot showing FOXF2 protein expression in HeLa cells transfected with FOXF2 WT, p.Q433P mutation and pCMV6-XL 'empty' vector constructs. Data presented correspond to the experiment shown in Figure V. 12 and were representative of at least 3 replicate experiments.

To investigate this further, RTqPCR was used to see if this might be due to increased expression, perhaps reflecting some undetected difference between the WT and mutant constructs. However, this in fact showed the opposite, that there was a modest 0.3 fold reduction in quantitative expression between the WT and p.Q433P constructs (Figure V. 14).

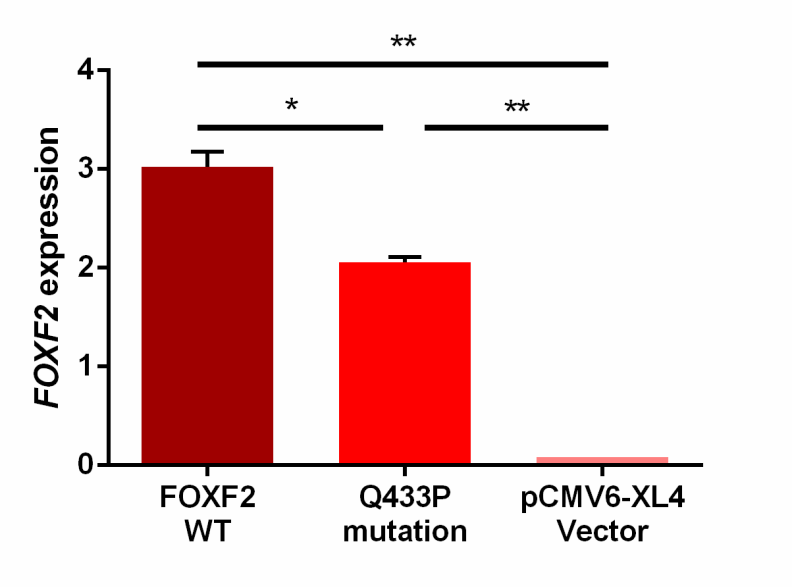

Figure V. 14. Quantitation of mRNA levels of WT and p.Q433P variant FOXF2 following transient transfection.

Quantitative expression difference between the WT and p.Q433P mutation constructs measured by RTqPCR in HeLa cells. Expression was normalized to *ACTB*. Data presented were representative of at least 3 replicate experiments. Error bars = standard deviation. *p<0.05; **p<0.01.

A similar result was also reproducibly obtained following transfection into HepG2 cells, while testing several independent clones of the constructs gave similar results (Figure V. 15).

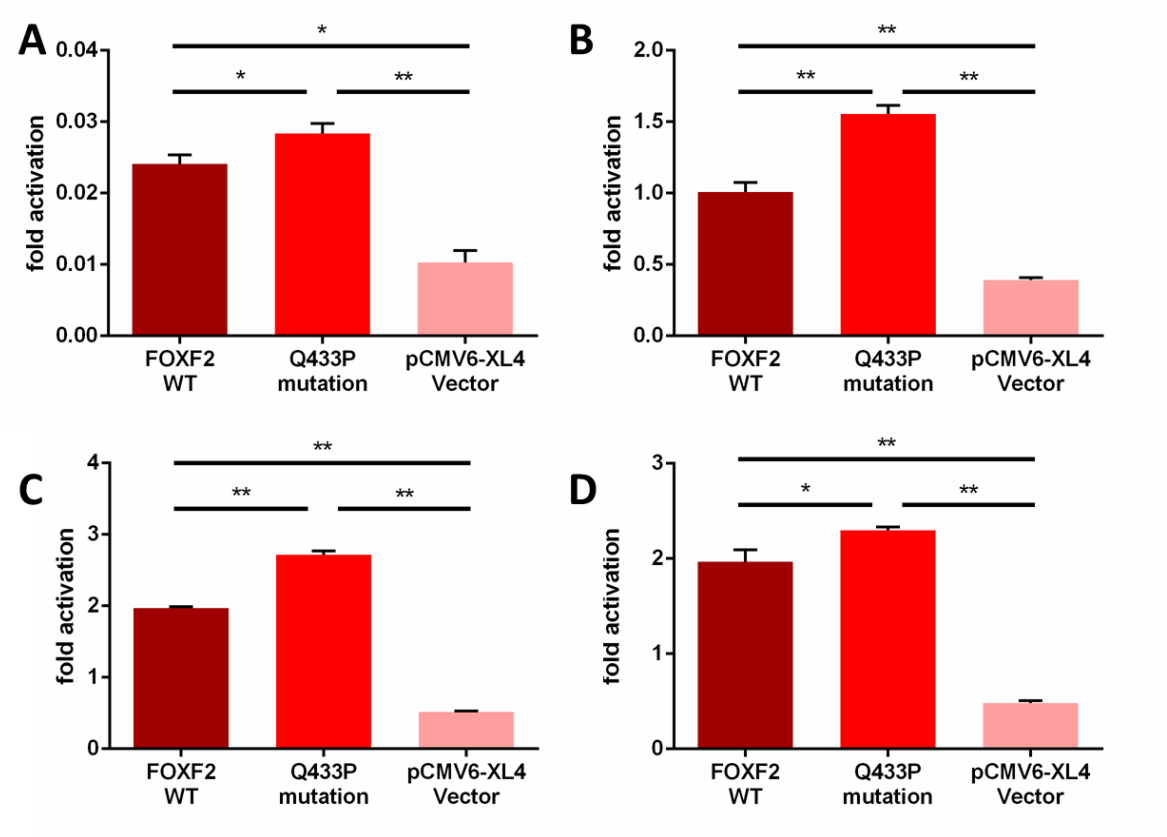

Figure V. 15. Effect of WT and p.Q433P variant FOXF2 on transcriptional activation. Transcriptional activation of FOXF2 WT and p.Q433P constructs in **A)** HepG2 cells. Data represent the average ± standard deviation (error bars) of triplicate samples at 24 hours post transfection; **B)** in HeLa cells. Data represent the average ± standard deviation (error bars) of triplicate samples at 48 hours post transfection; **C, D)** in HeLa cells. Data represent the average ± standard deviation (error bars) of triplicate samples at 24 hours post transfection with 2 independent clones. *p<0.05; **p<0.01.

Since the increased protein level did not seem to result from any of the possibilities tested, the results of the WT vs. mutant luciferase activity normalized to protein levels are also presented (Figure V. 16). We rationalized this since it is not known how the mutation might affect the translation of endogenous FOXF2 protein levels *in vivo* during embryonic development. This analysis shows effectively an 88% loss of activation relative to the amount of FOXF2 protein present.

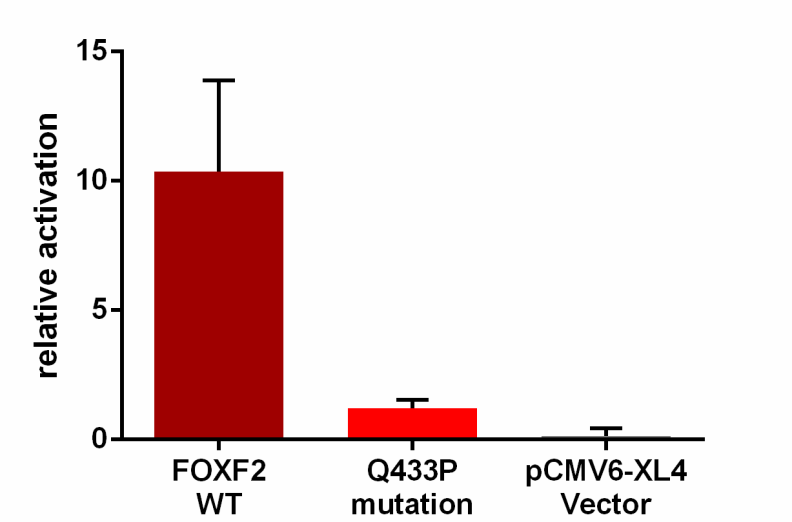

Figure V. 16. Effect of WT and p.Q433P variant FOXF2 on transcriptional activation by protein level.

Transcriptional activity was normalized according to protein level detected by Western blotting. Error bars = standard deviation. *p<0.05; **p<0.01.

Based on the findings of Xu et al. (2016) who reported upregulation of *Fgf18* and downregulation of *Shox2* expression in *Foxf2* knockout mice, the effect of overexpressing *FOXF2* was investigated on both of these genes in HeLa cells (Xu et al., 2016). Although no effect was detected for *SHOX2*, *FGF18* was found to be significantly upregulated when overexpressing the FOXF2-Q433P variant in comparison to the WT sequence (Figure V. 17).

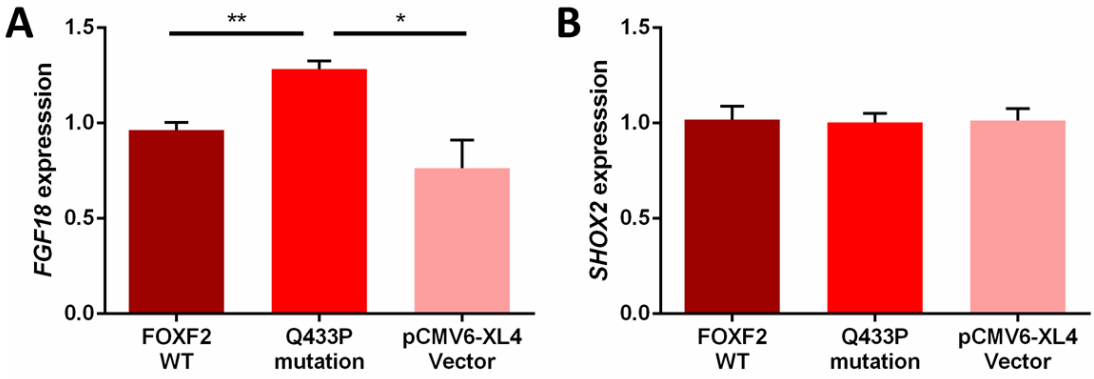

Figure V. 17. Effect of WT and p.Q433P variant FOXF2 constructs on the expression of putative downstream target genes.

A) *FGF18* and **B)** *SHOX2* transcript levels assessed by RTqPCR in HeLa cells at 24 hours following transfection of WT, p.Q433P constructs and 'empty' vector. Expression was normalised to *ACTB*. Data presented were representative of at least 3 replicate experiments. Error bars = standard deviation. *p<0.05; **p<0.01.

V. 4. 7. FOXF2 p.A25G and p.A41S effect on transcriptional activation

The effect of the variants p.A25G and p.A41S found in the CP and SMCP cohort was also investigated. Although these variants were predicted to be benign, a significant effect on transcriptional activity might influence our thinking on their impact. WT, p.A25G and p.A41S constructs were co-transfected into both HeLa and HepG2 cells along with the FOXF2 luciferase reporter plasmid (and *Renilla* plasmid).

WT, p.A25G and p.A41S constructs all produced significant activation compared to 'empty' vector, however, unlike the p.Q433P construct above, these variants showed no change in activation compared to the WT sequence (Figure V. 18). There was also no statistically significant difference observed in the quantity of protein of the FOXF2-A25G, FOXF2-A41S when compared to WT by Western blotting (Figure V. 19).

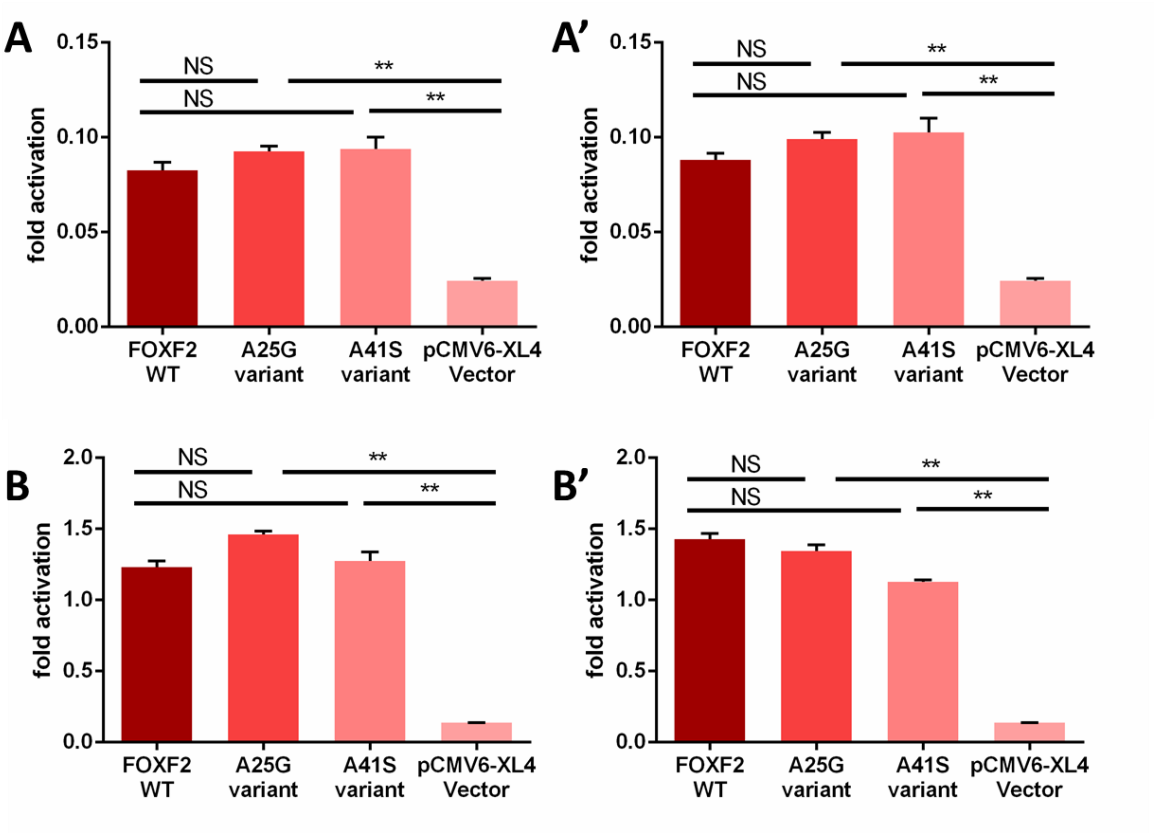

Figure V. 18. Comparative analysis of the effect of FOXF2 p.A25G and p.A41S variants on transcriptional activation.

Transcriptional activation of FOXF2 WT, p.A25G and p.A41S constructs in **A)** HepG2 cells; **B)** in HeLa cells. Data represent the average ± standard deviation (error bars) of triplicate samples at 24 hours post transfection with 2 independent clones (designated with or without '). **p*<0.05 ***p*<0.01; **NS** - not statistically significant, *p*≥0.05.

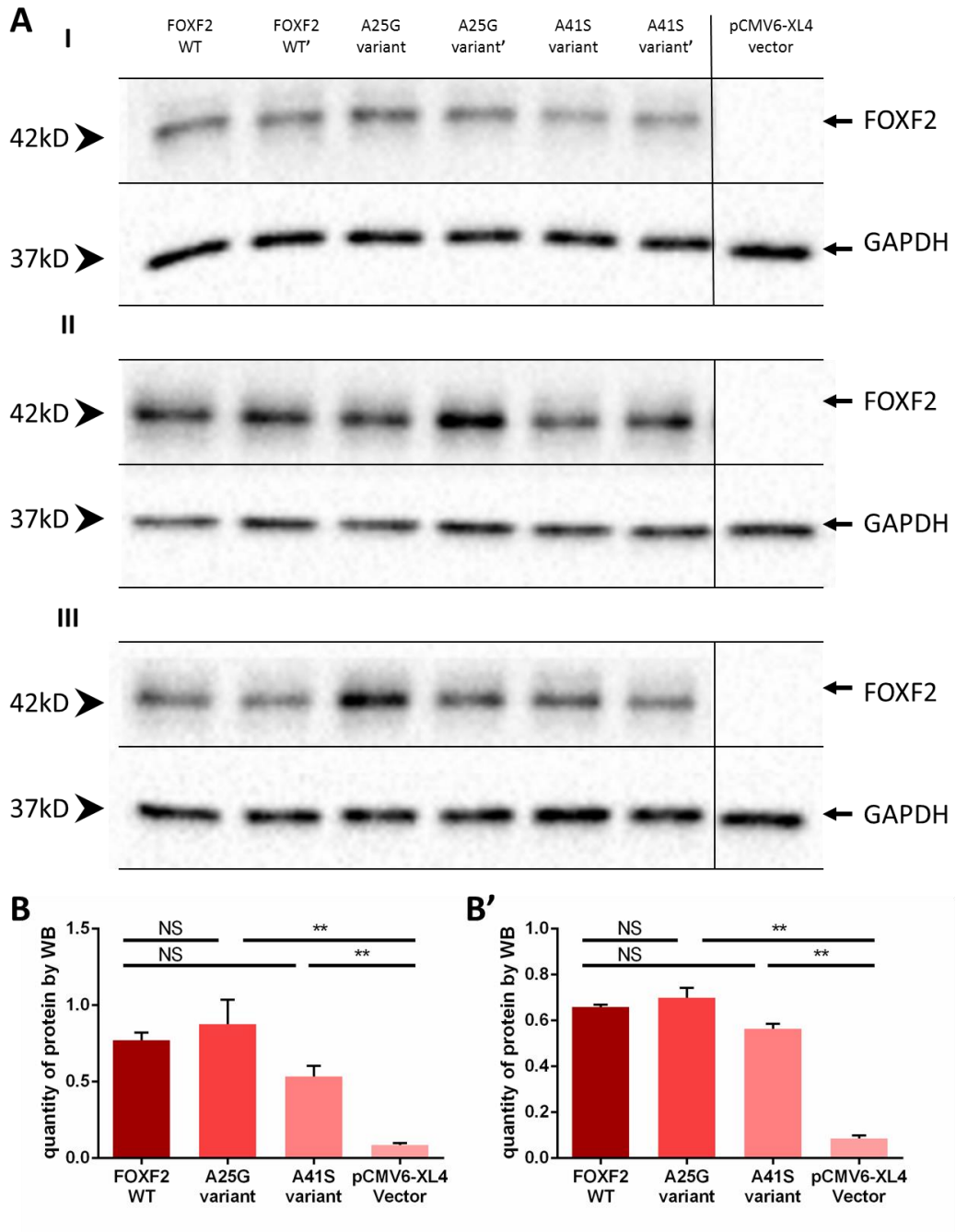

Figure V. 19. Detection and quantitation of FOXF2 proteins following transient transfection of WT and mutant constructs.

A) Western blot showing FOXF2 protein expression in HeLa cells transfected with FOXF2 WT, A25G, A41S mutations and pCMV6-XL 'empty' vector constructs using 2 independent clones (designated with or without '). Each experiment was carried out three times (I, II, III). Vertical line represents cut in the gel. **B), B)'** Quantitation and comparison of WT, FOXF2-A25G and FOXF2-A41S protein levels. Error bars = standard deviation. $^{**}p<0.01$; **NS** - not statistically significant, $p \geq 0.05$.

V. 4. 8. Expression of *FOXF2* in craniofacial tissues

As stated above, *Foxf2* has been previously established as required for normal palate closure in the mouse (Wang et al., 2003). Its expression in the developing orofacial region has been shown to be largely restricted to the posterior palate and tongue (Nik et al., 2016, Xu et al., 2016). However, nothing is known about *Foxf2* expression in the uvula since mice lack the equivalent of this structure. Therefore, *in situ* hybridisation was used to investigate *FOXF2* expression in coronal sections of human embryos from around the time of palatogenesis (Figure V. 20). This was conducted as a commissioned collaboration with the Medical Research Council, Wellcome Trust funded HDBR who both collect and perform projects using staged human fetal tissues (II. 42. Tissue *in situ* hybridization). I assisted by generating the *in situ* probe and selected suitable sections from staged human embryos but the *in situs* were performed by Ms Nadjeda Moreno of the HDBR. Similar to the mouse, *FOXF2* was found to be expressed in the human embryonic mesenchyme of the oral cavity and tongue (Nik et al., 2016, Xu et al., 2016). This was particularly notable in the posterior palatal shelves before fusion at stages CS22 and CS23, decreasing significantly in the fused palate at the later stage L8pcw. Expression was still seen in the most posterior region of the L8pcw embryo where the palatal shelves had not yet fused and extended to the oral epithelia in addition to the mesenchyme. This region is equivalent to the presumptive uvula.

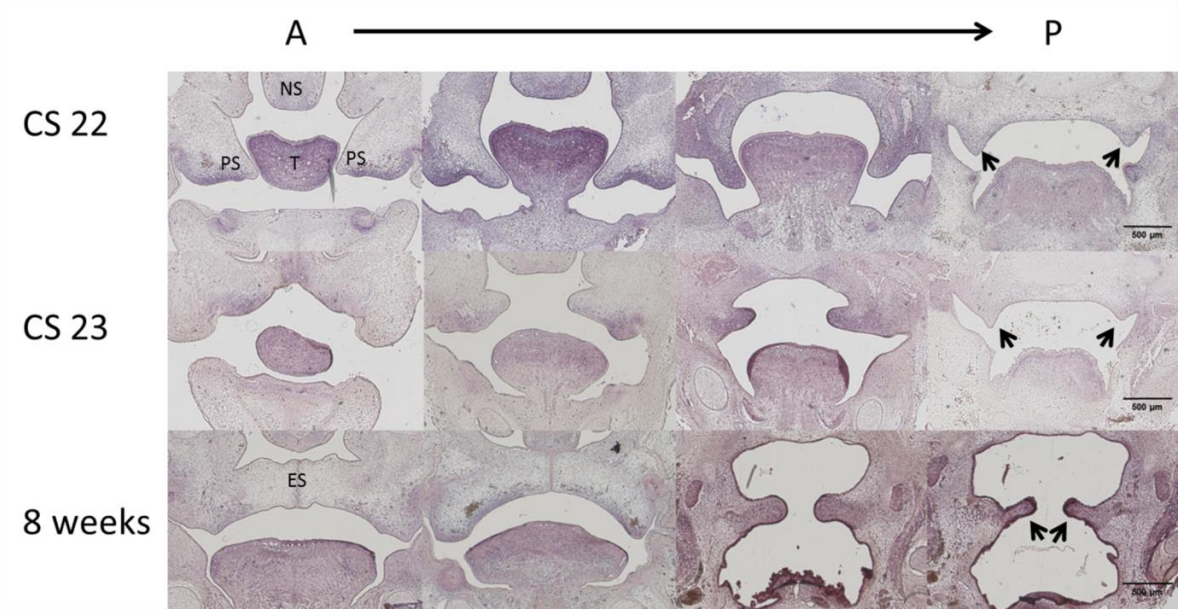

Figure V. 20. Expression of *FOXF2* in the oral cavity of human embryos.
Coronal sections of anterior to posterior (left to right) of human embryo heads at CS22, CS23 and L8pcw (top, middle and bottom panels respectively), showing maxilla, tongue and palatal shelves. The second column is approximately mid palate, the third column is towards the back of the palatal shelves and the fourth column is from among the last sections in each embryo that show the rudimentary palatal shelves (arrow heads) which on fusion will become the uvula. Expression of *FOXF2* is seen in the tongue and also in the palatal shelves. In the developing palate, expression is mostly on the oral half of anterior regions, but becomes more widely expressed throughout the posterior palatal shelf mesenchyme and bordering oral tissues. At later stages, expression includes the more posterior oral epithelial surfaces. **PS** - palatal shelf; **NS** - nasal septum; **T** - tongue; **ES** - epithelial seam.

V. 4. 9. Surgical management

As described above, the proband was found to have speech that was significantly affected by the VPI and a decision was made to proceed with surgical palate exploration and IVVP. Surgery was carried out by Mr Brian Sommerlad under general anaesthesia when the patient was nearly 3 years and 2 months of age. The findings on examination of the palate confirmed that there was no uvula and no anterior pillar of the fauces, with a rudimentary posterior pillar and a tight posterior border of the velum. The posterior nasal spine was broad but there was

no significant notch. There was significant adenoid tissue. On exploration of the velar musculature, the PP and levator muscles were directed anteriorly. They were retro-displaced and at the same time the palate lengthened by suturing the posterior pillars of fauces together and then releasing them postero-laterally at the junction with the tonsils. The levator muscles were of reasonable bulk and were sutured together in the midline as posteriorly as possible.

V. 4. 10. Outcome

The patient was seen for reassessment by the speech and language therapist seven months after surgery. In the interim period, he had received language therapy in Egypt twice a week by one therapist and therapy for the speech disorder thrice weekly by another. It was noted how he had made considerable progress in his language skills, now using 4 and sometimes 5 word sentences.

In his spontaneous speech, he was judged to have moderate hypernasality, but in words and syllables with the correct bilabial plosives, in the context of both high and low vowels, he had oral tone e.g. on words such as /baby/, /bay/, /poppy/, /piper/, /paper/. There was no longer accompanying nasal emission on targets such as /p/, /b/. The pattern of favoured placement of backed consonants to velar, with velar nasal fricatives and frequent syllabic nasals was still present. However, he was now inconsistently using targets /t/, /d/. There was still the developmental immaturity of consonant harmony, which needed to be taken into account in the vocabulary used in therapy. In terms of stimulability, a range of consonants not used in his sound system /f/, /n/, /s/, /sh/, /ge/ were elicited.

Follow-up videofluoroscopy showed improved palate mobility and lift to above the plane of the hard palate. The tongue was no longer involved in lifting the velum. The levator insertion, the point of maximum velar mobility, was posterior. Firm closure to the posterior pharyngeal wall appeared to be achieved on this view (Figure V. 21).

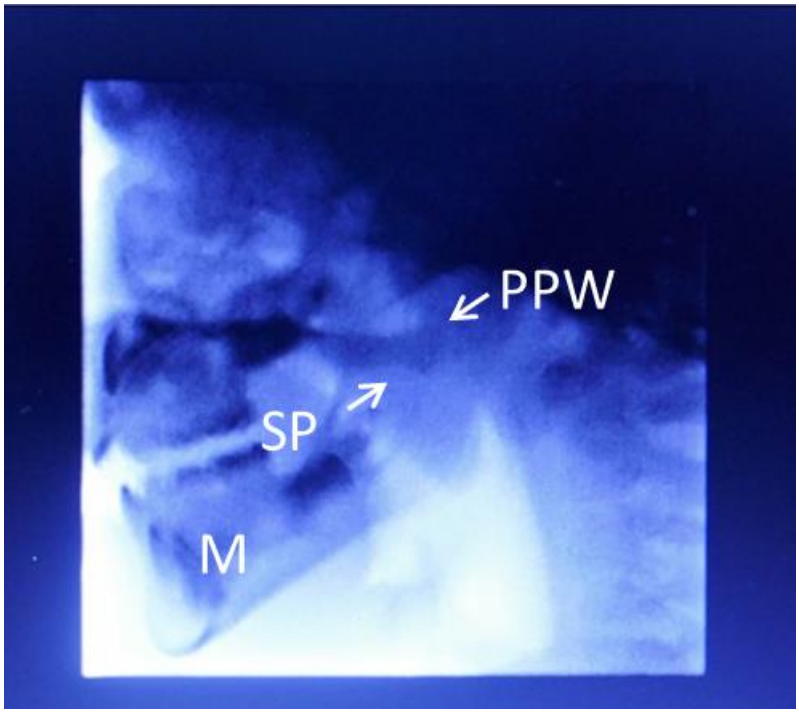

Figure V. 21. Still image from lateral X-ray video saying /i/. Postoperative view.
SP - soft palate; **PPW** - posterior pharyngeal wall; **M** - mandible.

In summary, the patient was judged to now have the structure to make considerable progress in establishing his sound system and resolving his unintelligibility problems. Parents were counselled that there may be some residual mild hypernasality, but this would only be known once the sound system difficulties had resolved. At further review at age 5 and 7 years, his speech was within normal limits.

V. 5. Discussion

In this study, a putative dominantly acting missense mutation in the activation domain of *FOXF2* was identified, which fully segregated in a multigeneration family that includes 8 affected individuals, presenting with absent uvula, short posterior border of the soft palate, and abnormal pillars of the fauces. From screening available literature and based on the extensive experience of Mr Brian Sommerlad and the North Thames Cleft team, this is a very rare disorder of palate development. In the mouse, *Foxf2* is expressed in the posterior region of the secondary palate, and homozygous loss of function results in a complete cleft of the secondary palate (Wang et al., 2003). Although mice naturally lack an uvula, we show here that *FOXF2* is also expressed in the posterior human palate during development, including the rudimentary uvula.

The *FOXF2* variant was identified using a combination of linkage analysis and exome sequencing, followed by more detailed segregation analysis. Cytogenetic analyses, which were also performed during the preliminary investigation, revealed two small duplicated regions in 6p25.3. These flank but do not overlap with the *FOXF2* locus and also fully segregate with the phenotype. The larger of these gains overlaps with two genes *FOXC1* and *GMDS*, known for their associated pathology. In fact, gains or losses of this interval, as well as dominant mutations in *FOXC1,* are reported to cause glaucoma and/or Axenfeld-Rieger syndrome, which is characterized by Dandy Walker malformation and cerebellar hypoplasia, sometimes including micro- or hypodontia (Gould et al., 1997, Aldinger et al., 2009). In another report, duplication of this interval was also reported, in a large pedigree that was characterized by glaucoma and iris hypoplasia (Lehmann et al., 2000). *GMDS* encodes a key enzyme required for fucose metabolism (Ohyama et al., 1998) and is associated with glaucoma due to its proximity to *FOXC1* and involvement in the same disease causing CNVs (Aldinger et al., 2009). However, in the Egyptian family, none of the individuals with the duplication display any obvious eye or brain malformations. The family was advised about the possibility of developing glaucoma and several members have been for ophthalmology checkups which were not remarkable. This collectively suggests that despite the overwhelming literature reporting pathology associated with this duplication, the

CNV at least in this family, is seemingly benign. We currently have no explanation for this, although one possibility is that the CNV could have occurred on a genetic background that was protective. There are several known examples of protective alleles such as in type 2 diabetes (Steinthorsdottir et al., 2014), lowering LDL cholesterol (Cohen et al., 2005) and cardiovascular disease (Wenquan et al., 2011).

Notably, the *FOXF2* variant lies only ~200 kb distant to the proximal duplication. Decipher lists >60 individuals who have chromosomal gains or losses encompassing this region (Firth et al., 2009). While the majority of these have eye anomalies, 1 individual with a 1.7 Mb duplication including *FOXF2* was reported to have a bifid uvula as well as hyperparathyroidism (Figure V. 5). This CNV was inherited from an unaffected father. Another individual with a small heterozygous deletion including only the *FOXQ1* and *FOXF2* loci (Figure V. 5) was reported to have a hypoplastic uvula and dysarthria, among other pathologies. This individual also had a *de novo* Chr5 duplication and a Chr2 duplication, while the 6p loss was implied benign, being inherited from his apparently unaffected father. Nevertheless, this rare description in Decipher and the precise location are striking.

A possible explanation for how a copy number gain could influence nearby gene expression during palate development is via disruption of a local topologically associated domain (TAD) (Lupianez et al., 2016, Thieme and Ludwig, 2017). TADs which define boundary regions where DNA sequences such as promoter-enhancer contacts occur are often marked by CTCF binding sites. Although cells relevant to fetal uvula development have not yet been investigated, numerous CTCF binding sites conserved across multiple cell lines have been identified (http://genome.ucsc.edu/). These include at least one within the CNV immediately distal to *FOXF2*, which, by impacting a relevant TAD, could compound with the effect of the missense mutation. In the context of the family reported here, given the proximity and shared segregation, it is therefore difficult to rule out a role for both the CNV and the missense variant in the causality of the uvula phenotype.

Forkhead genes encode transcription factors characterized by a 'winged helix' DNA binding domain. Mammals have two *FoxF* genes, *FoxF1* and *FoxF2*,

previously called *FREAC-1* and *FREAC-2* or *FKHL5* and *FKHL6* in man and *Lun* in mouse (Carlsson and Mahlapuu, 2002, Clevidence et al., 1994, Pierrou et al., 1994, Miura et al., 1998). *FOXF2* consist of two exons separated by an intron. The first exon encodes the forkhead DNA-binding domain and one of the transcriptional activation domains AD2. The second exon contains the coding sequence corresponding to the C-terminal activation domain AD1 (Figure V. 10) (Blixt et al., 1998). *Foxf2* is located on Chr6p25.3 and plays a crucial role in mouse and rat models (Bu et al., 2015). It is expressed in the mesenchyme of the oral cavity and the tongue, the fetal and adult lung, placenta, at low levels in the prostate, small intestine, colon and fetal brain. In the palate, it is particularly strongly expressed in the posterior secondary palate, especially immediately prior and during palatal shelf fusion (Nik et al., 2016, Xu et al., 2016). There is no difference between its expression in mouse and rat tissues, which suggest that the developmental role of the *Foxf2* gene may be universal in mammals (Aitola et al., 2000). *Foxf1* is more widely expressed in early embryogenesis, and knockout mice die by midgestation caused by the vascular system abnormalities (Ormestad et al., 2004).

Foxf2 is a downstream target of an epithelia-mesenchymal interference in the developing palate (Nik et al., 2016). It starts with Fgf10 from the mesenchyme activating *Shh* expression in the epithelium (Rice et al., 2004). *Shh* activates *Foxf2* expression in the mesenchyme. This pathway is linked to the expression of several genes responsible for Tgfβ signalling with consequences for collagen accumulation and mesenchymal proliferation. Suspension of Tgfβ signalling in palatal shelf mesenchyme by targeting *Tgfβr2* in neural crest leads to upregulation of *Foxf2* expression. Genetic inactivation of many components of this sequence, upstream and downstream of *Foxf2* causes CP with mesenchymal hypoplasia. Significant reduction in proliferation in posterior palate at E13.5 is observed where *Foxf2* expression is highest and is least overlapped with expression of *Foxf1*.

Between E13.5 and E14.5 cellular proliferation and ECM accumulation are responsible for rapid expansion of the palatal shelves. Both factors are reduced in the *Foxf2* mutant which can explain the developmental palate defect. Elimination of mesenchymal Tgfβ signalling by targeting the only Tgfβ ligand expressed in the mesenchyme, Tgfβ2 or the Tgfβ receptor specifically in the mesenchyme results in

CP phenotype with hypoplastic shelves, very similar to the *Foxf2* mutant (Varga et al., 1987). As a transcription factor with potentially targeting many genes, FOXF2 may influence palatal development in general, as well as Tgfβ signalling in particular, in several ways.

The majority of E18.5 *Foxf2*$^{-/-}$ pups have a wide CP with no intermediate forms observed. It is apparent that FOXF2 activity is limited to a short period at the initiation of palatal shelf expansion (Nik et al., 2016). Tgfβ is itself a potent activator of integrin and fibronectin expression (Hocevar et al., 1999). The positive feedback loop this creates (Margadant and Sonnenberg, 2010) is a likely mechanism basis for the 'all or nothing' palatal phenotype of *Foxf2* mutants (Nik et al., 2016, Xu et al., 2016).

Kaufmann and Knochel (1996) described the importance of the forkhead protein family in embryonic development (Kaufmann and Knochel, 1996). As examples, targeted disruption of the mouse *Foxa2* gene resulted in defects of node and notochord formation (Ang and Rossant, 1994), while *Foxc1* knockout mice die at birth with hydrocephalus and skeletal defects (Pierrou et al., 1994) and *Foxj1* mutant mice display an absence of cilia and random left-right asymmetry (Levin et al., 1995). Although the forkhead family has been studied extensively, the functions of most of its members are still unknown. Wang et al. (2003) investigated the significance of *Foxf2* in a number of ways including gene targeting, histology, immunohistochemistry, cell proliferation assays, *in situ* hybridization and skeletal analysis. The most notable defect was that new born *Foxf2*$^{-/-}$ mice were unable to suckle, as revealed by the absence of visible milk in their stomachs shortly after birth and died within 12-18 hours (Wang et al., 2003). Further investigation showed that this was caused by a CP and inability to achieve negative pressure in the oral cavity.

Xu et al. (2016) showed strikingly correspondent patterns of ectopic *Fgf18* expression in the palatal mesenchyme and concomitant loss of *Shh* expression in the palatal epithelium in *Foxf2* mutant embryos by *in situ* hybridization analysis. The palatal shelf expression zones correlated with areas where *Foxf2* but not *Foxf1* was expressed during normal palatogenesis. Also, inactivation of *Foxf2* and

Foxf1 resulted in ectopic activation of *Fgf18* expression throughout the palatal mesenchyme and dramatic loss of *Shh* expression throughout the palatal epithelium. Thus, Xu et al. (2016) described a novel Shh-Foxf-Fgf18-Shh circuit in the palate development molecular network, in which Foxf1 and Foxf2 regulate palatal shelf growth downstream of Shh signalling by repressing *Fgf18* expression in the palatal mesenchyme to ensure maintenance of *Shh* expression in the palatal epithelium (Xu et al., 2016). The expression pattern of *Shox2* marks the anterior half of the developing palatal mesenchyme (Xu et al., 2016). The level of *Shox2* mRNA expression in the anterior region of the palatal shelves was reduced in *Foxf2*$^{-/-}$ mutant embryos in comparison with the WT littermates. RTqPCR analysis validated the significantly increased expression of *Fgf18* and reduced expression of *Shox2* in the *Foxf2*$^{-/-}$ mutant palatal mesenchyme, consistent with results from whole mount *in situ* hybridization.

In a parallel study published around the same time, Nik et al. (2016) proposed that gene expression changes in palatal shelf mesenchyme that lead to reduced Tgfβ signalling contribute to the CP in *Foxf2*$^{-/-}$ mice. Expression of several genes encoding extracellular proteins important for Tgfβ signalling were reduced such as a fibronectin splice-isoform essential for formation of extracellular Tgfβ latency complexes. For example, Tgfβr3 which acts as a co-receptor and an extracellular reservoir of Tgfβ and integrins αV and β1, which are both Tgfβ targets and required for activation of latent Tgfβ (Nik et al., 2016). Mice lacking *Tgfβ3* exhibit a failure of the palate shelves to fuse, causing CP with incomplete penetrance (Proetzel et al., 1995). *TGFβ3* has also been reported to contribute to the aetiology of SMCP based on an association study of 12 candidate genes (Reiter et al., 2012). In this study, 24 SNPs were genotyped in a sample of 103 nonsyndromic SMCP patients of German origin and compared the allele frequencies with 279 healthy controls.

FOXF2 has been well characterized as a transcription factor and was found to consist of a DNA binding domain and 2 transcriptional activation domains, AD1 and AD2 (Blixt et al., 1998). The p.Q433P variant in *FOXF2* is located within AD1 (Hellqvist et al., 1998) and was predicted to be damaging by bioinformatics analysis. We therefore investigated transcriptional activity of WT and p.Q433P FOXF2 proteins with a luciferase reporter assay in HeLa and HepG2 cells as

previously described (Hellqvist et al., 1998). Surprisingly, we found that the variant resulted in significant upregulation of FOXF2 protein. Since transcript levels were constant, this might be explained by more efficient protein translation or by increased protein stability. Alternatively, high levels of overexpressed WT protein might be problematic for the cells; therefore, translation is actively restricted or the protein rapidly degraded. None of these possibilities were investigated further here but would be interesting to pursue in future work. In the context of increased protein levels, the reporter analysis showed a net increase in luciferase activity as compared with WT. However, expression levels are driven by the constitutive CMV promoter in the construct and are not designed to replicate regulation of this locus *in vivo*. By expressing the activity as a factor of the protein level, the variant resulted in a considerable loss of activity, which might more truly reflect the result of mutation in the activation domain. It was therefore interesting to note a comparative increase in *FGF18* expression (although not *Shox2*) (Xu et al., 2016) in HeLa cells overexpressing mutant versus WT FOXF2, which was the same general trend observed for mice lacking *Foxf2* (Nik et al., 2016). Despite these cells not being a biologically relevant cell type for native *FOXF2* expression, overall a similar effect was replicated.

Further evidence for a role of *FOXF2* in orofacial clefts was reported by Bu et al. (2015) who identified an association between two intronic SNPs within the gene and the occurrence of NS CL/P in an Asian population (Bu et al., 2015). Therefore, in an attempt to identify further mutations in *FOXF2*, we chose to investigate a cohort of CP and SMCP patients. In the absence of other cases with an absent uvula and hypernasality phenotype, these patients were considered the most likely to be on the same phenotypic spectrum, especially since SMCP is often associated with bifid uvula, however, we did not find any likely causal mutations. Instead, only two rare missense variants from the N-terminal portion of the protein were identified, both of which were predicted ‘benign’ by bioinformatics analysis. It is possible that patients with NS CLP might have been a better cohort, as suggested by the association data (Bu et al., 2015), but this remains to be tested. Furthermore, non-coding regulatory elements should not be ignored (Seto-Salvia and Stanier, 2014, Thieme and Ludwig, 2017). Nevertheless, our data potentially

reflects the rarity of the absent uvula and hypernasality phenotype and lack of phenotype-genotype overlap with other palate anomalies.

While *FOXF2* is strongly implicated for absent uvula, nearby chromosomal duplications are confounding factors that may also contribute, potentially in combination with the *FOXF2* variant, by affecting transcriptional regulation of this or nearby genes. Further detailed analysis will be required to investigate the precise mechanisms involved and for example whether this combination may have an effect on penetrance of this condition. In the future it would be very helpful to identify further families with a similar phenotype who also have mutations in this gene or nearby CNVs to further dissect their individual roles.

From a clinical perspective, we have described the clinical findings and management of a four-generational family with absent uvula and abnormal features of the oropharynx, associated with hypernasality. The presenting patient had a significant speech disorder and language delay associated with velopharyngeal incompetence, which led to a referral to a Cleft Lip and Palate Team for management. The other affected family members had less severe hypernasality, and did not present with significant problems in their sound systems (according to family reporting and assessment of II.2, II.3, III.3, III.4, III.5, III.6 family members by Mr Brian Sommerlad). As such, they were not considered candidates for surgery. This may be in part due to the more severe speech disorder in the patient, but may also reflect the general lack of available services in Egypt for the earlier generations, and comment on the society's acceptance of speech differences at that time.

Velar surgery was performed on the patient when he was 3 years and 2 months old. The operation involved lengthening the palate by suturing together the posterior pillars of the fauces and then releasing them inferiorly together with dissection and retropositioning of the palate musculature - especially the levator (Sommerlad, 2003). Follow-up seven months after surgery demonstrated significant improvement in speech, evidenced from the perceptual assessment, and velar function as demonstrated on lateral videofluoroscopy, and he went on to

completely resolve his speech difficulties supported by speech therapy intervention.

There are two interesting observations to be made. First, the degree of hypernasality was described as mild preoperatively and moderate postoperatively, suggesting perhaps a lack of improvement with surgery. However, there was important evidence for improvement in oral tone in the context of correct consonant production across both high and low vowels. This latter observation was very important in advising on the need for continuing therapy and likely success of the surgery. The apparent conflicting evidence of worsening hypernasality was a direct result of longer utterances postoperatively reflecting the resolving language delay observed at the initial appointment. Second, postoperative management recommended continuing therapy for the persistent articulation difficulties, rather than structurally related speech phenomena of hypernasality or nasal emission. Correcting the nasal fricatives and syllabic nasals resulted in habituating oral tone throughout speech, evidence for which was found at the postoperative assessment. He has continued to be seen annually by the surgeon. At the age of 5 and 7 years, his speech was recorded and assessed as having complete resolution of the articulatory difficulties.

V. 6. Conclusion

Disease causing gene identification enables a molecular diagnosis which is extremely valuable to the patient and their family. It provides insight and understanding as to why the condition has arisen in addition to future risk assessment, carrier testing and the possibility of prenatal diagnosis. From a research point of view, gene identification is the first step in understanding the disease and the physiological role of the underlying protein. In many cases, it is a key step in the development of therapeutic strategies and their translation into clinical practice. An important focus of this thesis was to study rare forms of palate phenotype, including the identification of novel genes that when disrupted cause such a palate abnormality. In this chapter, we have studied a multiplex Egyptian family who presented with a rare condition described as autosomal dominant hypernasality and absent uvula palate.

The extended pedigree was subjected to cytogenetic and linkage analysis. We then chose to use the unbiased screening strategy of WES rather than selecting and analysing candidate genes individually. WES analysis was performed on two distant affected cousins and one unaffected aunt who herself has 3 unaffected children, making it unlikely that she was a carrier of a non-penetrant mutant allele. Twenty-one candidate variants were identified following Ingenuity analysis and 11 of these were excluded when compared to the linkage analysis. The ten remaining variants were then examined as possible candidates, starting with Sanger sequencing which confirmed the validity of each. Bioinformatics screening was also used to assess the potential effects of the sequence change on protein function but the findings were not considered discriminatory. The recruitment of three additional family members, one affected and two unaffected individuals was extremely helpful allowing further segregation analysis. This proved highly informative and excluded 9 of the 10 genes, leaving *FOXF2* as the most likely candidate. Through WES, linkage analysis and functional studies, we have identified a missense variant in *FOXF2* as the likely cause of autosomal dominant hypernasality and absent uvula palate.

The original cytogenetic analyses revealed two small duplicated regions in 6p25.3 which flank but do not overlap with the *FOXF2* locus. These CNVs also fully segregated with the phenotype. The larger of these gains overlapped with two genes *FOXC1* and *GMDS*, known for their associated pathology. However, in the Egyptian family, none of the individuals with the duplication display any obvious eye or brain malformations. The family was advised about the possibility of developing glaucoma and several members have been for ophthalmology checkups which were not remarkable. This collectively suggests that despite the overwhelming literature reporting pathology associated with this duplication, the CNV at least in this family, is seemingly benign.

It is known that that *Foxf2* is expressed in mice palate tissue and knockout of the gene leads to CP in the majority of E18.5 null pups (Nik et al., 2016). Investigation of *FOXF2/Foxf2* gene has its own limitations. While mouse studies are extremely valuable, they also provide limited information in this case since mice are lacking the anatomical structure of an uvula. Furthermore, homozygous knockout mice develop a lethal overt CP. Studies of human embryos showed that *FOXF2* expression occurs at the back of the palatal shelves, but visualization of the fully formed uvula is not really possible at early stages of human embryos development. Nevertheless, the results of our study add to knowledge from previous studies and suggest *FOXF2* as a novel gene for posterior palate and velopharynx development.

Our findings are important for future counselling particularly in this extended Egyptian family. The clinical representation of this rare form of palate defect, assessment tools and treatment options could be a useful guide for any similar cases. Potential risk and prognosis based on current outcomes can be assessed based on the clinical history of this Egyptian family.

Close collaboration should be encouraged between clinicians, geneticist and researchers. Understanding this condition may allow health care professionals to better recognize rare forms of palate pathology, which can result in earlier referral of patients to specialized centres for diagnosis and treatment in a timely manner.

V. 7. Future work

Publication of this work will bring the case to the attention of the relevant scientific and clinical community. This is important as it may allow the identification of more families with autosomal dominant unusual velopharyngeal anatomy leading to hypernasality. This would help to confirm the role of *FOXF2* and may better explain the importance of the surrounding genomic environment.

Finding novel genes that interact with or are downstream of the FOXF2 transcriptional pathway will allow a better understanding of normal palate development and its pathogenesis. Further transcriptional targets could be identified by performing RNA-Seq on flow sorted palatal shelf tissue specific cells between WT and *Foxf2*$^{-/-}$ in both CM and CNC derived tissue (as described in Chapter IV: Investigation of transcriptional changes downstream of *Tbx22* during mouse palate development). This would complement similar studies performed by Xu et al. (2016), who used *Osr2*-Cre at E13.5 (*Foxf2* expression peak). It may be helpful to include earlier and later embryo stages to monitor the *Foxf2*-dependant differentially expressed genes during development (Xu et al., 2016).

Another line of inquiry would be to investigate the duplicated regions in 6p25.3 overlapping with two known genes *FOXC1* and *GMDS.* Our study suggests that despite the overwhelming literature reporting pathology associated with this duplication, the CNV at least in this family, is seemingly benign. There are several known examples of protective alleles and there is a possibility the CNV could have occurred on a genetic background that was protective (Steinthorsdottir et al., 2014, Cohen et al., 2005). It might be possible to answer this question by generating transgenic mice mimicking aspects of the Egyptian families Chr6p region, to look for effects on *Foxc1*-dependent phenotypes.

REFERENCE

ABDUELMULA, A., HUANG, R., PU, Q., TAMAMURA, H., MOROSAN-PUOPOLO, G. & BRAND-SABERI, B. 2016. SDF-1 controls the muscle and blood vessel formation of the somite. *Int J Dev Biol,* 60**,** 29-38.

ABOU-KHALIL, R., YANG, F., LIEU, S., JULIEN, A., PERRY, J., PEREIRA, C., RELAIX, F., MICLAU, T., MARCUCIO, R. & COLNOT, C. 2015. Role of muscle stem cells during skeletal regeneration. *Stem Cells,* 33**,** 1501-11.

ABYHOLM, F. E. 1976. Submucous cleft palate. *Scand J Plast Reconstr Surg,* 10**,** 209-12.

ACEVEDO, A. C., DA FONSECA, J. A., GRINHAM, J., DOUDNEY, K., GOMES, R. R., DE PAULA, L. M. & STANIER, P. 2010. Autosomal-dominant ankyloglossia and tooth number anomalies. *J Dent Res,* 89**,** 128-32.

ADAM, M. P., HUDGINS, L. & HANNIBAL, M. 1993. Kabuki Syndrome. *In:* ADAM, M. P., ARDINGER, H. H., PAGON, R. A., WALLACE, S. E., BEAN, L. J. H., STEPHENS, K. & AMEMIYA, A. (eds.) *GeneReviews.* University of Washington, Seattle.

ADOGA, A. A. & NIMKUR, T. L. 2011. The Traditionally Amputated Uvula amongst Nigerians: Still an Ongoing Practice. *ISRN Otolaryngol,* 2011**,** 704924.

ADZHUBEI, I., JORDAN, D. M. & SUNYAEV, S. R. 2013. Predicting functional effect of human missense mutations using PolyPhen-2. *Curr Protoc Hum Genet,* Chapter 7**,** Unit 7.20.

AITOLA, M., CARLSSON, P., MAHLAPUU, M., ENERBACK, S. & PELTO-HUIKKO, M. 2000. Forkhead transcription factor FoxF2 is expressed in mesodermal tissues involved in epithelio-mesenchymal interactions. *Dev Dyn,* 218**,** 136-49.

AKER, M., ROUVINSKI, A., HASHAVIA, S., TA-SHMA, A., SHAAG, A., ZENVIRT, S., ISRAEL, S., WEINTRAUB, M., TARABOULOS, A., BAR-SHAVIT, Z. & ELPELEG, O. 2012. An SNX10 mutation causes malignant osteopetrosis of infancy. *J Med Genet,* 49**,** 221-6.

ALAPPAT, S. R., ZHANG, Z., SUZUKI, K., ZHANG, X., LIU, H., JIANG, R., YAMADA, G. & CHEN, Y. 2005. The cellular and molecular etiology of the cleft secondary palate in Fgf10 mutant mice. *Dev Biol,* 277**,** 102-13.

ALDINGER, K. A., LEHMANN, O. J., HUDGINS, L., CHIZHIKOV, V. V., BASSUK, A. G., ADES, L. C., KRANTZ, I. D., DOBYNS, W. B. & MILLEN, K. J. 2009. FOXC1 is required for normal cerebellar development and is a major contributor to chromosome 6p25.3 Dandy-Walker malformation. *Nat Genet,* 41**,** 1037-42.

ALLORI, A. C., MULLIKEN, J. B., MEARA, J. G., SHUSTERMAN, S. & MARCUS, J. R. 2015. Classification of Cleft Lip/Palate: Then and Now. *Cleft Palate Craniofac J,* 54(2)**,** 175-188.

ALMAIDHAN, A., CESARIO, J., LANDIN MALT, A., ZHAO, Y., SHARMA, N., CHOI, V. & JEONG, J. 2014. Neural crest-specific deletion of Ldb1 leads to cleft secondary palate with impaired palatal shelf elevation. *BMC Dev Biol,* 14**,** 3.

AMELOT, A., CREVIER-BUCHMAN, L. & MAEDA, S. Observations of velopharyngeal closure mechanism in horizontal and lateral direction from fiberscopic data. 2003. 15th International Congress of Phonetic Sciences, 3021-3024.

ANDERS, S. & HUBER, W. 2010. Differential expression analysis for sequence count data. *Genome Biol,* 11**,** R106.

ANDL, T., AHN, K., KAIRO, A., CHU, E. Y., WINE-LEE, L., REDDY, S. T., CROFT, N. J., CEBRA-THOMAS, J. A., METZGER, D., CHAMBON, P., LYONS, K. M., MISHINA, Y., SEYKORA, J. T., CRENSHAW, E. B., 3RD & MILLAR, S. E. 2004. Epithelial Bmpr1a regulates differentiation and proliferation in postnatal hair follicles and is essential for tooth development. *Development,* 131**,** 2257-68.

ANDRADES, P., ESPINOSA-DE-LOS-MONTEROS, A., SHELL, D. H. T., THURSTON, T. E., FOWLER, J. S., XAVIER, S. T., RAY, P. D. & GRANT, J. H., 3RD 2008. The importance of radical intravelar veloplasty during two-flap palatoplasty. *Plast Reconstr Surg,* 122**,** 1121-30.

ANDREOU, A. M., PAUWS, E., JONES, M. C., SINGH, M. K., BUSSEN, M., DOUDNEY, K., MOORE, G. E., KISPERT, A., BROSENS, J. J. & STANIER, P. 2007. TBX22 missense mutations found in patients with X-linked cleft palate affect DNA binding, sumoylation, and transcriptional repression. *Am J Hum Genet,* 81**,** 700-12.

ANG, S. L. & ROSSANT, J. 1994. HNF-3 beta is essential for node and notochord formation in mouse development. *Cell,* 78**,** 561-74.

ANNUNEN, S., KORKKO, J., CZARNY, M., WARMAN, M. L., BRUNNER, H. G., KAARIAINEN, H., MULLIKEN, J. B., TRANEBJAERG, L., BROOKS, D. G., COX, G. F., CRUYSBERG, J. R., CURTIS, M. A., DAVENPORT, S. L., FRIEDRICH, C. A., KAITILA, I., KRAWCZYNSKI, M. R., LATOS-BIELENSKA, A., MUKAI, S., OLSEN, B. R., SHINNO, N., SOMER, M., VIKKULA, M., ZLOTOGORA, J., PROCKOP, D. J. & ALA-KOKKO, L. 1999. Splicing mutations of 54-bp exons in the COL11A1 gene cause Marshall syndrome, but other mutations cause overlapping Marshall/Stickler phenotypes. *Am J Hum Genet,* 65**,** 974-83.

ARNOLD, H. H. & BRAUN, T. 1996. Targeted inactivation of myogenic factor genes reveals their role during mouse myogenesis: a review. *Int J Dev Biol,* 40**,** 345-53.

BACK, G. W., NADIG, S., UPPAL, S. & COATESWORTH, A. P. 2004. Why do we have a uvula?: literature review and a new theory. *Clin Otolaryngol Allied Sci,* 29**,** 689-93.

BAEK, J. A., LAN, Y., LIU, H., MALTBY, K. M., MISHINA, Y. & JIANG, R. 2011. Bmpr1a signaling plays critical roles in palatal shelf growth and palatal bone formation. *Dev Biol,* 350**,** 520-31.

BARIS, I., ARISOY, A. E., SMITH, A., AGOSTINI, M., MITCHELL, C. S., PARK, S. M., HALEFOGLU, A. M., ZENGIN, E., CHATTERJEE, V. K. & BATTALOGLU, E. 2006. A novel missense mutation in human TTF-2 (FKHL15) gene associated with congenital hypothyroidism but not athyreosis. *J Clin Endocrinol Metab,* 91**,** 4183-7.

BEATY, T. H., MURRAY, J. C., MARAZITA, M. L., MUNGER, R. G., RUCZINSKI, I., HETMANSKI, J. B., LIANG, K. Y., WU, T., MURRAY, T., FALLIN, M. D., REDETT, R. A., RAYMOND, G., SCHWENDER, H., JIN, S. C., COOPER, M. E., DUNNWALD, M., MANSILLA, M. A., LESLIE, E., BULLARD, S., LIDRAL, A. C., MORENO, L. M., MENEZES, R., VIEIRA, A. R., PETRIN, A., WILCOX, A. J., LIE, R. T., JABS, E. W., WU-CHOU, Y. H., CHEN, P. K., WANG, H., YE, X., HUANG, S., YEOW, V., CHONG, S. S., JEE, S. H., SHI, B., CHRISTENSEN, K., MELBYE, M., DOHENY, K. F., PUGH, E. W., LING, H., CASTILLA, E. E., CZEIZEL, A. E., MA, L., FIELD, L. L., BRODY, L., PANGILINAN, F., MILLS, J. L., MOLLOY, A. M., KIRKE, P. N., SCOTT, J. M., ARCOS-BURGOS, M. & SCOTT, A. F. 2010. A genome-wide association study of cleft lip with and without cleft palate identifies risk variants near MAFB and ABCA4. *Nat Genet,* 42**,** 525-9.

BEATY, T. H., TAUB, M. A., SCOTT, A. F., MURRAY, J. C., MARAZITA, M. L., SCHWENDER, H., PARKER, M. M., HETMANSKI, J. B., BALAKRISHNAN, P., MANSILLA, M. A., MANGOLD, E., LUDWIG, K. U., NOETHEN, M. M., RUBINI, M., ELCIOGLU, N. & RUCZINSKI, I. 2013. Confirming genes influencing risk to cleft lip with/without cleft palate in a case-parent trio study. *Hum Genet,* 132**,** 771-81.

BEBEE, T. W., PARK, J. W., SHERIDAN, K. I., WARZECHA, C. C., CIEPLY, B. W., ROHACEK, A. M., XING, Y. & CARSTENS, R. P. 2015. The splicing regulators Esrp1 and Esrp2 direct an epithelial splicing program essential for mammalian development. *Elife,* 4.

BENKO, S., FANTES, J. A., AMIEL, J., KLEINJAN, D. J., THOMAS, S., RAMSAY, J., JAMSHIDI, N., ESSAFI, A., HEANEY, S., GORDON, C. T., MCBRIDE, D., GOLZIO, C., FISHER, M., PERRY, P., ABADIE, V., AYUSO, C., HOLDER-ESPINASSE, M., KILPATRICK, N., LEES, M. M., PICARD, A., TEMPLE, I. K., THOMAS, P., VAZQUEZ, M. P., VEKEMANS, M., ROEST CROLLIUS, H., HASTIE, N. D., MUNNICH, A., ETCHEVERS, H. C., PELET, A., FARLIE, P. G., FITZPATRICK, D. R. & LYONNET, S. 2009. Highly conserved non-coding elements on either side of SOX9 associated with Pierre Robin sequence. *Nat Genet,* 41**,** 359-64.

BICK, D., FRANCO, B., SHERINS, R. J., HEYE, B., PIKE, L., CRAWFORD, J., MADDALENA, A., INCERTI, B., PRAGLIOLA, A., MEITINGER, T. & BALLABIO, A. 1992. Brief report: intragenic deletion of the KALIG-1 gene in Kallmann's syndrome. *N Engl J Med,* 326**,** 1752-5.

BICKNELL, S., MCFADDEN, L. R. & CURRAN, J. B. 2002. Frequency of pharyngoplasty after primary repair of cleft palate. *J Can Dent Assoc,* 68**,** 688-92.

BIDDLE, F. G. 1980. Palate development in the mouse: a quantitative method that permits the estimation of time and rate of palate closure. *Teratology,* 22**,** 239-46.

BIRGBAUER, E., SECHRIST, J., BRONNER-FRASER, M. & FRASER, S. 1995. Rhombomeric origin and rostrocaudal reassortment of neural crest cells revealed by intravital microscopy. *Development,* 121**,** 935.

BIRNBAUM, S., LUDWIG, K. U., REUTTER, H., HERMS, S., STEFFENS, M., RUBINI, M., BALUARDO, C., FERRIAN, M., ALMEIDA DE ASSIS, N., ALBLAS, M. A., BARTH, S., FREUDENBERG, J., LAUSTER, C., SCHMIDT, G., SCHEER, M., BRAUMANN, B., BERGE, S. J., REICH, R. H., SCHIEFKE, F., HEMPRICH, A., POTZSCH, S., STEEGERS-THEUNISSEN, R. P., POTZSCH, B., MOEBUS, S., HORSTHEMKE, B., KRAMER, F. J., WIENKER, T. F., MOSSEY, P. A., PROPPING, P., CICHON, S., HOFFMANN, P., KNAPP, M., NOTHEN, M. M. & MANGOLD, E. 2009. Key susceptibility locus for nonsyndromic cleft lip with or without cleft palate on chromosome 8q24. *Nat Genet,* 41**,** 473-7.

BJORK, B. C., TURBE-DOAN, A., PRYSAK, M., HERRON, B. J. & BEIER, D. R. 2010. Prdm16 is required for normal palatogenesis in mice. *Hum Mol Genet,* 19**,** 774-89.

BJORNSSON, A., ARNASON, A. & TIPPET, P. 1989. X-linked cleft palate and ankyloglossia in an Icelandic family. *Cleft Palate J,* 26**,** 3-8.

BLIXT, A., MAHLAPUU, M., BJURSELL, C., DARNFORS, C., JOHANNESSON, T., ENERBACK, S. & CARLSSON, P. 1998. The two-exon gene of the human forkhead transcription factor FREAC-2 (FKHL6) is located at 6p25.3. *Genomics,* 53**,** 387-90.

BOHM, L. A., MILLER, J. E., MORRELL, N., SIDMAN, J. D. & ROBY, B. B. 2019. Surgical Outcomes for the Treatment of Velopharyngeal Insufficiency in 22q11.2 Deletion Syndrome. *Otolaryngol Head Neck Surg*.

BONAVENTURE, J., PHILIPPE, C., PLESSIS, G., VIGNERON, J., LASSELIN, C., MAROTEAUX, P. & GILGENKRANTZ, S. 1992. Linkage study in a large pedigree with Stickler syndrome: exclusion of COL2A1 as the mutant gene. *Hum Genet,* 90**,** 164-8.

BOORMAN, J. G. & SOMMERLAD, B. C. 1985. Levator palati and palatal dimples: their anatomy, relationship and clinical significance. *Br J Plast Surg,* 38**,** 326-32.

BOSMA, J. F. 1953. A correlated study of the anatomy and motor activity of the upper pharynx by cadaver dissection and by cinematic study of patients after maxillo-facial surgery. *Ann Otol Rhinol Laryngol,* 62**,** 51-72.

BOTSTEIN, D., WHITE, R. L., SKOLNICK, M. & DAVIS, R. W. 1980. Construction of a genetic linkage map in man using restriction fragment length polymorphisms. *Am J Hum Genet,* 32**,** 314-31.

BOYCE, J. O., KILPATRICK, N. & MORGAN, A. T. 2018. Speech and language characteristics in individuals with nonsyndromic submucous cleft palate-A systematic review. *Child Care Health Dev,* 44**,** 818-831.

BRAYBROOK, C., DOUDNEY, K., MARCANO, A. C., ARNASON, A., BJORNSSON, A., PATTON, M. A., GOODFELLOW, P. J., MOORE, G. E. & STANIER, P. 2001. The T-box transcription factor gene TBX22 is mutated in X-linked cleft palate and ankyloglossia. *Nat Genet,* 29**,** 179-83.

BRAYBROOK, C., LISGO, S., DOUDNEY, K., HENDERSON, D., MARCANO, A. C., STRACHAN, T., PATTON, M. A., VILLARD, L., MOORE, G. E., STANIER, P. & LINDSAY, S. 2002. Craniofacial expression of human and murine TBX22 correlates with the cleft palate and ankyloglossia phenotype observed in CPX patients. *Hum Mol Genet,* 11**,** 2793-804.

BREELAND, G. & MENEZES, R. G. 2019. Embryology, bone Ossification. *StatPearls.* StatPearls Publishing.

BRINKLEY, L. L. 1980. *In vitro studies of palatal shelf elevation*, Amsterdam: Elsevier/North-Holland.

BRINKLEY, L. L. & BOOKSTEIN, F. L. 1986. Cell distribution during mouse secondary palate closure. II. Mesenchymal cells. *J Embryol Exp Morphol,* 96**,** 111-30.

BRINKLEY, L. L. & MORRIS-WIMAN, J. 1984. The role of extracellular matrices in palatal shelf closure. *Curr Top Dev Biol,* 19**,** 17-36.

BROCK, L. J., ECONOMOU, A. D., COBOURNE, M. T. & GREEN, J. B. 2016. Mapping cellular processes in the mesenchyme during palatal development in the absence of Tbx1 reveals complex proliferation changes and perturbed cell packing and polarity. 228**,** 464-73.

BRONNER, M. E. & SIMOES-COSTA, M. 2016. The Neural Crest Migrating into the Twenty-First Century. *Curr Top Dev Biol,* 116**,** 115-34.

BROWN, N. L., YARRAM, S. J., MANSELL, J. P. & SANDY, J. R. 2002. Matrix metalloproteinases have a role in palatogenesis. *J Dent Res,* 81**,** 826-30.

BRUNEAU, B. G., NEMER, G., SCHMITT, J. P., CHARRON, F., ROBITAILLE, L., CARON, S., CONNER, D. A., GESSLER, M., NEMER, M., SEIDMAN, C. E. & SEIDMAN, J. G. 2001. A murine model of Holt-Oram syndrome defines roles of the T-box transcription factor Tbx5 in cardiogenesis and disease. *Cell,* 106**,** 709-21.

BRUNEEL, L., BETTENS, K., DE BODT, M., ROCHE, N., BONTE, K. & VAN LIERDE, K. 2018. Speech outcomes following Sommerlad primary palatoplasty: Results of the Ghent University Hospital. *J Commun Disord,* 72**,** 111-121.

BRYANT, D., LIU, Y., DATTA, S., HARIRI, H., SEDA, M., ANDERSON, G., PESKETT, E., DEMETRIOU, C., SOUSA, S., JENKINS, D., CLAYTON, P., BITNER-GLINDZICZ, M., MOORE, G. E., HENNE, W. M. & STANIER, P. 2018. SNX14 mutations affect endoplasmic reticulum associated neutral lipid metabolism in autosomal recessive spinocerebellar ataxia 20. *Hum Mol Genet*.

BU, L., CHEN, Q., WANG, H., ZHANG, T., HETMANSKI, J. B., SCHWENDER, H., PARKER, M., CHOU, Y. H., YEOW, V., CHONG, S. S., ZHANG, B., JABS, E. W., SCOTT, A. F. & BEATY, T. H. 2015. Novel evidence of association with nonsyndromic cleft lip with or without cleft palate was shown for single nucleotide polymorphisms in FOXF2 gene in an Asian population. *Birth Defects Res A Clin Mol Teratol,* 103**,** 857-62.

BURDI, A. R. 1968. Distribution of midpalatine cysts: a reevaluation of human palatal closure mechanisms. *J Oral Surg,* 26**,** 41-5.

BURDI, A. R. 2006. Developmental Biology and Morphogenesis of the Face, Lip and Palate. *In:* BERKOWITZ, S. (ed.) *Cleft Lip and Palate.* Berlin, Heidelberg: Springer Berlin Heidelberg.

BURDI, A. R. & FAIST, K. 1967. Morphogenesis of the palate in normal human embryos with special emphasis on the mechanisms involved. *American Journal of Anatomy,* 120**,** 149-159.

BURRIDGE, K. 2017. Focal adhesions: a personal perspective on a half century of progress. *Febs j,* 284**,** 3355-3361.

BUSH, J. O. & JIANG, R. 2012. Palatogenesis: morphogenetic and molecular mechanisms of secondary palate development. *Development,* 139**,** 231-43.

BUSH, J. O., LAN, Y., MALTBY, K. M. & JIANG, R. 2002. Isolation and developmental expression analysis of Tbx22, the mouse homolog of the human X-linked cleft palate gene. *Dev Dyn,* 225**,** 322-6.

BUSH, P. G. & WILLIAMS, A. J. 1983. Incidence of the Robin Anomalad (Pierre Robin syndrome). *Br J Plast Surg,* 36**,** 434-7.

BUTOW, K. W., HOOGENDIJK, C. F. & ZWAHLEN, R. A. 2009. Pierre Robin sequence: appearances and 25 years of experience with an innovative treatment protocol. *J Pediatr Surg,* 44**,** 2112-8.

CAI, Y., PATTERSON, K. E., REINIER, F., KEESECKER, S. E., BLUE, E., BAMSHAD, M. & HADDAD, J., JR. 2017. Copy Number Changes Identified Using Whole Exome Sequencing in Nonsyndromic Cleft Lip and Palate in a Honduran Population. *Birth Defects Res,* 109**,** 1257-1267.

CALNAN, J. 1954. Submucous cleft palate. *Br J Plast Surg,* 6**,** 264-82.

CALNAN, J. 1957. Modern views on Passavant's ridge. *Br J Plast Surg,* 10**,** 89-113.

CANDI, E., RUFINI, A., TERRINONI, A., GIAMBOI-MIRAGLIA, A., LENA, A. M., MANTOVANI, R., KNIGHT, R. & MELINO, G. 2007. DeltaNp63 regulates thymic development through enhanced expression of FgfR2 and Jag2. *Proc Natl Acad Sci U S A,* 104**,** 11999-2004.

CANICK, M. L. 1954. Cleft lip and cleft palate; a review of embryology, pathologic anatomy, and etiology. *Plast Reconstr Surg (1946),* 14**,** 30-46.

CAO, X., ZHANG, W., WAN, T., HE, L., CHEN, T., YUAN, Z., MA, S., YU, Y. & CHEN, G. 2000. Molecular cloning and characterization of a novel CXC chemokine macrophage inflammatory protein-2 gamma chemoattractant for human neutrophils and dendritic cells. *J Immunol,* 165**,** 2588-95.

CAOUETTE-LABERGE, L., BAYET, B. & LAROCQUE, Y. 1994. The Pierre Robin sequence: review of 125 cases and evolution of treatment modalities. *Plast Reconstr Surg,* 93**,** 934-42.

CARLSSON, P. & MAHLAPUU, M. 2002. Forkhead transcription factors: key players in development and metabolism. *Dev Biol,* 250**,** 1-23.

CARREIRA, S., DEXTER, T. J., YAVUZER, U., EASTY, D. J. & GODING, C. R. 1998. Brachyury-related transcription factor Tbx2 and repression of the melanocyte-specific TRP-1 promoter. *Mol Cell Biol,* 18**,** 5099-108.

CARSTENS, M. 2017. Pathologic anatomy of the soft palate, part 2: The soft tissue lever arm, pathology, and surgical correction. *Journal of Cleft Lip Palate and Craniofacial Anomalies,* 4**,** 83-108.

CARSTENS, M. H. 2002. Development of the facial midline. *J Craniofac Surg,* 13**,** 129-87; discussion 188-90.

CARVAJAL MONROY, P. L., GREFTE, S., KUIJPERS-JAGTMAN, A. M., HELMICH, M. P., ULRICH, D. J., VON DEN HOFF, J. W. & WAGENER, F. A. 2013. A rat model for muscle regeneration in the soft palate. *PLoS One,* 8**,** e59193.

CASEY, L. M., LAN, Y., CHO, E. S., MALTBY, K. M., GRIDLEY, T. & JIANG, R. 2006. Jag2-Notch1 signaling regulates oral epithelial differentiation and palate development. *Dev Dyn,* 235**,** 1830-44.

CASTELLUCCI, G. A., MCGINLEY, M. J. & MCCORMICK, D. A. 2016. Knockout of Foxp2 disrupts vocal development in mice. *Sci Rep,* 6**,** 23305.

CECCONI, F., ALVAREZ-BOLADO, G., MEYER, B. I., ROTH, K. A. & GRUSS, P. 1998. Apaf1 (CED-4 homolog) regulates programmed cell death in mammalian development. *Cell,* 94**,** 727-37.

CELLI, J., DUIJF, P., HAMEL, B. C., BAMSHAD, M., KRAMER, B., SMITS, A. P., NEWBURY-ECOB, R., HENNEKAM, R. C., VAN BUGGENHOUT, G., VAN HAERINGEN, A., WOODS, C. G., VAN ESSEN, A. J., DE WAAL, R., VRIEND, G., HABER, D. A., YANG, A., MCKEON, F., BRUNNER, H. G. & VAN BOKHOVEN, H. 1999. Heterozygous germline mutations in the p53 homolog p63 are the cause of EEC syndrome. *Cell,* 99**,** 143-53.

CHAABOUNI, M., SMAOUI, N., BENNEJI, N., M'RAD, R., JEMAA, L. B., HACHICHA, S. & CHAABOUNI, H. 2005. Mutation analysis of TBX22 reveals new mutation in Tunisian CPX family. *Clin Dysmorphol,* 14**,** 23-5.

CHAI, Y., JIANG, X., ITO, Y., BRINGAS, P., JR., HAN, J., ROWITCH, D. H., SORIANO, P., MCMAHON, A. P. & SUCOV, H. M. 2000. Fate of the mammalian cranial neural crest during tooth and mandibular morphogenesis. *Development,* 127**,** 1671-9.

CHAROENCHAIKORN, K., YOKOMIZO, T., RICE, D. P., HONJO, T., MATSUZAKI, K., SHINTAKU, Y., IMAI, Y., WAKAMATSU, A., TAKAHASHI, S., ITO, Y., TAKANO-YAMAMOTO, T., THESLEFF, I.,

YAMAMOTO, M. & YAMASHIRO, T. 2009. Runx1 is involved in the fusion of the primary and the secondary palatal shelves. *Dev Biol,* 326**,** 392-402.
CHEN, C. P., CHANG, S. J., CHERN, S. R., WU, P. S., CHEN, Y. T., SU, J. W., CHEN, W. L. & WANG, W. 2013. Prenatal diagnosis and molecular cytogenetic characterization of a de novo interstitial deletion of 7q (7q22.1-->q31.1). *Gene,* 521**,** 311-5.
CHEN, P. K., WU, J., HUNG, K. F., CHEN, Y. R. & NOORDHOFF, M. S. 1996. Surgical correction of submucous cleft palate with Furlow palatoplasty. *Plast Reconstr Surg,* 97**,** 1136-46; discussion 1147-9.
CHEN, P. K., WU, J. T., CHEN, Y. R. & NOORDHOFF, M. S. 1994. Correction of secondary velopharyngeal insufficiency in cleft palate patients with the Furlow palatoplasty. *Plast Reconstr Surg,* 94**,** 933-41; discussion 942-3.
CHEN, X., WANG, Z., DUAN, N., ZHU, G., SCHWARZ, E. M. & XIE, C. 2018. Osteoblast-osteoclast interactions. *Connect Tissue Res,* 59**,** 99-107.
CHILKOTI, G. T., MOHTA, M., KARTHIK, G. & SAXENA, A. K. 2017. Absent Uvula: What Mallampati Class? *Indian J Anaesth,* 61**,** 85-86.
CHIPETA, J., BANDA, J., MBINGA, M. & WA-SOMWE, S. 2009. Absent uvula and thrombocytopenia in an African infant with job's syndrome: Case report and review of literature. *J Infect Dis Immun***,** 1-5.
CHIQUET, M., BLUMER, S., ANGELINI, M., MITSIADIS, T. A. & KATSAROS, C. 2016. Mesenchymal Remodeling during Palatal Shelf Elevation Revealed by Extracellular Matrix and F-Actin Expression Patterns. *Front Physiol,* 7**,** 392.
CHOI, Y. & CHAN, A. P. 2015. PROVEAN web server: a tool to predict the functional effect of amino acid substitutions and indels. *Bioinformatics,* 31**,** 2745-7.
CHUO, C. B., SEARLE, Y., JEREMY, A., RICHARD, B. M., SHARP, I. & SLATOR, R. 2008. The continuing multidisciplinary needs of adult patients with cleft lip and/or palate. *Cleft Palate Craniofac J,* 45**,** 633-8.
CLEVIDENCE, D. E., OVERDIER, D. G., PETERSON, R. S., PORCELLA, A., YE, H., PAULSON, K. E. & COSTA, R. H. 1994. Members of the HNF-3/forkhead family of transcription factors exhibit distinct cellular expression patterns in lung and regulate the surfactant protein B promoter. *Dev Biol,* 166**,** 195-209.
COBOURNE, M. T. & SHARPE, P. T. 2003. Tooth and jaw: molecular mechanisms of patterning in the first branchial arch. *Arch Oral Biol,* 48**,** 1-14.
COHEN, J., PERTSEMLIDIS, A., KOTOWSKI, I. K., GRAHAM, R., GARCIA, C. K. & HOBBS, H. H. 2005. Low LDL cholesterol in individuals of African descent resulting from frequent nonsense mutations in PCSK9. *Nat Genet,* 37**,** 161-5.
COLE, P., BANERJI, S., HOLLIER, L. & STAL, S. 2008. Two hundred twenty-two consecutive pharyngeal flaps: an analysis of postoperative complications. *J Oral Maxillofac Surg,* 66**,** 745-8.
COLEMAN, R. D. 1965. Development of the rat palate. *Anat Rec,* 151**,** 107-17.
CONTE, F., OTI, M., DIXON, J., CARELS, C. E., RUBINI, M. & ZHOU, H. 2016. Systematic analysis of copy number variants of a large cohort of orofacial cleft patients identifies candidate genes for orofacial clefts. *Hum Genet,* 135**,** 41-59.
COSTA-SILVA, J., DOMINGUES, D. & LOPES, F. M. 2017. RNA-Seq differential expression analysis: An extended review and a software tool. 12**,** e0190152.
COULY, G., GRAPIN-BOTTON, A., COLTEY, P. & LE DOUARIN, N. M. 1996. The regeneration of the cephalic neural crest, a problem revisited: the regenerating cells originate from the contralateral or from the anterior and posterior neural fold. *Development,* 122**,** 3393-407.
CROCKETT, D. J. & GOUDY, S. L. 2014. Cleft lip and palate. *Facial Plast Surg Clin North Am,* 22**,** 573-86.

CUERVO, R. & COVARRUBIAS, L. 2004. Death is the major fate of medial edge epithelial cells and the cause of basal lamina degradation during palatogenesis. *Development,* 131**,** 15-24.

CUI, X. M., SHIOMI, N., CHEN, J., SAITO, T., YAMAMOTO, T., ITO, Y., BRINGAS, P., CHAI, Y. & SHULER, C. F. 2005. Overexpression of Smad2 in Tgf-beta3-null mutant mice rescues cleft palate. *Dev Biol,* 278**,** 193-202.

D'ANGELO, M., CHEN, J. M., UGEN, K. & GREENE, R. M. 1994. TGF beta 1 regulation of collagen metabolism by embryonic palate mesenchymal cells. *J Exp Zool,* 270**,** 189-201.

DARLING, D. S., STEARMAN, R. P., QI, Y., QIU, M. S. & FELLER, J. P. 2003. Expression of Zfhep/deltaEF1 protein in palate, neural progenitors, and differentiated neurons. *Gene Expr Patterns,* 3**,** 709-17.

DAS, S. & MUNSHI, A. 2018. Research advances in Apert syndrome. *J Oral Biol Craniofac Res,* 8**,** 194-199.

DAUGHERTY, A. 2017. Achondroplasia: Etiology, Clinical Presentation, and Management. *Neonatal Netw,* 36**,** 337-342.

DE BLACAM, C., SMITH, S. & ORR, D. 2018. Surgery for Velopharyngeal Dysfunction: A Systematic Review of Interventions and Outcomes. *Cleft Palate Craniofac J,* 55**,** 405-422.

DEPEW, M. J., SIMPSON, C. A., MORASSO, M. & RUBENSTEIN, J. L. 2005. Reassessing the Dlx code: the genetic regulation of branchial arch skeletal pattern and development. *J Anat,* 207**,** 501-61.

DICKSON, D. R. 1972. Normal and cleft palate anatomy. *Cleft Palate J,* 9**,** 280-93.

DICKSON, D. R. 1975. Anatomy of the normal velopharyngeal mechanism. *Clin Plast Surg,* 2**,** 235-48.

DIEFFENBACH, C. W., LOWE, T. M. & DVEKSLER, G. S. 1993. General concepts for PCR primer design. *PCR Methods Appl,* 3**,** S30-7.

DING, H., WU, X., BOSTROM, H., KIM, I., WONG, N., TSOI, B., O'ROURKE, M., KOH, G. Y., SORIANO, P., BETSHOLTZ, C., HART, T. C., MARAZITA, M. L., FIELD, L. L., TAM, P. P. & NAGY, A. 2004. A specific requirement for PDGF-C in palate formation and PDGFR-alpha signaling. *Nat Genet,* 36**,** 1111-6.

DIXON, M. J. 1996. Treacher Collins syndrome. *Hum Mol Genet,* 5 Spec No**,** 1391-6.

DIXON, M. J., MARAZITA, M. L., BEATY, T. H. & MURRAY, J. C. 2011. Cleft lip and palate: understanding genetic and environmental influences. *Nat Rev Genet,* 12**,** 167-78.

DIXON, P. 2010. Chapter One - Structure and function of the genome. *In:* BENNETT, P. & WILLIAMSON, C. (eds.) *Basic Science in Obstetrics and Gynaecology (Fourth Edition).* Churchill Livingstone.

DODE, C., LEVILLIERS, J., DUPONT, J. M., DE PAEPE, A., LE DU, N., SOUSSI-YANICOSTAS, N., COIMBRA, R. S., DELMAGHANI, S., COMPAIN-NOUAILLE, S., BAVEREL, F., PECHEUX, C., LE TESSIER, D., CRUAUD, C., DELPECH, M., SPELEMAN, F., VERMEULEN, S., AMALFITANO, A., BACHELOT, Y., BOUCHARD, P., CABROL, S., CAREL, J. C., DELEMARRE-VAN DE WAAL, H., GOULET-SALMON, B., KOTTLER, M. L., RICHARD, O., SANCHEZ-FRANCO, F., SAURA, R., YOUNG, J., PETIT, C. & HARDELIN, J. P. 2003. Loss-of-function mutations in FGFR1 cause autosomal dominant Kallmann syndrome. *Nat Genet,* 33**,** 463-5.

DOHERTY, T. J., VANDERVOORT, A. A. & BROWN, W. F. 1993. Effects of ageing on the motor unit: a brief review. *Can J Appl Physiol,* 18**,** 331-58.

DOUCET, J. C., HERLIN, C., CAPTIER, G., BAYLON, H., VERDEIL, M. & BIGORRE, M. 2013. Speech outcomes of early palatal repair with or without intravelar veloplasty in children with complete unilateral cleft lip and palate. *Br J Oral Maxillofac Surg,* 51**,** 845-50.

DUDAS, M., KIM, J., LI, W. Y., NAGY, A., LARSSON, J., KARLSSON, S., CHAI, Y. & KAARTINEN, V. 2006. Epithelial and ectomesenchymal role of the type I TGF-beta receptor ALK5 during facial morphogenesis and palatal fusion. *Dev Biol,* 296**,** 298-314.

DUDAS, M., LI, W. Y., KIM, J., YANG, A. & KAARTINEN, V. 2007. Palatal fusion - where do the midline cells go? A review on cleft palate, a major human birth defect. *Acta Histochem,* 109**,** 1-14.

DUDBRIDGE, F. 2003. A survey of current software for linkage analysis. *Hum Genomics,* 1**,** 63-5.

DUERR, R. H., TAYLOR, K. D., BRANT, S. R., RIOUX, J. D., SILVERBERG, M. S., DALY, M. J., STEINHART, A. H., ABRAHAM, C., REGUEIRO, M., GRIFFITHS, A., DASSOPOULOS, T., BITTON, A., YANG, H., TARGAN, S., DATTA, L. W., KISTNER, E. O., SCHUMM, L. P., LEE, A. T., GREGERSEN, P. K., BARMADA, M. M., ROTTER, J. I., NICOLAE, D. L. & CHO, J. H. 2006. A genome-wide association study identifies IL23R as an inflammatory bowel disease gene. *Science,* 314**,** 1461-3.

DURAIYAN, J., GOVINDARAJAN, R., KALIYAPPAN, K. & PALANISAMY, M. 2012. Applications of immunohistochemistry. *Journal of pharmacy & bioallied sciences,* 4**,** S307-S309.

EJAZ, R., CARTER, M. & GRIPP, K. 1993. Lateral Meningocele Syndrome. *GeneReviews.* University of Washington, Seattle.

ENOMOTO, H., NELSON, C. M., SOMERVILLE, R. P., MIELKE, K., DIXON, L. J., POWELL, K. & APTE, S. S. 2010. Cooperation of two ADAMTS metalloproteases in closure of the mouse palate identifies a requirement for versican proteolysis in regulating palatal mesenchyme proliferation. *Development,* 137**,** 4029-38.

ETTEMA, S. L., KUEHN, D. P., PERLMAN, A. L. & ALPERIN, N. 2002. Magnetic resonance imaging of the levator veli palatini muscle during speech. *Cleft Palate Craniofac J,* 39**,** 130-44.

EVANS, A. K., RAHBAR, R., ROGERS, G. F., MULLIKEN, J. B. & VOLK, M. S. 2006. Robin sequence: a retrospective review of 115 patients. *Int J Pediatr Otorhinolaryngol,* 70**,** 973-80.

EZZAT, A. E. & EL-SHENAWY, H. M. 2015. Palatopharyngeus the missing palatal muscles: Anatomical and physiological review. *Ann Maxillofac Surg,* 5**,** 226-8.

FADISTA, J., OSKOLKOV, N., HANSSON, O. & GROOP, L. 2017. LoFtool: a gene intolerance score based on loss-of-function variants in 60 706 individuals. *Bioinformatics,* 33**,** 471-474.

FAN, X., LOEBEL, D., BILDSOE, H., WILKIE, E., QIN, J., WANG, J. & TAM, P. 2016. Tissue interactions, cell signaling and transcriptional control in the cranial mesoderm during craniofacial development. 3**,** 74-98.

FARA, M. & DVORAK, J. 1970. Abnormal anatomy of the muscles of palatopharyngeal closure in cleft palates: anatomical and surgical considerations based on the autopsies of 18 unoperated cleft palates. *Plast Reconstr Surg,* 46**,** 488-97.

FERGUSON, M. W. 1978. Palatal shelf elevation in the Wistar rat fetus. *J Anat,* 125**,** 555-77.

FERGUSON, M. W. 1988. Palate development. *Development,* 103 Suppl**,** 41-60.

FERRANTE, M. I., GIORGIO, G., FEATHER, S. A., BULFONE, A., WRIGHT, V., GHIANI, M., SELICORNI, A., GAMMARO, L., SCOLARI, F., WOOLF, A. S., SYLVIE, O., BERNARD, L., MALCOLM, S., WINTER, R., BALLABIO, A. & FRANCO, B. 2001. Identification of the gene for oral-facial-digital type I syndrome. *Am J Hum Genet,* 68**,** 569-76.

FILIP, C., IMPIERI, D., AAGENAES, I., BREUGEM, C., HOGEVOLD, H. E., SAERVOLD, T., AUKNER, R., LIMA, K., TONSETH, K. & ABRAHAMSEN, T. G. 2017. Adults with 22q11.2 deletion syndrome have a different velopharyngeal anatomy with predisposition to velopharyngeal insufficiency. *J Plast Reconstr Aesthet Surg,* 71(4)**,** 524-536.

FINKELSTEIN, Y., MESHORER, A., TALMI, Y. P., ZOHAR, Y., BRENNER, J. & GAL, R. 1992. The riddle of the uvula. *Otolaryngol Head Neck Surg,* 107**,** 444-50.

FIRTH, H. V., RICHARDS, S. M., BEVAN, A. P., CLAYTON, S., CORPAS, M., RAJAN, D., VAN VOOREN, S., MOREAU, Y., PETTETT, R. M. & CARTER, N. P. 2009. DECIPHER: Database of Chromosomal Imbalance and Phenotype in Humans Using Ensembl Resources. *Am J Hum Genet,* 84**,** 524-33.

FITCHETT, J. E. & HAY, E. D. 1989. Medial edge epithelium transforms to mesenchyme after embryonic palatal shelves fuse. *Dev Biol,* 131**,** 455-74.

FITZPATRICK, D. R., DENHEZ, F., KONDAIAH, P. & AKHURST, R. J. 1990. Differential expression of TGF beta isoforms in murine palatogenesis. *Development,* 109**,** 585-95.

FOSTER, J. W., DOMINGUEZ-STEGLICH, M. A., GUIOLI, S., KWOK, C., WELLER, P. A., STEVANOVIC, M., WEISSENBACH, J., MANSOUR, S., YOUNG, I. D., GOODFELLOW, P. N. & ET AL. 1994. Campomelic dysplasia and autosomal sex reversal caused by mutations in an SRY-related gene. *Nature,* 372**,** 525-30.

FREBOURG, T., OLIVEIRA, C., HOCHAIN, P., KARAM, R., MANOUVRIER, S., GRAZIADIO, C., VEKEMANS, M., HARTMANN, A., BAERT-DESURMONT, S., ALEXANDRE, C., LEJEUNE DUMOULIN, S., MARRONI, C., MARTIN, C., CASTEDO, S., LOVETT, M., WINSTON, J., MACHADO, J. C., ATTIE, T., JABS, E. W., CAI, J., PELLERIN, P., TRIBOULET, J. P., SCOTTE, M., LE PESSOT, F., HEDOUIN, A., CARNEIRO, F., BLAYAU, M. & SERUCA, R. 2006. Cleft lip/palate and CDH1/E-cadherin mutations in families with hereditary diffuse gastric cancer. *J Med Genet,* 43**,** 138-42.

FRIEDRICH, G. & SORIANO, P. 1991. Promoter traps in embryonic stem cells: a genetic screen to identify and mutate developmental genes in mice. *Genes Dev,* 5**,** 1513-23.

FU, X., XU, J., CHATURVEDI, P., LIU, H., JIANG, R. & LAN, Y. 2017. Identification of Osr2 Transcriptional Target Genes in Palate Development. *J Dent Res,* 96**,** 1451-1458.

FUCHS, A., INTHAL, A., HERRMANN, D., CHENG, S., NAKATOMI, M., PETERS, H. & NEUBUSER, A. 2010. Regulation of Tbx22 during facial and palatal development. *Dev Dyn,* 239**,** 2860-74.

FUJIWARA, H., FERREIRA, M., DONATI, G., MARCIANO, D. K., LINTON, J. M., SATO, Y., HARTNER, A., SEKIGUCHI, K., REICHARDT, L. F. & WATT, F. M. 2011. The basement membrane of hair follicle stem cells is a muscle cell niche. *Cell,* 144**,** 577-89.

FUNATO, N. & YANAGISAWA, H. 2018. Deletion of the T-box transcription factor gene, Tbx1, in mice induces differential expression of genes associated with cleft palate in humans. *Arch Oral Biol,* 95**,** 149-155.

FURLOW, L. T., JR. 1986. Cleft palate repair by double opposing Z-plasty. *Plast Reconstr Surg,* 78**,** 724-38.

GANGOPADHYAY, N., MENDONCA, D. A. & WOO, A. S. 2012. Pierre robin sequence. *Semin Plast Surg,* 26**,** 76-82.

GARCIA-CASTRO, M. I., MARCELLE, C. & BRONNER-FRASER, M. 2002. Ectodermal Wnt function as a neural crest inducer. *Science,* 297**,** 848-51.

GENDRON-MAGUIRE, M., MALLO, M., ZHANG, M. & GRIDLEY, T. 1993. Hoxa-2 mutant mice exhibit homeotic transformation of skeletal elements derived from cranial neural crest. *Cell,* 75**,** 1317-31.

GERRELLI, D., LISGO, S., COPP, A. J. & LINDSAY, S. 2015. Enabling research with human embryonic and fetal tissue resources. *Development,* 142**,** 3073-6.

GHAFOORY, S., BREITKOPF-HEINLEIN, K., LI, Q., DZIERAN, J., SCHOLL, C., DOOLEY, S. & WOLFL, S. 2012. A fast and efficient polymerase chain reaction-based method for the preparation of in situ hybridization probes. *Histopathology,* 61**,** 306-13.

GILISSEN, C., HEHIR-KWA, J. Y., THUNG, D. T., VAN DE VORST, M., VAN BON, B. W., WILLEMSEN, M. H., KWINT, M., JANSSEN, I. M., HOISCHEN, A., SCHENCK, A., LEACH, R., KLEIN, R., TEARLE, R., BO, T., PFUNDT, R., YNTEMA, H. G., DE VRIES, B. B., KLEEFSTRA, T., BRUNNER, H. G., VISSERS, L. E. & VELTMAN, J. A. 2014. Genome sequencing identifies major causes of severe intellectual disability. *Nature,* 511**,** 344-7.

GILISSEN, C., HOISCHEN, A., BRUNNER, H. G. & VELTMAN, J. A. 2012. Disease gene identification strategies for exome sequencing. *Eur J Hum Genet,* 20**,** 490-7.

GIRARDOT, C., SCHOLTALBERS, J., SAUER, S., SU, S. Y. & FURLONG, E. E. 2016. Je, a versatile suite to handle multiplexed NGS libraries with unique molecular identifiers. *BMC Bioinformatics,* 17**,** 419.

GLASER, E. R., SKOLNICK, M. L., MCWILLIAMS, B. J. & SHPRINTZEN, R. J. 1979. The dynamics of Passavant's ridge in subjects with and without velopharyngeal insufficiency--a multi-view videofluoroscopic study. *Cleft Palate J,* 16**,** 24-33.

GOLDING-KUSHNER, K. J., ARGAMASO, R. V., COTTON, R. T., GRAMES, L. M., HENNINGSSON, G., JONES, D. L., KARNELL, M. P., KLAIMAN, P. G., LEWIN, M. L., MARSH, J. L. & ET AL. 1990. Standardization for the reporting of nasopharyngoscopy and multiview videofluoroscopy: a report from an International Working Group. *Cleft Palate J,* 27**,** 337-47; discussion 347-8.

GORDON, C. T., WADE, C., BRINAS, I. & FARLIE, P. G. 2011. CXCL14 expression during chick embryonic development. *Int J Dev Biol,* 55**,** 335-40.

GOULD, D. B., MEARS, A. J., PEARCE, W. G. & WALTER, M. A. 1997. Autosomal dominant Axenfeld-Rieger anomaly maps to 6p25. *Am J Hum Genet,* 61**,** 765-8.

GRANT, S. F., WANG, K., ZHANG, H., GLABERSON, W., ANNAIAH, K., KIM, C. E., BRADFIELD, J. P., GLESSNER, J. T., THOMAS, K. A., GARRIS, M., FRACKELTON, E. C., OTIENO, F. G., CHIAVACCI, R. M., NAH, H. D., KIRSCHNER, R. E. & HAKONARSON, H. 2009. A genome-wide association study identifies a locus for nonsyndromic cleft lip with or without cleft palate on 8q24. *J Pediatr,* 155**,** 909-13.

GREENE, R. M. & PISANO, M. M. 2011. Issue overview: epigenetic processes in development. *Birth Defects Res A Clin Mol Teratol,* 91**,** 649-51.

GREENE, R. M. & PRATT, R. M. 1976. Developmental aspects of secondary palate formation. *J Embryol Exp Morphol,* 36**,** 225-45.

GREFTE, S., KUIJPERS, M. A., KUIJPERS-JAGTMAN, A. M., TORENSMA, R. & VON DEN HOFF, J. W. 2012. Myogenic capacity of muscle progenitor cells from head and limb muscles. *Eur J Oral Sci,* 120**,** 38-45.

GRENIER, J., TEILLET, M. A., GRIFONE, R., KELLY, R. G. & DUPREZ, D. 2009. Relationship between neural crest cells and cranial mesoderm during head muscle development. *PLoS One,* 4**,** e4381.

GRIPP, K. W., WOTTON, D., EDWARDS, M. C., ROESSLER, E., ADES, L., MEINECKE, P., RICHIERI-COSTA, A., ZACKAI, E. H., MASSAGUE, J., MUENKE, M. & ELLEDGE, S. J. 2000. Mutations in TGIF cause holoprosencephaly and link NODAL signalling to human neural axis determination. *Nat Genet,* 25**,** 205-8.

GRITLI-LINDE, A. 2007. Molecular control of secondary palate development. *Dev Biol,* 301**,** 309-26.

GRITLI-LINDE, A. 2012. The mouse as a developmental model for cleft lip and palate research. *Front Oral Biol,* 16**,** 32-51.

HA, S., KOH, K. S., MOON, H., JUNG, S. & OH, T. S. 2015. Clinical Outcomes of Primary Palatal Surgery in Children with Nonsyndromic Cleft Palate with and without Lip. *Biomed Res Int,* 2015**,** 185459.

HAMLET, S. L. & MOMIYAMA, Y. 1992. Velar activity and timing of eustachian tube function in swallowing. *Dysphagia,* 7**,** 226-33.

HAMMOND, N. L., BROOKES, K. J. & DIXON, M. J. 2018. Ectopic Hedgehog Signaling Causes Cleft Palate and Defective Osteogenesis. *J Dent Res,* 97**,** 1485-1493.

HAN, J., MAYO, J., XU, X., LI, J., BRINGAS, P., JR., MAAS, R. L., RUBENSTEIN, J. L. & CHAI, Y. 2009. Indirect modulation of Shh signaling by Dlx5 affects the oral-nasal patterning of palate and rescues cleft palate in Msx1-null mice. *Development,* 136**,** 4225-33.

HAN, Y. & GU, Y. 2016. Review: imaging technologies for flow cytometry. 16**,** 4639-4647.

HARDWICKE, J. T., RICHARDS, H., CAFFERKY, L., UNDERWOOD, I., TER HORST, B. & SLATOR, R. 2016. Outcomes of Cleft Palate Repair in Patients with Pierre Robin Sequence: A Matched Case-Control Study. *Plast Reconstr Surg,* 137**,** 927-35.

HARKIN, L. F., GERRELLI, D., GOLD DIAZ, D. C., SANTOS, C., ALZU'BI, A., AUSTIN, C. A. & CLOWRY, G. J. 2016. Distinct expression patterns for type II topoisomerases IIA and IIB in the early foetal human telencephalon. *J Anat,* 228**,** 452-63.

HARVILLE, E. W., WILCOX, A. J., LIE, R. T., VINDENES, H. & ABYHOLM, F. 2005. Cleft lip and palate versus cleft lip only: are they distinct defects? *Am J Epidemiol,* 162**,** 448-53.

HE, F., POPKIE, A. P., XIONG, W., LI, L., WANG, Y., PHIEL, C. J. & CHEN, Y. 2010a. Gsk3beta is required in the epithelium for palatal elevation in mice. *Dev Dyn,* 239**,** 3235-46.

HE, F., XIONG, W., WANG, Y., LI, L., LIU, C., YAMAGAMI, T., TAKETO, M. M., ZHOU, C. & CHEN, Y. 2011. Epithelial Wnt/beta-catenin signaling regulates palatal shelf fusion through regulation of Tgfbeta3 expression. *Dev Biol,* 350**,** 511-9.

HE, F., XIONG, W., WANG, Y., MATSUI, M., YU, X., CHAI, Y., KLINGENSMITH, J. & CHEN, Y. 2010b. Modulation of BMP signaling by Noggin is required for the maintenance of palatal epithelial integrity during palatogenesis. *Dev Biol,* 347**,** 109-21.

HE, F., XIONG, W., YU, X., ESPINOZA-LEWIS, R., LIU, C., GU, S., NISHITA, M., SUZUKI, K., YAMADA, G., MINAMI, Y. & CHEN, Y. 2008. Wnt5a regulates directional cell migration and cell proliferation via Ror2-mediated noncanonical pathway in mammalian palate development. *Development,* 135**,** 3871-9.

HELLQVIST, M., MAHLAPUU, M., BLIXT, A., ENERBACK, S. & CARLSSON, P. 1998. The human forkhead protein FREAC-2 contains two functionally redundant activation domains and interacts with TBP and TFIIB. *J Biol Chem,* 273**,** 23335-43.

HELLQVIST, M., MAHLAPUU, M., SAMUELSSON, L., ENERBACK, S. & CARLSSON, P. 1996. Differential activation of lung-specific genes by two forkhead proteins, FREAC-1 and FREAC-2. *J Biol Chem,* 271**,** 4482-90.

HIDALGO-BRAVO, A., POMPA-MERA, E. N., KOFMAN-ALFARO, S., GONZALEZ-BONILLA, C. R. & ZENTENO, J. C. 2005. A novel filamin A D203Y mutation in a female patient with otopalatodigital type 1 syndrome and extremely skewed X chromosome inactivation. *Am J Med Genet A,* 136**,** 190-3.

HIGASHIHORI, N., BUCHTOVA, M. & RICHMAN, J. M. 2010. The function and regulation of TBX22 in avian frontonasal morphogenesis. *Dev Dyn,* 239**,** 458-73.

HOCEVAR, B. A., BROWN, T. L. & HOWE, P. H. 1999. TGF-beta induces fibronectin synthesis through a c-Jun N-terminal kinase-dependent, Smad4-independent pathway. *Embo j,* 18**,** 1345-56.

HODGINS, N., HOO, C., MCGEE, P. & HILL, C. 2015. A survey of assessment and management of velopharyngeal incompetence (VPI) in the UK and Ireland. *J Plast Reconstr Aesthet Surg,* 68**,** 485-91.

HOLZINGER, E. R., LI, Q., PARKER, M. M., HETMANSKI, J. B., MARAZITA, M. L., MANGOLD, E., LUDWIG, K. U., TAUB, M. A., BEGUM, F., MURRAY, J. C., ALBACHA-HEJAZI, H., ALQOSAYER, K., AL-SOUKI, G., ALBASHA HEJAZI, A., SCOTT, A. F., BEATY, T. H. & BAILEY-WILSON, J. E. 2017. Analysis of sequence data to identify potential risk variants for oral clefts in multiplex families. *Mol Genet Genomic Med,* 5**,** 570-579.

HOSHINO, A. 2011. The Role of TBX22 in Craniofacial Development. *PhD Thesis*.

HOSOKAWA, R., DENG, X., TAKAMORI, K., XU, X., URATA, M., BRINGAS, P., JR. & CHAI, Y. 2009. Epithelial-specific requirement of FGFR2 signaling during tooth and palate development. *J Exp Zool B Mol Dev Evol,* 312b**,** 343-50.

HOSSEINABAD, H. H., DERAKHSHANDEH, F., MOSTAAJERAN, F., ABDALI, H., DAVARI, H. A., HASSANZADEH, A. & KUMMER, A. W. 2015. Incidence of velopharyngeal insufficiency and oronasal fistulae after cleft palate repair: A retrospective study of children referred to Isfahan Cleft Care Team between 2005 and 2009. *Int J Pediatr Otorhinolaryngol,* 79**,** 1722-6.

HOWARD, T. D., PAZNEKAS, W. A., GREEN, E. D., CHIANG, L. C., MA, N., ORTIZ DE LUNA, R. I., GARCIA DELGADO, C., GONZALEZ-RAMOS, M., KLINE, A. D. & JABS, E. W. 1997. Mutations in TWIST, a basic helix-loop-helix transcription factor, in Saethre-Chotzen syndrome. *Nat Genet,* 15**,** 36-41.

HROMAS, R., BROXMEYER, H. E., KIM, C., NAKSHATRI, H., CHRISTOPHERSON, K., 2ND, AZAM, M. & HOU, Y. H. 1999. Cloning of BRAK, a novel divergent CXC chemokine preferentially expressed in normal versus malignant cells. *Biochem Biophys Res Commun,* 255**,** 703-6.

HUANG, J. T. & LEE, V. 2005. Identification and characterization of a novel human nephronectin gene in silico. *Int J Mol Med,* 15**,** 719-24.

HUANG, M. H., LEE, S. T. & RAJENDRAN, K. 1997. A fresh cadaveric study of the paratubal muscles: implications for eustachian tube function in cleft palate. *Plast Reconstr Surg,* 100**,** 833-42.

HUANG, M. H., LEE, S. T. & RAJENDRAN, K. 1998. Anatomic basis of cleft palate and velopharyngeal surgery: implications from a fresh cadaveric study. *Plast Reconstr Surg,* 101**,** 613-27; discussion 628-9.

HUANG, M. H., RISKI, J. E., COHEN, S. R., SIMMS, C. A. & BURSTEIN, F. D. 1999. An anatomic evaluation of the furlow double opposing Z-plasty technique of cleft palate repair. *Ann Acad Med Singapore,* 28**,** 672-6.

IKEHATA, M., YAMADA, A., MORIMURA, N., ITOSE, M., SUZAWA, T., SHIROTA, T., CHIKAZU, D. & KAMIJO, R. 2017. Wnt/beta-catenin signaling activates nephronectin expression in osteoblasts. *Biochem Biophys Res Commun,* 484**,** 231-234.

INGRAHAM, C. R., KINOSHITA, A., KONDO, S., YANG, B., SAJAN, S., TROUT, K. J., MALIK, M. I., DUNNWALD, M., GOUDY, S. L., LOVETT, M., MURRAY, J. C. & SCHUTTE, B. C. 2006. Abnormal skin, limb and craniofacial morphogenesis in mice deficient for interferon regulatory factor 6 (Irf6). *Nat Genet,* 38**,** 1335-40.

ISHIDA, M., CULLUP, T., BOUSTRED, C., JAMES, C., DOCKER, J., ENGLISH, C., LENCH, N., COPP, A. J., MOORE, G. E., GREENE, N. D. E. & STANIER, P. 2018. A targeted sequencing panel identifies rare damaging variants in multiple genes in the cranial neural tube defect, anencephaly. *Clin Genet,* 93**,** 870-879.

ITO, Y., YEO, J. Y., CHYTIL, A., HAN, J., BRINGAS, P., JR., NAKAJIMA, A., SHULER, C. F., MOSES, H. L. & CHAI, Y. 2003. Conditional inactivation of Tgfbr2 in cranial neural crest causes cleft palate and calvaria defects. *Development,* 130**,** 5269-80.

ITTNER, L. M., WURDAK, H., SCHWERDTFEGER, K., KUNZ, T., ILLE, F., LEVEEN, P., HJALT, T. A., SUTER, U., KARLSSON, S., HAFEZI, F., BORN, W. & SOMMER, L. 2005. Compound developmental eye disorders following inactivation of TGFbeta signaling in neural-crest stem cells. *J Biol,* 4**,** 11.

IWATA, J., SUZUKI, A., YOKOTA, T., HO, T. V., PELIKAN, R., URATA, M., SANCHEZ-LARA, P. A. & CHAI, Y. 2014. TGFbeta regulates epithelial-mesenchymal interactions through WNT signaling activity to control muscle development in the soft palate. *Development,* 141**,** 909-17.

IWATA, J., TUNG, L., URATA, M., HACIA, J. G., PELIKAN, R., SUZUKI, A., RAMENZONI, L., CHAUDHRY, O., PARADA, C., SANCHEZ-LARA, P. A. & CHAI, Y. 2012. Fibroblast growth factor 9 (FGF9)-pituitary homeobox 2 (PITX2) pathway mediates transforming growth factor beta (TGFbeta) signaling to regulate cell proliferation in palatal mesenchyme during mouse palatogenesis. *J Biol Chem,* 287**,** 2353-63.

IZUMI, K., KONCZAL, L. L., MITCHELL, A. L. & JONES, M. C. 2012. Underlying genetic diagnosis of Pierre Robin sequence: retrospective chart review at two children's hospitals and a systematic literature review. *J Pediatr,* 160**,** 645-650.e2.

JÄNICKE, S. & HUBER, A. 1996. Comparison of different animal models in cleft lip and palate research. *British Journal of Oral and Maxillofacial Surgery,* 34**,** 340-341.

JEZEWSKI, P. A., VIEIRA, A. R., NISHIMURA, C., LUDWIG, B., JOHNSON, M., O'BRIEN, S. E., DAACK-HIRSCH, S., SCHULTZ, R. E., WEBER, A., NEPOMUCENA, B., ROMITTI, P. A., CHRISTENSEN, K., ORIOLI, I. M., CASTILLA, E. E., MACHIDA, J., NATSUME, N. & MURRAY, J. C. 2003. Complete sequencing shows a role for MSX1 in non-syndromic cleft lip and palate. *J Med Genet,* 40**,** 399-407.

JIANG, R., LAN, Y., CHAPMAN, H. D., SHAWBER, C., NORTON, C. R., SERREZE, D. V., WEINMASTER, G. & GRIDLEY, T. 1998. Defects in limb, craniofacial, and thymic development in Jagged2 mutant mice. *Genes Dev,* 12**,** 1046-57.

JIN, J. Z. & DING, J. 2006a. Analysis of cell migration, transdifferentiation and apoptosis during mouse secondary palate fusion. *Development,* 133**,** 3341-7.

JIN, J. Z. & DING, J. 2006b. Analysis of Meox-2 mutant mice reveals a novel postfusion-based cleft palate. *Dev Dyn,* 235**,** 539-46.

JIN, J. Z., LEI, Z., LAN, Z. J., MUKHOPADHYAY, P. & DING, J. 2018. Inactivation of Fgfr2 gene in mouse secondary palate mesenchymal cells leads to cleft palate. *Reprod Toxicol,* 77**,** 137-142.

JIN, J. Z., LI, Q., HIGASHI, Y., DARLING, D. S. & DING, J. 2008. Analysis of Zfhx1a mutant mice reveals palatal shelf contact-independent medial edge epithelial differentiation during palate fusion. *Cell Tissue Res,* 333**,** 29-38.

JIN, J. Z., TAN, M., WARNER, D. R., DARLING, D. S., HIGASHI, Y., GRIDLEY, T. & DING, J. 2010. Mesenchymal cell remodeling during mouse secondary palate reorientation. *Dev Dyn,* 239**,** 2110-7.

JIN, S. W., SIM, K. B. & KIM, S. D. 2016. Development and Growth of the Normal Cranial Vault : An Embryologic Review. *J Korean Neurosurg Soc,* 59**,** 192-6.

JIN, Y. R., TURCOTTE, T. J., CROCKER, A. L., HAN, X. H. & YOON, J. K. 2011. The canonical Wnt signaling activator, R-spondin2, regulates craniofacial patterning and morphogenesis within the branchial arch through ectodermal-mesenchymal interaction. *Dev Biol,* 352**,** 1-13.

JOHNSTON, J. J., SAPP, J. C., TURNER, J. T., AMOR, D., AFTIMOS, S., ALECK, K. A., BOCIAN, M., BODURTHA, J. N., COX, G. F., CURRY, C. J., DAY, R., DONNAI, D., FIELD, M., FUJIWARA, I., GABBETT, M., GAL, M., GRAHAM, J. M., HEDERA, P., HENNEKAM, R. C., HERSH, J. H., HOPKIN, R. J., KAYSERILI, H., KIDD, A. M., KIMONIS, V., LIN, A. E., LYNCH, S. A., MAISENBACHER, M., MANSOUR, S., MCGAUGHRAN, J., MEHTA, L., MURPHY, H., RAYGADA, M., ROBIN, N. H., ROPE, A. F., ROSENBAUM, K. N., SCHAEFER, G. B., SHEALY, A., SMITH, W., SOLLER, M., SOMMER, A., STALKER, H. J., STEINER, B., STEPHAN, M. J., TILSTRA, D., TOMKINS, S., TRAPANE, P., TSAI, A. C., VAN ALLEN, M. I., VASUDEVAN, P. C., ZABEL, B., ZUNICH, J., BLACK, G. C. & BIESECKER, L. G. 2010. Molecular analysis expands the spectrum of phenotypes associated with GLI3 mutations. *Hum Mutat,* 31**,** 1142-54.

JONES, K. L., JONES, M. C. & CAMPO, M. D. 2013. *Smith's recognizable patterns of human malformation*.

JORGENSON, R. J., SHAPIRO, S. D., SALINAS, C. F. & LEVIN, L. S. 1982. Intraoral findings and anomalies in neonates. *Pediatrics,* 69**,** 577-82.

JUMLONGRAS, D., BEI, M., STIMSON, J. M., WANG, W. F., DEPALMA, S. R., SEIDMAN, C. E., FELBOR, U., MAAS, R., SEIDMAN, J. G. & OLSEN, B. R. 2001. A nonsense mutation in MSX1 causes Witkop syndrome. *Am J Hum Genet,* 69**,** 67-74.

JURILOFF, D. M. & HARRIS, M. J. 2008. Mouse genetic models of cleft lip with or without cleft palate. *Birth Defects Res A Clin Mol Teratol,* 82**,** 63-77.

KAARTINEN, V., CUI, X. M., HEISTERKAMP, N., GROFFEN, J. & SHULER, C. F. 1997. Transforming growth factor-beta3 regulates transdifferentiation of medial edge epithelium during palatal fusion and associated degradation of the basement membrane. *Dev Dyn,* 209**,** 255-60.

KAARTINEN, V., VONCKEN, J. W., SHULER, C., WARBURTON, D., BU, D., HEISTERKAMP, N. & GROFFEN, J. 1995. Abnormal lung development and cleft palate in mice lacking TGF-beta 3 indicates defects of epithelial-mesenchymal interaction. *Nature genetics,* 11**,** 415.

KAHRILAS, P. 1993. Pharyngeal structure and function. *Dysphagia,* 8**,** 303-307.

KALAY, E., SEZGIN, O., CHELLAPPA, V., MUTLU, M., MORSY, H., KAYSERILI, H., KREIGER, E., CANSU, A., TORAMAN, B., ABDALLA, E. M., ASLAN, Y., PILLAI, S. & AKARSU, N. A. 2012. Mutations in RIPK4 cause the autosomal-recessive form of popliteal pterygium syndrome. *Am J Hum Genet,* 90**,** 76-85.

KANTAPUTRA, P. N., PARAMEE, M., KAEWKHAMPA, A., HOSHINO, A., LEES, M., MCENTAGART, M., MASROUR, N., MOORE, G. E., PAUWS, E. & STANIER, P. 2011. Cleft lip with cleft palate, ankyloglossia, and hypodontia are associated with TBX22 mutations. *J Dent Res,* 90**,** 450-5.

KAPLAN, E. N. 1975. The occult submucous cleft palate. *Cleft Palate J,* 12**,** 356-68.

KAUFMANN, E. & KNOCHEL, W. 1996. Five years on the wings of fork head. *Mech Dev,* 57**,** 3-20.

KEREM, B., ROMMENS, J. M., BUCHANAN, J. A., MARKIEWICZ, D., COX, T. K., CHAKRAVARTI, A., BUCHWALD, M. & TSUI, L. C. 1989. Identification of the cystic fibrosis gene: genetic analysis. *Science,* 245**,** 1073-80.

KERRISK, M. E., CINGOLANI, L. A. & KOLESKE, A. J. 2014. ECM receptors in neuronal structure, synaptic plasticity, and behavior. *Prog Brain Res,* 214**,** 101-31.

KEYNES, R. & COOK, G. M. 1995. Axon guidance molecules. *Cell,* 83**,** 161-9.

KHANDELWAL, K. D., ISHORST, N., ZHOU, H., LUDWIG, K. U., VENSELAAR, H., GILISSEN, C., THONISSEN, M., VAN ROOIJ, I. A., DREESEN, K., STEEHOUWER, M., VAN DE VORST, M., BLOEMEN, M., VAN BEUSEKOM, E., ROOSENBOOM, J., BORSTLAP, W., ADMIRAAL, R., DORMAAR, T., SCHOENAERS, J., VANDER POORTEN, V., HENS, G., VERDONCK, A., BERGE, S., ROELEVELDT, N., VRIEND, G., DEVRIENDT, K., BRUNNER, H. G., MANGOLD, E., HOISCHEN, A., VAN BOKHOVEN, H. & CARELS, C. E. 2016. Novel IRF6 Mutations Detected in Orofacial Cleft Patients by Targeted Massively Parallel Sequencing. *J Dent Res*.

KIRSCHNER, R. E. & BAYLIS, A. L. 2014. Surgical considerations in 22Q11.2 deletion syndrome. *Clin Plast Surg,* 41**,** 271-82.

KISPERT, A. & HERMANN, B. G. 1993. The Brachyury gene encodes a novel DNA binding protein. *Embo j,* 12**,** 4898-9.

KIYOZUMI, D., TAKEICHI, M., NAKANO, I., SATO, Y., FUKUDA, T. & SEKIGUCHI, K. 2012. Basement membrane assembly of the integrin alpha8beta1 ligand nephronectin requires Fraser syndrome-associated proteins. *J Cell Biol,* 197**,** 677-89.

KOLMODIN, L. A. & BIRCH, D. E. 2002. Polymerase chain reaction. Basic principles and routine practice. *Methods Mol Biol,* 192**,** 3-18.

KONDO, S., SCHUTTE, B. C., RICHARDSON, R. J., BJORK, B. C., KNIGHT, A. S., WATANABE, Y., HOWARD, E., DE LIMA, R. L., DAACK-HIRSCH, S., SANDER, A., MCDONALD-MCGINN, D. M., ZACKAI, E. H., LAMMER, E. J., AYLSWORTH, A. S., ARDINGER, H. H., LIDRAL, A. C., POBER, B. R., MORENO, L., ARCOS-BURGOS, M., VALENCIA, C., HOUDAYER, C., BAHUAU, M., MORETTI-FERREIRA, D., RICHIERI-COSTA, A., DIXON, M. J. & MURRAY, J. C. 2002. Mutations in IRF6 cause Van der Woude and popliteal pterygium syndromes. *Nat Genet,* 32**,** 285-9.

KRANTZ, I. D., MCCALLUM, J., DESCIPIO, C., KAUR, M., GILLIS, L. A., YAEGER, D., JUKOFSKY, L., WASSERMAN, N., BOTTANI, A., MORRIS, C. A., NOWACZYK, M. J., TORIELLO, H., BAMSHAD, M. J., CAREY, J. C., RAPPAPORT, E., KAWAUCHI, S., LANDER, A. D., CALOF, A. L., LI, H. H., DEVOTO, M. & JACKSON, L. G. 2004. Cornelia de Lange syndrome is caused by mutations in NIPBL, the human homolog of Drosophila melanogaster Nipped-B. *Nat Genet,* 36**,** 631-5.

KRAUSE, A., ZACHARIAS, W., CAMARATA, T., LINKHART, B., LAW, E., LISCHKE, A., MILJAN, E. & SIMON, H. G. 2004. Tbx5 and Tbx4 transcription factors interact with a new chicken PDZ-LIM protein in limb and heart development. *Dev Biol,* 273**,** 106-20.

KRIENS, O. B. 1969. An anatomical approach to veloplasty. *Plast Reconstr Surg,* 43**,** 29-41.

KRIENS, O. B. 1970. Fundamental anatomic findings for an intravelar veloplasty. *Cleft Palate J,* 7**,** 27-36.

KUEHN, D. P. & MOON, J. B. 2005. Histologic study of intravelar structures in normal human adult specimens. *Cleft Palate Craniofac J,* 42**,** 481-9.

KUMMER, A. W. 2011a. Disorders of resonance and airflow secondary to cleft palate and/or velopharyngeal dysfunction. *Semin Speech Lang,* 32**,** 141-9.

KUMMER, A. W. 2011b. Perceptual assessment of resonance and velopharyngeal function. *Semin Speech Lang,* 32**,** 159-67.

KUMMER, A. W., MARSHALL, J. L. & WILSON, M. M. 2015. Non-cleft causes of velopharyngeal dysfunction: implications for treatment. *Int J Pediatr Otorhinolaryngol,* 79**,** 286-95.

KUROTAKI, N., IMAIZUMI, K., HARADA, N., MASUNO, M., KONDOH, T., NAGAI, T., OHASHI, H., NARITOMI, K., TSUKAHARA, M., MAKITA, Y., SUGIMOTO, T., SONODA, T., HASEGAWA, T., CHINEN, Y., TOMITA HA, H. A., KINOSHITA, A., MIZUGUCHI, T., YOSHIURA KI, K., OHTA, T., KISHINO, T., FUKUSHIMA, Y., NIIKAWA, N. & MATSUMOTO, N. 2002. Haploinsufficiency of NSD1 causes Sotos syndrome. *Nat Genet,* 30**,** 365-6.

KUSCH, T., STORCK, T., WALLDORF, U. & REUTER, R. 2002. Brachyury proteins regulate target genes through modular binding sites in a cooperative fashion. *Genes Dev,* 16**,** 518-29.

LAN, Y. & JIANG, R. 2009. Sonic hedgehog signaling regulates reciprocal epithelial-mesenchymal interactions controlling palatal outgrowth. *Development,* 136**,** 1387-96.

LAN, Y., OVITT, C. E., CHO, E. S., MALTBY, K. M., WANG, Q. & JIANG, R. 2004. Odd-skipped related 2 (Osr2) encodes a key intrinsic regulator of secondary palate growth and morphogenesis. *Development,* 131**,** 3207-16.

LAN, Y., ZHANG, N., LIU, H., XU, J. & JIANG, R. 2016. Golgb1 regulates protein glycosylation and is crucial for mammalian palate development. *Development,* 143**,** 2344-55.

LANDER, E. S. & BOTSTEIN, D. 1987. Homozygosity mapping: a way to map human recessive traits with the DNA of inbred children. *Science,* 236**,** 1567-70.

LANZA, I. R. & SREEKUMARAN NAIR, K. 2010. Regulation of skeletal muscle mitochondrial function: genes to proteins. *Acta Physiol (Oxf),* 199**,** 529-47.

LARSSON, K. S. 1960. Studies on the closure of the secondary palate. II. Occurrence of sulpho-mucopolysaccharides in the palatine processes of the normal mouse embryo. *Exp Cell Res,* 21**,** 498-503.

LATTOUF, R., YOUNES, R., LUTOMSKI, D., NAAMAN, N., GODEAU, G., SENNI, K. & CHANGOTADE, S. 2014. Picrosirius red staining: a useful tool to appraise collagen networks in normal and pathological tissues. *J Histochem Cytochem,* 62**,** 751-8.

LAUMONNIER, F., HOLBERT, S., RONCE, N., FARAVELLI, F., LENZNER, S., SCHWARTZ, C. E., LESPINASSE, J., VAN ESCH, H., LACOMBE, D., GOIZET, C., PHAN-DINH TUY, F., VAN BOKHOVEN, H., FRYNS, J. P., CHELLY, J., ROPERS, H. H., MORAINE, C., HAMEL, B. C. & BRIAULT, S. 2005. Mutations in PHF8 are associated with X linked mental retardation and cleft lip/cleft palate. *J Med Genet,* 42**,** 780-6.

LAZZARO, C. 1940. Sul meccanismo di chiusura del palato secondario. *Monit. Zool. Ital.***,** 51, 249-273.

LEDERER, D., GRISART, B., DIGILIO, M. C., BENOIT, V., CRESPIN, M., GHARIANI, S. C., MAYSTADT, I., DALLAPICCOLA, B. & VERELLEN-DUMOULIN, C. 2012. Deletion of KDM6A, a histone demethylase interacting with MLL2, in three patients with Kabuki syndrome. *Am J Hum Genet,* 90**,** 119-24.

LEE, H. T., LIU, S. P., LIN, C. H., LEE, S. W., HSU, C. Y., SYTWU, H. K., HSIEH, C. H. & SHYU, W. C. 2017. A Crucial Role of CXCL14 for Promoting Regulatory T Cells Activation in Stroke. *Theranostics,* 7**,** 855-875.

LEE, K. K. L., PESKETT, E., QUINN, C. M., AIELLO, R., ADEEVA, L., MOULDING, D. A., STANIER, P. & PAUWS, E. 2018. Overexpression of Fgfr2c causes craniofacial bone hypoplasia and ameliorates craniosynostosis in the Crouzon mouse. 11.

LEHMANN, O. J., EBENEZER, N. D., JORDAN, T., FOX, M., OCAKA, L., PAYNE, A., LEROY, B. P., CLARK, B. J., HITCHINGS, R. A., POVEY, S., KHAW, P. T. & BHATTACHARYA, S. S. 2000. Chromosomal duplication involving the forkhead transcription factor gene FOXC1 causes iris hypoplasia and glaucoma. *Am J Hum Genet,* 67**,** 1129-35.

LEOW, A. M. & LO, L. J. 2008. Palatoplasty: evolution and controversies. *Chang Gung Med J,* 31**,** 335-45.

LEOYKLANG, P., SUPHAPEETIPORN, K., SIRIWAN, P., DESUDCHIT, T., CHAOWANAPANJA, P., GAHL, W. A. & SHOTELERSUK, V. 2007. Heterozygous nonsense mutation SATB2 associated with cleft palate, osteoporosis, and cognitive defects. *Hum Mutat,* 28**,** 732-8.

LESLIE, E. J., CARLSON, J. C., SHAFFER, J. R., BUTALI, A., BUXO, C. J., CASTILLA, E. E., CHRISTENSEN, K., DELEYIANNIS, F. W., LEIGH FIELD, L., HECHT, J. T., MORENO, L., ORIOLI, I. M., PADILLA, C., VIEIRA, A. R., WEHBY, G. L., FEINGOLD, E., WEINBERG, S. M., MURRAY, J. C., BEATY, T. H. & MARAZITA, M. L. 2017. Genome-wide meta-analyses of nonsyndromic orofacial clefts identify novel associations between FOXE1 and all orofacial clefts, and TP63 and cleft lip with or without cleft palate. *Hum Genet,* 136**,** 275-286.

LESLIE, E. J., LIU, H., CARLSON, J. C., SHAFFER, J. R., FEINGOLD, E., WEHBY, G., LAURIE, C. A., JAIN, D., LAURIE, C. C., DOHENY, K. F., MCHENRY, T., RESICK, J., SANCHEZ, C., JACOBS, J., EMANUELE, B., VIEIRA, A. R., NEISWANGER, K., STANDLEY, J., CZEIZEL, A. E., DELEYIANNIS, F., CHRISTENSEN, K., MUNGER, R. G., LIE, R. T., WILCOX, A., ROMITTI, P. A., FIELD, L. L., PADILLA, C. D., CUTIONGCO-DE LA PAZ, E. M., LIDRAL, A. C., VALENCIA-RAMIREZ, L. C., LOPEZ-PALACIO, A. M., VALENCIA, D. R., ARCOS-BURGOS, M., CASTILLA, E. E., MEREB, J. C., POLETTA, F. A., ORIOLI, I. M., CARVALHO, F. M., HECHT, J. T., BLANTON, S. H., BUXO, C. J., BUTALI, A., MOSSEY, P. A., ADEYEMO, W. L., JAMES, O., BRAIMAH, R. O., AREGBESOLA, B. S., ESHETE, M. A., DERIBEW, M., KORUYUCU, M., SEYMEN, F., MA, L., DE SALAMANCA, J. E., WEINBERG, S. M., MORENO, L., CORNELL, R. A., MURRAY, J. C. & MARAZITA, M. L. 2016. A Genome-wide Association Study of Nonsyndromic Cleft Palate Identifies an Etiologic Missense Variant in GRHL3. *Am J Hum Genet,* 98**,** 744-54.

LESLIE, E. J. & MARAZITA, M. L. 2013. Genetics of cleft lip and cleft palate. *Am J Med Genet C Semin Med Genet,* 163c**,** 246-58.

LEUNG, K. 2004. 4-[(18)F]Fluorobenzoyl-Arg-Arg-Natl-Cys-Tyr-Cit-Lys-d-Lys-Pro-Tyr-Arg-Cit-Cys-Arg -NH2. *Molecular Imaging and Contrast Agent Database (MICAD).* Bethesda (MD): National Center for Biotechnology Information (US).

LEVIN, M., JOHNSON, R. L., STERN, C. D., KUEHN, M. & TABIN, C. 1995. A molecular pathway determining left-right asymmetry in chick embryogenesis. *Cell,* 82**,** 803-14.

LI, C., LAN, Y., KRUMLAUF, R. & JIANG, R. 2017a. Modulating Wnt Signaling Rescues Palate Morphogenesis in Pax9 Mutant Mice. *J Dent Res,* 96**,** 1273-1281.

LI, D., LIU, T., MENG, X., GUO, Q., SHI, J., HAO, Y., JIAO, X., LV, K. & SONG, T. 2017b. Polymorphic variants in VAX1 and the risk of nonsyndromic cleft lip with or without cleft palate in a population from northern China. *Medicine (Baltimore),* 96**,** e6550.

LI, J., RODRIGUEZ, G., HAN, X., JANECKOVA, E., KAHNG, S., SONG, B. & CHAI, Y. 2019a. Regulatory Mechanisms of Soft Palate Development and Malformations. *J Dent Res,* 98**,** 959-967.

LI, L., LIN, M., WANG, Y., CSERJESI, P., CHEN, Z. & CHEN, Y. 2011. Bmprla is required in mesenchymal tissue and has limited redundant function with BmprIb in tooth and palate development. *Dev Biol,* 349**,** 451-61.

LI, Q. & DING, J. 2007. Gene expression analysis reveals that formation of the mouse anterior secondary palate involves recruitment of cells from the posterior side. *Int J Dev Biol,* 51**,** 167-72.

LI, R., CHEN, Z., YU, Q., WENG, M. & CHEN, Z. 2019b. The Function and Regulatory Network of Pax9 Gene in Palate Development. 98**,** 277-287.

LI, W., FU, Y., JIANG, B., LO, A. Y., AMEER, G. A., BARNETT, C. & WANG, B. 2019c. Polymer-integrated amnion scaffold significantly improves cleft palate repair. *Acta Biomater,* 92**,** 104-114.

LIANG, J., VON DEN HOFF, J., LANGE, J., REN, Y., BIAN, Z. & CARELS, C. E. 2016. MSX1 mutations and associated disease phenotypes: genotype-phenotype relations. *Eur J Hum Genet,* 24**,** 1663-1670.

LIBERZON, A., SUBRAMANIAN, A., PINCHBACK, R., THORVALDSDOTTIR, H., TAMAYO, P. & MESIROV, J. P. 2011. Molecular signatures database (MSigDB) 3.0. *Bioinformatics,* 27**,** 1739-40.

LIN, K., ZOU, R., LIN, F., ZHENG, S., SHEN, X. & XUE, X. 2014. Expression and effect of CXCL14 in colorectal carcinoma. *Mol Med Rep,* 10**,** 1561-8.

LINDMAN, R., PAULIN, G. & STAL, P. S. 2001. Morphological characterization of the levator veli palatini muscle in children born with cleft palates. *Cleft Palate Craniofac J,* 38**,** 438-48.

LINGALA, S. G., SUTTON, B. P., MIQUEL, M. E. & NAYAK, K. S. 2016. Recommendations for real-time speech MRI. *J Magn Reson Imaging,* 43**,** 28-44.

LIU, K., YU, W., TANG, M., TANG, J., LIU, X., LIU, Q., LI, Y., HE, L., ZHANG, L., EVANS, S. M. & TIAN, X. 2018. A dual genetic tracing system identifies diverse and dynamic origins of cardiac valve mesenchyme. 145**,** dev167775.

LIU, K. J., ARRON, J. R., STANKUNAS, K., CRABTREE, G. R. & LONGAKER, M. T. 2007. Chemical rescue of cleft palate and midline defects in conditional GSK-3beta mice. *Nature,* 446**,** 79-82.

LIU, W., LAN, Y., PAUWS, E., MEESTER-SMOOR, M. A., STANIER, P., ZWARTHOFF, E. C. & JIANG, R. 2008. The Mn1 transcription factor acts upstream of Tbx22 and preferentially regulates posterior palate growth in mice. *Development (Cambridge, England),* 135**,** 3959-3968.

LIU, W., SUN, X., BRAUT, A., MISHINA, Y., BEHRINGER, R. R., MINA, M. & MARTIN, J. F. 2005. Distinct functions for Bmp signaling in lip and palate fusion in mice. *Development,* 132**,** 1453-61.

LIU, Y., WANG, M., ZHAO, W., YUAN, X., YANG, X., LI, Y., QIU, M., ZHU, X. J. & ZHANG, Z. 2015. Gpr177-mediated Wnt Signaling Is Required for Secondary Palate Development. *J Dent Res,* 94**,** 961-7.

LOEYS, B. L., CHEN, J., NEPTUNE, E. R., JUDGE, D. P., PODOWSKI, M., HOLM, T., MEYERS, J., LEITCH, C. C., KATSANIS, N., SHARIFI, N., XU, F. L., MYERS, L. A., SPEVAK, P. J., CAMERON, D. E., DE BACKER, J., HELLEMANS, J., CHEN, Y., DAVIS, E. C., WEBB, C. L., KRESS, W., COUCKE, P., RIFKIN, D. B., DE PAEPE, A. M. & DIETZ, H. C. 2005. A syndrome of altered cardiovascular, craniofacial, neurocognitive and skeletal development caused by mutations in TGFBR1 or TGFBR2. *Nat Genet,* 37**,** 275-81.

LOGEMANN, J. A., PAULOSKI, B. R., RADEMAKER, A. W., COLANGELO, L. A., KAHRILAS, P. J. & SMITH, C. H. 2000. Temporal and biomechanical characteristics of oropharyngeal swallow in younger and older men. *J Speech Lang Hear Res,* 43**,** 1264-74.

LOVE, M. I., HUBER, W. & ANDERS, S. 2014. Moderated estimation of fold change and dispersion for RNA-seq data with DESeq2. *Genome Biol,* 15**,** 550.

LŐW, P., MOLNÁR, K. & KRISKA, G. 2016. Dissection of a Chicken (Gallus domesticus).

LU, J., CHATTERJEE, M., SCHMID, H., BECK, S. & GAWAZ, M. 2016. CXCL14 as an emerging immune and inflammatory modulator. *J Inflamm (Lond),* 13**,** 1.

LUDWIG, K. U., MANGOLD, E., HERMS, S., NOWAK, S., REUTTER, H., PAUL, A., BECKER, J., HERBERZ, R., ALCHAWA, T., NASSER, E., BOHMER, A. C., MATTHEISEN, M., ALBLAS, M. A., BARTH, S., KLUCK, N., LAUSTER, C., BRAUMANN, B., REICH, R. H., HEMPRICH, A., POTZSCH, S., BLAUMEISER, B., DARATSIANOS, N., KREUSCH, T., MURRAY, J. C., MARAZITA, M. L., RUCZINSKI, I., SCOTT, A. F., BEATY, T. H., KRAMER, F. J., WIENKER, T. F., STEEGERS-THEUNISSEN, R. P., RUBINI, M., MOSSEY, P. A., HOFFMANN, P., LANGE, C., CICHON, S.,

PROPPING, P., KNAPP, M. & NOTHEN, M. M. 2012. Genome-wide meta-analyses of nonsyndromic cleft lip with or without cleft palate identify six new risk loci. *Nat Genet,* 44**,** 968-71.

LUKE, D. A. 1984. Epithelial proliferation and development of rugae in relation to palatal shelf elevation in the mouse. *J Anat,* 138 (Pt 2)**,** 251-8.

LUMAKA, A., VAN HOLE, C., CASTEELS, I., ORTIBUS, E., DE WOLF, V., VERMEESCH, J. R., LUKUSA, T. & DEVRIENDT, K. 2012. Variability in expression of a familial 2.79 Mb microdeletion in chromosome 14q22.1-22.2. *Am J Med Genet A,* 158a**,** 1381-7.

LUPIANEZ, D. G., SPIELMANN, M. & MUNDLOS, S. 2016. Breaking TADs: How Alterations of Chromatin Domains Result in Disease. *Trends Genet,* 32**,** 225-237.

LUYTEN, A., BETTENS, K., D'HAESELEER, E., DE LEY, S., HODGES, A., GALIWANGO, G., VERMEERSCH, H. & VAN LIERDE, K. 2013. Impact of early synchronous lip and palatal repair on speech. *Folia Phoniatr Logop,* 65**,** 303-11.

MA H, S. K., CHEN G, QIAO XT, CHUANG MY 2006. Application of Real-time Polymerase Chain Reaction (RT-PCR). *J Am Science,* 2.

MAAS, C. & POETS, C. F. 2014. Initial treatment and early weight gain of children with Robin Sequence in Germany: a prospective epidemiological study. *Arch Dis Child Fetal Neonatal Ed,* 99**,** F491-4.

MAAS, S. M., DE JONG, T. P., BUSS, P. & HENNEKAM, R. C. 1996. EEC syndrome and genitourinary anomalies: an update. *Am J Med Genet,* 63**,** 472-8.

MADANI, M. 2007. Laser assisted uvulopalatopharyngoplasty (LA-UPPP) for the treatment of snoring and mild to moderate obstructive sleep apnea. *Atlas Oral Maxillofac Surg Clin North Am,* 15**,** 129-37.

MADDIESON, I. 1984. *Patterns of Sounds,* Cambridge, Cambridge University Press.

MADISEN, L., ZWINGMAN, T. A., SUNKIN, S. M., OH, S. W., ZARIWALA, H. A., GU, H., NG, L. L., PALMITER, R. D., HAWRYLYCZ, M. J., JONES, A. R., LEIN, E. S. & ZENG, H. 2010. A robust and high-throughput Cre reporting and characterization system for the whole mouse brain. *Nat Neurosci,* 13**,** 133-40.

MAJEWSKI, J., SCHWARTZENTRUBER, J., LALONDE, E., MONTPETIT, A. & JABADO, N. 2011. What can exome sequencing do for you? *J Med Genet,* 48**,** 580-9.

MAMMADOVA, A., ACKERMANS, M. M., BLOEMEN, M., OOSTENDORP, C., ZHOU, H., CARELS, C. E. & VON DEN HOFF, J. W. 2014. Effects of retinoic acid on proliferation and gene expression of cleft and non-cleft palatal keratinocytes. *Eur J Orthod,* 36**,** 727-34.

MANGOLD, E., BOHMER, A. C., ISHORST, N., HOEBEL, A. K., GULTEPE, P., SCHUENKE, H., KLAMT, J., HOFMANN, A., GOLZ, L., RAFF, R., TESSMANN, P., NOWAK, S., REUTTER, H., HEMPRICH, A., KREUSCH, T., KRAMER, F. J., BRAUMANN, B., REICH, R., SCHMIDT, G., JAGER, A., REITER, R., BROSCH, S., STAVUSIS, J., ISHIDA, M., SESELGYTE, R., MOORE, G. E., NOTHEN, M. M., BORCK, G., ALDHORAE, K. A., LACE, B., STANIER, P., KNAPP, M. & LUDWIG, K. U. 2016. Sequencing the GRHL3 Coding Region Reveals Rare Truncating Mutations and a Common Susceptibility Variant for Nonsyndromic Cleft Palate. *Am J Hum Genet,* 98**,** 755-62.

MANGOLD, E., LUDWIG, K. U., BIRNBAUM, S., BALUARDO, C., FERRIAN, M., HERMS, S., REUTTER, H., DE ASSIS, N. A., CHAWA, T. A., MATTHEISEN, M., STEFFENS, M., BARTH, S., KLUCK, N., PAUL, A., BECKER, J., LAUSTER, C., SCHMIDT, G., BRAUMANN, B., SCHEER, M., REICH, R. H., HEMPRICH, A., POTZSCH, S., BLAUMEISER, B., MOEBUS, S., KRAWCZAK, M., SCHREIBER, S., MEITINGER, T., WICHMANN, H. E., STEEGERS-THEUNISSEN, R. P., KRAMER, F. J., CICHON, S., PROPPING, P., WIENKER, T. F., KNAPP, M., RUBINI, M., MOSSEY, P. A., HOFFMANN, P. & NOTHEN, M. M. 2010. Genome-wide association study identifies two susceptibility loci for nonsyndromic cleft lip with or without cleft palate. *Nat Genet,* 42**,** 24-6.

MAO, X., FUJIWARA, Y., CHAPDELAINE, A., YANG, H. & ORKIN, S. H. 2001. Activation of EGFP expression by Cre-mediated excision in a new ROSA26 reporter mouse strain. *Blood,* 97**,** 324-6.

MAPAR, D., KHANLAR, F., SADEGHI, S., ABDALI, H., MEMARZADEH, M., DAVARI, H. A. & DERAKHSHANDEH, F. 2019. The incidence of velopharyngeal insufficiency and oronasal fistula after primary palatal surgery with Sommerlad intravelar veloplasty: A retrospective study in Isfahan Cleft Care Team. *Int J Pediatr Otorhinolaryngol,* 120**,** 6-10.

MARCANO, A. C., DOUDNEY, K., BRAYBROOK, C., SQUIRES, R., PATTON, M. A., LEES, M. M., RICHIERI-COSTA, A., LIDRAL, A. C., MURRAY, J. C., MOORE, G. E. & STANIER, P. 2004. TBX22 mutations are a frequent cause of cleft palate. *J Med Genet,* 41**,** 68-74.

MARDINI, S., CHIM, H., SESELGYTE, R. & CHEN, P. K. 2016. Predictors of Success in Furlow Palatoplasty for Submucous Clefts: An Experience with 91 Consecutive Patients. *Plast Reconstr Surg,* 137**,** 135e-141e.

MARGADANT, C. & SONNENBERG, A. 2010. Integrin-TGF-beta crosstalk in fibrosis, cancer and wound healing. *EMBO Rep,* 11**,** 97-105.

MARIONI, J. C., MASON, C. E., MANE, S. M., STEPHENS, M. & GILAD, Y. 2008. RNA-seq: an assessment of technical reproducibility and comparison with gene expression arrays. *Genome Res,* 18**,** 1509-17.

MARK, M., GHYSELINCK, N. B. & CHAMBON, P. 2009. Function of retinoic acid receptors during embryonic development. *Nucl Recept Signal,* 7**,** e002.

MARTINEZ-ALVAREZ, C., BLANCO, M. J., PEREZ, R., RABADAN, M. A., APARICIO, M., RESEL, E., MARTINEZ, T. & NIETO, M. A. 2004. Snail family members and cell survival in physiological and pathological cleft palates. *Dev Biol,* 265**,** 207-18.

MATSUMURA, K., TAKETOMI, T., YOSHIZAKI, K., ARAI, S., SANUI, T., YOSHIGA, D., YOSHIMURA, A. & NAKAMURA, S. 2011. Sprouty2 controls proliferation of palate mesenchymal cells via fibroblast growth factor signaling. *Biochem Biophys Res Commun,* 404**,** 1076-82.

MAUE-DICKSON, W. 1979. The craniofacial complex in cleft lip and palate: an update review of anatomy and function. *Cleft Palate J,* 16**,** 291-317.

MAZZETTI, M. P. V., ALONSO, N., BROCK, R. S., AYOUB, A., MASSUMOTO, S. M. & ECA, L. P. 2018. Importance of Stem Cell Transplantation in Cleft Lip and Palate Surgical Treatment Protocol. *J Craniofac Surg,* 29**,** 1445-1451.

MCDONALD-MCGINN, D. M., LAROSSA, D., GOLDMUNTZ, E., SULLIVAN, K., EICHER, P., GERDES, M., MOSS, E., WANG, P., SOLOT, C., SCHULTZ, P., LYNCH, D., BINGHAM, P., KEENAN, G., WEINZIMER, S., MING, J. E., DRISCOLL, D., CLARK, B. J., 3RD, MARKOWITZ, R., COHEN, A., MOSHANG, T., PASQUARIELLO, P., RANDALL, P., EMANUEL, B. S. & ZACKAI, E. H. 1997. The 22q11.2 deletion: screening, diagnostic workup, and outcome of results; report on 181 patients. *Genet Test,* 1**,** 99-108.

MCGRATH, K. E., KONISKI, A. D., MALTBY, K. M., MCGANN, J. K. & PALIS, J. 1999. Embryonic expression and function of the chemokine SDF-1 and its receptor, CXCR4. *Dev Biol,* 213**,** 442-56.

MCHUGH, M. L. 2011. Multiple comparison analysis testing in ANOVA. *Biochem Med (Zagreb),* 21**,** 203-9.

MCKEOWN, S. J., WALLACE, A. S. & ANDERSON, R. B. 2013. Expression and function of cell adhesion molecules during neural crest migration. *Dev Biol,* 373**,** 244-57.

MEGARBANE, A., PANGRAZIO, A., VILLA, A., CHOUERY, E., MAARAWI, J., SABBAGH, S., LEFRANC, G. & SOBACCHI, C. 2013. Homozygous stop mutation in the SNX10 gene in a consanguineous Iraqi boy with osteopetrosis and corpus callosum hypoplasia. *Eur J Med Genet,* 56**,** 32-5.

MEHENDALE, F. V., BIRCH, M. J., BIRKETT, L., SELL, D. & SOMMERLAD, B. C. 2004. Surgical management of velopharyngeal incompetence in velocardiofacial syndrome. *Cleft Palate Craniofac J,* 41**,** 124-35.

MEHENDALE, F. V., LANE, R., LAVERTY, A., DINWIDDIE, R. & SOMMERLAD, B. C. 2013. Effect of palate re-repairs and hynes pharyngoplasties on pediatric airways: an analysis of preoperative and postoperative cardiorespiratory sleep studies. *Cleft Palate Craniofac J,* 50**,** 257-67.

MERRITT, L. 2005. Part 1. Understanding the embryology and genetics of cleft lip and palate. *Adv Neonatal Care,* 5**,** 64-71.

MESKIN, L. H., GORLIN, R. J. & ISAACSON, R. J. 1964. ABNORMAL MORPHOLOGY OF THE SOFT PALATE. I. THE PREVALENCE OF CLEFT UVULA. *Cleft Palate J,* 35**,** 342-6.

METWALLI, K. A., DO, M. A., NGUYEN, K., MALLICK, S., KIN, K., FAROKHNIA, N., JUN, G. & FAKHOURI, W. D. 2018. Interferon Regulatory Factor 6 Is Necessary for Salivary Glands and Pancreas Development. *J Dent Res,* 97**,** 226-236.

MEUTER, S., SCHAERLI, P., ROOS, R. S., BRANDAU, O., BOSL, M. R., VON ANDRIAN, U. H. & MOSER, B. 2007. Murine CXCL14 is dispensable for dendritic cell function and localization within peripheral tissues. *Mol Cell Biol,* 27**,** 983-92.

MI, H., MURUGANUJAN, A., CASAGRANDE, J. T. & THOMAS, P. D. 2013. Large-scale gene function analysis with the PANTHER classification system. *Nat Protoc,* 8**,** 1551-66.

MILLS, A. A., ZHENG, B., WANG, X. J., VOGEL, H., ROOP, D. R. & BRADLEY, A. 1999. p63 is a p53 homologue required for limb and epidermal morphogenesis. *Nature,* 398**,** 708-13.

MILUNSKY, J. M., MAHER, T. A., ZHAO, G., ROBERTS, A. E., STALKER, H. J., ZORI, R. T., BURCH, M. N., CLEMENS, M., MULLIKEN, J. B., SMITH, R. & LIN, A. E. 2008. TFAP2A mutations result in branchio-oculo-facial syndrome. *Am J Hum Genet,* 82**,** 1171-7.

MING, J. E., KAUPAS, M. E., ROESSLER, E., BRUNNER, H. G., GOLABI, M., TEKIN, M., STRATTON, R. F., SUJANSKY, E., BALE, S. J. & MUENKE, M. 2002. Mutations in PATCHED-1, the receptor for SONIC HEDGEHOG, are associated with holoprosencephaly. *Hum Genet,* 110**,** 297-301.

MINOUX, M. & RIJLI, F. M. 2010. Molecular mechanisms of cranial neural crest cell migration and patterning in craniofacial development. *Development,* 137**,** 2605-21.

MISSAGIA, R. V. & PERINI, F. A. 2018. Skull morphology of the Brazilian shrew mouse Blarinomys breviceps (Akodontini; Sigmodontinae), with comparative notes on Akodontini rodents. *Zoologischer Anzeiger,* 277**,** 148-161.

MITCHELL, C. J., KIM, M. S., ZHONG, J., NIRUJOGI, R. S., BOSE, A. K. & PANDEY, A. 2016. Unbiased identification of substrates of protein tyrosine phosphatase ptp-3 in C. elegans. *Mol Oncol,* 10**,** 910-20.

MITCHELL, K., O'SULLIVAN, J., MISSERO, C., BLAIR, E., RICHARDSON, R., ANDERSON, B., ANTONINI, D., MURRAY, J. C., SHANSKE, A. L., SCHUTTE, B. C., ROMANO, R. A., SINHA, S., BHASKAR, S. S., BLACK, G. C., DIXON, J. & DIXON, M. J. 2012. Exome sequence identifies RIPK4 as the Bartsocas-Papas syndrome locus. *Am J Hum Genet,* 90**,** 69-75.

MITRA, A. K., STESSMAN, H. A., SCHAEFER, R. J., WANG, W., MYERS, C. L., VAN NESS, B. G. & BEIRAGHI, S. 2016. Fine-Mapping of 18q21.1 Locus Identifies Single Nucleotide Polymorphisms Associated with Nonsyndromic Cleft Lip with or without Cleft Palate. *Front Genet,* 7**,** 88.

MITSUI, S. N., YASUE, A., MASUDA, K., NARUTO, T., MINEGISHI, Y., OYADOMARI, S., NOJI, S., IMOTO, I. & TANAKA, E. 2016. Novel human mutation and CRISPR/Cas genome-edited mice reveal the importance of C-terminal domain of MSX1 in tooth and palate development. *Sci Rep,* 6**,** 38398.

MIURA, N., KAKINUMA, H., SATO, M., AIBA, N., TERADA, K. & SUGIYAMA, T. 1998. Mouse forkhead (winged helix) gene LUN encodes a transactivator that acts in the lung. *Genomics,* 50**,** 346-56.

MOHAMAD SHAH, N. S., SALAHSHOURIFAR, I., SULONG, S., WAN SULAIMAN, W. A. & HALIM, A. S. 2016. Discovery of candidate genes for nonsyndromic cleft lip palate through genome-

wide linkage analysis of large extended families in the Malay population. *BMC Genet,* 17**,** 39.

MONEMI, M., ERIKSSON, P. O., DUBAIL, I., BUTLER-BROWNE, G. S. & THORNELL, L. E. 1996. Fetal myosin heavy chain increases in human masseter muscle during aging. *FEBS Lett,* 386**,** 87-90.

MOON, J. B., SMITH, A. E., FOLKINS, J. W., LEMKE, J. H. & GARTLAN, M. 1994. Coordination of velopharyngeal muscle activity during positioning of the soft palate. *Cleft Palate Craniofac J,* 31**,** 45-55.

MOON, J. B., THOMPSON, S. A., JAECKEL, E. & CANADY, J. W. 1998. Muscle fiber type distribution in the normal human levator veli palatini muscle. *Cleft Palate Craniofac J,* 35**,** 419-24.

MOORE, G. E., IVENS, A., CHAMBERS, J., FARRALL, M., WILLIAMSON, R., PAGE, D. C., BJORNSSON, A., ARNASON, A. & JENSSON, O. 1987. Linkage of an X-chromosome cleft palate gene. *Nature,* 326**,** 91-2.

MOOTHA, V. K., LINDGREN, C. M., ERIKSSON, K. F., SUBRAMANIAN, A., SIHAG, S., LEHAR, J., PUIGSERVER, P., CARLSSON, E., RIDDERSTRALE, M., LAURILA, E., HOUSTIS, N., DALY, M. J., PATTERSON, N., MESIROV, J. P., GOLUB, T. R., TAMAYO, P., SPIEGELMAN, B., LANDER, E. S., HIRSCHHORN, J. N., ALTSHULER, D. & GROOP, L. C. 2003. PGC-1alpha-responsive genes involved in oxidative phosphorylation are coordinately downregulated in human diabetes. *Nat Genet,* 34**,** 267-73.

MORGAN, N. V., BRUETON, L. A., COX, P., GREALLY, M. T., TOLMIE, J., PASHA, S., ALIGIANIS, I. A., VAN BOKHOVEN, H., MARTON, T., AL-GAZALI, L., MORTON, J. E., OLEY, C., JOHNSON, C. A., TREMBATH, R. C., BRUNNER, H. G. & MAHER, E. R. 2006. Mutations in the embryonal subunit of the acetylcholine receptor (CHRNG) cause lethal and Escobar variants of multiple pterygium syndrome. *Am J Hum Genet,* 79**,** 390-5.

MORICE, A., RENAULT, F., SOUPRE, V., CHAPUIS, C., TRICHET ZBINDEN, C., KADLUB, N., GIUDICE, A., VAZQUEZ, M. P. & PICARD, A. 2018. Predictors of speech outcomes in children with Pierre Robin sequence. *J Craniomaxillofac Surg,* 46**,** 479-484.

MORROW, B. E., MCDONALD-MCGINN, D. M., EMANUEL, B. S., VERMEESCH, J. R. & SCAMBLER, P. J. 2018. Molecular genetics of 22q11.2 deletion syndrome. *Am J Med Genet A,* 176**,** 2070-2081.

MORTAZAVI, A., WILLIAMS, B. A., MCCUE, K., SCHAEFFER, L. & WOLD, B. 2008. Mapping and quantifying mammalian transcriptomes by RNA-Seq. *Nat Methods,* 5**,** 621-8.

MOSSEY, P. A., LITTLE, J., MUNGER, R. G., DIXON, M. J. & SHAW, W. C. 2009. Cleft lip and palate. *Lancet,* 374**,** 1773-85.

MULLER, C. W. & HERRMANN, B. G. 1997. Crystallographic structure of the T domain-DNA complex of the Brachyury transcription factor. *Nature,* 389**,** 884-8.

MURPHY, K. C. & SCAMBLER, P. J. 2005. *Velo-Cardio-Facial Syndrome*, Cambridge University Press.

MURRAY, S. A., ORAM, K. F. & GRIDLEY, T. 2007. Multiple functions of Snail family genes during palate development in mice. *Development,* 134**,** 1789-97.

NAGY, A., GERTSENSTEIN, M., VINTERSTEN, K. & BEHRINGER, R. 2009. Alizarin red staining of post-natal bone in mouse. *Cold Spring Harb Protoc,* 2009**,** pdb.prot5171.

NAICHE, L. A., HARRELSON, Z., KELLY, R. G. & PAPAIOANNOU, V. E. 2005. T-box genes in vertebrate development. *Annu Rev Genet,* 39**,** 219-39.

NAKAJIMA, A., SHULER, F. C., GULKA, A. O. D. & HANAI, J. I. 2018. TGF-beta Signaling and the Epithelial-Mesenchymal Transition during Palatal Fusion. *Int J Mol Sci,* 19.

NARAN, S., FORD, M. & LOSEE, J. E. 2017. What's New in Cleft Palate and Velopharyngeal Dysfunction Management? *Plast Reconstr Surg,* 139**,** 1343e-1355e.

NG, D., THAKKER, N., CORCORAN, C. M., DONNAI, D., PERVEEN, R., SCHNEIDER, A., HADLEY, D. W., TIFFT, C., ZHANG, L., WILKIE, A. O., VAN DER SMAGT, J. J., GORLIN, R. J., BURGESS, S. M., BARDWELL, V. J., BLACK, G. C. & BIESECKER, L. G. 2004. Oculofaciocardiodental and Lenz

microphthalmia syndromes result from distinct classes of mutations in BCOR. *Nat Genet,* 36**,** 411-6.

NG, S. B., BIGHAM, A. W., BUCKINGHAM, K. J., HANNIBAL, M. C., MCMILLIN, M. J., GILDERSLEEVE, H. I., BECK, A. E., TABOR, H. K., COOPER, G. M., MEFFORD, H. C., LEE, C., TURNER, E. H., SMITH, J. D., RIEDER, M. J., YOSHIURA, K., MATSUMOTO, N., OHTA, T., NIIKAWA, N., NICKERSON, D. A., BAMSHAD, M. J. & SHENDURE, J. 2010a. Exome sequencing identifies MLL2 mutations as a cause of Kabuki syndrome. *Nat Genet,* 42**,** 790-3.

NG, S. B., BUCKINGHAM, K. J., LEE, C., BIGHAM, A. W., TABOR, H. K., DENT, K. M., HUFF, C. D., SHANNON, P. T., JABS, E. W., NICKERSON, D. A., SHENDURE, J. & BAMSHAD, M. J. 2010b. Exome sequencing identifies the cause of a mendelian disorder. *Nat Genet,* 42**,** 30-5.

NIEMANN, S., ZHAO, C., PASCU, F., STAHL, U., AULEPP, U., NISWANDER, L., WEBER, J. L. & MULLER, U. 2004. Homozygous WNT3 mutation causes tetra-amelia in a large consanguineous family. *Am J Hum Genet,* 74**,** 558-63.

NIK, A. M., JOHANSSON, J. A., GHIAMI, M., REYAHI, A. & CARLSSON, P. 2016. Foxf2 is required for secondary palate development and Tgfbeta signaling in palatal shelf mesenchyme. *Dev Biol,* 415**,** 14-23.

NISHIHARA, H., KOBAYASHI, N., KIMURA-YOSHIDA, C., YAN, K., BORMUTH, O., DING, Q., NAKANISHI, A., SASAKI, T., HIRAKAWA, M., SUMIYAMA, K., FURUTA, Y., TARABYKIN, V., MATSUO, I. & OKADA, N. 2016. Coordinately Co-opted Multiple Transposable Elements Constitute an Enhancer for wnt5a Expression in the Mammalian Secondary Palate. *PLoS Genet,* 12**,** e1006380.

NODEN, D. M. & TRAINOR, P. A. 2005. Relations and interactions between cranial mesoderm and neural crest populations. Oxford, UK.

O'RAHILLY, R. & GARDNER, E. 1972. The initial appearance of ossification in staged human embryos. *Am J Anat,* 134**,** 291-301.

OHYAMA, C., SMITH, P. L., ANGATA, K., FUKUDA, M. N., LOWE, J. B. & FUKUDA, M. 1998. Molecular cloning and expression of GDP-D-mannose-4,6-dehydratase, a key enzyme for fucose metabolism defective in Lec13 cells. *J Biol Chem,* 273**,** 14582-7.

ONNIS, L., TRUZZI, A. & MA, X. 2018. Language development and disorders: Possible genes and environment interactions. *Res Dev Disabil,* 82**,** 132-146.

ORIOLI, I. M., VIEIRA, A. R., CASTILLA, E. E., MING, J. E. & MUENKE, M. 2002. Mutational analysis of the Sonic Hedgehog gene in 220 newborns with oral clefts in a South American (ECLAMC) population. *Am J Med Genet,* 108**,** 12-5.

ORMEROD, M. G. 1994. *Flow cytometry,* Oxford, BIOS Scientific Publishers in association with the Royal Microscopical Society.

ORMESTAD, M., ASTORGA, J. & CARLSSON, P. 2004. Differences in the embryonic expression patterns of mouse Foxf1 and -2 match their distinct mutant phenotypes. *Dev Dyn,* 229**,** 328-33.

ORTEGA, N., BEHONICK, D. J. & WERB, Z. 2004. Matrix remodeling during endochondral ossification. *Trends Cell Biol,* 14**,** 86-93.

OWEN, N. & MOOSAJEE, M. 2019. RNA-sequencing in ophthalmology research: considerations for experimental design and analysis. 11**,** 2515841419835460.

OZTURK, F., LI, Y., ZHU, X., GUDA, C. & NAWSHAD, A. 2013. Systematic analysis of palatal transcriptome to identify cleft palate genes within TGFbeta3-knockout mice alleles: RNA-Seq analysis of TGFbeta3 Mice. *BMC Genomics,* 14**,** 113.

PAN, W., LIN, J. & LE, C. T. 2002. How many replicates of arrays are required to detect gene expression changes in microarray experiments? A mixture model approach. *Genome Biol,* 3.

PAN, Y., HAN, Y., ZHANG, H., ZHOU, L., LI, D., CAI, Q., MA, J., ZHANG, W. & WANG, L. 2013. Association and cumulative effects of GWAS-identified genetic variants for nonsyndromic orofacial clefts in a Chinese population. *Environ Mol Mutagen,* 54**,** 261-7.

PAPAIOANNOU, V. E. 2014. The T-box gene family: emerging roles in development, stem cells and cancer. *Development,* 141**,** 3819-33.

PAPAIOANNOU, V. E. & SILVER, L. M. 1998. The T-box gene family. *Bioessays,* 20**,** 9-19.

PARK, J. W., CAI, J., MCINTOSH, I., JABS, E. W., FALLIN, M. D., INGERSOLL, R., HETMANSKI, J. B., VEKEMANS, M., ATTIE-BITACH, T., LOVETT, M., SCOTT, A. F. & BEATY, T. H. 2006. High throughput SNP and expression analyses of candidate genes for non-syndromic oral clefts. *J Med Genet,* 43**,** 598-608.

PARK, M., AHN, S. H., JEONG, J. H. & BAEK, R. M. 2015. Evaluation of the levator veli palatini muscle thickness in patients with velocardiofacial syndrome using magnetic resonance imaging. *J Plast Reconstr Aesthet Surg,* 68**,** 1100-5.

PARK, S., SASO, Y., ITO, O., TOKIOKA, K., KATO, K., NITTA, N. & KITANO, I. 2000. A retrospective study of speech development in patients with submucous cleft palate treated by four operations. *Scand J Plast Reconstr Surg Hand Surg,* 34**,** 131-6.

PASSAVANT, G. 1869. Ueber die verschliessung des Schlundes beim Sprechen. *Archiv f. pathol. Anat.,* 46**,** 1-31.

PAUL, B. J., PALMER, K., SHARP, J. C., PRATT, C. H., MURRAY, S. A. & DUNNWALD, M. 2017. ARHGAP29 Mutation Is Associated with Abnormal Oral Epithelial Adhesions. *J Dent Res,* 96**,** 1298-1305.

PAUWS, E., HOSHINO, A., BENTLEY, L., PRAJAPATI, S., KELLER, C., HAMMOND, P., MARTINEZ-BARBERA, J. P., MOORE, G. E. & STANIER, P. 2009a. Tbx22null mice have a submucous cleft palate due to reduced palatal bone formation and also display ankyloglossia and choanal atresia phenotypes. *Hum Mol Genet,* 18**,** 4171-9.

PAUWS, E., MOORE, G. E. & STANIER, P. 2009b. A functional haplotype variant in the TBX22 promoter is associated with cleft palate and ankyloglossia. *J Med Genet,* 46**,** 555-61.

PAYLOR, R., GLASER, B., MUPO, A., ATALIOTIS, P., SPENCER, C., SOBOTKA, A., SPARKS, C., CHOI, C. H., OGHALAI, J., CURRAN, S., MURPHY, K. C., MONKS, S., WILLIAMS, N., O'DONOVAN, M. C., OWEN, M. J., SCAMBLER, P. J. & LINDSAY, E. 2006. Tbx1 haploinsufficiency is linked to behavioral disorders in mice and humans: implications for 22q11 deletion syndrome. *Proc Natl Acad Sci U S A,* 103**,** 7729-34.

PELTON, R. W., HOGAN, B. L., MILLER, D. A. & MOSES, H. L. 1990. Differential expression of genes encoding TGFs beta 1, beta 2, and beta 3 during murine palate formation. *Dev Biol,* 141**,** 456-60.

PERKINS, J. A., LEWIS, C. W., GRUSS, J. S., EBLEN, L. E. & SIE, K. C. 2005. Furlow palatoplasty for management of velopharyngeal insufficiency: a prospective study of 148 consecutive patients. *Plast Reconstr Surg,* 116**,** 72-80; discussion 81-4.

PERRY, J. L. 2011. Anatomy and physiology of the velopharyngeal mechanism. *Semin Speech Lang,* 32**,** 83-92.

PERRY, J. L., KUEHN, D. P., SUTTON, B. P. & FANG, X. 2017. Velopharyngeal Structural and Functional Assessment of Speech in Young Children Using Dynamic Magnetic Resonance Imaging. *Cleft Palate Craniofac J,* 54**,** 408-422.

PEYRARD-JANVID, M., LESLIE, E. J., KOUSA, Y. A., SMITH, T. L., DUNNWALD, M., MAGNUSSON, M., LENTZ, B. A., UNNEBERG, P., FRANSSON, I., KOILLINEN, H. K., RAUTIO, J., PEGELOW, M., KARSTEN, A., BASEL-VANAGAITE, L., GORDON, W., ANDERSEN, B., SVENSSON, T., MURRAY, J. C., CORNELL, R. A., KERE, J. & SCHUTTE, B. C. 2014. Dominant mutations in GRHL3 cause Van der Woude Syndrome and disrupt oral periderm development. *Am J Hum Genet,* 94**,** 23-32.

PIERROU, S., HELLQVIST, M., SAMUELSSON, L., ENERBACK, S. & CARLSSON, P. 1994. Cloning and characterization of seven human forkhead proteins: binding site specificity and DNA bending. *Embo j,* 13**,** 5002-12.

PODVINEC, S. 1952. The physiology and pathology of the soft palate. *J Laryngol Otol,* 66**,** 452-61.

POSWILLO, D. & ROY, L. J. 1965. The pathogenesis of cleft palate. An animal study. *Br J Surg,* 52**,** 902-12.

PRINTZLAU, A. & ANDERSEN, M. 2004. Pierre Robin sequence in Denmark: a retrospective population-based epidemiological study. *Cleft Palate Craniofac J,* 41**,** 47-52.

PROETZEL, G., PAWLOWSKI, S. A., WILES, M. V., YIN, M., BOIVIN, G. P., HOWLES, P. N., DING, J., FERGUSON, M. W. & DOETSCHMAN, T. 1995. Transforming growth factor-beta 3 is required for secondary palate fusion. *Nat Genet,* 11**,** 409-14.

QUADERI, N. A., SCHWEIGER, S., GAUDENZ, K., FRANCO, B., RUGARLI, E. I., BERGER, W., FELDMAN, G. J., VOLTA, M., ANDOLFI, G., GILGENKRANTZ, S., MARION, R. W., HENNEKAM, R. C., OPITZ, J. M., MUENKE, M., ROPERS, H. H. & BALLABIO, A. 1997. Opitz G/BBB syndrome, a defect of midline development, is due to mutations in a new RING finger gene on Xp22. *Nat Genet,* 17**,** 285-91.

RADBRUCH, A. 1992. *Flow cytometry and cell sorting; Berlin, New York: Springer-Verlag*.

RAHIMOV, F., MARAZITA, M. L., VISEL, A., COOPER, M. E., HITCHLER, M. J., RUBINI, M., DOMANN, F. E., GOVIL, M., CHRISTENSEN, K., BILLE, C., MELBYE, M., JUGESSUR, A., LIE, R. T., WILCOX, A. J., FITZPATRICK, D. R., GREEN, E. D., MOSSEY, P. A., LITTLE, J., STEEGERS-THEUNISSEN, R. P., PENNACCHIO, L. A., SCHUTTE, B. C. & MURRAY, J. C. 2008. Disruption of an AP-2alpha binding site in an IRF6 enhancer is associated with cleft lip. *Nat Genet,* 40**,** 1341-7.

RAINGER, J. K., BHATIA, S., BENGANI, H., GAUTIER, P., RAINGER, J., PEARSON, M., ANSARI, M., CROW, J., MEHENDALE, F., PALINKASOVA, B., DIXON, M. J., THOMPSON, P. J., MATARIN, M., SISODIYA, S. M., KLEINJAN, D. A. & FITZPATRICK, D. R. 2014. Disruption of SATB2 or its long-range cis-regulation by SOX9 causes a syndromic form of Pierre Robin sequence. *Hum Mol Genet,* 23**,** 2569-79.

RAUCH, F. & GLORIEUX, F. H. 2004. Osteogenesis imperfecta. *Lancet,* 363**,** 1377-85.

REITER, R., BROSCH, S., LUDEKE, M., FISCHBEIN, E., HAASE, S., PICKHARD, A., ASSUM, G., SCHWANDT, A., VOGEL, W., HOGEL, J. & MAIER, C. 2012. Genetic and environmental risk factors for submucous cleft palate. *Eur J Oral Sci,* 120**,** 97-103.

RICE, J. P., SACCONE, N. L. & CORBETT, J. 2001. The lod score method. *Adv Genet,* 42**,** 99-113.

RICE, R., CONNOR, E. & RICE, D. P. 2006. Expression patterns of Hedgehog signalling pathway members during mouse palate development. *Gene Expr Patterns,* 6**,** 206-12.

RICE, R., SPENCER-DENE, B., CONNOR, E. C., GRITLI-LINDE, A., MCMAHON, A. P., DICKSON, C., THESLEFF, I. & RICE, D. P. 2004. Disruption of Fgf10/Fgfr2b-coordinated epithelial-mesenchymal interactions causes cleft palate. *J Clin Invest,* 113**,** 1692-700.

RICHARDSON, R. J., DIXON, J., JIANG, R. & DIXON, M. J. 2009. Integration of IRF6 and Jagged2 signalling is essential for controlling palatal adhesion and fusion competence. *Hum Mol Genet,* 18**,** 2632-42.

RICHARDSON, R. J., DIXON, J., MALHOTRA, S., HARDMAN, M. J., KNOWLES, L., BOOT-HANDFORD, R. P., SHORE, P., WHITMARSH, A. & DIXON, M. J. 2006. Irf6 is a key determinant of the keratinocyte proliferation-differentiation switch. *Nat Genet,* 38**,** 1329-34.

RICHARDSON, R. J., HAMMOND, N. L., COULOMBE, P. A., SALORANTA, C., NOUSIAINEN, H. O., SALONEN, R., BERRY, A., HANLEY, N., HEADON, D., KARIKOSKI, R. & DIXON, M. J. 2014. Periderm prevents pathological epithelial adhesions during embryogenesis. *J Clin Invest,* 124**,** 3891-900.

RILEY, B. M., MANSILLA, M. A., MA, J., DAACK-HIRSCH, S., MAHER, B. S., RAFFENSPERGER, L. M., RUSSO, E. T., VIEIRA, A. R., DODE, C., MOHAMMADI, M., MARAZITA, M. L. & MURRAY, J. C.

2007. Impaired FGF signaling contributes to cleft lip and palate. *Proc Natl Acad Sci U S A,* 104**,** 4512-7.
RINNE, T., BRUNNER, H. G. & VAN BOKHOVEN, H. 2007. p63-associated disorders. *Cell Cycle,* 6**,** 262-8.
ROBIN, P. 1994. A fall of the base of the tongue considered as a new cause of nasopharyngeal respiratory impairment: Pierre Robin sequence, a translation. 1923. *Plast Reconstr Surg,* 93**,** 1301-3.
ROCKSTROH, D., PFAFFLE, H., LE DUC, D., ROSSLER, F., SCHLENSOG-SCHUSTER, F., HEIKER, J. T., KRATZSCH, J., KIESS, W., LEMKE, J. R., ABOU JAMRA, R. & PFAFFLE, R. 2019. A new p.(Ile66Serfs*93) IGF2 variant is associated with pre- and postnatal growth retardation. *Eur J Endocrinol,* 180**,** K1-k13.
ROESSLER, E., DU, Y. Z., MULLOR, J. L., CASAS, E., ALLEN, W. P., GILLESSEN-KAESBACH, G., ROEDER, E. R., MING, J. E., RUIZ I ALTABA, A. & MUENKE, M. 2003. Loss-of-function mutations in the human GLI2 gene are associated with pituitary anomalies and holoprosencephaly-like features. *Proc Natl Acad Sci U S A,* 100**,** 13424-9.
ROGERS, B. O. 1967. Palate surgery prior to von Graefe's pioneering staphylorrhaphy (1819): an historical review of the early causes of surgical indifference in repairing the cleft palate. *Plast Reconstr Surg,* 39**,** 1-19.
ROGERS, C. D., JAYASENA, C. S., NIE, S. & BRONNER, M. E. 2012. Neural crest specification: tissues, signals, and transcription factors. *Wiley Interdiscip Rev Dev Biol,* 1**,** 52-68.
ROGERS, M. F., SHIHAB, H. A., MORT, M., COOPER, D. N., GAUNT, T. R. & CAMPBELL, C. 2018. FATHMM-XF: accurate prediction of pathogenic point mutations via extended features. *Bioinformatics,* 34**,** 511-513.
ROURKE, R., WEINBERG, S. M., MARAZITA, M. L. & JABBOUR, N. 2017. Diagnosing subtle palatal anomalies: Validation of video-analysis and assessment protocol for diagnosing occult submucous cleft palate. *Int J Pediatr Otorhinolaryngol,* 100**,** 242-246.
ROUX, P. J. 1825. Memoire sur la Staphylorraphie, ou Suture du Voile du Palais.**,** 84.
RUVINSKY, I., SILVER, L. M. & GIBSON-BROWN, J. J. 2000. Phylogenetic analysis of T-Box genes demonstrates the importance of amphioxus for understanding evolution of the vertebrate genome. *Genetics,* 156**,** 1249-57.
SADOVE, A. M., VAN AALST, J. A. & CULP, J. A. 2004. Cleft palate repair: art and issues. *Clin Plast Surg,* 31**,** 231-41.
SAGAR, P. & NIMKIN, K. 2015. Feasibility study to assess clinical applications of 3-T cine MRI coupled with synchronous audio recording during speech in evaluation of velopharyngeal insufficiency in children. *Pediatr Radiol,* 45**,** 217-27.
SAKAMOTO, M. K., NAKAMURA, K., HANDA, J., KIHARA, T. & TANIMURA, T. 1989. Morphogenesis of the secondary palate in mouse embryos with special reference to the development of rugae. *Anat Rec,* 223**,** 299-310.
SALEEM, A. A. & SIDDIQUI, S. N. 2015. Fraser Syndrome. *J Coll Physicians Surg Pak,* 25 Suppl 2**,** S124-6.
SAMBASIVAN, R., GAYRAUD-MOREL, B., DUMAS, G., CIMPER, C., PAISANT, S., KELLY, R. G. & TAJBAKHSH, S. 2009. Distinct regulatory cascades govern extraocular and pharyngeal arch muscle progenitor cell fates. *Dev Cell,* 16**,** 810-21.
SAMBASIVAN, R., KURATANI, S. & TAJBAKHSH, S. 2011. An eye on the head: the development and evolution of craniofacial muscles. *Development,* 138**,** 2401-15.
SANDY, J., WILLIAMS, A., MILDINHALL, S., MURPHY, T., BEARN, D., SHAW, B., SELL, D., DEVLIN, B. & MURRAY, J. 1998. The Clinical Standards Advisory Group (CSAG) Cleft Lip and Palate Study. *Br J Orthod,* 25**,** 21-30.
SANDY, J. R. 2019. Making a difference for children born with a cleft in the UK. *J Orthod,* 46**,** 77-80.

SANDY, J. R., WILLIAMS, A. C., BEARN, D., MILDINHALL, S., MURPHY, T., SELL, D., MURRAY, J. J. & SHAW, W. C. 2001. Cleft lip and palate care in the United Kingdom--the Clinical Standards Advisory Group (CSAG) Study. Part 1: background and methodology. *Cleft Palate Craniofac J,* 38**,** 20-3.

SANGER, F. 1988. Sequnces, sequnces and sequnces. *Annual Review of Biochemistry,* 57**,** 1-29.

SANGER, F., NICKLEN, S. & COULSON, A. R. 1992. DNA sequencing with chain-terminating inhibitors. 1977. *Biotechnology,* 24**,** 104-8.

SARDONE, V., ELLIS, M., TORELLI, S., FENG, L., CHAMBERS, D., EASTWOOD, D., SEWRY, C., PHADKE, R., MORGAN, J. E. & MUNTONI, F. 2018. A novel high-throughput immunofluorescence analysis method for quantifying dystrophin intensity in entire transverse sections of Duchenne muscular dystrophy muscle biopsy samples. *PLoS One,* 13**,** e0194540.

SASAKI, Y., ISHIDA, S., MORIMOTO, I., YAMASHITA, T., KOJIMA, T., KIHARA, C., TANAKA, T., IMAI, K., NAKAMURA, Y. & TOKINO, T. 2002. The p53 family member genes are involved in the Notch signal pathway. *J Biol Chem,* 277**,** 719-24.

SATOKATA, I. & MAAS, R. 1994. Msx1 deficient mice exhibit cleft palate and abnormalities of craniofacial and tooth development. *Nat Genet,* 6**,** 348-56.

SCHIAFFINO, S., ROSSI, A. C., SMERDU, V., LEINWAND, L. A. & REGGIANI, C. 2015. Developmental myosins: expression patterns and functional significance. *Skeletal muscle,* 5**,** 22-22.

SCHNEIDER, L. & D'ADDA DI FAGAGNA, F. 2012. Neural stem cells exposed to BrdU lose their global DNA methylation and undergo astrocytic differentiation. *Nucleic Acids Res,* 40**,** 5332-42.

SCHREURS, M., SUTTORP, C. M., MUTSAERS, H. A. M., KUIJPERS-JAGTMAN, A. M., VON DEN HOFF, J. W., ONGKOSUWITO, E. M., CARVAJAL MONROY, P. L. & WAGENER, F. 2019. Tissue engineering strategies combining molecular targets against inflammation and fibrosis, and umbilical cord blood stem cells to improve hampered muscle and skin regeneration following cleft repair. *Med Res Rev***,** 1-18.

SCHURCH, N. J., SCHOFIELD, P., GIERLINSKI, M., COLE, C., SHERSTNEV, A., SINGH, V., WROBEL, N., GHARBI, K., SIMPSON, G. G., OWEN-HUGHES, T., BLAXTER, M. & BARTON, G. J. 2016. Erratum: How many biological replicates are needed in an RNA-seq experiment and which differential expression tool should you use? *Rna,* 22**,** 1641.

SCHWARZ, J. M., RODELSPERGER, C., SCHUELKE, M. & SEELOW, D. 2010. MutationTaster evaluates disease-causing potential of sequence alterations. *Nat Methods,* 7**,** 575-6.

SCOTT, J. K., LEARY, S. D., NESS, A. R., SANDY, J. R., PERSSON, M., KILPATRICK, N. & WAYLEN, A. E. 2015. Perceptions of team members working in cleft services in the United kingdom: a pilot study. *Cleft Palate Craniofac J,* 52**,** e1-7.

SEDGWICK, A. E. & D'SOUZA-SCHOREY, C. 2016. Wnt Signaling in Cell Motility and Invasion: Drawing Parallels between Development and Cancer. *Cancers (Basel),* 8.

SELL, D., HARDING, A. & GRUNWELL, P. 1999. GOS.SP.ASS.'98: an assessment for speech disorders associated with cleft palate and/or velopharyngeal dysfunction (revised). *Int J Lang Commun Disord,* 34**,** 17-33.

SESELGYTE, R., BRYANT, D., DEMETRIOU, C., ISHIDA, M., PESKETT, E., MORENO, N., MORROGH, D., SELL, D., LEES, M., FARRALL, M., MOORE, G. E., SOMMERLAD, B., PAUWS, E. & STANIER, P. 2019. Disruption of FOXF2 as a Likely Cause of Absent Uvula in an Egyptian Family. 98**,** 659-665.

SETO-SALVIA, N. & STANIER, P. 2014. Genetics of cleft lip and/or cleft palate: association with other common anomalies. *Eur J Med Genet,* 57**,** 381-93.

SHAMBLOTT, M. J., BUGG, E. M., LAWLER, A. M. & GEARHART, J. D. 2002. Craniofacial abnormalities resulting from targeted disruption of the murine Sim2 gene. *Dev Dyn,* 224**,** 373-80.

SHAPIRO, H. M. 2018. Flow Cytometry: The Glass Is Half Full. *Methods Mol Biol,* 1678**,** 1-10.

SHIMOMURA, T., KAWAKAMI, M., TATSUMI, K., TANAKA, T., MORITA-TAKEMURA, S., KIRITA, T. & WANAKA, A. 2019. The Role of the Wnt Signaling Pathway in Upper Jaw Development of Chick Embryo. *Acta Histochem Cytochem,* 52**,** 19-26.

SHIOMI, N., CUI, X. M., YAMAMOTO, T., SAITO, T. & SHULER, C. F. 2006. Inhibition of SMAD2 expression prevents murine palatal fusion. *Dev Dyn,* 235**,** 1785-93.

SHIOTA, K., KOSAZUMA, T., KLUG, S. & NEUBERT, D. 1990. Development of the fetal mouse palate in suspension organ culture. *Acta Anat (Basel),* 137**,** 59-64.

SHU, X., SHU, S. & CHENG, H. 2019. Genome-Wide mRNA-Seq Profiling Reveals that LEF1 and SMAD3 Regulate Epithelial-Mesenchymal Transition Through the Hippo Signaling Pathway During Palatal Fusion. *Genet Test Mol Biomarkers,* 23**,** 197-203.

SILVER, A. L., NIMKIN, K., ASHLAND, J. E., GHOSH, S. S., VAN DER KOUWE, A. J., BRIGGER, M. T. & HARTNICK, C. J. 2011. Cine magnetic resonance imaging with simultaneous audio to evaluate pediatric velopharyngeal insufficiency. *Arch Otolaryngol Head Neck Surg,* 137**,** 258-63.

SIMOES-COSTA, M., TAN-CABUGAO, J., ANTOSHECHKIN, I., SAUKA-SPENGLER, T. & BRONNER, M. E. 2014. Transcriptome analysis reveals novel players in the cranial neural crest gene regulatory network. *Genome Res,* 24**,** 281-90.

SLAVOTINEK, A. M. & TIFFT, C. J. 2002. Fraser syndrome and cryptophthalmos: review of the diagnostic criteria and evidence for phenotypic modules in complex malformation syndromes. *J Med Genet,* 39**,** 623-33.

SLEEMAN, M. A., FRASER, J. K., MURISON, J. G., KELLY, S. L., PRESTIDGE, R. L., PALMER, D. J., WATSON, J. D. & KUMBLE, K. D. 2000. B cell- and monocyte-activating chemokine (BMAC), a novel non-ELR alpha-chemokine. *Int Immunol,* 12**,** 677-89.

SNYDER-WARWICK, A. K., PERLYN, C. A., PAN, J., YU, K., ZHANG, L. & ORNITZ, D. M. 2010. Analysis of a gain-of-function FGFR2 Crouzon mutation provides evidence of loss of function activity in the etiology of cleft palate. *Proc Natl Acad Sci U S A,* 107**,** 2515-20.

SOLER ARTIGAS, M., WAIN, L. V., MILLER, S., KHEIRALLAH, A. K., HUFFMAN, J. E., NTALLA, I., SHRINE, N., OBEIDAT, M., TROCHET, H., MCARDLE, W. L., ALVES, A. C., HUI, J., ZHAO, J. H., JOSHI, P. K., TEUMER, A., ALBRECHT, E., IMBODEN, M., RAWAL, R., LOPEZ, L. M., MARTEN, J., ENROTH, S., SURAKKA, I., POLASEK, O., LYYTIKAINEN, L. P., GRANELL, R., HYSI, P. G., FLEXEDER, C., MAHAJAN, A., BEILBY, J., BOSSE, Y., BRANDSMA, C. A., CAMPBELL, H., GIEGER, C., GLASER, S., GONZALEZ, J. R., GRALLERT, H., HAMMOND, C. J., HARRIS, S. E., HARTIKAINEN, A. L., HELIOVAARA, M., HENDERSON, J., HOCKING, L., HORIKOSHI, M., HUTRI-KAHONEN, N., INGELSSON, E., JOHANSSON, A., KEMP, J. P., KOLCIC, I., KUMAR, A., LIND, L., MELEN, E., MUSK, A. W., NAVARRO, P., NICKLE, D. C., PADMANABHAN, S., RAITAKARI, O. T., RIED, J. S., RIPATTI, S., SCHULZ, H., SCOTT, R. A., SIN, D. D., STARR, J. M., VINUELA, A., VOLZKE, H., WILD, S. H., WRIGHT, A. F., ZEMUNIK, T., JARVIS, D. L., SPECTOR, T. D., EVANS, D. M., LEHTIMAKI, T., VITART, V., KAHONEN, M., GYLLENSTEN, U., RUDAN, I., DEARY, I. J., KARRASCH, S., PROBST-HENSCH, N. M., HEINRICH, J., STUBBE, B., WILSON, J. F., WAREHAM, N. J., JAMES, A. L., MORRIS, A. P., JARVELIN, M. R., HAYWARD, C., SAYERS, I., STRACHAN, D. P., HALL, I. P. & TOBIN, M. D. 2015. Sixteen new lung function signals identified through 1000 Genomes Project reference panel imputation. *Nat Commun,* 6.

SOMMERLAD, B. C. 2003. A technique for cleft palate repair. *Plast Reconstr Surg,* 112**,** 1542-8.

SOMMERLAD, B. C. 2006. Surgery of the cleft palate: repair using the operating microscope with radical muscle retropositioning--the GostA approach. *B-ent,* 2 Suppl 4**,** 32-4.

SOMMERLAD, B. C., FENN, C., HARLAND, K., SELL, D., BIRCH, M. J., DAVE, R., LEES, M. & BARNETT, A. 2004. Submucous cleft palate: a grading system and review of 40 consecutive submucous cleft palate repairs. *Cleft Palate Craniofac J,* 41**,** 114-23.

SORIANO, P. 1999. Generalized lacZ expression with the ROSA26 Cre reporter strain. *Nat Genet,* 21**,** 70-1.

SPALICE, A., PARISI, P., NICITA, F., PIZZARDI, G., DEL BALZO, F. & IANNETTI, P. 2009. Neuronal migration disorders: clinical, neuroradiologic and genetics aspects. *Acta Paediatr,* 98**,** 421-33.

STAL, P., ERIKSSON, P. O. & THORNELL, L. E. 1996. Differences in capillary supply between human oro-facial, masticatory and limb muscles. *J Muscle Res Cell Motil,* 17**,** 183-97.

STAL, P. S. & LINDMAN, R. 2000. Characterisation of human soft palate muscles with respect to fibre types, myosins and capillary supply. *J Anat,* 197 (Pt 2)**,** 275-90.

STAL, S. & HICKS, M. J. 1998. Classic and occult submucous cleft palates: a histopathologic analysis. *Cleft Palate Craniofac J,* 35**,** 351-8.

STANIER, P. & MOORE, G. E. 2004. Genetics of cleft lip and palate: syndromic genes contribute to the incidence of non-syndromic clefts. *Hum Mol Genet,* 13 Spec No 1**,** R73-81.

STANIER, P. & PAUWS, E. 2012. Development of the lip and palate: FGF signalling. *Front Oral Biol,* 16**,** 71-80.

STANIER, P., SESELGYTE, R., MOORE, G. E. & PAUWS, E. 2018. TBX22-Associated Syndrome. *Reference Module in Biomedical Sciences.* Elsevier.

STEINTHORSDOTTIR, V., THORLEIFSSON, G. & SULEM, P. 2014. Identification of low-frequency and rare sequence variants associated with elevated or reduced risk of type 2 diabetes. 46**,** 294-8.

STENNARD, F. A., COSTA, M. W., ELLIOTT, D. A., RANKIN, S., HAAST, S. J., LAI, D., MCDONALD, L. P., NIEDERREITHER, K., DOLLE, P., BRUNEAU, B. G., ZORN, A. M. & HARVEY, R. P. 2003. Cardiac T-box factor Tbx20 directly interacts with Nkx2-5, GATA4, and GATA5 in regulation of gene expression in the developing heart. *Dev Biol,* 262**,** 206-24.

STRANSKY, C., BASTA, M., SOLOT, C., COHEN, M., LOW, D. W., LAROSSA, D. & JACKSON, O. 2013. Do patients with Pierre Robin sequence have worse outcomes after cleft palate surgery? *Ann Plast Surg,* 71**,** 292-6.

STROMLAND, K., SJOGREEN, L., JOHANSSON, M., EKMAN JOELSSON, B. M., MILLER, M., DANIELSSON, S., BILLSTEDT, E., GILLBERG, C., JACOBSSON, C., NORINDER, J. A. & GRANSTROM, G. 2005. CHARGE association in Sweden: malformations and functional deficits. *Am J Med Genet A,* 133a**,** 331-9.

STRONG, E. B. & BUCKMILLER, L. M. 2001. Management of the cleft palate. *Facial Plast Surg Clin North Am,* 9**,** 15-25, vii.

SUBRAMANIAN, A., TAMAYO, P., MOOTHA, V. K., MUKHERJEE, S., EBERT, B. L., GILLETTE, M. A., PAULOVICH, A., POMEROY, S. L., GOLUB, T. R., LANDER, E. S. & MESIROV, J. P. 2005. Gene set enrichment analysis: a knowledge-based approach for interpreting genome-wide expression profiles. *Proc Natl Acad Sci U S A,* 102**,** 15545-50.

SULLIVAN, S. R., VASUDAVAN, S., MARRINAN, E. M. & MULLIKEN, J. B. 2011. Submucous cleft palate and velopharyngeal insufficiency: comparison of speech outcomes using three operative techniques by one surgeon. *Cleft Palate Craniofac J,* 48**,** 561-70.

SUN, Y., KUEK, V., QIU, H., TICKNER, J., CHEN, L., WANG, H., HE, W. & XU, J. 2018. The emerging role of NPNT in tissue injury repair and bone homeostasis. *J Cell Physiol,* 233**,** 1887-1894.

SUPHAPEETIPORN, K., TONGKOBPETCH, S., SIRIWAN, P. & SHOTELERSUK, V. 2007. TBX22 mutations are a frequent cause of non-syndromic cleft palate in the Thai population. *Clin Genet,* 72**,** 478-83.

SUZUKI, K., HU, D., BUSTOS, T., ZLOTOGORA, J., RICHIERI-COSTA, A., HELMS, J. A. & SPRITZ, R. A. 2000. Mutations of PVRL1, encoding a cell-cell adhesion molecule/herpesvirus receptor, in cleft lip/palate-ectodermal dysplasia. *Nat Genet,* 25**,** 427-30.

SWANSON, J. W., MITCHELL, B. T., COHEN, M., SOLOT, C., JACKSON, O., LOW, D., BARTLETT, S. P. & TAYLOR, J. A. 2017. The Effect of Furlow Palatoplasty Timing on Speech Outcomes in Submucous Cleft Palate. *Ann Plast Surg,* 79**,** 156-161.

SWIBEL ROSENTHAL, L. H., WALSH, K. & THOMPSON, D. M. 2018. Velopharyngeal incompetence: role in paediatric swallowing deficits. *Curr Opin Otolaryngol Head Neck Surg,* 26**,** 356-366.

SZKLARCZYK, D., FRANCESCHINI, A., WYDER, S., FORSLUND, K., HELLER, D., HUERTA-CEPAS, J., SIMONOVIC, M., ROTH, A., SANTOS, A., TSAFOU, K. P., KUHN, M., BORK, P., JENSEN, L. J. & VON MERING, C. 2015. STRING v10: protein-protein interaction networks, integrated over the tree of life. *Nucleic Acids Res,* 43**,** D447-52.

TABLER, J. M., BARRELL, W. B., SZABO-ROGERS, H. L., HEALY, C., YEUNG, Y., PERDIGUERO, E. G., SCHULZ, C., YANNAKOUDAKIS, B. Z., MESBAHI, A., WLODARCZYK, B., GEISSMANN, F., FINNELL, R. H., WALLINGFORD, J. B. & LIU, K. J. 2013. Fuz mutant mice reveal shared mechanisms between ciliopathies and FGF-related syndromes. *Dev Cell,* 25**,** 623-35.

TADA, M. & SMITH, J. C. 2001. T-targets: clues to understanding the functions of T-box proteins. *Dev Growth Differ,* 43**,** 1-11.

TAIB, B. G., TAIB, A. G., SWIFT, A. C. & VAN EEDEN, S. 2015. Cleft lip and palate: diagnosis and management. *Br J Hosp Med (Lond),* 76**,** 584-5, 588-91.

TALBOT, J. C., NICHOLS, J. T., YAN, Y. L., LEONARD, I. F., BREMILLER, R. A., AMACHER, S. L., POSTLETHWAIT, J. H. & KIMMEL, C. B. 2016. Pharyngeal morphogenesis requires fras1-itga8-dependent epithelial-mesenchymal interaction. *Dev Biol,* 416**,** 136-148.

TAN, T. Y., KILPATRICK, N. & FARLIE, P. G. 2013. Developmental and genetic perspectives on Pierre Robin sequence. *Am J Med Genet C Semin Med Genet,* 163c**,** 295-305.

TANG, Q., LI, L., JIN, C., LEE, J. M. & JUNG, H. S. 2015. Role of region-distinctive expression of Rac1 in regulating fibronectin arrangement during palatal shelf elevation. *Cell Tissue Res,* 361**,** 857-68.

TANIKAWA, D. Y., AGUENA, M., BUENO, D. F., PASSOS-BUENO, M. R. & ALONSO, N. 2013. Fat grafts supplemented with adipose-derived stromal cells in the rehabilitation of patients with craniofacial microsomia. *Plast Reconstr Surg,* 132**,** 141-52.

TARDIF, M., BERTI, L. C., MARINO, V. C. C., PARDO, J. & BRESSMANN, T. 2018. Hypernasal Speech Is Perceived as More Monotonous than Typical Speech. *Folia Phoniatr Logop,* 70**,** 183-190.

TEMPEST, M. N. 1981. Cleft craft: The evolution of its surgery. Vol. III alveolar and palatal deformities. *British Journal of Plastic Surgery,* 34**,** 370-371.

THESLEFF, I., VAAHTOKARI, A., VAINIO, S. & JOWETT, A. 1996. Molecular mechanisms of cell and tissue interactions during early tooth development. *Anat Rec,* 245**,** 151-61.

THIEME, F. & LUDWIG, K. U. 2017. The Role of Noncoding Genetic Variation in Isolated Orofacial Clefts. *J Dent Res,* 96**,** 1238-1247.

THIEME, V., SELZER, G., GUNTHER, L., RUSTEMEYER, J. & BREMERICH, A. 2005. [Pierre Robin sequence: postoperative complications following cleft palate surgery. A retrospective study covering 25 years]. *Mund Kiefer Gesichtschir,* 9**,** 306-11.

THIENPONT, B., MERTENS, L., DE RAVEL, T., EYSKENS, B., BOSHOFF, D., MAAS, N., FRYNS, J. P., GEWILLIG, M., VERMEESCH, J. R. & DEVRIENDT, K. 2007. Submicroscopic chromosomal imbalances detected by array-CGH are a frequent cause of congenital heart defects in selected patients. *Eur Heart J,* 28**,** 2778-84.

THOMASON, H. A., ZHOU, H., KOUWENHOVEN, E. N., DOTTO, G. P., RESTIVO, G., NGUYEN, B. C., LITTLE, H., DIXON, M. J., VAN BOKHOVEN, H. & DIXON, J. 2010. Cooperation between the transcription factors p63 and IRF6 is essential to prevent cleft palate in mice. *J Clin Invest,* 120**,** 1561-9.

TONKIN, E. T., WANG, T. J., LISGO, S., BAMSHAD, M. J. & STRACHAN, T. 2004. NIPBL, encoding a homolog of fungal Scc2-type sister chromatid cohesion proteins and fly Nipped-B, is mutated in Cornelia de Lange syndrome. *Nat Genet,* 36**,** 636-41.

TRAINOR, P. A. & TAM, P. P. 1995. Cranial paraxial mesoderm and neural crest cells of the mouse embryo: co-distribution in the craniofacial mesenchyme but distinct segregation in branchial arches. *Development,* 121**,** 2569-82.

TRAN, F. H. & ZHENG, J. J. 2017. Modulating the wnt signaling pathway with small molecules. 26**,** 650-661.

TRAPPE, S. W., COSTILL, D. L., FINK, W. J. & PEARSON, D. R. 1995. Skeletal muscle characteristics among distance runners: a 20-yr follow-up study. *J Appl Physiol (1985),* 78**,** 823-9.

TSIEN, J. Z., CHEN, D. F., GERBER, D., TOM, C., MERCER, E. H., ANDERSON, D. J., MAYFORD, M., KANDEL, E. R. & TONEGAWA, S. 1996. Subregion- and cell type-restricted gene knockout in mouse brain. *Cell,* 87**,** 1317-26.

VAN DEN BOOGAARD, M. J., DORLAND, M., BEEMER, F. A. & VAN AMSTEL, H. K. 2000. MSX1 mutation is associated with orofacial clefting and tooth agenesis in humans. *Nat Genet,* 24**,** 342-3.

VAN DEN ELZEN, A. P., SEMMEKROT, B. A., BONGERS, E. M., HUYGEN, P. L. & MARRES, H. A. 2001. Diagnosis and treatment of the Pierre Robin sequence: results of a retrospective clinical study and review of the literature. *Eur J Pediatr,* 160**,** 47-53.

VAN, L., HEUNG, T., GRAFFI, J., NG, E., MALECKI, S., VAN MIL, S., BOOT, E., CORRAL, M., CHOW, E. W. C., HODGKINSON, K. A., SILVERSIDES, C. & BASSETT, A. S. 2019. All-cause mortality and survival in adults with 22q11.2 deletion syndrome. *Genet Med*.

VARGA, J., ROSENBLOOM, J. & JIMENEZ, S. A. 1987. Transforming growth factor beta (TGF beta) causes a persistent increase in steady-state amounts of type I and type III collagen and fibronectin mRNAs in normal human dermal fibroblasts. *Biochem J,* 247**,** 597-604.

VASER, R., ADUSUMALLI, S., LENG, S. N., SIKIC, M. & NG, P. C. 2016. SIFT missense predictions for genomes. 11**,** 1-9.

VATLACH, S., MAAS, C. & POETS, C. F. 2014. Birth prevalence and initial treatment of Robin sequence in Germany: a prospective epidemiologic study. *Orphanet J Rare Dis,* 9**,** 9.

VAZIRI SANI, F., HALLBERG, K., HARFE, B. D., MCMAHON, A. P., LINDE, A. & GRITLI-LINDE, A. 2005. Fate-mapping of the epithelial seam during palatal fusion rules out epithelial-mesenchymal transformation. *Dev Biol,* 285**,** 490-5.

VISSERS, L. E., VELTMAN, J. A., VAN KESSEL, A. G. & BRUNNER, H. G. 2005. Identification of disease genes by whole genome CGH arrays. *Hum Mol Genet,* 14 Spec No. 2**,** R215-23.

VOGEL, H. & ZAMECNIK, J. 2005. Diagnostic immunohistology of muscle diseases. *J Neuropathol Exp Neurol,* 64**,** 181-93.

WALKER, B. E. & FRASER, F. C. 1956. Closure of the Secondary Palate in Three Strains of Mice. *Journal of Embryology and Experimental Morphology,* 4**,** 176-189.

WALLIS, D. E., ROESSLER, E., HEHR, U., NANNI, L., WILTSHIRE, T., RICHIERI-COSTA, A., GILLESSEN-KAESBACH, G., ZACKAI, E. H., ROMMENS, J. & MUENKE, M. 1999. Mutations in the homeodomain of the human SIX3 gene cause holoprosencephaly. *Nat Genet,* 22**,** 196-8.

WAN, Y., LANTZ, B., CUSACK, B. J. & SZABO-ROGERS, H. L. 2018. Prickle1 regulates differentiation of frontal bone osteoblasts. 8**,** 18021.

WANG, C., YUE, F. & KUANG, S. 2017. Muscle Histology Characterization Using H&E Staining and Muscle Fiber Type Classification Using Immunofluorescence Staining. *Bio Protoc,* 7.

WANG, T., TAMAKOSHI, T., UEZATO, T., SHU, F., KANZAKI-KATO, N., FU, Y., KOSEKI, H., YOSHIDA, N., SUGIYAMA, T. & MIURA, N. 2003. Forkhead transcription factor Foxf2 (LUN)-deficient mice exhibit abnormal development of secondary palate. *Dev Biol,* 259**,** 83-94.

WANG, Y., LI, D., XU, Y., MA, L., LU, Y., WANG, Z., WANG, L., ZHANG, W. & PAN, Y. 2018. Functional Effects of SNPs in MYH9 and Risks of Nonsyndromic Orofacial Clefts. *J Dent Res,* 97**,** 388-394.

WANG, Z., GERSTEIN, M. & SNYDER, M. 2009. RNA-Seq: a revolutionary tool for transcriptomics. *Nat Rev Genet,* 10**,** 57-63.

WEATHERLEY-WHITE, R. C., SAKURA, C. Y., JR., BRENNER, L. D., STEWART, J. M. & OTT, J. E. 1972. Submucous cleft palate. Its incidence, natural history, and indications for treatment. *Plast Reconstr Surg,* 49**,** 297-304.

WEINTRAUB, H., DAVIS, R., TAPSCOTT, S., THAYER, M., KRAUSE, M., BENEZRA, R., BLACKWELL, T. K., TURNER, D., RUPP, R., HOLLENBERG, S. & ET AL. 1991. The myoD gene family: nodal point during specification of the muscle cell lineage. *Science,* 251**,** 761-6.

WELSH, I. C., HAGGE-GREENBERG, A. & O'BRIEN, T. P. 2007. A dosage-dependent role for Spry2 in growth and patterning during palate development. *Mech Dev,* 124**,** 746-61.

WENQUAN, N., YUE, Q., PINGJIN, G. & DINGLIANG, Z. 2011. Review: association between angiotensin converting enzyme G2350A polymorphism and hypertension risk: a meta-analysis. *J Renin Angiotensin Aldosterone Syst,* 12**,** 8-14.

WILKINSON, D. G., BHATT, S. & HERRMANN, B. G. 1990. Expression pattern of the mouse T gene and its role in mesoderm formation. *Nature,* 343**,** 657-9.

WITT, P. D., MYCKATYN, T., MARSH, J. L., GRAMES, L. M. & DOWTON, S. B. 1997. Need for velopharyngeal management following palatoplasty: an outcome analysis of syndromic and nonsyndromic patients with Robin sequence. *Plast Reconstr Surg,* 99**,** 1522-9; discussion 1530-4.

WONG, L. S., LIM, E., LU, T. C. & CHEN, P. K. T. 2019. Management of velopharyngeal insufficiency by modified Furlow palatoplasty with pharyngeal flap: a retrospective outcome review. *Int J Oral Maxillofac Surg,* 48**,** 703-707.

WU, T., CHEN, G., TIAN, F. & LIU, H. X. 2017. Contribution of cranial neural crest cells to mouse skull development. *Int J Dev Biol,* 61**,** 495-503.

WYLEZINSKA, M., PINKSTONE, M., HAY, N., SCOTT, A. D., BIRCH, M. J. & MIQUEL, M. E. 2015. Impact of orthodontic appliances on the quality of craniofacial anatomical magnetic resonance imaging and real-time speech imaging. *Eur J Orthod,* 37**,** 610-7.

XIE, X., LU, J., KULBOKAS, E. J., GOLUB, T. R., MOOTHA, V., LINDBLAD-TOH, K., LANDER, E. S. & KELLIS, M. 2005. Systematic discovery of regulatory motifs in human promoters and 3' UTRs by comparison of several mammals. *Nature,* 434**,** 338-45.

XING, P. R., PAN, J. Y. & ZHANG, H. R. 2019. [Expression and significance of Shh and Wnt5a genes in Cornelia de Lange syndrome]. *Zhongguo Dang Dai Er Ke Za Zhi,* 21**,** 485-490.

XIONG, W., HE, F., MORIKAWA, Y., YU, X., ZHANG, Z., LAN, Y., JIANG, R., CSERJESI, P. & CHEN, Y. 2009. Hand2 is required in the epithelium for palatogenesis in mice. *Dev Biol,* 330**,** 131-41.

XU, J., LIU, H., LAN, Y., ARONOW, B. J., KALINICHENKO, V. V. & JIANG, R. 2016. A Shh-Foxf-Fgf18-Shh Molecular Circuit Regulating Palate Development. *PLoS Genet,* 12**,** e1005769.

XU, X., HAN, J., ITO, Y., BRINGAS, P., JR., DENG, C. & CHAI, Y. 2008. Ectodermal Smad4 and p38 MAPK are functionally redundant in mediating TGF-beta/BMP signaling during tooth and palate development. *Dev Cell,* 15**,** 322-9.

XU, X., HAN, J., ITO, Y., BRINGAS, P., JR., URATA, M. M. & CHAI, Y. 2006. Cell autonomous requirement for Tgfbr2 in the disappearance of medial edge epithelium during palatal fusion. *Dev Biol,* 297**,** 238-48.

YAGI, H., FURUTANI, Y., HAMADA, H., SASAKI, T., ASAKAWA, S., MINOSHIMA, S., ICHIDA, F., JOO, K., KIMURA, M., IMAMURA, S., KAMATANI, N., MOMMA, K., TAKAO, A., NAKAZAWA, M., SHIMIZU, N. & MATSUOKA, R. 2003. Role of TBX1 in human del22q11.2 syndrome. *Lancet,* 362**,** 1366-73.

YANG, A., SCHWEITZER, R., SUN, D., KAGHAD, M., WALKER, N., BRONSON, R. T., TABIN, C., SHARPE, A., CAPUT, D., CRUM, C. & MCKEON, F. 1999. p63 is essential for regenerative proliferation in limb, craniofacial and epithelial development. *Nature,* 398**,** 714-8.

YANG, L. T. & KAARTINEN, V. 2007. Tgfb1 expressed in the Tgfb3 locus partially rescues the cleft palate phenotype of Tgfb3 null mutants. *Dev Biol,* 312**,** 384-95.

YANG, T., JIA, Z., BRYANT-PIKE, W., CHANDRASEKHAR, A., MURRAY, J. C., FRITZSCH, B. & BASSUK, A. G. 2014. Analysis of PRICKLE1 in human cleft palate and mouse development demonstrates rare and common variants involved in human malformations. *Mol Genet Genomic Med,* 2**,** 138-51.

YANG, Y., YUAN, J., YAO, X., ZHANG, R., YANG, H., ZHAO, R., GUO, J., JIN, K., MEI, H., LUO, Y., ZHAO, L., TU, M. & ZHU, Y. 2017. BMPR1B mutation causes Pierre Robin sequence. *Oncotarget,* 8**,** 25864-25871.

YE, L., MORSE, L. R., ZHANG, L., SASAKI, H., MILLS, J. C., ODGREN, P. R., SIBBEL, G., STANLEY, J. R., WONG, G., ZAMARIOLI, A. & BATTAGLINO, R. A. 2015. Osteopetrorickets due to Snx10 deficiency in mice results from both failed osteoclast activity and loss of gastric acid-dependent calcium absorption. *PLoS Genet,* 11**,** e1005057.

YOSHIDA, T., VIVATBUTSIRI, P., MORRISS-KAY, G., SAGA, Y. & ISEKI, S. 2008. Cell lineage in mammalian craniofacial mesenchyme. *Mech Dev,* 125**,** 797-808.

YOUNKIN, S. G., SCHARPF, R. B., SCHWENDER, H., PARKER, M. M., SCOTT, A. F., MARAZITA, M. L., BEATY, T. H. & RUCZINSKI, I. 2014. A genome-wide study of de novo deletions identifies a candidate locus for non-syndromic isolated cleft lip/palate risk. *BMC Genet,* 15**,** 24.

YSUNZA, A., PAMPLONA, C., RAMIREZ, E., MOLINA, F., MENDOZA, M. & SILVA, A. 2002. Velopharyngeal surgery: a prospective randomized study of pharyngeal flaps and sphincter pharyngoplasties. *Plast Reconstr Surg,* 110**,** 1401-7.

YSUNZA, P. A., BLOOM, D., CHAIYASATE, K., RONTAL, M., VANHULLE, R., SHAHEEN, K. & GIBSON, D. 2016. Velopharyngeal videofluoroscopy: Providing useful clinical information in the era of reduced dose radiation and safety. *Int J Pediatr Otorhinolaryngol,* 89**,** 127-32.

YSUNZA, P. A., REPETTO, G. M., PAMPLONA, M. C., CALDERON, J. F., SHAHEEN, K., CHAIYASATE, K. & RONTAL, M. 2015. Current Controversies in Diagnosis and Management of Cleft Palate and Velopharyngeal Insufficiency. *Biomed Res Int,* 2015**,** 196240.

YU, H., SMALLWOOD, P. M., WANG, Y., VIDALTAMAYO, R., REED, R. & NATHANS, J. 2010. Frizzled 1 and frizzled 2 genes function in palate, ventricular septum and neural tube closure: general implications for tissue fusion processes. *Development,* 137**,** 3707-17.

YU, K. & ORNITZ, D. M. 2011. Histomorphological study of palatal shelf elevation during murine secondary palate formation. *Dev Dyn,* 240**,** 1737-44.

YU, L., GU, S., ALAPPAT, S., SONG, Y., YAN, M., ZHANG, X., ZHANG, G., JIANG, Y., ZHANG, Z., ZHANG, Y. & CHEN, Y. 2005. Shox2-deficient mice exhibit a rare type of incomplete clefting of the secondary palate. *Development,* 132**,** 4397-406.

YUAN, G., SINGH, G., CHEN, S., PEREZ, K. C., WU, Y., LIU, B. & HELMS, J. A. 2017. Cleft Palate and Aglossia Result From Perturbations in Wnt and Hedgehog Signaling. *Cleft Palate Craniofac J,* 54**,** 269-280.

YUAN, X., BAI, J., ZHANG, J., YANG, L., DUAN, J., LI, Y. & GAO, M. 2018. CONDEL: Detecting Copy Number Variation and Genotyping Deletion Zygosity from Single Tumor Samples using Sequence Data. *IEEE/ACM Trans Comput Biol Bioinform*.

ZAMORA, E. A. & SALINI, U. B. 2019. Axenfield Anomaly. *StatPearls.* Treasure Island (FL): StatPearls Publishing LLC.

ZARAGOZA, M. V., LEWIS, L. E., SUN, G., WANG, E., LI, L., SAID-SALMAN, I., FEUCHT, L. & HUANG, T. 2004. Identification of the TBX5 transactivating domain and the nuclear localization signal. *Gene,* 330**,** 9-18.

ZEMLIN, W. R. 1964. *Speech and hearing science : anatomy and physiology*, Stipes Publishing Co.

ZHANG, Z., SONG, Y., ZHAO, X., ZHANG, X., FERMIN, C. & CHEN, Y. 2002. Rescue of cleft palate in Msx1-deficient mice by transgenic Bmp4 reveals a network of BMP and Shh signaling in the regulation of mammalian palatogenesis. *Development,* 129**,** 4135-46.

ZHAO, S., FUNG-LEUNG, W. P., BITTNER, A., NGO, K. & LIU, X. 2014. Comparison of RNA-Seq and microarray in transcriptome profiling of activated T cells. *PLoS One,* 9**,** e78644.

ZHAO, Y., GUO, Y. J., TOMAC, A. C., TAYLOR, N. R., GRINBERG, A., LEE, E. J., HUANG, S. & WESTPHAL, H. 1999. Isolated cleft palate in mice with a targeted mutation of the LIM homeobox gene lhx8. *Proc Natl Acad Sci U S A,* 96**,** 15002-6.

ZHOU, J., GAO, Y., LAN, Y., JIA, S. & JIANG, R. 2013. Pax9 regulates a molecular network involving Bmp4, Fgf10, Shh signaling and the Osr2 transcription factor to control palate morphogenesis. *Development,* 140**,** 4709-18.

ZLOTOGORA, J., SAGI, M., SCHUPER, A., LEIBA, H. & MERIN, S. 1992. Variability of Stickler syndrome. *Am J Med Genet,* 42**,** 337-9.

ZOUPA, M., XAVIER, G. M., BRYAN, S., THEOLOGIDIS, I., ARNO, M. & COBOURNE, M. T. 2018. Gene expression profiling in the developing secondary palate in the absence of Tbx1 function. 19**,** 429.

ZWEIER, C., STICHT, H., AYDIN-YAYLAGUL, I., CAMPBELL, C. E. & RAUCH, A. 2007. Human TBX1 missense mutations cause gain of function resulting in the same phenotype as 22q11.2 deletions. *Am J Hum Genet,* 80**,** 510-7.